Literature review on sand and mud

TKI MUSA project

Literature review on sand and mud
TKI MUSA project

Author(s)
Prof. dr. ir. L.C. van Rijn
ir. A. Colina Alonso
Prof. dr. A.J. Manning

Literature review on sand and mud

TKI MUSA project

Client	
Contact	Leo van Rijn (info@leovanrijn-sediment.com) and Y. Huismans (Ymkje.Huismans@deltares.nl)
Reference	TKI MUSA Project: 11204950
Keywords	Sand, Slit, Clay, Biota, Consolidation, Erosion, Flocculation, Sedimentation, Field Measurements, Laboratory Experiments

Document control	
Version	1,0
Date	16-11-2020
Project nr.	11204950-001
Document ID	-
Pages	144
Status	final

Author(s)		
	dr. ir. L.C. van Rijn	
	ir. A. Colina Alonso	
	Prof. dr. A.J, Manning	

Doc. version	Main Author	Reviewer
1.0	dr. ir. L.C. van Rijn	dr. D.S. van Maren

MUSA

About the MUSA project

Estuaries and tidal basins form the transition zones between land and sea. They contain important habitats for flora and fauna and are extensively used by people, like for navigation. For ecological and navigational purposes, it is important to understand and predict the evolution of channels and shoals, including sedimentation rates and the composition of the bed sediments. The bed material of large estuaries and tidal basins largely consists of mixtures of mud and sand, with predominantly sandy channels and mainly muddy intertidal areas. The interaction between sand and mud, in combination with currents and waves, leads to complex dynamics in these areas, with migrating channels and shoals.

Much is known about the behaviour of the individual sediment fractions, but the knowledge and understanding of sand-mud interaction remains limited (especially under the combined forcing of waves and currents), as do the available tools and models to accurately predict the bed evolution and sediment transport rates in sand-mud areas. Existing models, like the ones by Van Ledden (2003), Soulsby & Clarke (2005) or Van Rijn (2007) have only limitedly been verified with observations due to a lack of good quality observational data. Also, none of the available approaches cover the complete spectrum of sand-mud interaction, which includes settling, erosion processes, waves and currents, and the bed shear stress. Therefore, in practice, sand- and mud fractions are often treated separately. This decoupled approach limits the predictive capacity of numerical models, and therefore the impact of human intervention such as deepening of channels and port construction on maintenance dredging volumes and other morphological changes.

In the MUSA-research project, a consortium contractors, consultants and research organizations join forces to increase the understanding of sand-mud dynamics by means of fieldwork campaigns and lab experiments, and to implement this knowledge in engineering tools and advanced models for the prediction of mud and sand transport and associated morphology in tidal conditions with both currents and waves.

Contents

1 Introduction

Mixtures of clay, silt and fine sand generally characterize the bed of the major estuaries and tidal basins around the world. The interaction of the cohesive and non-cohesive sediment fractions in response to the hydrodynamic forces of nature results in a rather complex sedimentary environment with large-scale migrating/shifting tidal channels, mud flats and islands, which we hardly understand from a physical point of view. The tidal channels often are sand-dominated with migrating sandy bed features, whereas the tidal flats are dominated by the finer fractions (silts and muds) with additional biotic processes affecting the composition of intertidal and subtidal sediments. As most of these estuaries nowadays act as important navigation routes, their hydrography and sediment dynamics are affected by large-scale dredging activities. In order to minimize the dredging effort and to anticipate undesired ecological and morphological effects of these activities, reliable tools for prediction of sand and mud transport and associated morphological changes are needed. Yet, no models are available that can predict the morphological changes and associated deposition rates in the case of a combined sand-mud bed in an estuary with sufficient accuracy. Often, complex calibration procedures (Van Maren et al., 2020) are required to get meaningful results. In most cases, the present approach is (Mengual et al., 2017):

- use separate sand and mud transport models;
- combine the results based on the fraction percentages.

In some cases, field data of mud concentrations at a limited number of locations are available for calibration of the many model parameters involved. Most often, detailed data of mud and sand concentrations, settling velocities and bed composition in the near-bed region are not available. Generally, this leads to a crude calibration focussing on the dominant mechanisms.

Using this approach, the detailed interaction of the sand and mud fractions cannot sufficiently be taken into account and very conservative overall results may be obtained (significant overprediction of siltation rates).

The most basic objective of the MUSA-research to extend our knowledge of the detailed physical near-bed sediment exchange processes in combined current and waves over a mixed mud-sand bed for implementation in detailed numerical models and other more simple excel/matlab/python-tools.

A substantial amount of work has been done in the past 30 years on the erosion of sand and mud individually, and to a lower degree, on mixtures of sand and mud. The MUSA project extends previous work, filling in gaps of knowledge but also using similar terminologies and methodologies. Therefore, the present report presents an extensive review of the existing literature of papers, documents and reports on mud-sand beds and identifies knowledge gaps and key research questions, outlining an approach to address the formulated remaining research questions. Information of ongoing projects on mud-sand beds elsewhere will be incorporated as much as possible (GIP Seine-Aval Project; www.seine-aval.fr).

The setup of this report is as follows. A process overview and definitions are provided in Chapter 2. Chapters 3, 4 and 5 present respectively reviews on erosion experiments of soft and firm mud-sand beds, settling experiments and consolidation experiments related to bed densities. Detailed descriptions of the existing literature (summarized in chapters 3-5) are given in Appendices A, B, C, D, E and F. Based on the evaluation of all review results, new laboratory and field experiments are proposed in Chapter 6.

Literature review on sand and mud
16 November 2020

2　Basic definitions and processes

2.1　Sediment bed

2.1.1　Grain size scales

Mud is defined as a mixture of clay and silt particles, including organic/calcareous materials and minor contents (<10%) of sand. Sand, silt and clay are defined by their grain size, see Table 2.1. However, multiple definitions exist to differentiate sand silt and clay:

Table 2.1 Sand, silt, clay definitions and US-Wentworth scale

Classification method	sand	silt	clay
American Geophysical Union sacle and Wentworth scale	0.063-2 mm	0.04 - 0.063 mm	< 0.004 mm
ASTM D422	0.075-4.75 mm	0.05 - 0.075 mm	< 0.005 mm
B.S. 1377	0.060-2 mm	0.02 - 0.060 mm	< 0.002 mm
NEN 5104	0.063-2 mm	0.02 - 0.063 mm	< 0.002 mm

Size (Millimeters)	Wentworth Grade	Phi (Φ) Scale	Sediment	Sedimentary Rock
>256	Boulder	−8	GRAVEL	CONGLOMERATE
256-64	Cobble	−6		
64-4	Pebble	−2		
4-2	Granule	−1		
2-1	Very coarse sand	0	SAND	SANDSTONE
1-1/2	Coarse sand	1		
1/2-1/4	Medium sand	2		
1/4-1/8	Fine sand	3		
1/8-1/16	Very fine sand	4		
1/16-1/32	Coarse silt	5	MUD	MUDSTONE
1/32-1/64	Medium silt	6		
1/64-1/128	Fine silt	7		
1/128-1/256	Very fine silt	8		
<1/256	Clay	>8		

Studies on the erosion and settling of sand-mud mixtures have therefore defined sand, but especially clay and mud in different ways which hampers mutual comparison of existing datasets. Most pure clay minerals have a grain size smaller than 2 µm (lutum) or 4 µm (Wentworth-scale). For practical reasons (laboratory determination of the percentage<2 µm is extremely difficult), the cohesive fraction with clay and very fine silt is defined to consist of particles with diameters smaller than 4 µm (clay-dominated fraction). Therefore, we follow the definition of the American Geophysical Union.

The grain size scale of the American Geophysical Union for sediments with particle sizes smaller than 2 mm consists of many subclasses ranging from very coarse sand to very fine clay.

MUSA

Herein, the following six subclasses are distinguished:

coarse sand (non-cohesive)	0.5 to 2 mm	(500 to 2000 µm)
fine sand (non-cohesive)	0.063 to 0.5 mm	(63 to 500 µm)
coarse silt	0.032 to 0.063 mm	(32 to 63 µm)
medium silt	0.016 to 0.032 mm	(16 to 32 µm)
fine silt (weakly cohesive)	0.08 to 0.016 mm	(8 to 16 µm)
very fine silt (weakly cohesive)	0.04 to 0.08 mm	(4 to 8 µm)
coarse clay (cohesive)	0.02 to 0.04 mm	(2 to 4 µm)
medium clay	0.01 to -0.02 mm	(1 to 2 µm)
fine clay	< 0.005 to 0.01 mm	(0.5 to 1 µm)
very fine clay	<0.005 mm	(< 0.5 µm)

Mud beds consist of primary particles (of silt and clay) but also of flocs. Flocs are aggregates of 10's to 100's of µm formed by clay particles bound together by polymeric and bacterial substances and van der Waals forces, and are characterised by a very open structure.

2.1.2 Mud-sand mixtures

Sediment bed mixtures consisting of mud (particles and flocs < 63 µm) and sand are known as mud-sand mixtures and are generally found along marine and estuarine beds, banks and coasts. Mud-sand bed mixtures are mixtures with appreciable fractions of clay, silt and (fine) sand. Based on Shepard (1954), a bed of muddy sand is a mixture with a minor percentage of mud (less than mass percentage of about 30%) and a sandy mud is a mixture with a major percentage of mud (more than 70%). McLaughlin (1959), Gibbs (1985), Stevens (1991), (Van Ledden, 2004) and many others have found that cohesive effects strongly depend on the amount of fine clay, silt and organic materials.

Bed samples consisting of mixtures of clay, silt and sand are herein classified as: mud, sandy mud, silty mud or clayey mud, depending on the percentages of sand, silt, clay and organic material (Table 2.2). The percentage of clay, silt and mud are in this report are defined as weight percentages, and not as volume percentage (unless specifically mentioned).

Table 2.2 Types of sand-mud mixtures (mass percentages)

Type of sediment		Percentage of organic material	Percentage of Clay + Fine Silt (< 8 µm)	Percentage of Silt (8 - 63 µm)	Percentage of Sand (> 63 µm)
Sand	(non-cohesive)	0%	0%	0%	100%
Muddy Sand	(weakly-cohesive)	0-10%	0-5%	20-40%	60-80%
Sandy Mud	(cohesive)	0-10%	5-10%	30-60%	60-30%
Mud	(cohesive)	0-20%	10-20%	50-70%	0-10%
Silty Mud	(cohesive)	0-20%	10-40%	60-80%	0%
Clayey Mud	(cohesive)	0-20%	40-60%	40-60%	0%

The clay fraction of mud-sand beds has cohesive properties and has the ability to retain water. Cohesion is caused by van der Waals forces and /or organic polymers binding the very fine plate-type clay particles. The ability of clay to retain water is related to the relatively open structure of flocs. The fine particles consist of various clay and quartz minerals (very fine silt). The most important clay minerals are kaolinite, illite and montmorillonite (subclass of smectites). The latter has a relatively large absorption capacity for other particulate substances in the water (organic matter) stimulating floc growth. If possible, the dominant

clay mineral should be identified (chemistry, microscopy, spectroscopy, x-ray diffraction) and reported to provide an idea of the clay activity.

Mud-sand beds also contains organic materials in the form of the remains of plant and animal organisms (microscopic and larger organisms), fibres, active bacteria and fungi, and organic molecules. Of relevance is also the bed structure which is related to the presence of cracks, plant rests and biological activity. Cracking occurs due to shrinking and swelling as a result of the clay becoming wet and dry. Biological activity consists of burrowing animals (worms, insects, moles) and root penetration from vegetation. Biological activity also includes ingestion.

Mehta (1991b, 1992) and Berlamont et al. (1993) have identified and categorized the sediment properties describing the behaviour of sand-mud mixtures, such as yield stress, shear strength, plasticity index, dry density, percentages clay, silt and sand, organic matter and salinity. According to Parchure et al. (2002) and Parchure and Davis (2005), the most significant parameters to characterize cohesive sediment beds are particle size distribution, organic content, plasticity and bulk density. Plasticity is characterized by the Atterberg limits (liquid and plastic limits, see also section), which are a measure of the of the critical water contents of a fine-grained soil, and therewith the soil state of the muddy mixture (solid, semi-solid, plastic and liquid). A decreasing water content increases the stiffness of the saturated clay. At low water content the clay can behave more like a plastic solid than a thick fluid. The water content at the transition point between thick fluid and plastic clay is known as the Liquid Limit LL. At a lower water content, the Plastic Limit PL is reached at which plastic soil can no longer deform without breaking. The difference between the flow and plastic limits is known as the plasticity index (PI = LL - PL). The plasticity index increases with increasing clay content, as the soil's capacity to retain water depends on the clay content. See section 2.1.7 for more details on the Atterberg limits.

2.1.3 Layered beds

Bed deposits formed in sedimentary environments often have layered structures due to differential settling and sediment sorting. Each layer may have a different structure, bulk density (degree of consolidation) and strength against erosion resulting in a stepwise erosional behaviour. Generally, the topmost layer is a thin muddy layer as the very fine particles will settle at the end of the settling process. The upper muddy layer generally is soft and can be easily eroded if it is freshly deposited. The mud particles will almost immediately be suspended, when the flow-induced bed-shear stress exceeds the critical shear stress for erosion (defined in section 2.1.10). A sandy sub-layer underneath a thin mud layer will be eroded as bed load transport with ripple features occurring. Other more consolidated mud layers underneath sand layers may have a much higher erosion strength due to consolidation processes.

2.1.4 Mixed beds

Homogeneously mixed sediment beds of clay, slit and sand particles are rare in nature. A typical example of a rather homogeneously mixed bed is the bed surface of an intertidal flat exposed to waves due to the active reworking of the bed surface by the surface waves and bioturbation by benthic organisms.

Homogeneously mixed beds have been used in most laboratory experiments. These types of laboratory mixtures generally are somewhat bimodal by mixing fine sand and natural mud with low silt contents. The presence of sand improves the drainage, resulting in more compaction. The degree of compaction increases with the percentage of sand. The sediment properties are approximately constant over the depth of the homogeneous layer.

MUSA

2.1.5 Network structure

Cohesive effects in mud-sand mixtures become important in the case that the sand particles are surrounded (coated) by fine cohesive particles. At lower mud content, the soil structure is dominated by the sand skeleton, as all sand particles are still in contact see Figure 2.1 (upper). At higher mud content (lower panel of Figure 2.1), the sand particles are no longer in contact. The structure of the bed is then dominated by the clay-water matrix, and the bed has cohesive properties. Whether the sand particles are in contact or not depends on the volumetric sand concentration c_{sand}. C_{sand} can be defined as the ratio of the sand particle volume ($0.16\pi D^3$ for a sphere) and the cube volume (D^3) resulting in $c_{sand} \approx 0.5$ (volume concentration) for a cube packing (see Figure 2.1). Thus, all sand particles are in contact for a volume concentration of about 0.5. A stronger network is obtained for a hexagonal-packing resulting in a volume concentration of about 0.7, see Figure 2.1 (upper).
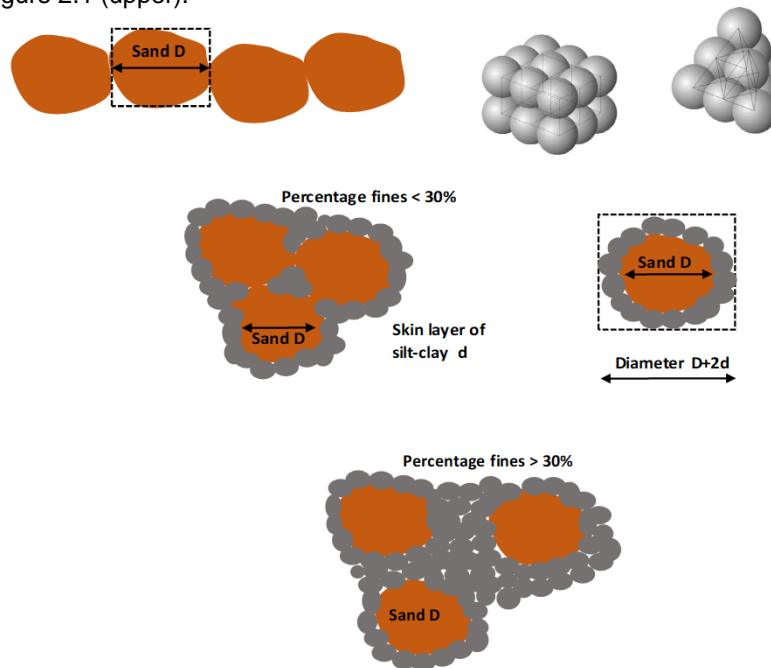

Figure 2.1 Network structures of mud-sand mixtures. Upper: sand particles without mud. Middle: sand particles with skin layer of silt-clay particles (percentage fines < 30%). Lower: sand particles drowned in mud particles (percentage fines > 30%).

Determination of volume concentration of fines for complete coating of sand particles

If one sand particle with diameter D is surrounded by a layer of fine particles with diameter d, the total volume of the fine particles in the skin layer is about: $V_{fines} = (1-\varepsilon)\ 1.33\pi[(0.5D+d)^3-(0.5D)^3]$, with ε= pore volume of the fine particles (about 0.4).

The cube around a sand particle (diameter D) plus the skin layer of fine particles (diameter d) has a volume of $V_{cube,sand+fines}=(D+2d)^3$.

The volume concentration of fine particles is: $c_{fines}=V_{fines}/V_{cube,sand+fines}= (1-\varepsilon)1.33\pi[(0.5D+d)^3-(0.5D)^3]/(D+2d)^3$. Using: $\varepsilon=0.4$, $d/D=0.08$, $d=0.000008$ m (8 µm) and $D=0.0001$ m (100 µm), it follows that: $c_{fines}\approx 0.1$.

Thus, a minimum of about $p_{clay-finesilt}=0.1$ (10% by volume) of fine particles (< 8 µm) is required for complete coating of the sand particles (63 to 200 µm) by a skin layer of fine particles.

Assuming $p_{clay-finesilt}=0.1$ and a silt-clay ratio of $p_{silt}/p_{clay-finesilt}=2$ for natural mixed sediment beds, the critical clay-silt content (< 63 µm) will be about $p_{silt,cr}+p_{clay-fine\ silt,cr}=p_{mud,cr} \approx 0.3$. A fully space-filling network will be present for clay-silt contents > 30%. The distance between the sand particles will increase for increasing clay-silt content, see Figure 2.1 (middle and lower panel).

If the mud content is below the critical value ($p_{mud}<p_{mud,cr}$), the bed only has weak cohesive or non-cohesive properties.

A fully cohesive bed is different from a non-cohesive bed in the sense that the density of the bed is not constant in time due to consolidation processes taking place in the near-bed region. Particle-particle interaction of very fine cohesive particles results in aggregation (flocs) of the particles. In the final stage of the (hindered) settling process near the bed, these flocs become space-filling and form a network structure (gelling structure), which is the onset of the consolidation process (Winterwerp, 1999, 2001). The concentration at the transition from hindered settling to consolidation (or from mobile fluid mud to immobile consolidating mud) is defined as the gelling concentration c_{gel}.

Quantitative information can be obtained from field observations at the mouth of the Amazon in Brazil (Vinzon and Mehta, 2003). They have made detailed concentration and velocity measurements through the mobile fluid mud layer. The gelling/maximum concentrations at the bottom of the mobile hyperpycnal layer were of the order of 200 to 250 kg/m^3 (mass concentration). Just above the immobile bed the sediment concentrations were of the order of 200 kg/m^3 decreasing to about 10 kg/m^3 and transported at velocities of 0.1 to 0.7 m/s.

Li et al. (2004) report a value of about 280 kg/m^3 (wet bulk density of about 1200 kg/m^3) as the transition from the mobile fluid mud to the immobile consolidating bed (with a median grain size of about 10 µm) for the mouth of the Yangtze Estuary in China.

Consolidation tests with koalinite (< 4 µm) in saline water (Van Rijn, 1993) show that the consolidation process commences at a concentration of about c_{gel}= 150 to 250 kg/m^3.

Dankers (2006) found much lower values of c_{gel}= 70 to 90 kg/m^3 for kaolinite (< 4 µm) in saline water.

Others have found values in the range of 30 to 180 kg/m^3 (Whitehouse et al., 2000; Merckelbach and Kranenburg, 2004; Camenen and Pham Van Bang, 2011; Te Slaa et al., 2013).

MUSA

2.1.6 Bed density

The bed density can be defined in different ways. The most common method is to define the wet or dry density as the ratio of the wet or dry sediment mass (resp.) in a volume V. Wu and Li (2017), however, state that it is more appropriate to define the density of the mud as the mass of mud in the volume occupied by the mud (including pores).

Determination of bulk density of mud-sand mixtures

The bulk density of the mixture of mud and sand is: $\rho_{wet, mixture} = M_{wet}/V$,

The dry density of the mixture of mud and sand is: $\rho_{dry, mixture} = M_{dry}/V$,

with M_{wet}= mass water and sediment per volume V; $M_{dry} = M_{dry,mud} + M_{dry,sand}$= mass of dry sediment per volume V.

The percentage of mud and sand in volume V is: $p_{sand} = M_{dry,sand}/M_{dry}$ and $p_{mud} = M_{dry,mud}/M_{dry}$

The dry density of sand is: $\rho_{dry, sand} = M_{dry, sand}/V = (M_{dry, sand}/M_{dry})(M_{dry}/V) = p_{sand}\,\rho_{dry, mixture}$

The dry density of mud is: $\rho_{dry, mud} = M_{dry, mud}/V = (M_{dry,mud}/M_{dry})(M_{dry}/V) = p_{mud}\,\rho_{dry, mixture}$

Using: $p_{mud} + p_{sand} = 1$, it follows that: $M_{dry, mud}/M_{dry} + M_{dry, sand}/M_{dry} = 1$

$(\rho_{dry, mud}\,V)/M_{dry} + (\rho_{dry, sand}\,V)/M_{dry} = 1$

$\rho_{dry, mud} + \rho_{dry, sand} = M_{dry}/V$

$\rho_{dry, mud} + \rho_{dry, sand} = \rho_{dry, mixture}$

Wu and Li (2017) state that it is better to define the densities in terms of the volumes of each sediment fraction.

The (true) dry density of mud and sand is then defined as: $\rho_{dry, mud,*} = M_{dry, mud}/V_{mud}$ and $\rho_{dry,sand,*} = M_{dry,sand}/V_{sand}$

with V_{mud}= volume of the mud fraction including pores and V_{sand}= volume of the sand fraction including pores.

$V_{mud} + V_{sand} = V$

$M_{dry,mud}/\rho_{dry, mud,*} + M_{dry,sand}/\rho_{dry,sand,*} = M_{dry}/\rho_{dry, mixture}$

Using: $M_{dry,mud} = p_{mud}\,M_{dry}$ and $M_{dry,sand} = p_{sand}\,M_{dry}$, it follows that:

$p_{mud}\,M_{dry}/\rho_{dry, mud,*} + p_{sand}\,M_{dry}/\rho_{dry,sand,*} = M_{dry}/\rho_{dry, mixture}$

$p_{mud}/\rho_{dry, mud,*} + p_{sand}/\rho_{dry,sand,*} = 1/\rho_{dry, mixture}$

This latter equation, first given by Colby (1963). This equation is only valid for a mixture in which the mud and sand fractions are fully separated.

In natural mixtures, the mud particles are between and around the sand particles, see Figure 2.2.

In that case the V_{mud} including remaining voids can not easily be determined.

Wu and Li (2017) have proposed to use:

$(1-B)\,p_{sand}/\rho_{dry,sand,*} + B\,p_{sand}/\rho_s + p_{mud}/\rho_{dry,mud,*} = 1/\rho_{dry, mixture}$

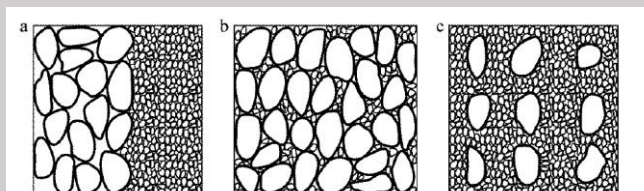with: B=filling coefficient, ρ_s = sediment density

Figure 2.2

MUSA

2.1.7 Plasticity

Depending on its water content, a soil may appear in one of four states: solid, semi-solid, plastic and liquid. In each state, the consistency and behavior of a soil is different. The boundary between each state can be defined based on a change in the soil's behavior. The Atterberg limits can be used to distinguish between different types of soils. The water content at which the soil changes from one state to the other are known as consistency limits or Atterberg's limit.

Plasticity is a property exhibited by soils when an appreciable percentage of the soil consists of clay size particles. The plasticity index (PI) is used as a measure of the plastic properties of the soil samples tested.

The plasticity index is defined as the numerical difference between the liquid limit (LL) and the plastic limit (PL). The liquid limit (LL) is the moisture content at which the soil possesses an arbitrarily small shear strength. This limit can be determined by standard test procedures (Casagrande bowl test based on horizontal movement of soil in a bowl or fall cone test based on the measurement of penetration into the soil of a standardized stainless-steel cone). The plastic limit (PL) is the moisture content at which the soil begins to crumble when rolled into thin threads based on a standard test procedure.

Soils with a high PI tend to be muddy, those with a lower PI tend to have more sand, and those with a PI of 0 (non-plastic) tend to have little or no mud. PI<7: slightly plastic soils; PI=7-17: medium plastic soils; PI>17: highly plastic soils.

2.1.8 Organic material

Several organic substances are found in natural sediments. They include bacteria, diatoms, leaves, roots, dead animals, macroscopic and microscopic vegetation, industrial organic compounds, etc. Due to the electro-chemical properties of cohesive sediments, organics are attached to the fine sediment particles. Therefore, they are often found with sediments that have a substantial percent of fine clay-type sediments such as in estuaries, lakes, wetlands, harbors, marinas and navigation channels (Parchure and Davis, 2005).

Standard sediment analysis includes determination of the total organic matter as a percentage of the sediment weight. The procedure involves complete burning of the organic matter and is referred to as the Loss on Ignition (LOI). This is not always a reliable measurement of total organic matter. Some sediments may include calcium carbonate, which also burns and adds to the loss in weight after ignition. Some organisms contain appreciable ash weight. Hence, LOI results offer only an approximate quantity of organic matter present in sediment.

Only limited information is available in published literature (Mehta et al. 1997; Mehta 2002). Mehta (2002) has found that the erosion rate of mud from Florida (Newnan's Lake) increased by factor of 7 at a shear stress of 0.2 N/m^2 when the organic contents changed from 10% to 60%.

2.2 Processes

2.2.1 Bed shear stress

This section provides a fairly simple approach for the mean bed shear stress by currents and waves. It does not account for more complex methods (Bijker, Grant & Madsen, Fredsoe, as synthesized by Soulsby et al 1993) or methods accounting for sandy or muddy beds (Soulsby and Clarke, 2005; Malarkey et al., 2012).

The bed-shear stress by currents is given by:

$$\tau_{b,c} = \rho g \, (u_m/C)^2 = 0.125 \, f_w \, (u_m)^2$$

MUSA

with: ρ= fluid density; g= acceleration of gravity; u_m= depth-mean current velocity; f_w= $8g/C^2$=friction coefficient; Chézy coefficient=$5.75g^{0.5}$ log(12h/k_s) for rough flow conditions; h= water depth; k_s= bed roughness height.

The maximum (peak) bed-shear stress in waves is given by:

$$\tau_{b,w,max}= 0.5\ \rho\ f_w\ (U_{max})^2$$

with: f_w= exp[-6+5.2(A_{max}/k_s)$^{-0.19}$]=friction coefficient for rough conditions; U_{max}= $\pi H/[T\ sinh(kh)]$= maximum orbital velocity near the bed (at edge of wave boundary layer) based on linear wave theory; H= wave height; T= wave period; h= water depth to mean sea level; A_{max}= maximum orbital excursion (U_{max}= $2\pi A_{max}/T$); k=$2\pi/L$=wave number; L= wave length.

The time-averaged bed-shear stress over the wave cycle is given by:

$$\tau_{b,w,mean}= 0.25\ \rho\ f_w\ (U_{max})^2$$

Various complex parameterizations exist to determine the combines bed shear stress under currents and waves – see Soulsby et al. (1993) for an overview. Here we use a fairly simple methodology to compute the time-averaged bed-shear stress from the combination of waves and current, based on the Bijker-approach (Van Rijn 1993), which is given as:

$$\tau_{b,cw,mean} = \tau_{b,c} + \tau_{b,w,mean}$$

2.2.2 Erosion

The onset of motion of cohesionless (sand) particles by water flow in rivers, estuaries and coastal seas depends on three basic forces: lift and drag forces exerted by the fluid flow and the stabilizing force of gravity. A sand particle resting on the bed will be set in motion when the flow velocity is above a threshold velocity which is known as the critical flow velocity. As the flow depth has a strong effect on flow velocity, a more general approach is to use the concept of critical bed shear stress (τ_{cr}). The critical bed-shear stress of cohesionless sand particles is fairly well-known based on the work of Shields (1936) and many others.

In tidal rivers (estuaries) the bed often consists of a mixture of sand, silt, clay and organic materials. Many researchers have found that there is a lower limit of mud/clay content (critical mud/clay content) below which the sediment can be described as "sand" with a known erosion threshold. Above this critical mud/clay content, an increased erosion threshold is assumed to be present. According to Van ledden (2004), a mixture of sand, silt and clay generally behaves as a mixture with cohesive properties when the mud content is larger than a critical mud content ($p_{mud,cr}$) and a non-cohesive mixture when the mud content is smaller than the critical mud content. The proposed critical clay content is about 0.1 (Van Ledden, 2003) and the proposed critical mud content is typically 0.3. (depending on the clay:silt ratio). This critical mud content is related to the Plasticity Index PI: soils with a PI > 0 are cohesive. The PI is primarily related to the clay content (typically >0 for a clay content >10%%, but this depends on the clay type),). The critical clay content can also be expressed as a critical mud content as many systems exhibit a fairly constant clay:silt ratio (van Ledden et al., 2004; Flemming, 2000).) and the mud content is more easy to measure and therefore more widely available. It is not yet clear whether the critical clay content or the critical mud content is the best parameter to distinguish between cohesive and non-cohesive behaviour. More research on this will be done in the MUSA-project.

Laboratory work (Mitchener and Torfs, 1996; Van Rijn 2019) show that there is an optimal mud content between 30% and 50% at which the critical erosion shear stress of the sand-

Literature review on sand and mud
16 November 2020

MUSA

mud mixture is maximal. The critical shear stress of soft mud beds decreases for relatively high mud contents > 50%.

The particles of a bed consisting of cohesive sediments (mixture of mud and sand) with a mud/clay content above the critical content are affected by cohesive and adhesive forces, which both have relatively strong stabilizing effects. Similarly, a critical bed-shear stress can be defined, but generally-accepted relationships are not yet available. Experimental work has shown that influential parameters are: the percentage of clay, silt, sand and organic materials, the dry density and biological parameters. Many researchers have found a strong relationship between the critical shear stress and the dry density (see Van Rijn 1993; 2019), because, the dry density is affected for a mud content > 30% (Van Rijn and Barth, 2019). Depending on the compaction time scale and sand content, the dry bulk density may vary in the range of 400 to 1200 kg/m^3.

Others (Smerdon and Beasley, 1959; Winterwerp 2012) have found a clear relationship with the plasticity index (PI). Smerdon and Beasley (1959) have tested various clay-type soils from Missouri (USA) ranging from a silty loam soil with little cohesion to highly cohesive clay soils in a laboratory flume to determine the critical bed-shear stress for erosion. The plasticity index ranged from 6.6 to 44.1. The critical shear stress was found to be well correlated with the plasticity index ($\tau_{cr} \sim PI^{0.84}$).

Various methods have been used to determine the critical shear stress for erosion and the erosion rates at higher shear stresses, as follows:

Laboratory
- small compartment filled with mud in false floor of flume (Van Rijn 2020);
- sediment lift in floor of flume (Van Rijn 1984; Jacobs 2011; Roberts et al. 1998);
- carrousel flume (Winterwerp et al., 1991; Manning et al. 2010);
- tube with rotating propeller above a mud core (Geesthacht 1991, 1995; Van Rijn 2020, Thomsen and Gust, 2000).

Field
- submerged carrousel (Amos et al., 1992; Sutherland et al., 1998; Thompson 2011);
- submerged in-situ erosion bell (ISIS; Mitchener and Torfs, 1996);
- submerged straight flume (Aberle et al., 2003; Debnath et al., 2004, 2007);
- partly submerged bended flume for intertidal zone (Houwing 2000);
- erosion volume measurements (sounding instruments in combination with shear stress measurements).

Various types of erosion of muddy beds can be distinguished (see Winterwerp et al., 2012) as follows:
- floc erosion, which is the pick-up of individual particles and small-scale flocs of the fluffy top layer (millimeters) of the bed by the turbulent vortices of the fluid flow just above the bed. Floc erosion occurs for $0.5\tau_{cr} < \tau_b < 1.5\tau_{cr}$ with τ_{cr} = erosion threshold stress and τ_b = applied time-averaged bed-shear stress. Some erosion may already occur for $\tau_b < \tau_{cr}$ due to higher turbulent stresses;
- surface erosion for $1.5\tau_{cr} < \tau_b < 3\tau_{cr}$, which is the simultaneous mobilization of several layers of particles and flocs (failure of the bonds of particles-floc skeleton/network). Surface erosion is a drained process as porewater can freely flow away. Some swelling of the top layers is involved and the erosion rate is restricted by the rate of water inflow into the bed;
- mass erosion for $\tau_b > 3\tau_{cr}$, which is the erosion of lumps of bed material when the applied fluid stresses are larger than the undrained (remoulded) soil strength of the bed. Mass erosion is an undrained process as pore water cannot easily flow

inward the bed (pore water under-pressures) and is most often observed for more compacted beds (low permeability).

2.2.3 Liquefaction and bed failure

For eroding soils of mud and sand, it is important whether the soil is in drained or undrained conditions. The undrained condition is a state where outflow rates of pore water from the soil is very low in relation to the deformation rate (driven by the applied shear stress). Erosion of sand occurs generally in drained conditions because of its low porosity. The fluid can freely drain out of the pores, then the pore pressures will remain constant resulting in drained shear stresses. Erosion of mud is drained or undrained, depending on the permeability of the material and the deformation rate (resulting from the applied stress and shear strength of the bed). Under drained conditions water can flow into the bed and mud particles are eroded from the surface, whereas mass erosion takes place under undrained conditions (Winterwerp et al., 2012 – see also the previous section on erosion).

Bed failure (mass erosion) of a soft cohesive soil is strongly related to the shear strength within the soil. The shear strength (or resistance) of soil is a result of friction between and interlocking of particles, and possibly cementation or bonding at particle contacts. Due to interlocking, particulate material may expand or contract in volume as it is subject to shear-related deformation. For contractive soils the water is driven out as the soil is sheared, and its strength increases. If soil expands its volume in response to an external stress (dilatation), the density of the soil decreases and the strength decreases – this is typical for densely packed sand.

Various mechanisms for bed failure, slope instability and deformation can be distinguished:
- slope sliding/slumping, which occurs along very steep cohesionless slopes and milder cohesive mud slopes;
- liquefaction (and successive mass slide for sloping deposits), which generally occurs in sediment beds exposed to a sudden increase of fluid pressure (overpressure)
- breaching and retrogressive erosion, which generally starts from a local steep initial slope producing a quasi-steady turbidity current of sediment (Mastbergen and Van den Berg, 2003; Van den Berg et al., 2002).

Bed failure by breaching refers to a thin surficial layer of sediment and is restricted to very steep subaqueous slopes, composed of medium to densely (hexagonally) packed sand. This sand is known as dilatant material because, when subject to shear deformation, its volume expands, causing a negative pore pressure with respect to the hydrostatic pore pressure. Due to this under-pressure, the sand is able to maintain a steep (up to vertical) subaqueous slope, which gradually fails because the negative pore pressure at the surface is only slowly compensated by inflowing porewater.

Liquefaction of sand beds involves thick layers of very loosely packed sand (with a pore volume larger than about 42%). This type of sand is known as contractant-type material because, after a small disturbance, it is liable to volume contraction with a consequent rise in pore pressure. Liquefaction of mud waves requires a repetitive strain such as wave action (or earthquakes). Sea waves in shallow water generate horizontal and vertical pressure fluctuations at the bed and therefore repetitive overpressures in the soil. The overpressures cannot escape from the bed as loading is cyclic. When the overpressures exceed the stresses exerted by the resisting stresses of the sediment particles, the bed liquefies.

MUSA

Flume experiments with waves over a consolidated mud bed have shown that large waves can easily liquefy the top layer of the mud bed and generate a thin fluid mud layer with concentrations larger than 100 kg/m^3 (Maa and Mehta, 1986; Van Rijn and Louisse, 1987). Liquefaction of the top mud layer is initiated by wave-induced pressure variations at the bed, which lead to an increase of the water pressure in the pores and hence to a reduction of the internal soil shear strength.

Lu et al. (2009) and Zuo (2018) show examples of liquefaction of the upper layer of mud bed due to wave motion. Using a gamma-ray densitometer, they measured the wet bulk density of the top layer of the mud bed after storm events. The wet bulk density varied from 1100 to 1600 kg/m³ over a layer of about 0.2 m at the Caofeidian coast in the North Bohai Sea (China) after storm events.

Peng Yao et al. (2015) have performed detailed flume tests with combined currents and waves using fine silt and sand beds from the silty tidal flats of the Jiangsu Coast in China. Two types of sediments (45 μm and 85 μm), with different sand-silt-clay ratios, were collected. Visual observation showed that the oscillatory wave motion over a silty bed helps to build up the excess pore pressure in the sediment bed. Over time, the excess pore pressure reaches a maximum value resulting in the beginning of the bed liquefaction. The bed liquefaction initiates the sediment-water interface progressively extending downward. Meanwhile, the pore water escapes from the bed, starting at the bottom of the sediment bed progressively moving upward. These two processes shape the bed into a two-layer system: the sublayer (bottom layer) in a densely packed state, and the surface layer in a liquefied state. Finally, the surface layer develops as a high concentration layer under waves, and the sublayer is turned into a hard (high-strength) layer with a rippled surface. When the currents are superimposed to the waves, not only the high concentration layer, but also the surface sediments of the sublayer (i.e., ripples) are eroded and transported by the currents. The remaining part of the sublayer is left behind; the erosion of this hardened layer requires a higher critical erosion velocity.

Muddy-silty sea beds are easily liquefied by storm waves. Surveys immediately after a storm period shows the presence of a very soft top layer with wet bulk density values in the range of 1300 to 1800 kg/m³ (Kerala coast, Bohai Sea coast). Channel slopes in these conditions should be very mild (milder than 1 to 20) to reduce the risk of rapid infill due to liquefaction of the top layer of the slopes, particularly during extreme storms (cyclones).

2.2.4 Bed forms

The majority of subaqueous sediment at many places around the world consists of mixtures of cohesive clay and cohesionless sand and silt, but the role of cohesion on the development and stability of sedimentary bedforms is poorly understood.

The development of bed forms is strongly suppressed if appreciable quantities of mud are present in the bed. Van Rijn and Louisse (1987) have done experiments with mixtures of fine sand (= 100 μm) and kaolinite showing that a bed consisting of 25 % kaolinite and 75 % fine sand had a completely different erosional behaviour than a bed of 75 % kaolinite and 25 % fine sand. A bed with 75% kaolinite was liquefied under the action of waves and ripples were absent. Liquefaction of the top layer did not occur in the bed with only 25% kaolinite and the kaolinite concentrations in the water column were not larger than about 300 mg/l, because only the top layer of the bed was washed out. The sand concentrations were also quite small (factor 30 smaller than in case of 100% sand bed) due to a strong suppression of sand ripples (height = 0.002 m).

Based on the work of Baas et al. (2013), current ripples are mostly developing on the cohesive, mixed sand–mud beds, with mud fractions of up to about 20%, but they are significantly smaller than equivalent bedforms in non-cohesive sand. Their findings are summarized in Table 2.3.

MUSA

Table 2.3 Bed form development in mud-sand beds (based on Baas et al., 2013)

Cohesive forces in *bed* dominate bedform dynamics	Cohesive forces in *flow* dominate bedform dynamics
Erosional bedforms prevail	Depositional bedforms prevail
Deep erosional scours, and erosional base of bedforms	Scouring is most common below high-concentration clay flows
Bedforms evolve through stage with sandy crest and mixed sand-mud core; angle-of-repose cross-lamination prevails	Bedforms go through same stage, but low angle cross lamination is more common
Highly efficient winnowing of clay; sandy bedforms	Clay winnowing is less common; bedforms consist of muddy sand
Texture of bedforms contrasts with texture of mixed sand-mud bed underneath	Less contrast in textures
Winnowed sand tends to 'heal' irregular scoured topography; thus re-establishing classic quasi-triangular bedform shapes	Healing processes are confined to LTPF (Lower Transitional Plug Flows); bedforms have variable shapes
Bedform height tends to decrease with increasing initial clay content in the bed; wavelength is constant	Bedform height and wavelength tend to increase with increasing clay concentration in the flow
No backflow ripples present in bedform trough	Backflow ripples present in bedform trough
No dewatering structures observed	Dewatering structures in mixed sand-mud

Bedforms developing under the cohesive clay flows tend to increase in size with increasing suspended clay concentration until turbulence in the flow is fully suppressed (Baas et al., 2013). Selective removal of clay from the mixed beds (clay winnowing) is found to be an important process. This winnowing process led to the development of a sand-rich armouring layer. This armouring layer protects the underlying mixed sand–mud from prolonged erosion. Winnowing is less efficient for the bedforms developing under the cohesive clay flows, where bedforms consisting of muddy sand were more characteristic. The winnowed sand is found to smoothen irregularly scoured topography, thus re-establishing classic quasi-triangular bedform shapes (Baas et al., 2013).

In general terms, erosional bedforms prevail when non-cohesive forces in the bed dominate bedform dynamics, whereas depositional bedforms prevail when cohesive forces in the flow dominate bedform dynamics.

The findings of Baas et al. (2013) are confirmed by the experimental study of Schindler et al. (2015). They also found a strong influence of initial bed clay content on mean bedform dimensions, but also on the steepness. Hence, the bedforms in clay-rich sand have lower amplitudes, lower wavelengths, and flatter geometries than in clay-poor sand.

Lichtman et al. (2018) collected data on three intertidal flats in the Dee Estuary (near West Kirby, NW England) over a spring-neap cycle to determine the bed material transport rates of bedforms in biologically-active mixed sand-mud. From the data, the effects of physical and biological cohesion could not be distinguished from each another, as the variation in bio-related content (EPS) is linearly related to the variation in cohesive clay content. Therefore, the term cohesive clay represents both physical and biological cohesion. An inverse relationship between the duration of tidal inundation and clay content was found: as the tide progressed from spring towards neap, and wave forcing decreased, the sediment bed at the field sites changed rapidly from weakly cohesive (<2 vol% cohesive clay) to strongly cohesive (up to 5.4 vol% cohesive clay). The results furthermore demonstrate that the bedform migration rate and the bed material transport rate of mixed

MUSA

sediments in the field were significantly different from that of sand-only bedforms, even when clay and EPS fractions in the bed were below 2.8 vol% and 0.05 wt%, respectively.

2.2.5 Settling

A basic parameter for modelling of deposition is the in-situ settling velocity of the (flocculated) sediments. Analysis of laboratory and field data has shown that the settling velocity of the flocs is strongly related to the salinity, organic content, degree of turbulence, and the sediment concentration and composition. According to Gratiot and Manning (2004), the organic content is the most influential parameter.

Salinity acts as a flocculant, reducing the electrochemical repulsion of individual clay particles. Without a flocculant (salinity or organic polymers) clay particles do not flocculate. Flocculation is possible at a salinity exceeding 1-5 ppt. Flocculation is also possible in fresh water (Gratriot and Manning 2004). Sand and mud can also flocculate together because of biological activity.

In saline suspensions with sediment concentrations up to about 1000 mg/l an increase of the settling velocity with concentration has been observed as a result of the flocculation effect both in laboratory and in field conditions.

When the sediment concentrations are larger than approximately 5 g/l, the settling velocity decreases with increasing concentrations due to the hindered settling effect. Hindered settling is the effect that the settling velocity of the flocs is reduced due to an upward flow of fluid displaced by the settling flocs. At very large concentrations the vertical fluid flow can be so strong that the upward fluid drag forces on the flocs become equal to the downward gravity forces resulting in a temporary state of dynamic equilibrium with no net vertical movement of the flocs. This state which occurs close to bed, generally is called fluid mud. In the laboratory, the hindered settling velocity can be quite accurately determined from settling/consolidation tests by measuring the sinking of the sediment-fluid interface.

Settling velocities based on in-situ settling measurements (settling tubes) as a function of concentration in saline conditions from all over the world are shown in Figure 2.3 (Severn, Avonmouth, Thames, Mersey in England; Western Scheldt in The Netherlands; River Scheldt in Belgium; Brisbane in Australia; Chao Phya in Thailand, Demerara in South America; Van Rijn, 1993).
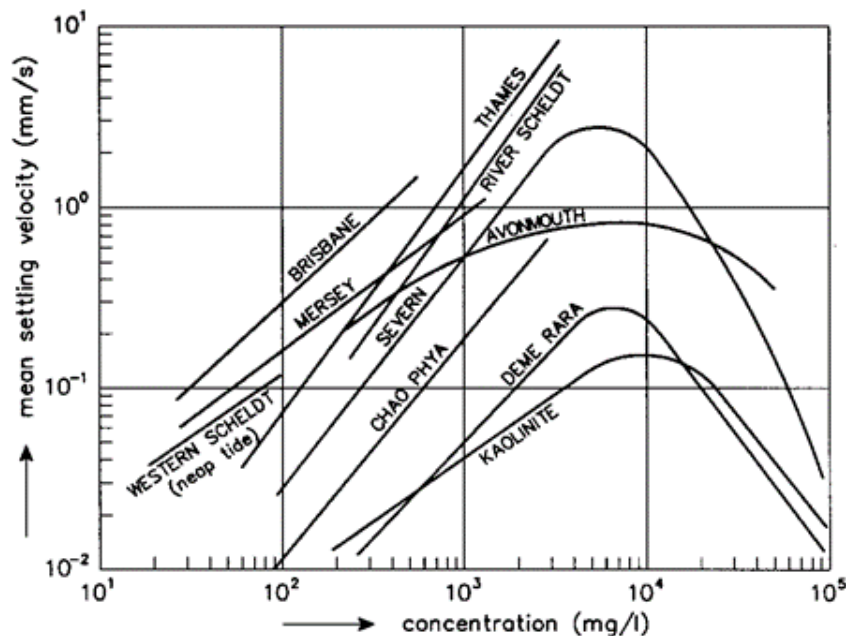

Figure 2.3 The influence of sediment concentration on the settling velocity

MUSA

Various methods and instruments can be used to determine the settling velocity of natural mud particles and flocs from in-situ water-sediment samples, as follows:

- in-situ settling tubes;
- in-situ video or photo-cameras;
- in-situ Laser-Diffraction (LD) instruments.

Detailed settling velocity processes are described in Chapter 4.

2.2.6 Effect of biogenetic factors

The interaction between bed sediment and ecology is a two-way interaction, although in this literature we restrict ourselves to the effects of biota on sediment dynamics. Many plant and animal species are so-called ecosystem engineers, i.e. organisms whose presence or activity alters the abiotic properties of a habitat (Jones et al., 1994; 1997). Autogenic engineers change the environment via their own physical structures (e.g. corals and trees). Allogenic engineers change the environment by transforming living or on-living materials from one physical state to another, via mechanical or other means (e.g. beavers creating dams and burrowing marine macrofauna).

In the past decades many fundamental studies have been executed describing significant effects of biota on sedimentation and erosion rates of fine sediment (mud), by either stabilizing or destabilizing the sediment:

- Marine vegetation enhances the bottom dissipation of current energy and reduces shear stress at the sediment–water interface, which is especially significant when the shoot density is high.
- Microphytobenthos and secreted bio-related content (EPS) stabilize the sediment, and an increase of up to a factor of 5 can be assigned to the erosion threshold on muddy beds (e.g. Le Hir et al., 2007; Andersen et al, 2010). The development of benthic diatoms tends to be seasonal, so that stabilising effects are likely to be minimal in winter. Although most studies focus on the surface phenomenon caused by EPS, biogenic stabilization is not necessarily confined to the presence of a surface biofilm: EPS may penetrate the surface of the sediment matrix and establish a vertical profile (Chen et al., 2017). Therefore, after full erosion of the biofilm protection, the high EPS content in the sublayers continues to stabilize the sediment (hindered erosion) by binding individual grains. Consequently, the bed strength does not immediately revert to the abiotic condition.
- Macrofaunal effects are characterized by extreme variability, and they can have two distinct effects on benthic–pelagic exchange (see also Willows et al. 1998; Willows et al., 2000). Their filtration of suspended matter can result in bio-deposition of fines (stabilizing effect). However, the bioturbation caused by their movement through the upper sediment layers, can result in a significant increase of the mass eroded once the critical erosion current velocity has been reached (destabilizing effect). For muddy sediments, destabilization seems to be the general trend (Herman et al., 2001; Le Hir et al., 2007). Note that bioturbation can change the structure of the sediment to a considerable depth, changing the sediment stratigraphy by mixing fine particles in a sandy bed for instance. Biogeochemical consequences in the distribution of organic matter are also to be expected: Chennu et al. (2015) showed that within days to weeks after the addition of a lugworm to a homogenized and recomposed sediment, the average surficial mycro-phytobenthos biomass and its spatial heterogeneity were, respectively, 150-250% and 280% higher than in sediments without lugworms.

MUSA

The study of Harris et al. (2016) reveal differences in biological effects among different measures of erosion potential, suggesting that multiple stages/depths of erosion should be considered when accounting for ecological processes. For instance, local biota was important to early/ surface erosion, yet once the surface layer was eroded/resuspended, mud/microbes appeared to stabilize sediments. In other words, the importance of biotic and abiotic predictors varies with erosion stage.

Although many measuring campaigns have been carried out on tidal flats, only limited have carried out in tidal channels (Sutherland et al., 1998; Andersen et al., 2001; Dickhudt et al., 2009). These showed that minor effects of biota in subtidal environments, which were attributed to little light penetration at greater depths. However, it is possible (and likely) that other fine-grained channel-beds may show different characteristics as a result of different texture and/or biological community.

The traditional line of thinking was that large-scale morphology of many sand-mud systems (such as the Wadden Sea) is a physical process, and that biota can have a significant effect on the sediment dynamics. The exception being saltmarshes, which can trap fine sediment for long time-scales and significantly influence large-scale morphological evolution (Morris, 2007). However, Borsje et al. (2008) showed that on local spatial scales and at seasonal timescales biota can certainly have a major effect. In addition, le Hir et al. (2007) showed that whereas the effects of the presence of microphytobenthos are only seasonal and have little to no effect on the long-term morphodynamics, vegetation on salt marshes can induce significant seaward shifts of upper flats, that remain present in the long-term.

De Lucas (2014) studied the effect of biota on flocculation in the Markermeer Lake (NL). He showed that when sediments suspended from the bed interact with biota in the water column, organic-inorganic flocs are formed. The flocs have different properties depending on the type of algae involved. For instance, the size of flocs containing Aphanothece (a colonial blue-green algae) exceeds the equilibrium Kolmogorov micro-length scale, and flocculate faster than mineral flocs. On the other hand, in case of interaction with Aphanizomenon (a filamentous blue-green algae) the floc size may be limited by filaments concentration and steric repulsion (preventing chemical reactions), resulting in a smaller floc-size. Consequently, the type of algae in the water column also will influence the relationship between the total amount of suspended matter and the turbidity level, since for the same amount of suspended sediment, smaller floc size will induce a higher turbidity.

2.3   Base parameters

2.3.1   Erosion
percentage sand > 63 μm,
percentage fines < 63 μm,
percentage fine silt-clay < 8 μm,
percentage clay < 2 μm
percentage organic material;
dry density
permeability
shear strength
plasticity index
Critical shear stress particle erosion, surface erosion, mass erosion

2.3.2   Settling velocity
initial concentration;
shear stress/current velocity and turbulence,
water depth,

MUSA

salinity
Settling velocities $w_{s,10}$, $w_{s,50}$, $w_{s,90}$,
floc sizes and floc densities

2.3.3 Bulk densities

Bed including gel point density
percentage of sand > 63 μm, percentage fines < 63 μm,
percentage fine silt-clay < 8 μm,
percentage of clay < 2 μm,
plasticity index,
percentage organic material;
depth below sediment surface
time scale of primary consolidation: permeability and undrained shear strength

3 Erosion of mud-sand beds

3.1 Critical bed-shear stress for erosion due to currents

Many data sets on the erosion of soft mud beds in both laboratory and field conditions with (tidal) currents are available, see Appendix A. Various laboratory and in situ methods have been used so far: erosion tubes with rotating propellers, annular carrousels and straight flumes. The critical bed-shear stress for surface and mass erosion is found to be related to the percentage of clay (albeit differently defined throughout literature, see section 2.1), percentage of fines (< 63 um), plasticity and the dry bed density. Experiments on the effect of oscillatory wave motion on the critical stress for erosion are very scarce. In the following paragraphs a summary of the research on erosion by currents is given, in which subsequently the findings for different types of erosion (particle, surface and bulk erosion) are described.

3.1.1 Erosion of fresh mud deposits

The critical bed shear stress for erosion of freshly deposited mud is as low as several 0.01 to 0.25 Pa (Widdows et al., 2007; Dickhudt et al, 2011; Ahmad et al., 2011; Wiberg et al., 2013). This is typically material depositing in a thin, low-density layer often referred to as the fluff layer. Sediment in the fluff layer is typically resuspended at peak flow velocities. A depth-averaged sediment concentration of 0.2 kg/m^3 in a 10 m deep channel corresponds to 2 kg/m^2; at low density (100 kg/m^3) this corresponds to 2 cm of mud. Part of this sediment consolidates, reaching much higher critical shear stresses (see sections hereafter).

3.1.2 Particle erosion of sand and mud fraction

The critical bed shear stresses for particle erosion of the fine fraction are given in Figure 3.1 (based on the data from the Literature and van Rijn 2019) for four bed density ranges:
- low dry density < 400 kg/m³ (LD);
- low to medium dry density 400 to 800 kg/m^3 (LMD);
- medium to high dry density 800-1200 kg/m³ (MHD) and
- high dry density 1200 to 1600 kg/m³ (HD).

The critical bed shear stress is shown on the outside of the vertical axis, whereas the critical depth-averaged flow velocity (based C=90 m$^{0.5}$/s for depth of h=3 m) is shown on the inside of the vertical axis. Bed shear stresses involved are the grain-related bed shear stress values.

The erosion type (particle erosion p.e. or surface erosion s.e), is unknown for most of the literature data. Most of the critical stress values are in the range of 0.15 to 0.4 Pa for LD- and LMD-beds (Figure 3.1 upper).

The particle erosion of fines for soft, almost pure mud beds (p_{fines} > 80%) occurs at relatively low bed shear stresses in the range of 0.15 to 0.25 Pa (open circles, triangles).

In the case of medium to high density beds, the critical stresses are larger and clearly increase for increasing percentages of fines < 63 μm (Figure 3.1 lower). The maximum critical bed shear stress is of the order of 2 Pa for a HD-bed of pure mud with p_{fines} > 80%. Discrepancies between various datasets are most likely related to the sediment composition of the mixtures (percentage of clay; percentage organic materials), the degree of consolidation of the mud (as also suggested by the large differences in the critical shear stress for the upper and lower panels of Figure 3.1), and the various definitions of particle, surface and mass erosion.

MUSA

The results for artificial mud-sand beds and in situ mud-sand beds (IS) show no major differences. The critical bed shear stress for particle/surface erosion is in the range of 0.2 to 0.8 Pa for both type of beds.

Predictive relationships for particle erosion are given by Ahmad et al. (2011), Wu et al. (2017) and Van Rijn (2019). These latter two relationships refer to the critical stress for the mixture (no distinction between the fine fraction and the sand fraction). Overall, it can be concluded that the equations are close together for soft mud-sand beds (LD and LMD) and in reasonably good agreement with measured data.
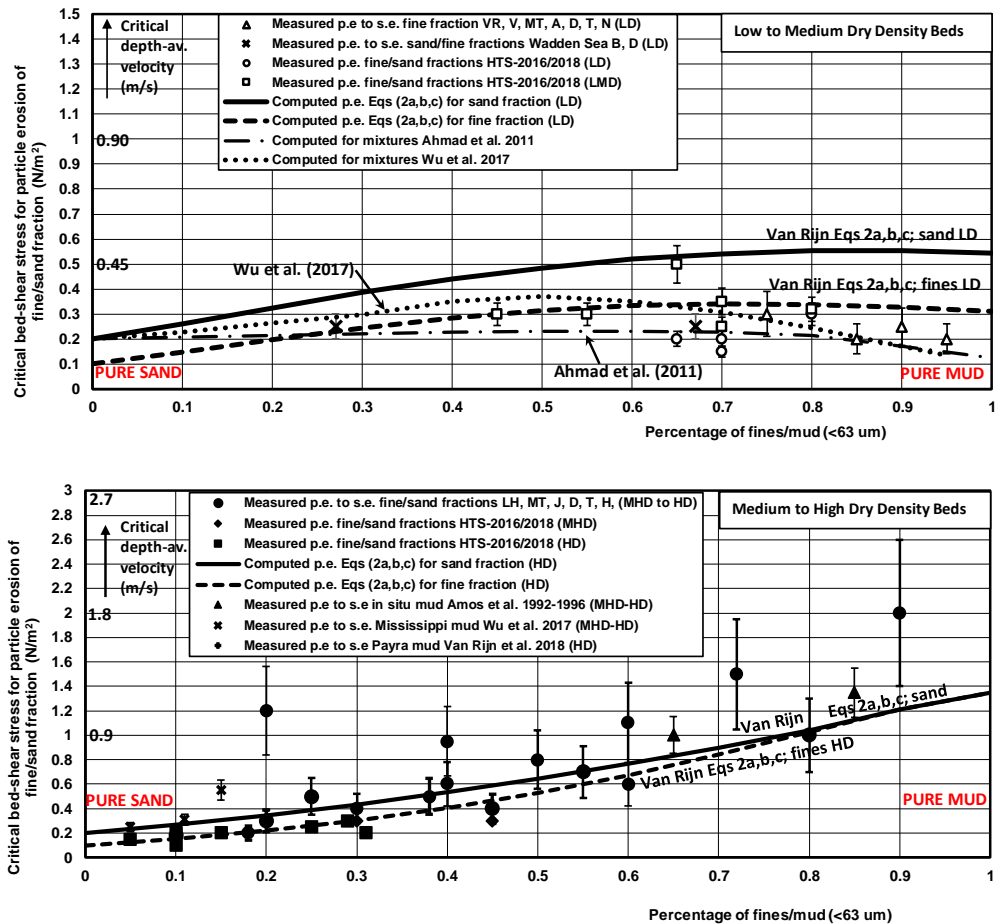
Figure 3.1 Critical bed shear stress for particle erosion. Upper: Low to medium dry density beds. Lower: Medium to high dry density beds. An= Andersen 2001; B= Bauaamt 1987; De= Deltares 1989, 1991, 2016; D= Dou 2000, J= Jacobs 2011; H= Houwing 2000, LH= Le Hir et al. 2008; MT= Mitchener and Torfs 1996; N= Noack et al. 2015; T= Thorn 1981; To=Tolhurst et al. 2000; V= Van et al. 2012; VR= Van Rijn 1993; HTS= flume data Hanze Techical School, Groningen, Netherlands. p.e.= particle erosion; s.e.= surface erosion. LD= low dry density beds < 400 kg/m³; LMD= low to medium dry density beds 400-800 kg/m³; MHD= medium to high dry density beds 800-1200 kg/m³; HD= high dry density beds > 1200 kg/m³

3.1.3 Surface and mass erosion of mixture

Surface and mass erosion are most important for the engineering practice, as these processes create relatively high mud concentrations in the water column and are the main contributors to morphodynamic changes. The transition from surface to mass erosion is reasonably continuous for low to medium density beds (compare closed and open circles of HTS-data; LD and LMD), but discontinuous for higher density beds (MHD and HD), as

shown in Figure 3.2. Both the measured data points and the trend lines are shown in Figure 3.2:

- For p_{fines} between 0.1 and 0.5, the bed dry density is mostly > 800 kg/m³ (MHD to HD) and the critical shear stress for surface erosion gradually increases from 0.2 to 1 Pa.
- For p_{fines}> 0.5, the bed dry density is generally much smaller (LD to LMD) and the critical shear stress for surface erosion is gradually decreasing to about 0.2 Pa for p_{fines}=0.9.
- The critical shear stress of particle and surface erosion tend to approach a value of about 0.15 to 0.2 Pa for LD-beds with p_{fines} > 0.9 (close to gelling point of sediment; dry density of 100 to 150 kg/m³).

An important data set stems from Mitchener and Torfs (1996). For relatively high percentages of fines (> 70%) the MT-data related to surface erosion are in the same range as the present HTS-data (critical stress values of 0.2 to 0.5 Pa). A marked difference occurs for mixtures with relatively low percentages of fines (< 63 μm) in the range of 10% to 20% (muddy sands), see percentage fines=0.2 in Figure 3.1. Mixtures of clay (kaolinite/montmorillonite) and 150/230 μm-sand with percentage of clay of about 10% and dry density values > 800 kg/m³ of the MT-data, had relatively high critical stresses in the range of 0.7 to 3 Pa. These values are much higher than those of the present HTS-data. The main difference between MT and HTS is the percentage of the clay fraction within the fine fraction. The pure clay fraction is relatively high for the MT-data and relatively small for the HTS-data. Hence, relatively high percentages of clay within the fine fraction may lead to relatively high critical stresses (see also §2.1.5 Network structure: 5% to 10% clay can give complete coating of 200 μm-sand particles). This makes it important to specify the percentage of clay as a basic parameter based on the particle size distribution of the bed samples involved. The important role of the clay fraction was recently confirmed based on erosion tests with mud from Guayaquil (Ecuador) having about 20% fines < 63 μm and 10% clay (50% clay within the fine fraction) and critical stress values for surface erosion in the range of 0.5 to 1.5 Pa (Van Rijn 2019). More research is required on the effect of the clay fraction on the critical shear stress.

Mass erosion of LD, LMD, MHD and HD-beds of the HTS-data occur at critical stresses of in the range of 0.7 to 2 Pa. It is noted that the measured bed-shear stress values related to mass erosion are less accurate than those for particle and surface erosion, because the mud-sand bed was eroded over maximum 10 mm resulting in a larger water depth and varying bed roughness. This was taken into account (to some extent) by using a larger water depth and a larger bed roughness (k_s). The inaccuracy of the bed-shear stress for mass erosion may be as large as ±30%.

MUSA
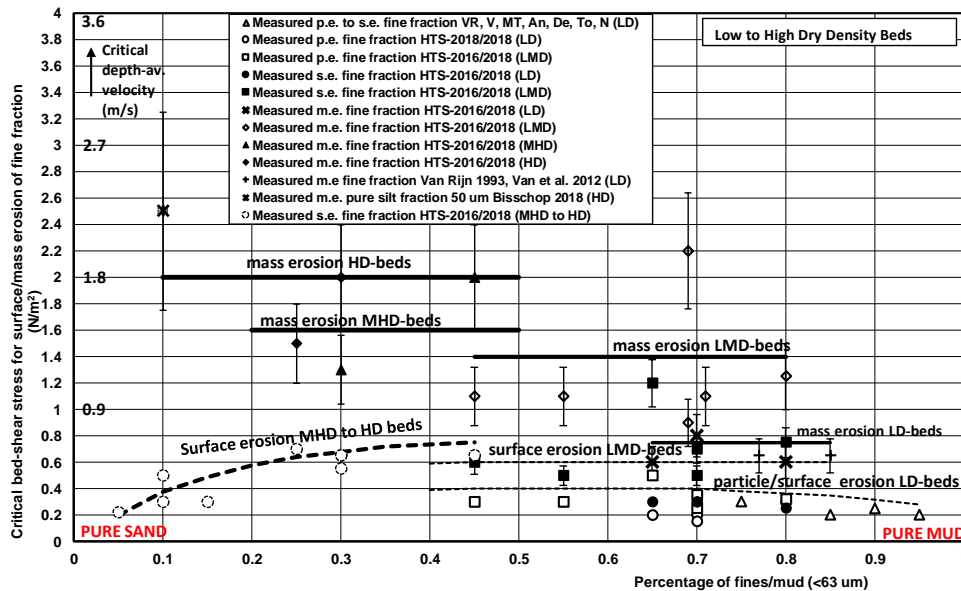
Figure 3.2 Critical bed shear stress for surface and mass erosion; low to high dry density beds

The critical bed-shear stresses of all available literature data on erosion of high-density clay-type soils (Appendix A) are shown in Figure 3.3. The most influential parameters are the percentage of clay (<8 μm) and the dry density of the soil expressing the degree of compaction. The precise type of erosion (particle or surface erosion) is not the same for all literature data. Most data are based on visual observations of particle/surface erosion. Four compaction stages are herein distinguished:

- medium to firm soil with dry density of 400 to 800 kg/m^3;
- firm soil with dry density of 800 to 1200 kg/m^3;
- stiff soil and with dry density of 1200 to 1600 kg/m^3;
- very stiff soil with dry density of 1600 to 2000 kg/m^3.

The critical bed-shear for particle/surface erosion of a firmly consolidated mud bed with a percentage of clay of 15% and a dry density of 800 kg/m^3 is of the order of 1±0.5 N/m^2 (Van Rijn 2019).

The critical bed-shear for erosion of firm soils with a clay percentage <15% is below 1 N/m^2. Mostafa et al. (2008) have found critical stresses for surface and mass erosion of 0.5 to 2 N/m² for stiff clay from South Carolina (USA) with a clay percentage of 40% to 50% and a dry density of 1350 to 1450 kg/m³.

Literature review on sand and mud
16 November 2020
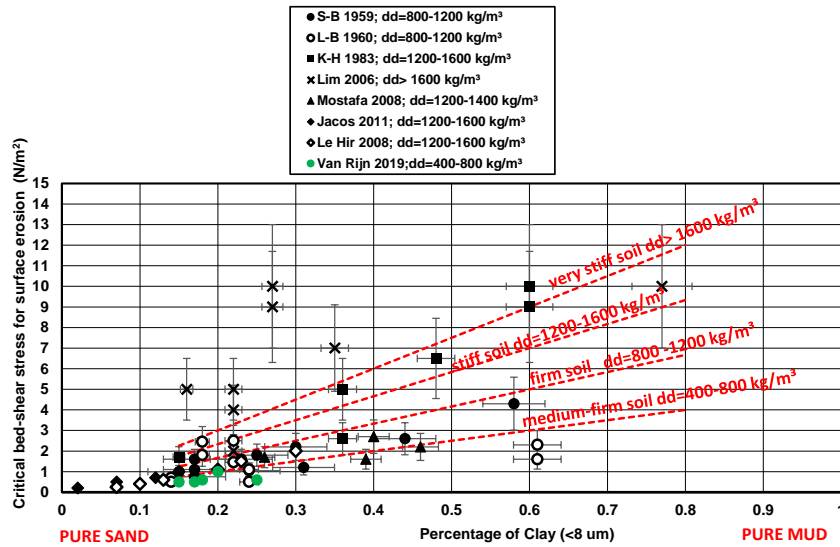
Figure 3.3 Critical bed-shear stress for erosion of firm to very stiff clay-type soils

3.2   Erosion of mud-sand beds due to currents and waves

Experiments on mud-sand beds in combined currents and waves are extremely scarce. Panagiotopoulos et al. (1997) have determined the critical erosion velocity of sediment mixtures. The sediment mixtures consisted of fine sand (152 μm and 215 μm) and estuarine mud ranging from 0 to 50%. The pure clay content (< 2 μm) of the mud varied from 0 to 18%. The results are given in Table 3.1. The critical erosion velocity of sand shows an increase of 30% to 50% for a mud content of 50%. The wave tests show that the critical wave-related bed-shear stress of sand is not affected for mud contents smaller than about 30%. It also shows that the 215 μm-sand is slightly more easily erodible than the 150 μm-sand and that the wave-related critical shear stress is significantly lower than the current-related critical stress.

Table 3.1 Critical conditions (laboratory) for erosion of sand-mud mixtures (Panagiotopoulos 1997)

Mud content and pure Clay (<2 μm) content	Mixtures with sand 152 μm			Mixtures with sand 215 μm		
	Critical velocity at 4 mm above bed (m/s)	Current-related bed-shear stress (N/m^2)	Critical wave-related bed-shear stress (N/m^2)	Critical velocity at 4 mm above bed (m/s)	Current-related bed-shear stress (N/m^2)	Critical wave-related bed-shear stress (N/m^2)
0% (0%)	0.14	0.094	0.05	0.125	0.074	0.045
10% (3%)	0.145	0.098	0.05	0.135	0.085	0.045
20% (7%)	0.155	0.108	0.05	0.14	0.092	0.045
30% (11%)	0.16	0.114	0.05	0.145	0.096	0.045
40% (15%)	0.17	0.132	0.08	0.16	0.114	0.07
50% (18%)	0.18	0.144	0.10	0.18	0.142	0.07

MUSA

3.3 Erosion rates

At the bed, two simultaneous processes occur: erosion and deposition. A very rough indication of the erosion rates of mud-sand mixtures is given in Figure 3.4, based on the data of Van Rijn (2019). For clarity the measured values are omitted. The erosion rate increases for increasing bed-shear stress ($E \sim \tau_b^2$) and decreases strongly for increasing dry density (400, 600, 700, 800 and > 1000 kg/m³). The erosion rate of fine cohesionless sand of 63 μm measured in a high-velocity pipeline circuit is also shown (Van Rijn et al. 2018). Strong damping of turbulence at high bed-shear stress was observed for cohesionless fine sand resulting in a less steep increase of the erosion rate of fine sand. The erosion rate of mixtures of clay-silt-sand is smaller than that of fine cohesionless sand due to the cohesive effects of the very fine clay fraction reducing the erosion rate of cohesive mixtures.

The deposition flux is defined as: $D = c_b\, w_s$ with c_b = near-bed concentration of fines (range of 1 to 100 kg/m³) and w_s = settling velocity near the bed (range of 0.5 to 1 mm/s). Using these values, an estimate of the deposition flux is 1 to 100 gram/m²/s, which is of the same order of magnitude as the erosion rate. Hence, fairly stable channel beds are possible in muddy conditions when the near-bed sediment concentration is high (i.e. the vertical mixing rate is low).
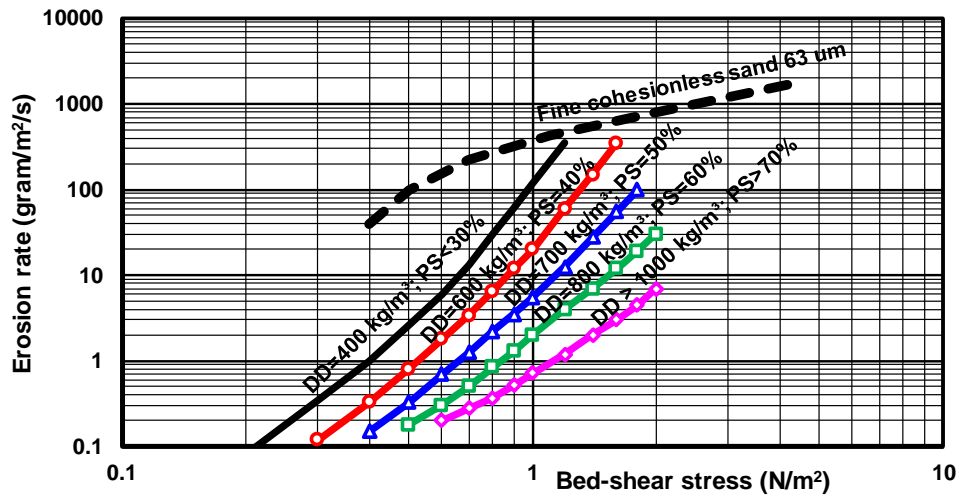
Figure 3.4 Erosion rates of mud-sand mixtures (DD=dry density; PS= percentage of sand)

3.4 Sediment concentrations and transport due to currents and waves

3.4.1 Fine sediment concentrations

Few datasets are available for fine sediment concentrations in conditions with combined currents and waves.

A flume study has been done by Peng Yao (2016), Peng Yao et al. (2015). They have performed detailed flume tests with currents and waves over a bed of fine silts and sands. Two types of sediments, with different sand–silt–clay ratios, were collected from the silty tidal flats of the Jiangsu Coast, China. The sediment samples were collected from the upper zone (referred to as sediment S1) and the middle zone (referred to as sediment S2) of the tidal flat, respectively. The sediments deposited at the surface layer of the tidal flats with a thickness of approximate 10 cm were sampled. The grain size distributions of the two bed samples (sediments S1 and S2) were measured by a Malvern Mastersize 3000 laser particle size analyzer at the beginning and at the end of the experiments.

MUSA

The sediment S1 is a silt-enriched mixture with a median grain size of about 45 µm (70% < 63 µm; 10% < 8 µm; 2% < 2 µm; 30% sand), while the sediment S2 is a very fine sand-enriched mixture with a median size of about 85 µm (30%< 63 µm; 70% sand). Measured concentration profiles are available for comparison with numerical model results.

S1-Silty bed: Visual observation showed that the oscillatory wave motion helps to build up the excess pore pressure in the sediment bed resulting in the beginning of the bed liquefaction and extending gradually downward. Simultaneously, the pore water escapes from the bed, starting at the bottom of the sediment bed progressively moving upward. Due to these processes, two bed layers are formed: the sublayer (bottom layer) in a densely packed state with a rippled surface, and the surface layer in a liquefied state with a high-concentration top layer.

When the current is superimposed on the waves, not only the high concentration layer, but also the topmost of the sublayer (i.e., ripples) is eroded and transported by the current. Part of the sublayer is left behind, as the erosion of this hardened layer requires a higher critical erosion velocity.

Small ripples with height=8 mm and length 50 mm are formed at bed-shear stress of 0.3 N/m^2

Finer sediments usually yield smaller wave ripples. However, during the steady states of the experiments of sediment S1, it is found that the median grain size in the ripples (i.e., 80 µm) was larger than the original bed materials (i.e., 45 µm). It means that the ripples were formed mainly by coarser sand grains of sediment S1, as the finer grains are more easily washed out and suspended.

A thin layer of high concentrations (mostly fine sand and coarsest silt) is generated in wave-only cases: δ_{hcl}=15-25 mm; c_{mean}=10-40 gr/l for H/h=0.3-0.45 (regular waves).

Silt concentrations above the high concentration layer (hcl) vary in the range of 0.5-1 kg/m^3 for H/h=0.3-0.45 (no current).

Sand concentrations are washed out and vary in range 0.01-0.1 kg/m³ for H/h=0.3-0.45 (no current).

Silt concentrations above the hcl-layer vary in the range of 1-3 kg/m^3 for H/h=0.4 (with current 0.3-0.4 m/s).

S2-Sandy bed: Sandy behaviour with ripples with heights 8 to 15 mm and length 50 to 100 mm.

A thin layer of high concentrations is generated in wave-only cases: δ_{hcl}=20-30 mm; c_{mean}= 7-20 gr/l for H/h=0.28-0.42 (regular waves). With no current, silt concentrations above the hcl-layer are washed out and vary in the range of 0.3-0.5 kg/m^3 for H/h=0.28-0.42. With currents ranging between 0.3-0.4 m/s silt concentrations above the hcl-layer are washed out and vary in the range of 0.5-1 kg/m^3 for H/h=0.4.

Various field datasets of sediment concentrations in tidal flows are available for comparison with results from numerical model simulations. The basic data and conditions are given in Table 3.2**.** Detailed data of mud-silt coasts are given in Table 3.3. The depth-averaged concentrations during peak tidal flow have been estimated from the available concentration profile data or from the ratio q_s/q with q_s representing the depth-integrated transport rate and q representing the water discharge rate.

Figure 3.5 shows measured depth-averaged concentrations of mud, silt and fine sand at various locations with tidal and river flow. The mud concentrations are somewhat larger (factor 2 to 3) than the silt-fine sand concentrations. Mud concentrations in very large water depths are smaller than mud concentrations in smaller depths at the same depth-averaged velocity, because the bed-shear stresses are smaller for larger depths at the same flow velocity. Mud concentrations generated above a fluid mud bed are relatively large as the top layer of the fluid mud bed is eroded during tidal flow (over 0.1 to 0.5 m, Jiufa et al., 2001). Background mud concentrations for conditions with a sandy channel bed are also

MUSA

shown. The background mud concentrations, which are strongly supply-limited, are much smaller (factor 10) than the sub-saturated mud concentrations over a muddy bed.

The available data have been used to construct a plot of mud concentrations as function of depth-mean velocity and significant wave height in a water depth of 7 m, see Figure 3.6. The upper and lower limits of mud concentrations for each wave height class for a muddy bed (range of 10-30 μm) are shown.

Table 3.2 Basic data of measured mud, silt and fine sand concentrations

Location	Water depth (m)	Bed conditions	Suspended sediment	Source
Nessmersiel mud Germany 1982-1987	0.5 to 1.5	fresh mud deposits < 200 kg/m^3	mud	Bauamt Kustenschutz, Norden 1987
Nessmersiel silt-mud Germany 1982-1987	0.5 to 1.5	sand-mud mixture > 500 kg/m^3	silt, fine sand and mud	Bauamt Kustenschutz, Norden 1987
Ems tidal river mud Germany June 1990	5 to 7	fluid mud (thin) 200-500 kg/m^3	mud	Winterwerp 2011
Ems tidal river mud Germany February 2006	5 to 7	fluid mud (thick) 200-500 kg/m^3	mud	Winterwerp 2011
Amazone tidal mouth Brasil 1990	15-20	fluid mud (thick) 200-500 kg/m^3	mud	Vinzon and Mehta 2003
Yangtze tidal estuary China September 1991	8-10	fluid mud (thick) 200-500 kg/m^3	mud	Jiufa et al., 2001
Elbe tidal river Germany 2002	13-15	sand-mud mixture > 500 kg/m^3	mud, silt and fine sand	BAW 2006/2007 Van Rijn 2016
Huanghe river China September 1987	5-10	sand-mud mixture > 500 kg/m^3	mud, silt and fine sand	Van den Berg and Van Gelder 1993
Ems tidal outer estuary Germany 2012	10-12	sand-mud mixture > 500 kg/m^3	mud, silt and fine sand	Van Maren et al. 2015
Elbe tidal outer estuary Germany 2002	10-15	sand-mud mixture > 500 kg/m^3	mud, silt and fine sand	BAW 2006/2007 Van Rijn 2016
Rotterdam tidal Water way Holland 2006	10-12	sand-mud mixture > 500 kg/m^3	sand-mud mixture	De Nijs 2012
Thames Estuary 2004	5-10 m	sand-mud mixture	mud	Baugh and Littlewood 2006

MUSA

Table 3.3 Mud concentrations of mud-silt coasts of Brazil (Amazon), China, India (Kerala)

| Coast	Bed sediments (μm)	Wet bulk density of bed (kg/³)	Water depth (m)	Max. Tidal current (m/s)	Significant wave height (m)	Mud concentrations (kg/m³)			
						near-bed layer 0-1 m	at 1 m above bed	at middepth	near surface
Amazon coast Brasil	< 10 (muddy)	n.m	15-20	1.5	1-2	1-10	1 (1000mg/l)	0.01 (10 mg/l)	<0.01 (< 10 mg/l)
	< 10 (muddy)	n.m	15-20	1	1-2	1-50	0.5 (500 mg/l)	0.01 (10 mg/l)	<0.01 (< 10 mg/l)
Bohai Sea Coast near Huanghua Port China	10-30 (silty)	n.m	6-7	0.5	0.5	>0.3	0.3	0.25	0.2
	10-30	n.m	6-7	0.5	0.8-1.2	>0.5	0.5	0.4	0.3
	10-30	n.m	6-7	0.5	2-2.5	3-10	3	2.5	2
Caofeidian coast, North Bohai Sea, China	10-50	1100-1600	2.5-5	0.6	0.5-0.6	0.2-0.35	<0.2		
	10-50	1100-1600 (0.1-0.2 m) after storm BF7	2.5-5	0.6	<0.5	<0.1	<0.1		
Jiangsu coast north of Yangtze estuary, china	50-80 (p_{clay}=2-15%)	n.m.	3-4	0.7	0.35-0.45	0.4-0.6	0.4-0.6	0.4-0.6	
	50-80	n.m.	1.7-2.3	0.7	0.35-0.45	1-3	1-3	1-3	
	50-80	n.m.	1.5-2	0.7	0.35-0.45	0.5-1.5	0.5-1.5	0.5-1.5	
Kerala Coast India	10-30 (silty)	1300-1800	6	0.8	1	0.1-0.15	<0.1	0.01	<0.01
	10-30	1300-1800	6	0.8	2-2.5	< 10	<0.1	0.01	<0.01
	10-30	1400-1600	11	0.2	1-1.5	0.-0.15	<0.1	0.01	<0.01
	10-30	1400-1600	11	0.2	2-3	<5	<0.1	0.01	<0.01

MUSA
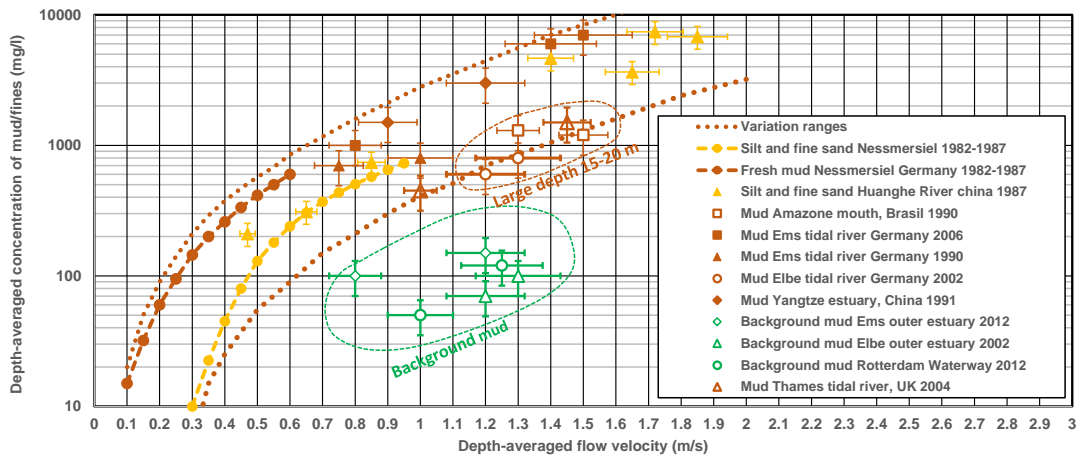
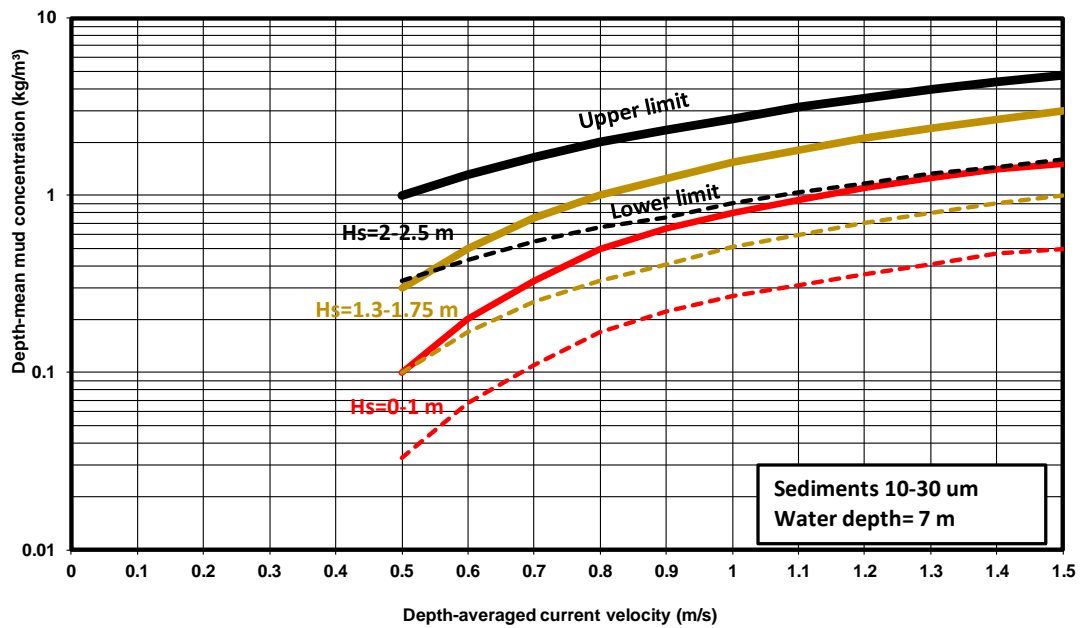*Figure 3.5 Mud and silt concentrations as function of depth-averaged flow velocity*

Figure 3.6 Depth-mean mud concentration as function of depth-mean velocity and significant wave height (Hs); muddy bed 10-30 μm and water depth of 7 m.

4 Settling velocities in mud-sand environments

4.1 Detailed processes

A basic parameter for modelling of deposition is the in-situ settling velocity of the (flocculated) sediments (Baugh and Manning, 2007; Soulsby et al., 2013; Sheremet et al., 2017). Kranck and Milligan (1992) observed that most suspended particulate matter (SPM) within an estuary occurs in the form of flocs under the majority of estuarine conditions. Flocculation is therefore a principal mechanism that controls how fine sediments are transported throughout an estuary and coastal regions. Analysis of laboratory and field data has shown that the settling velocity of the flocs is strongly related to the salinity, organic content, degree of turbulence, and the sediment concentration (Mietta et al., 2009; Mikeš and Manning, 2010; Manning, 2004a).

Flocculating sediments with increasing settling velocities occur in conditions with concentrations up to 5 g/l. Hindered settling with decreasing settling velocities occurs in the near-bed region with concentrations higher than 5 g/l.

4.1.1 Flocculating range

The degree of flocculation is highly dependent on both the particle collision frequency and the collision mechanism. Van Leussen (1988), following Friedlander (1977), quantitatively demonstrated that the latter tends to be dominated by turbulent shear stresses (e.g., Krone, 1962; Parker et al., 1972; McCave, 1984; Burban et al. 1989; van Leussen, 1994; Winterwerp, 1998; Manning, 2004b), and to a lesser extent by Brownian motion (van Leussen, 1994) and differential settling (Wacholder and Sather, 1974; Lick et al., 1993; Stolzenbach and Elimelich, 1994). Both

the concentration and turbulence parameters can vary spatially and temporally throughout an estuary. A conceptual model that attempts to explain the linkage between floc structure and floc behaviour in an aquatic environment is provided by Droppo (2001). As a result of dynamic interparticle collisions, floc growth implies large variations in the sediment settling flux, with direct implications for the vertical distribution of sediment loading (Manning and Dyer, 2007).

Velocity gradients create turbulent mixing; the energy for turbulent mixing is derived from the kinetic energy dissipated by the water flowing across a rough boundary. The frictional force exerted by the flow per unit area of the bed is the shear stress. The turbulent shear stress generated within the water column during turbulent flow conditions interacts with the suspended sediment. The inertia of larger sediment particles, responding more slowly to local accelerations than significantly smaller particles, produces 'orthokinetic' interparticle collisions that can stimulate flocculation (McAnally and Mehta, 2001). Dyer (1989) proposed a schematic relationship between the floc diameter and SPM concentration and shear stress.

The efficiency with which suspended particles coagulate is a reflection of the stability of the suspension (van Leussen, 1994). As the abundance of particles in a suspension rises, the statistical occurrence of collisions also increases. A suspension is classified as unstable when it becomes fully flocculated and is stable when all its particles remain as individual entities.

Too much turbulence can break flocs into smaller aggregates and primary particles (Eisma, 1986; Dyer, 1989). Even the act of a floc breaking up causes energy to be removed from the surrounding turbulent shear field. The floc-structure model of van de Ven and Hunter

(1977) described various sources of energy loss due to breakup. The model identified that energy is dissipated in stretching the internal bonds to the limit of their tensile strength during floc rupture. Also, viscous dissipation occurs as a result of the interstitial water flowing in response to a change in floc shape as it is distorted.

Based on extensive floc data it is proposed that there is a range of nominal turbulent shear stress 'regions' that typically relate to mud flocculation (Manning et al., 2017; 1 Pa = 1 N m^{-2}):

- Low turbulent shear stress: < 0.2 Pa;
- Moderate turbulent shear stress: 0.2–0.45 Pa;
- Moderate to high turbulent shear stress: 0.45–0.7 Pa;
- Very high turbulent shear stress: > 0.7 Pa.

Because low to moderate levels of turbulent shear stress can promote floc growth, high levels of turbulence that occur during a tidal cycle can, in turn, cause disruption to the flocculation process by instigating floc breakup and eventually pull the constituent components of a floc apart. As turbulent activity increases, both turbulent pressure differences and turbulent shear stresses in the flow rise. If the floc structural integrity is less than can be tolerated by the imposed turbulence-induced forces, the floc will fracture. Also, aggregate breakup can occur as a result of high-impact particle collisions during very turbulent events. Floc breakup by three-particle collisions tends to be
the most effective (Burban et al., 1989).

McCave (1984) found that turbulence determines the maximum floc size in tidally dominated estuaries. Tambo and Hozumi (1979) showed that an aggregate would break up when the floc diameter was larger than the length-scale of the energy dissipating eddies. Similarly, Eisma (1986) observed a general agreement between the maximum floc size and the smallest turbulent eddies, as categorised by Kolmogorov (1941a, b). Fettweis et al. (2006) and van der Lee et al. (2009) both showed that floc size and the Kolmogorov microscale vary in a similar way with the root mean
square of the gradient in the turbulent velocity fluctuations. Puls et al. (1988) and Kranck and Milligan (1992) have hypothesised that both concentration and turbulence are thought to have an effect on the maximum floc size and the resulting size spectra.

Velocity gradients are largest in the lowest 10–20 per cent of the water column, and approximately 80 per cent of the turbulent energy generated by the flow occurs within this zone. It is here that the strongest lift and shear forces occur, and Mehta and Partheniades (1975) have suggested that it is these forces that control the maximum size of the flocs in suspension. Thus, floc measurements in this turbulent, near-bed region are extremely important. On a smaller scale, both Argaman and Kaufman (1970) and Parker et al. (1972) suggested that flocs might decrease in size by gradual breakup through surface erosion of the floc by turbulent drag. The rate at which this takes place
is proportional to the floc surface area and the surface shearing stress. These processes of floc breakup are more significant at low SPM concentrations.

Salinity acts as a flocculant, reducing the electrochemical repulsion of individual clay particles (e.g., van Olphen, 1977; Manning, 2001). Without a flocculant (salinity or organic polymers) clay particles do not flocculate. Flocculation is possible at a salinity exceeding 1-5 ppt (Krone, 1963). Salinity is therefore primarily a binary factor: the water is saline (ppt > 1-5 ppt; flocculation is possible) or not saline (no flocculation). In terms of gauging the importance of salt flocculation, engineering practice (as a simple rule-of-thumb) categorises this behaviour in terms of NaCl concentration. Critical salinities for coagulation of three common clays, expressed both as salinity and milli-equivalents per litre, are (Winterwerp and van Kesteren, 2004):

MUSA

- Kaolinite: 0.6 or 10 mEq l^{-1};
- Illite: 1.1 or 19 mEq l^{-1};
- Smectite (or Montmorillonite): 2.4 or 36 mEq l^{-1}.

In sea water it might be expected that these critical values of salinity are greatly exceeded (Al Ani et al., 1991). On that basis, the role of salt flocculation should not be one that induces a clay mineral dependency, whereas in brackish environments it could lead to slight dependency of mineral type (Manning et al., 2017).

It is increasingly recognised that there is a strong mediation of the physical behaviour of particles and flocs by the biological components of the system. Mineral cohesion effects are further enhanced by the presence of extracellular polymeric substances (EPS; e.g., Tolhurst et al., 2002), such as mucopolysaccharides produced by microphytobenthos. EPS has a *stabilising* effect on cohesive sediments (Parsons et al., 2016; Hope et al., 2020). In estuarine environments, where sediments are predominantly mud and silt, benthic microphytobenthos contribute up to half the total autotrophic production (Cahoon, 1999; Underwood and Kromkamp, 1999). For example, epipelic diatoms (e.g., Paterson and Hagerthey, 2001) secrete long-chain molecule EPS as they move within the sediments. EPS is regarded as a highly effective biostabiliser of muddy sediments (e.g., Uncles et al., 2003; Underwood and Paterson, 2003; de Brouwer et al. 2005; Gerbersdorf et al. 2009; Grabowski et al., 2011) and can significantly enhance interparticle cohesion. Flocculation and deflocculation can result from adsorbed polymers. In general, flocs held together by polymers are stronger than those held together solely by electrostatic, London–van der Waals forces (Kitchener, 1972). It is noted that polymers indeed lead to stronger flocs, but floc break-up is irreversible (a broken EPS strain can no be repaired). So, EPS flocs will behave differently when they have been subjected to large shear.

Edzwald and O'Melia (1975) conducted experiments with pure kaolinite and found that the flocculation efficiency was less than 10 per cent. Experiments by Kranck (1984) have shown that the flocculation of mineral particles that contained some organic matter greatly enhanced the settling velocity of the resultant aggregates. This result was also obtained by Gratiot and Manning (2004) using a grid oscillation tank and video-capture techniques. Both Cadee (1985) and Kranck and Milligan (1988) reported enhanced flocculation following diatom and coccolith blooms at the entrance of tidal inlets; coccolithophorids may also act as nuclei around which flocs are created. Jackson (1990) modelled flocculation during a diatom bloom by considering both aggregation processes and algal growth. It was concluded that the important parameters were turbulent shear, the algal (particle) concentration and the size and stickiness of the algae.

Owen tube measurements generally show an exponentially increasing relationship between median floc settling velocity, $W_{s,50}$, and SPM concentration, C, for concentrations <10 gl^{-1}, in the form of:

$$W_{s,50} = k\ C^m$$

This relationship has been reported for numerous estuaries (Odd, 1988; van Leussen, 1988; Delo and Ockenden, 1992). An exponent m of 1.05 was measured for the Severn Estuary and 0.69 for the neighbouring Parrett Estuary. Variations in m between estuaries are, probably, a result of floc density variations and differences in ambient hydrodynamic conditions.

Floc sizes (D) can range over four orders of magnitude, from individual clay particles to stringer-type floc structures several centimetres in length. An individual floc might comprise up to an order of 10^6 individual particulates, and as it grows in size its effective density (i.e.,

MUSA

bulk density minus water density), ρ_e, generally decreases (Tambo and Watanabe, 1979; Klimpel and Hogg, 1986; Droppo et al., 2000). The general trend exhibited by a floc's effective density, as a function of floc size, has been observed by a number of authors (Manning and Dyer, 1999; Al Ani et al., 1991; Alldredge and Gotschalk, 1988; Fennessy et al., 1994a, b; Gibbs, 1985; McCave, 1975, 1984).

Settling velocity, in addition to effective floc density, is regarded as a basic variable in determining suspended sediment deposition rates in both still and flowing waters. Much has been documented on non-cohesive sediments (coarse silts and larger), and because the only forces involved are gravity and the flow resistance of the particles (e.g. Soulsby, 1997), it is possible to calculate the settling velocity of low-concentration suspensions of these particles from the relative density, size and shape of the particles, using well-defined expressions (e.g., Stokes' law; Stokes, 1851). However, the settling velocity of flocculated, cohesive sediments in estuaries is significantly greater than the constituent particles because floc settling velocity rises due to the size-dependent Stokes' law relationship (Mehta and Lott, 1987; Dyer and Manning, 1999). Based on the research of Stolzenbach and Elimelich (1994) and Gregory (1978), Winterwerp and van Kesteren (2004) concluded that although flocs are porous in composition, they can be treated as impermeable entities when considering their settling velocities. For a constant floc settling velocity there is a wide range of D and effective density ρ_e. Similarly, for a constant D there is a large spread in both settling velocity and effective floc density ρ_e . As with floc sizes, settling velocities typically can range over four orders of magnitude, from an order of 0.01 mms^{-1} up to several cm s^{-1} (Lick, 1994). As a result, the sizes and settling velocities of flocs are key parameters when modelling cohesive sediment transport in near-shore waters (e.g. Mehta and Lott, 1987; Geyer et al., 2000; Cheviet et al., 2002).

Manning (2001) defined microflocs and macroflocs as flocs with diameters such that D < 160μm and D > 160μm, respectively. Flocculation is a dynamically active process that readily reacts to changes in turbulent hydrodynamic conditions (e.g. Krone, 1962; Parker et al., 1972; McCave, 1984; van Leussen, 1994; Winterwerp, 1998; Manning, 2004a). For example, during spring-tide tidal conditions in the Tamar Estuary (UK), Uncles et al. (2010) showed that median-diameter floc sizes could exceed 700 μm, and Manning et al. (2006) showed that macroflocs typically can reach 1–2 mm in diameter with settling velocities up to 20 mm s^{-1}; however, the effective densities of these large 1–2 mm macroflocs generally are <50 kg m^{-3}, which means that they are prone to break up when settling through a region of high turbulent shear.

The degree of flocculation, often referred to as the stability (van Leussen, 1994), is highly dependent on a number of variables, including: mineralogy (Winterwerp and van Kesteren, 2004); electrolytic levels, which tend to be altered because of salinity gradients in an estuary (van Olphen, 1977; Krone, 1963), which can in turn affect the zeta-potential of clay particles (Chassagne et al., 2009); suspended sediment (solids) concentration (SSC; Ross, 1988; Burban et al., 1989); organic content (Gregory, 1978; Kranck, 1984); and turbulent mixing (e.g., Krone, 1962; Argaman and Kaufman, 1970; Parker et al., 1972; McCave, 1984; van Leussen, 1994; Winterwerp, 1998; McAnally, 1999; Manning, 2004a). A conceptual model that attempts to explain the linkage between floc structure and floc behaviour in an aquatic environment is provided by Droppo (2001). The rate of flocculation is a function of: suspended particulate matter concentration, salinity, mineralogy, biological stickiness and the physical mechanisms that bring the cohesive particles into contact (e.g. Manning, 2004b; Mehta, 2014; Winterwerp and van Kesteren, 2004).

The larger the floc, the larger its settling velocity (although also depending on floc density). Turbulence destroys flocs but also provides microscale water motions that bring clay particles together, thereby promoting the formation of floc. In absence of turbulence, the

MUSA

growth rate of flocs would be extremely low. Therefore, an optimal turbulence regime exists, at which the flow size (and therefore settling velocity) is maximal.

Sediment mixtures may either behave in a segregated way or may interact through flocculation. The phenomenon of mud–sand segregation considers the mud and sand to operate as two independent suspensions (van Ledden, 2002). When a segregated regime dominates there is very little bonding, and flocculation interaction between the fine fraction and the larger, non-cohesive sediment fraction is non-existent. Mixed sediment experiments have shown that fine sediment particles and sand grains, which behave in a segregated manner, settle simultaneously (but at different speeds) at the bed–water interface, thereby forming two well-sorted layers (Migniot, 1968; Ockenden and Delo, 1988; Williamson and Ockenden, 1993; Torfs et al., 1996). However, where the fine fraction and the larger non-cohesive sediment coexist as a single mixture (Mitchener et al., 1996), this creates the potential for these two fractions to combine and exhibit some degree of interactive flocculation (Manning et al., 2010, 2013). Whitehouse et al. (2000) describe a process whereby cohesive sediments that are mixed into a predominately cohesionless sandy region can create a 'cage-like' structure that can fully encompass the sand grains, thereby trapping the sand within a clay floc envelope. Within a mixed sediment environment, the degree of cohesion between the various sediment fractions tends to increase with the content of fine clay minerals within the sediment and starts to become significant when the sediment contains more than 5–10 per cent of clay by weight (Dyer, 1986; Raudkivi, 1998; Whitehouse et al., 2000, van Ledden, 2003).

In addition to physical processes, biological activity, more commonly associated with cohesive sediments, has been highlighted to play an important role in the cohesion of mixed sediments (e.g. Paterson and Hagerthey, 2001) and is an important component that makes mixed sediment flocculation possible. The influence of biology on sand has been reported to a much lesser extent; however, sand grains that are exposed to long-term biological activity may also develop a cohesive bio-coating, which could increase the particle collision efficiency when they are entrained. Hickman and Round (1970) reported that sand particles can be joined by epipsammic (i.e., attached to or moving through sand particles) diatoms that attach to sand grains. Epipsammic macro-algae either adnate (i.e., grow strongly) to the grain surface or attach to sand grains using their mucilage stalks. Epipsammic diatoms that are attached to sand grains demonstrate strong adhesive properties to the grain surface (Harper and Harper, 1967).

When fine sand and biology are combined into a single matrix they can form microbial mats, and the binding strength of these mats can be extremely high. Little (2000) states that because these types of algal threads are sticky with EPS, they can efficiently trap fine sand grains. These sticky bio-coatings can increase the collision efficiency (Edzwald and O'Melia, 1975) of particles when entrained into suspension, thus allowing fine sand grains to adhere with the clay fraction. Using microscopic photography, Wolanski (2007) reports the formation of large, muddy flocs formed by
mud that creates a sticky membrane around large, non-cohesive silt particles. Recent laboratory experiments that examined the effects of EPS bio-stabilisers on both ripple (Malarkey et al., 2015) and dune (Parsons et al., 2016) evolution in sand–mud sedimentary environments found that just 0.1 per cent EPS was sufficient to prevent the formation of significant bedforms.

The process of bioturbation (i.e., the reworking of bed sediments by living organisms) can also potentially enhance the mixing of bed sediment particles prior to resuspension (e.g., Nowell et al., 1981; Paterson et al., 1990; Widdows et al., 2004). Thus, a bed that is initially deposited as a discretely segregated layering of mud and sand may be transformed into a quasi-homogeneous mixture as a result of bioturbation.

MUSA

4.1.2 Hindered settling range

When the sediment concentrations are larger than approximately 5 g/l, the settling velocity decreases with increasing concentrations due to the hindered settling effect. Hindered settling is the effect that the settling velocity of the flocs is reduced due to an upward flow of fluid displaced by the settling flocs (e.g. Dankers and Winterwerp, 2007; Spearman and Manning, 2017). Furthermore, the viscosity of high-concentration mixtures increases markedly (factor 10 to 100) compared to that of clear water.

In the laboratory, the hindered settling velocity can be quite accurately determined from settling/consolidation tests by measuring the sinking of the sediment-fluid interface. Manning et al. (2017) have proposed a laboratory experimental protocol to measure the settling velocity of interfaces formed within a muddy suspension for both dilute and hindered settling suspensions.

At very large concentrations the vertical fluid flow can be so strong that the upward fluid drag forces on the flocs become equal to the downward gravity forces resulting in a temporary state of dynamic equilibrium with no net vertical movement of the flocs. This state which occurs close to bed, generally is called fluid mud, which can rheologically behave in a non-Newtonian manner.

High-concentration suspensions can display different settling behaviours depending on the initial condition. For volume concentrations above a value, $\phi > \phi_{crit}$ (see Figure 4.1), analysis of settling behaviour in settling columns shows that only one interface (between clear water and the settled bed) will be created, as segregation of grains is increasingly suppressed. Below this value $\phi < \phi_{crit}$, two interfaces are created: one between overlying clearer water and the settling suspension and the second between the suspension and the bed (Dankers 2006).

When the average distance between flocs becomes sufficiently small, they join together to form a volume-filling network. This point, known as the gel point with a volume concentration of ϕ_{gel} (see Figure 4.1), marks the transition between hindered settling and the permeability phase of consolidation, where the settling velocity function is mainly driven by the compression of flocs and expulsion of pore water (where effective stresses are zero) as shown in Figure 4.1 (Spearman and Manning, 2017).

Spearman and Manning (2017) have proposed a correction to the Richardson–Zaki equation to better describe the settling behaviour in the ultra-high concentration range up the maximum volumetric concentration (ϕ_{max}).
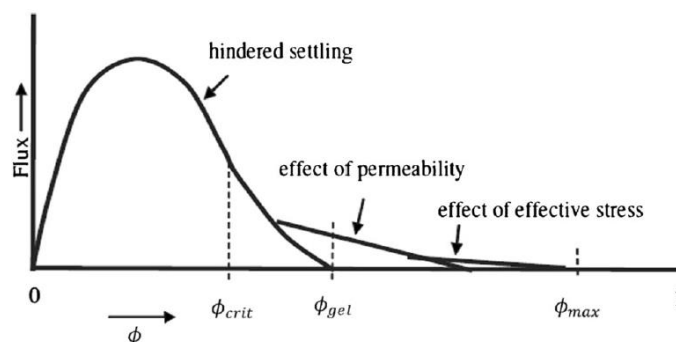
Figure 4.1 Schematic representation of settling flux variation with volumetric concentration (ϕ) showing effects of hindered settling, permeability and consolidation (Spearman and Manning 2017).

4.2 Measuring instruments

Various methods and instruments can be used to determine the settling velocity of natural mud particles and flocs from water-sediment samples. The samples can be analyzed either in the laboratory or in the field. For muddy sediments, the settling velocity (or grain size

MUSA

distribution) can be measured in its flocculated state, or of the primary particles. The flocculated state can be measured only in the field because for laboratory analysis the sample needs to be transferred from the sample location to the laboratory where it is resuspended by mechanical stirring, which influences the floc distribution (either by destroying or generating flocs) and thus on the settling velocity. Therefore, immediate in-situ analysis of the samples is highly preferred.

The determination of the settling velocity of natural flocculated suspended sediments can best achieved by in-situ systems, as follows:

- in-situ settling tubes;
- in-situ video or photo-cameras;
- in-situ Laser-Diffraction (LD) instruments.

The development of video-based floc devices has provided tools with which floc sizes and floc settling velocities can be measured simultaneously within a natural flow, whilst creating minimal interference to the aggregates. Furthermore, unlike many standard particle-size instruments, these permit an estimate of an individual floc's effective density, ρ_e, defined as the bulk density minus the water density, using a modified Stokes' law. Therefore, these measurements make possible the computation of floc-mass distribution across a range of sizes (Fennessy et al., 1997; Manning, 2004,a, b) and can provide an insight into the interaction of flocs within the lower layers of the flow, where the suspended concentration gradients are greatest. Such site-specific information on floc settling velocity spectra is a prerequisite for the accurate parameterization of aggregation processes, especially for implementation into sediment transport models (Manning, 2004b, 2008; Baugh and Manning, 2007).

Of note, the video-based LabSFLOC – Laboratory Spectral Flocculation Characteristics – instrument (Manning,2006; Manning et al., 2017) is often widely regarded as a benchmark system when measuring a wide range of floc characteristics, dynamical properties and types (e.g. Manning et al., 2007a, b, 2010; Spearman et al., 2020). It is a portable laboratory derivation of the prototype in situ INSSEV (IN-Situ SEttling Velocity) instrument (Manning and Dyer, 2002) that enables floc properties to be measured in laboratory studies using suspended particulate matter (SPM) concentrations of several gl^{-1}. LabSFLOC utilizes a low-intrusive, high resolution video camera to observe flocs as they settle in a settling column constructed of Perspex. The video camera utilizes a back-illumination system, whereby floc images are manifested as silhouettes; i.e., particles appear to be dark on a light background. This reduces image smearing and renders the floc structure more visible. A floc sample is extracted from its original environment (e.g., a flume) and is immediately transferred to the column using a modified pipette. The video camera, the centre of which is positioned 0.075 m above the base of the column, views all particles in the centre of the column as they settle from within a predetermined sampling volume. All of the flocs viewed by the LabSFLOC video camera, for each sample, are measured both for floc size and settling velocity. Clear, greyscale, 2-D optical images of the flocs are recorded by the video suite (analogue-to-digital for version 1 and fully digital for version 2). LabSFLOC-2 (e.g. Ye et al., 2018) can measure floc sizes of 8 mm in diameter and settling velocities approaching 45 mm s^{-1}, providing the flexibility to measure both pure mud and mud–sand mixed sediment floc dynamics. By implementing a sequence of image-analysis algorithms, the floc porosity, fractal dimensions, floc dry mass and the mass settling flux of a floc population can be computed (Manning et al., 2017). The calculated dry mass also can be compared with the measured SPM concentration (i.e. a mass-balanced referenced floc population), thus providing an estimate of the efficiency and reliability of each sampling procedure. It follows that the data obtained from LabSFLOC is both qualitative and quantitative.

The portability of the LabSFLOC instrument has led to the development of the INSSEV-LF: IN-Situ Settling Velocity instrument. The LF (LabSFLOC) version of INSSEV is a hybrid

MUSA

system that combines two key components: (1), the low-intrusive LabSFLOC system and (2), an in situ estuarine floc sampling acquisition unit (to initially obtain the suspension sample). For the latter, a 2.2 l van Dorn horizontal sampling tube with a 10–14 kg weight suspended from the underside of the tube has been used to collect a water sample at a nominal height above the estuary bed. Manning and Schoellhamer (2013) have deployed the INSSEV-LF throughout San Francisco Bay
and the Northern Californian River Delta, USA.

The determination of the settling velocity of the primary particles is determined in a laboratory. The sample is first deflocculated (mechanically or chemically using Peptiser or Calgon) and subsequently measured using a settling tube method, a camera, or laser diffraction. Laser diffraction (Coulter or Malvern) is an often-used method to measure the size distribution of sediment samples, but these methods tend to underestimate the clay fraction significantly when analysing the sample as whole because the larger particles shade the smaller particles. This can be partly overcome by separately analysing the smaller and larger particles. Still, settling tubes provide the most accurate estimate of the clay fraction.

4.3   Measured settling velocities

Most common methods for measuring the settling velocities are settling tubes and video-camera systems**.**

Figure 4.2 shows settling velocities based on settling tube results (Van Rijn 2018). The observed settling velocities are in the range of 0.1 to 3 mm/s.

Figure 4.3 and Figure 4.4 show settling velocities based on the LabSFLOC video camera system of HR Wallingford (Manning et al., 2010). The observed settling velocities are in the range of 0.5 to 10 mm/s. Macroflocs are clearly observed by the camera system.

Based on these results, it may be concluded that the settling tube tests may lead to smaller settling velocities (Figure 4.2), which may be caused by the destruction of macroflocs during the sampling operation. On the other hand, the camera systems may not detect the smaller microflocs and may thus have a slight bias towards the larger macroflocs.
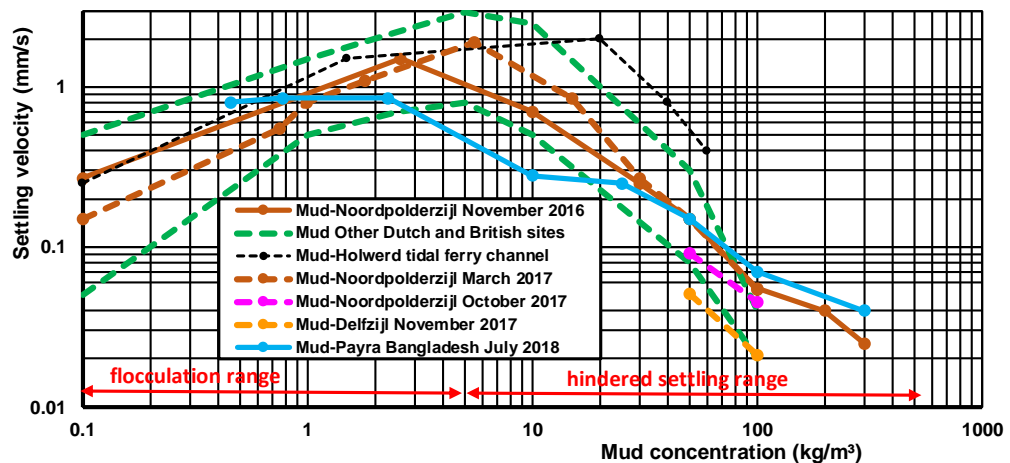
Figure 4.2 Median settling velocity as function of mud concentration of various mud samples (Van Rijn 2018)

MUSA
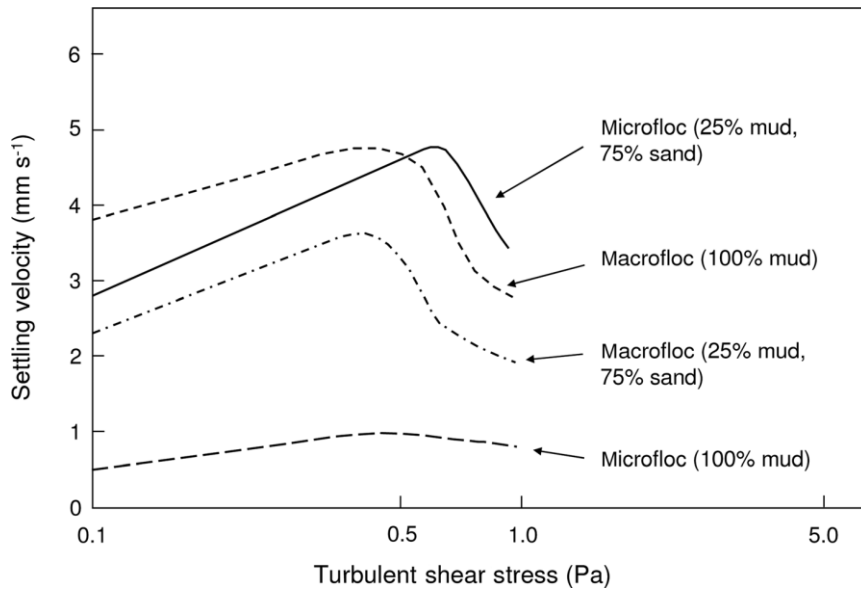
Figure 4.3 Settling velocities of macroflocs and microflocs, plotted against shear stress, for a mixed sediment suspension comprising a ratio of 25 per cent mud to 75 per cent sand and a pure mud suspension, all for a total SPM concentration of 5 gl⁻¹.
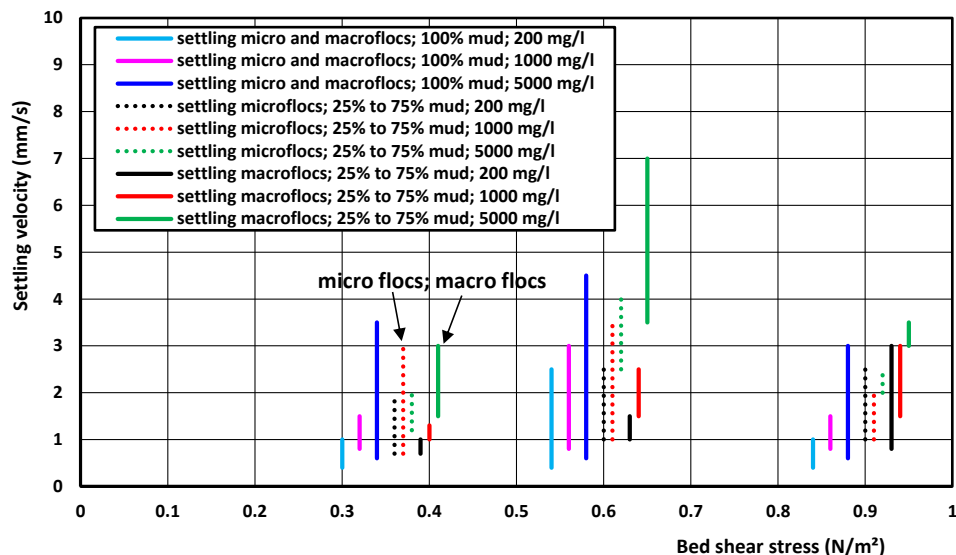
Figure 4.4 Settling velocities of macroflocs and microflocs, plotted against shear stress for concentrations of 0.2 to 5 g/l based on data of Manning et al. (2010)

Different ratios of mud and sand can vary the level of cohesion and influence the resultant level of flocculation. However, due to the wide-ranging variability of mixed sediment compositional properties, it is extremely difficult to quantitatively describe such a complex sedimentary matrix in a fundamental manner; this is primarily the result of a lack of verification data. Therefore, in order to quantify mixed-sediment flocculation characteristics, a series of laboratory studies were conducted on a range of mud–sand mixtures that possessed different SPM concentrations and were sheared by different levels of turbulent mixing (Manning et al., 2007, 2010). The results revealed the following general, mixed-sediment floc properties:

- $W_{s,micro}$ increases in response to a rising sand content.
- $W_{s,macro}$ decreases with rising sand content.
- The greater the sand content of a mixed suspension, the higher the total mass settling flux (MSF).

MUSA

- The SPMratio (defined as the ratio of macrofloc to microfloc SPM concentrations) steadily rises as overall sediment concentration increases, which is similar to a fully cohesive suspension. However, the SPM_{ratio} generally decreases across the suspended particulate matter.

These factors have been included in a set of empirically derived algorithms that describe mixed-sediment flocculation (Manning et al., 2011). It should be noted that any mixed-sediment flocculation effects and sediment–fraction interactions can only be demonstrated empirically through rigorous laboratory settling experiments. A review of the testing of the mixed sediment flocculation algorithms is provided by Spearman et al. (2011).

The settling velocity strongly depends on the sediment composition (percentage clay, silt and fine sand) of the mud sample considered. For example, the settling velocity in the muddy Scheldt river near Antwerp (Belgium) was found to be rather low with values ($w_{s,50}$) between 0.07 and 0.1 mm/s (0.085 ± 0.015 mm/s; equivalent size of about 10 μm) at concentrations of 300 mg/l, which points to a low degree of flocculation. The largest settling velocity ($w_{s,90}$) of Scheldt mud was in the range of 1.5 to 3.5 mm/s. The settling velocity in the silty ferry channel near Holwerd (The Netherlands) is much higher (factor 5), with values of about $w_{s,50} \cong 0.8$ mm/s (equivalent size of 20 to 30 μm), because the percentage of silt in the ferry channel near Holwerd is much higher than in the Scheldt river. The largest settling velocity ($w_{s,90}$) of Holwerd mud is in the range of 1.5 to 6.5 mm/s (mud concentrations in range 1000 to 10000 mg/l). These examples show that the settling velocity can vary substantially, both spatially and most likely also temporally.

Of specific interest is the deposition flux of fine sediments. The deposition flux was originally thought to depend on a so-called shear stress for deposition (the Partheniades equation; Ariathurai and Arulanadan, 1978). Later Sanford and Halka (1993) and Winterwerp (2007) argued that such a critical shear stress for deposition does not exist. Still, permanent deposition as argued by these authors appears to be a too rigid definition, poorly explaining the formation of high concentration layers close to the bed. This led to the definition of the co-called reduced deposition factor (van Kessel and Van Lede, 2009) which appears to be related to amongst others the near-bed suspended sediment concentration through consolidation effects (through which the critical bed shear stress only gradually increases in time) and hindered settling effects (van Maren et al., 2020). The need to apply a factor to reduce the deposition flux is likely to be the result of many over-simplified processes near the bed: hindered settling, vertical mixing, damping of turbulence. Having a simple parameter enables some of the right behaviour to be modelled without needing to include lots of model complexity.

Literature review on sand and mud
16 November 2020

MUSA

5 Consolidation and bulk densities of sand-mud mixtures

Deposition and consolidation of mud are basic processes in natural, low-energy environments. The composition and structure of the deposited sediment bed is dependent on the input concentrations, clay, silt and sand content supplied by the water system, layer thickness and sedimentological, chemical and biological properties of the sediments involved.

Knowledge of the consolidation of soft muddy layers can be obtained from settling tests in laboratory columns.
This type of research work has shown that the consolidation process of soft materials consists of three distinct phases (Migniot 1968 and 1989):
  1. hindered settling phase (initial hours);
  2. primary (short-term) consolidation phase accompanied by large strains (weeks to months);
  3. secondary (long-term) consolidation phase accompanied by small strains (Terzaghi-type consolidation; years).

The settling and consolidation processes are essentially vertical processes with downward movement of sediments and upward movement of expelled pore water and can therefore be studied in laboratory settling columns. Early work on the self-weight consolidation of mud has been done by Been and Sills (1981), by Lin (1983) using mud with very low sand content and by Torfs et al. (1996) with varying sand contents. The amount of literature of pure muds is vast and will not be elaborated on here – we restrict ourselves here to effect of silt and sand on consolidation processes.

Lin (1983) studied the self-weight consolidation of a lake mud with 25% clay, 65% silt and 10% sand (Lake Panora, Iowa, USA) in fresh water using a settling column height of about 2 m. The initial consolidation time of a suspension with a dry density (concentration) of about 225 kg/m^3 was found to be of the order of 1 week to obtain an end density of about 450 to 500 kg/m^3.
Torfs et al. (1996) carried out consolidation tests with Scheldt-mud and Hong Kong-mud in settling columns with various types of mud and varying sand contents (0% to 60%) in saline water. Most of their tests concern the settling and consolidation of relatively thin Hong Kong-mud layers < 0.2 m with initial concentrations < 50 kg/m^3. Some tests with Scheldt-mud were done in a long settling column of 2 m with an initial concentration of 150 kg/m^3. The settling procedure was varied to study its effect on the bed structure, as follows: (1) almost instantaneous filling of the column, (2) continuous filling by pumping the mixture from a base container and (3) intermittent filling with intervals of days to weeks resulting in layered beds. They found that the filling procedure affects the formation of a matrix structure prior to consolidation. When the bed matrix structure is formed, the sand particles are held within the structure of the bed. In the case of low concentrations << 100 kg/m^3, compact flocs and sand particles can sink through the mixture to form a bottom layer of higher density, and segregation occurs with an almost sand-free upper layer. Segregation occurs at low concentrations (<< 100 kg/m^3) and high sand contents (10% to 30%) resulting in a layered density profile. The degree of segregation is limited to a maximum sand content (about 30%), which is a function of the mud type. The presence of large quantities of sand increases the consolidation rate as small drainage paths are created by sand pockets through which the pore water is expelled during consolidation.

MUSA

Torfs et al. (1996) have also studied layered beds in a flume resulting from sequential events of deposition due to differences in conditions as present during storm and post-storm conditions. Layered beds are most pronounced in conditions with high sand contents and relatively large time intervals between events resulting in a bed of mud and sand layers. A few hours between input events is long enough for the bed to develop a mud layer with gelling structure and support the next layer of sand. Layer thickness decreases with increasing sand content to a limiting value at about 30%. The intermittent deposition of thin mud layers without sand also lead to more rapid consolidation as the pore water path remains relatively small.

Dankers (2006) focused on the effect of fine sand particles on the consolidation behaviour of mud in saline water. The dry density of the top mud layer was about 50 to 100 kg/m^3 on which a suspension of settling sand particles (110 μm and 360 μm) in concentrations < 10 kg/m^3 was poured. The experimental results show the generation of small pockets of sand in the upper layers of the mud. Coarse sand particles move relatively far through the mud layer creating drainage paths for pore water. The consolidation rate of the upper mud layers increased by about 10%.

Fossati et al. (2015) presented several self-weight consolidation tests performed with Río de la Plata sediments (Uruguay). Samples with a relatively small clay/silt ratio (<0.15) showed faster settling and consolidation rates with a stable height during the first day of the experiment. The end density was about 700 kg/m^3 after 1 day for a mixture of 10% clay, 90% silt. The end density increased to about 770 kg/m^3 for a mixture of 10% clay, 70% silt and 20 % sand. A different behaviour is observed for cohesive sediment with a clay/silt ratio of about 0.5 showing a continuous consolidation process during several days with a decreasing rate. The end dry density was about 350 kg/m^3 for a mixture with 35% clay and 65% silt. Their results show a strong effect of the clay-silt ratio.

Te Slaa et al. (2013) and Te Slaa (2020) studied the settling and consolidation behaviour of silt-rich sediment as present in Chinese rivers under laboratory conditions in specially designed settling columns. Results show that a transition in consolidation behaviour occurs around clay contents of about 10 %, which is in analogy with the transition from non-cohesive to cohesive erosion behaviour. Above this threshold, sediment mixtures consolidate in a cohesive way, whereas for smaller clay percentages only weak cohesive behaviour occurs. The settling behaviour of silt-rich sediment is found to be in analogy with granular material at concentration below 150 g/l. Above 150–200 g/l, the material settles in a hindered settling regime where segregation is limited or even prevented.

Van Rijn and Barth (2019) studied the effect of sand on the primary consolidation time and end dry density of mud layers based on consolidation tests in laboratory conditions. Two types of natural muds and various artificial mud-sand mixtures with high percentages of sand were used. Based on the test results and literature (Table 5.1), it is found that the primary (short-term) consolidation process proceeds fairly quickly (10 to 50 days) if the percentage of sand (> 62 μm) is larger than about 30%, as shown in Figure 5.1. Natural muds with low sand content ($\cong$ 20%) and thickness of 1 to 2 m can consolidate to 400 to 450 kg/m^3 after 20 to 50 days. Natural muds with a high sand content of 40% to 50% and thickness of 1 to 3 m can consolidate to dry density values of 600 to 700 kg/m^3 after 10 to 30 days. The time scale is relatively small (up to 60 days) for a small thickness of 1 m and relatively large (up to 180 days) for a large mud thickness of about 3 m and low sand content. The available data suggest an almost linear relationship between the primary consolidation period and the mud layer thickness.

The vertical distribution of the dry density shows relatively high values (15% to 20% larger than depth-mean) in the near-bottom zone and relatively low values (15% to 20% smaller) in the near-surface zone. The end density values of the N-mud (Noordpolderzijl-mud) and

MUSA

D-mud (Delfzijl-mud) in the laboratory columns were about 10% smaller than the in-situ density values at the field site where the base mud was taken.

The final dry bulk density of the primary (short-term) consolidation phase of mud mixtures with a layer thickness of 1 to 3 m strongly depends on the percentage of sand (p_s), as shown in Figure 5.2 with data from the present study and from the literature (Table 5.1). The final density increases from about 450 kg/m³ for p_s=20% to about 880 kg/m³ for p_s=73%. The final density is higher if the percentage of clay is lower. The dry density values derived from laboratory columns with vertical drainage processes only are somewhat smaller than the values based on field tests. In field conditions, the consolidation processes are also influenced by lateral drainage resulting in larger dry density values (15%).

The final density can be increased by 5% to 10% by placing a sand layer load on top of the mud surface after about 10 days, once the upper mud layer has developed a network structure (and sand does no longer sink into the mud matrix). This only minor effect of placement of a top sand load is because the draining structure of the mud layer itself is not affected, except for the upper mud layer in contact with the sand load layer. If sand is available, it is much more effective to mix the available sand through the mud beforehand than to use the sand as a top load. By mixing of mud and sand, the (final) density at the end of the primary consolidation process can be increased by about 50%.

An empirical equation (Van Rijn and Barth, 2019) is also shown in Figure 5.2 for realistic values of p_{org}, p_{clay} and p_{silt}. This equation reads as:

$$\rho_{dry,mix} = (1-p_{org}/100)[400\ (p_{clay}/100) + 800\ (p_{silt}/100) + 1600(p_{sand}/100)]$$

with: p_{org}= percentage organic materials (%), p_{clay}=percentage clay (<8 μm), p_{silt}=percentage silt (8-63 μm), p_{sand}=percentage sand (%).
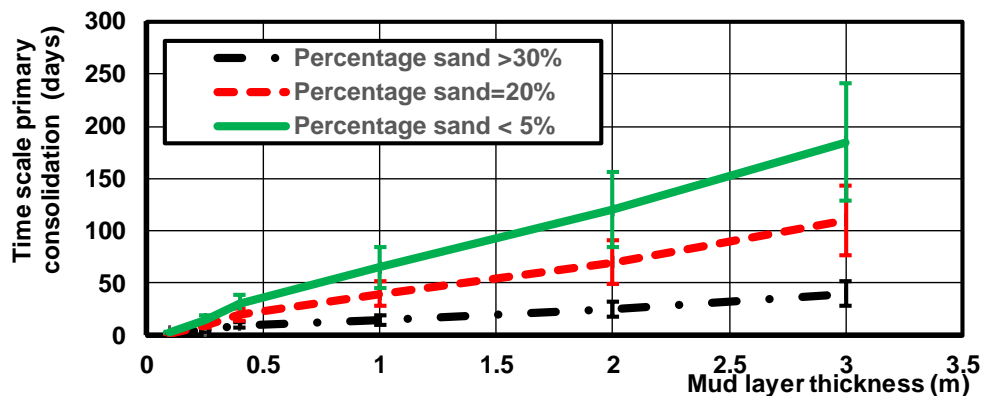
Figure 5.1 Time scale of primary consolidation process
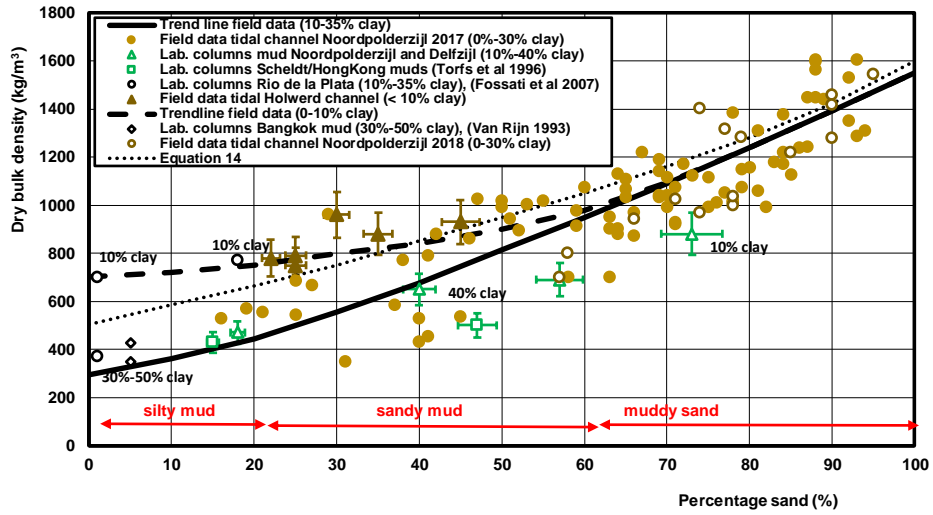
Figure 5.2 End dry density of primary consolidation period as function of percentage of sand and clay

Literature review on sand and mud
16 November 2020

Table 5.1 Laboratory and field data of end dry density values at end of short-term consolidation period.

n.m.= not measured

Type of mud	Layer thickness (m)	Percentage clay < 2/4 µm (%)	Percentage sand > 63 µm (%)	Percentage organic materials (%)	Time scale of primary consolidation period (days)	End dry density of primary consolidation (kg/m³)
Lab. colums: Bangkok mud (Van Rijn 1993)	1	30-50	5	-	90	420
	2	30-50	5	-	180	350
Lab. columns: Scheldt mud (Torfs et al. 1996)		n.m	15	n.m.	60	430
Lab. columns; Hong Kong mud (Torfs et al. 1996)	0.1	40	47	n.m.	<5	500
Lab. columns: Rio de la Plata muds (Fossati et al. 2015)	1	35	1	n.m.	60	370
	1	10	1	n.m.	<1	700
	1	10	18	n.m.	<1	770
Lab. columns: Delfzijl mud (present study)	2	40	18	10	50	470
Lab. columns: Noordpolderzijl mud (present study)	2-3	30-40	40	7	40	650
	2-3	20	57	7	40	690
	2-3	10	73	7	40	880
Field: Holwerd channel (Deltares 2016; Van Rijn 2016)	1-2	<10	22	7	<30	780
	1-2	<10	25	7	<30	750
	1-2	<10	25	7	<30	790
	1-2	<10	30	7	<30	960
	1-2	<10	35	7	<30	880
	1-2	<10	45	7	<30	930
Field: Noordpolderzijl (Van Rijn 2017)	<1	n.m.	20-50	n.m.	<90	400-800
	<1	n.m.	50-60	n.m.	<90	800-1000
	<1	n.m.	60-70	n.m.	<60	800-1200
	<1	n.m.	70-80	n.m.	<30	1000-1400
	<1	n.m.	80-90	n.m.	<30	1000-1600

Literature review on sand and mud
16 November 2020

MUSA

6 Evaluation of available experimental results and proposal for additional research

6.1 Erosion of mud-sand beds

Many data sets on the erosion of soft mud beds in both laboratory and field conditions with (tidal) currents are available, see Appendix A. Various laboratory and in situ methods to measure the erosion of the bed have been described in the literature: erosion tubes with rotating propellers, annular carrousels and straight flumes. Based on analysis of existing data sets for current-dominated conditions, the critical bed-shear stress for surface and mass erosion is found to be related to the percentage of clay (< 8 μm), percentage of fines (< 63 um), plasticity and the dry bed density.

Since most earlier experimental work on mud-sand beds has been done for (tidal) currents without surface waves, the effect of waves on the erosion of mixed mud-sand beds is a focus point in the MUSA-project.

The basic philosophy is to design a series of laboratory and field experiments which can be used to derive fairly simple and partly empirical relationships describing the most relevant erosion processes in terms of the size distribution, the mineral composition and the bed density for a range of mixed mud-sand conditions.

It is realized that some detailed erosion-related parameters and processes such as the stress conditions and stress history of the bed may also be important, but this will not be studied in great detail in the MUSA-project given the available budget. Furthermore, it may require a detailed geotechnical approach which is beyond the scope of the present MUSA-Project.

The role of bacterial films and other biological effects will also not be taken into account at this stage of research. However, the organic content of samples will be determined as an added value (if possible) to distinguish between types of mud-sand mixtures.

Based on the literature survey the following research questions are formulated:

Research questions
1. What is the critical bed shear stress and erosion rate of soft mud-sand beds in laboratory and field conditions with currents?
2. What is the role of oscillatory wave motion on the erosion of mud-sand mixtures?
3. What is the effect of varying percentages of clay, silt and sand and consolidation on the erodibility of mud-sand mixtures?
4. What is the role of bed irregularities (gravel, shells) on the erodibility of mud-sand mixtures?
5. How are the critical stresses and erosion rates of the sand and mud fractions related to bulk sediment properties and basic hydrodynamic parameters?

The methodology to address the above-listed research questions will also determine the research findings. For example, sample transfer from the field to the lab or the way the laboratory bed is prepared will influence the bed density and structure, which in turn are expected to determine the erodibility of the bed. As such, the research program will detail the set-up of each experiment (allowing for experimental reproduction) and will include a laboratory assessment on the effects of various bed layering (deposited layered bed, mixed bed) and bed density on the measured erosion rates.

Proposed type of activities

In addition to the already existing data sets for current-dominated conditions, we propose to carry out new laboratory experiments with natural and artificial mud-sand mixtures, in which the clay, silt and sand components and consolidation will be varied in a systematic way. The natural muds will be taken from various sites in the Netherlands, England and Denmark. To extend our knowledge of the effect of waves on the erosion of mud-sand mixtures, a series of tests with the same samples will be done in a wave-current flume.

To achieve this, we propose the following activities:
1. perform erosion tests in a laboratory current flume
   a. use mud-sand samples from different field sites; vary percentage of sand, clay type (and with varying sand and mud type also the plasticity index) and bed density/consolidation;
   b. do simultaneous tests in small current flume and erosion tube with propeller (mud samples from Western Scheldt estuary and Scheldt river).
2. perform similar erosion tests in large wave-current flume with long bed of mud-sand; focus on detailed velocities and concentrations of sand and mud in lowest 20 cm above the bed (at least 10 points).
3. perform erosion tests in field conditions with mud-sand beds under both tidal currents and waves; focus on detailed velocities and concentrations of sand and mud in lowest 50 cm above the bed (at 10 points).

It is proposed to do the field tests at a number of sites in the Netherlands, e.g. the tidal flats near Holwerd in Wadden Sea, tidal flat Ossenisse in Western Scheldt and an inland located (fresh water) site. Field sites will as much as possible be selected at locations where initial samples have been taken. The instruments (high-resolution acoustic and electromagnetic sensors for instantaneous velocities from which current and wave motions are determined; optical concentrations; pump sampler; echo sounder for bed detection) are mounted in a small tripod operated from a survey boat.

6.2   Settling velocity and deposition fluxes

Settling velocities and deposition fluxes are key parameters for deposition of sediment from suspension to the bed. Settling velocities in muddy environments have been measured at many locations around the world using mechanical settling tubes and/or video-camera systems, see Appendix C. The different methods to measure settling velocities both have advantages and disadvantages, as follows:

Settling tubes
- determination of the settling velocity distribution representing the full settling velocity range ($w_s,10$; $w_s,50$ and $w_s,90$) of particles and flocs is possible;
- larger settling velocities of macroflocs may be underestimated due to destruction of flocs during sampling;
- a long tube (>700 mm) is required for accurate determination of larger settling velocities in the range of 1 to 10 mm/s;
- accurate results only for concentrations > 200 mg/l.

Video-camera systems
- accurate detection of macroflocs (> 150µm) with relatively large settling velocities of 1 to 10 mm/s;
- less accurate detection of mud particles and microflocs (10 to 50µm);

MUSA

- determination of representative distribution of floc size and settling velocity is laborious requiring sophisticated object recognition software (automatic or semi-automatic analysis is required).

To extend our knowledge of settling velocities and fluxes, also in relation to measuring methods, new laboratory and field experiments (partly in combination with the experiments of Section 6.1) will be done with a focus on the near-bed layer. The following research questions are formulated:

Research questions
1. What is the influence of settling velocity and sediment concentration distribution on the deposition flux close to the bed, and how can this be related to hydrodynamic forcing and sediment properties?
2. What is the role of sand on mud flocs size, shape, and density and the resulting settling rates?
3. How to obtain an accurate settling velocity distribution from settling tube and video-camera results? And, related to this, determine the effect of sample transfer to the laboratory on the floc sizes and settling velocities.

Proposed type of activities
1. measure sediment concentrations and settling velocities close to the bed in laboratory and field conditions with currents and/or waves;
2. develop a simple settling tube instrument which can be used for in situ determination of mud settling velocities in laboratory and field conditions;
3. determine the best way of measuring fall velocities (accurate but also practical) by performing comparative tests at field sites with mud concentrations > 200 mg/l using both settling tube and in situ camera

6.3   Bed density

Deposition and consolidation of mud are basic processes in natural, low-energy conditions (slack water period) resulting in a bed with a soft upper layer and more firm deeper layers (increasing bed density at deeper layers). The composition and structure of the deposited sediment bed is dependent on the concentrations in the near-bed layer, the clay, silt and sand content supplied by the water system, the layer thickness and sedimentological, chemical and biological properties of the sediments involved.

A basic problem of many erosion studies at mud-sand beds is the variation of the bed density over the upper 50 cm of the bed, because the erodibility of the bed is primarily determined by the bed density. To extend our knowledge, a simple method to measure the bed density in field conditions should be developed, tested and applied at many locations in combination with sample analysis in thin layers to determine the sediment composition of the upper 50 cm.

Research questions
1. What is the best method to measure the density of the upper 50 cm of the bed, with a focus on the transition layer between water and seabed?
2. What is the dry bed density of the upper 50 cm of mud-sand beds in tidal conditions and how does this relate to sediment properties (e.g. composition, compaction)?
3. What is a simple method for extraction and analysis of samples in shallow and in deep water?

Proposed type of activities
1. perform comparative field tests at sites with soft mud-sand beds using various sampling instruments (e.g. Sonidens, Admodus, Graviprobe, dropcorer).

MUSA

2. develop a simple but accurate sampling instrument for bed density and sediment composition.
3. measure the bed density and sediment composition of the upper 50 cm at various tidal field sites.

References

Aberle, J., Nikora, V. and Walters, R., 2006. Data interpretation for in situ measurements of cohesive erosion. Journal of Hydraulic Engineering, ASCE, Vol. 132 (6), 581-588

Ahmad, M.F.; Dong, P.; Mamat, M.; Wan Nik, W.B.; Mohd, M.H., 2011. The critical shear stresses for sand and mud mixture. Applied Mathematical Sciences 5(2): 53–71.

Al Ani, S., Dyer, K. R., Huntley, D. A., 1991. Measurement of the influence of salinity on floc

density and strength. Geo-Marine Letters 11, 154–158.

Alldredge, A. L., Gotschalk, C., 1988. In situ settling behavior of marine snow. Limnology and Oceanography 33, 339–351.

Amos, C.L., Daborn, G.R., Christian, H.A., Atkinson, A. and Robertson, A., 1992. In situ erosion measurements on fine-grained sediments from the Bay of Fundy. Marine Geology, Vol. 108, 175-196.

Amos, C.L., Sutherland, T.F. and Zevenhuizen, J., 1996. The stability of sublittoral, fine-grained sediments in a subarctic estuary. Sedimentology, Vol. 43, 1-19.

Amos, C.L., Feeney, T., Sutherland, T.F. and Luternauer, J.L., 1997. The stability of fine-grained sediments from the Fraser River Delta. Estuarine, Coastal and Shelf Science, Vol. 45, 507-524.

Andersen, T.J., 2001. Seasonal variation of erodibility of two temperate, microtidal mudflats. Estuarine, Coastal and Shelf Science, 53, 1-12.

Andersen, T.J., Lund-Hansen, L., Pejrup, M., Jensen, K.T., Mouritsen, K.N., 2005. Biologically induced differences in erodibility and aggregation of subtidal and intertidal sediments: a possible cause for seasonal changes in sediment deposition. Journal of Marine Systems 55 (3/4), 123–138.

Andersen, T.J., Lanaru, M., Van Bernem, C., Pejrup, M. and Riethmueller, R., 2010. Erodibility of a mixed mudflat dominated by microphytobenthos and Cerastoderma edule, East Frisian Wadden Sea, Germany. Estuarine, Coastal and Shelf Science, Vol. 87, 197-206.

Argaman, Y., Kaufman, W. J., 1970. Turbulence and flocculation. Journal of the Sanitary Engineering Division 96, 223–241.

Ariathurai, C.R., Arulanandan, K., 1978. Erosion rates of cohesive soils. Journal of Hydraulics Division 104 (2),279–282

Baas, J.H., Best, J.L., Peakall, J., 2011. Depositional processes, bedform development and hybrid bed formation in rapidly decelerated cohesive (mud-sand) sediment flows. Sedimentology 58:1953–1987. https://doi.org/10.1111/j.1365-3091.2011.01247.x.

Baas, J.H., Davies, A.G., Malarkey, J., 2013. Bedform development in mixed sand-mud: the contrasting role of cohesive forces in flow and bed. Geomorphology 182, 19–39.

Baas, J.H.,Westlake, A., Eggenhuisen, J., Amoudry, L., Cartigny, M., Coultish, N., McLelland, S., Mouazé, D., Bauamt fur Kustenschutz, 1987. Tiefenstabilisierung von Aussentiefs mit Naturuntersuchungen am Nessmersieler Aussentief (In German). Norden, Germany

Baugh, J.V. and Manning, A.J., 2007. An Assessment of a New Settling Velocity Parameterization for Cohesive Sediment Transport Modeling. Continental Shelf Research, doi:10.1016/j.csr.2007.03.003.

Baugh, J.V. and Littlewood, M.A., 2006. Development of a cohesive sediment transport model of the Thames estuary. Estuarine and coastal modeling, South-Carolina, USA

BAW 2006/2007. Anpassung der Fahrrinne von Unter- und Außenelbe an die Containerschifffahrt; Gutachten zur ausbaubedingten Änderung der morphodynamischen Prozesse, A3955 03 10062 H.1c

Been, K. and Sills, G.C., 1981. Self weighed consolidation of soft soils: an experimental and theoretical study. Geotechnique, Vol. 31 (4), 519-535.

Berlamont, J., Ockenden, M., Toorman, E. and Winterwerp, J., 1993. The characterization of cohesive sediment properties. Coastal Engineering, 21, 105- 128.

Bisschop, R., 2018. Erosion of sand at high velocities; an experimental study. Doctoral Thesis, Department of Civil Engineering, Delft University of Technology, Delft, The Netherlands.

Borsje B.W., de Vries M.B., Hulscher S., de Boer G.J., 2008. Modeling large-scale cohesive sediment transport affected by small-scale biological activity. Estuarine Coastal and Shelf Science 78:468-480

Burban, P.-Y., Lick, W., Lick, J., 1989. The flocculation of fine-grained sediments in estuarine waters. Journal of Geophysical Research 94 (C6), 8323–8330.

Cadee, G. C., 1985. Macroaggregates of Emiliana huxleyi in sediment traps. Marine Ecology

Progress Series 24, 193–196.

Cahoon, L. B., 1999. The role of benthic microalgae in neritic ecosystems. Oceanography and Marine Biology: An Annual Review 37, 47–86.

Chassagne, C., Mietta, F., Winterwerp, J. C., 2009. Electrokinetic study on kaolinite suspensions. Journal of Colloid and Interface Science 336, 352–359.

Chen, X. D., Zhang, C. K., Paterson, D. M., Thompson, C. E. L., Townend, I. H., Gong, Z., … Feng, Q. (2017). Hindered erosion: The biological mediation of non-cohesive sediment behaviour. Water Resources Research, 53(6), 4787–4801. https://doi.org/10.1002/2016WR020105

Cheviet, C., Violeau, D., Guesmia, M., 2002. Numerical simulation of cohesive sediment transport in the Loire estuary with a three-dimensional model including new parameterisations. In: Winterwerp, J. C., Kranenburg, C. (eds.), Fine Sediment Dynamics in the Marine Environment – Proc. in Mar. Sci. 5. Amsterdam: Elsevier, 529–543.

Colby, B.R., 1963. Discussion of Sediment transportation mechanics: Introduction and properties of sediment, Progress report by the Task Committee on Preparation of Sediment Manual of the Committee on Sedimentation of the Hydraulics Division, V.A. Vanoni, Chmm, J. Hydr. Div., ASCE, 89(1), 266-268.

Dankers, P.J.T., 2006. On the hindered settling of suspensions of mud and mud-sand mixtures. Doctoral Thesis. Department of Civil Engineering. Technical University of Delft, Delft, The Netherlands

Dankers, P. J. T., Winterwerp, J. C., 2007. Hindered settling of mud flocs: Theory and validation.

Continental Shelf Research 27, 1893–1907.

Debnath, K., Nikora, V., Aberle, J., Westrich, B. and Muste, M., 2007. Erosion of cohesive sediments: resuspension, bed load and erosion patterns from field experiments. Journal of Hydraulic Engineering, ASCE, Vol. 133 (5), 508-520

de Brouwer, J. F. C., Wolfstein, K., Ruddy, G. K., 2005. Biogenic stabilization of intertidal sediments: The importance of extracellular polymeric substances produced by benthic diatoms. Microbial Ecology 49, 501–512.

Delo, E. A., Ockenden, M. C., 1992. Estuarine Muds Manual. HR Wallingford Report, SR 309.

Deltares, 1989. NOGAT Offshore Pipeline; report on erodibility tests. Report H1050, Delft, The Netherlands.

Deltares, 1991. Erosion of natural sediments from the Netherlands. Report Z161-35/37. Delft, The Netherlands.

Deltares, 2016. KPP Navigation channel Holwerd; analysis of dredging data, bottom soundings and bottom composition. Report No. 1230378 (in Dutch), Delft, The Netherlands.

Deltares 2016. Analysis ferry channel Holwerd-Ameland; field measurements (in Dutch). Report 1230378, Delft, The Netherlands

MUSA

Deltares, 2016. KPP Analysis tidal channel Holwerd-Ameland; Overview laboratory analyses. Report 1230378.002, Delft, The Netherlands

Deltares, 2016. KPP Analysis tidal channel Holwerd-Ameland; Analysis of dredging data. Report 1230378.000, Delft, The Netherlands

De Nijs, M.A.J., 2012. On sedimentation processes in a stratified estuarine system. Doctoral Thesis, Department of Civil Engineering, Technical University of Delft, The Netherlands

Dickhudt, P.J.,Friedrichs,C.T.,Schaffner,L.C.,Sanford,L.P., 2009.Spatia land temporal variation in cohesive sediment erodibility in theYork River estuary eastern USA: abiologically influenced equilibrium modified by seasonal deposition. MarineGeology267,128–140.

Dickhudt, P.J., C. T. Friedrichs, L. P. Sanford, 2011. Mud matrix solids fraction and bed erodibility in the York River estuary, USA, and other muddy environments, Continental Shelf Research, Volume 31, Issue 10, Supplement, p. S3-S13, doi 10.1016/j.csr.2010.02.008.

Dou, Guoren, 2000. Incipient motion of sediment under currents. China Ocean Engineering, Vol. 14, No. 4, 391-406.

Droppo, I. G., 2001. Rethinking what constitutes suspended sediments. Hydrological Processes
15, 1551–1564.

Droppo, I. G., Walling, D., Ongley, E., 2000. The influence of floc size, density and porosity
on sediment and contaminant transport. Journal of the National Centre for Scientific Research 4, 141–147.

Dunn, L.S., 1959. Tractive resistance of cohesive channels. Journal of Soil Mechanics and Foundations, ASCE, June

Dyer, K. R., 1986. Coastal and Estuarine Sediment Dynamics. Chichester: John Wiley and Sons.

Dyer, K. R., 1989. Sediment processes in estuaries: future research requirements. Journal of Geophysical Research 94 (C10), 14327–14339.

Dyer, K. R., Manning, A. J., 1999. Observation of the size, settling velocity and effective density of flocs, and their fractal dimensions. Journal of Sea Research 41, 87–95.

Edzwald, J. K., O'Melia, C. R., 1975. Clay distributions in recent estuarine sediments. Clays and Clay Minerals 23: 39–44.

Eisma, D., 1986. Flocculation and de-flocculation of suspended matter in estuaries. Netherlands Journal of Sea Research 20, 183–199.

Fennessy, M. J.; Dyer, K. R., Huntley, D. A., 1994a. INSSEV: an instrument to measure the size and settling velocity of flocs in-situ. Marine Geology 117, 107–117.

Fennessy, M. J., Dyer, K. R., Huntley, D. A., 1994b. Size and settling velocity distributions of
flocs in the Tamar Estuary during a tidal cycle. Netherlands Journal of Aquatic Ecology 28, 275–282.

Fennessy, M. J., Dyer, K. R., Huntley, D. A., Bale, A. J., 1997. Estimation of settling flux spectra in estuaries using INSSEV. In: Burt, N., Parker R., Watts J. (eds.), Cohesive Sediments – Proceedings of INTERCOH Conference (Wallingford, England). Chichester: John Wiley and Sons, 87–104.

Fettweis, M., Francken, F., Pison, V., Van den Eynde, D., 2006. Suspended particulate matter dynamics and aggregate sizes in a high turbidity area. Marine Geology 235, 63–74.

Fossati, M., Mosquera, R., Pedocchi, F. and Piedra-Cueva, I., 2015. Self-weight consolidation tests of the Rio de la Plata sediments. Proceedings INTERCOH2015, International Conference on Cohesive Sediment Transport Processes, Leuven, Belgium; published by Vlaams Institute for the Sea, ISSN1377-0950

Friedlander, S. K., 1977. Smoke, dust and haze. In: Fundamentals of Aerosol Behaviour, New York: Wiley.

Geesthacht 1991. A device for erosion measurements on naturally formed muddy sediments; the EROMES system. Paper GKSS 91/E/18. GKSS Forschungszentrum Geesthacht GMBH, Geesthacht, Germany

Geesthacht 1995. Schubspannungscharakteristik des EROMES-systems; Messungen zur Hydrodynamik und Erosionsversuche mit Kaolinit. Paper GKSS 95/E/43. GKSS Forschungszentrum Geesthacht GMBH, Geesthacht, Germany

Gerbersdorf, S. U., Bittner, R., Lubarsky, H., Manz, W., Paterson, D. M., 2009. Microbial assemblages as ecosystem engineers of sediment stability. Journal of Soils and Sediments 9, 640–652.

Geyer, W. R., Hill, P. S., Milligan, T. G., Traykovski, P., 2000. The structure of the Eel River

plume during floods. Continental Shelf Research 20, 2067–2093.

Gibbs, R.J., 1985. Estuarine flocs; their size, settling velocity and density. Journal of Geophysical Research, Vol. 90 (C2), 3249-3251.

Grabowski, R. C., Droppo, I. G., Wharton, G., 2011. Erodibility of cohesive sediment: The importance of sediment properties. Earth-Science Reviews 105, 101–120.

Gratiot, N., Manning, A. J., 2004. An experimental investigation of floc characteristics in a

diffusive turbulent flow. Journal of Coastal Research 41, 105–113.

Gregory, J., 1978. Effects of polymers on colloid stability. In: Ives, K. J. (ed.), The Scientific Basis of Flocculation. Alphen aan den Rijn, The Netherlands: Sijthoff and Noordhoff, 89–99.

Harper, M. A., Harper, J. F., 1967. Measurements of diatom adhesion and their relationship with movement. British Phycological Bulletin 3, 195–207.

Harris, R.J., C.A. Pilditch, B.L. Greenfield, V. Moon, and I. Krncke. 2016. The influence of benthic macrofauna on the erodibility of intertidal sediments with varying mud content in three New Zealand estuaries. Estuaries and Coasts 39: 815–828.

Herman P.M.J, Middelburg J.J., Heip C.H.R., 2001. Benthic community structure and sediment processes on an intertidal flat: results from the ECOFLAT project. Continental Shelf Research 21:2055-2071

Hope, J.A., Malarkey, J., Baas, J.H., Peakall, J., Parsons, D.R., Manning, A.J., Bass, S.J., Lichtman, I.D., Thorne, P.D., Ye, L. and Paterson, D.M., 2020. Interactions between sediment microbial ecology and physical dynamics drive heterogeneity in contextually similar depositional systems. Limnology and Oceanography, DOI: 10.1002/lno.11461.

Houwing, E.J., 2000. Sediment dynamics in the pioneer zone in the land reclamation area of the Waddenzee, The Netherlands. Doctoral Thesis, Department of Physical Geography, University of Utrecht, The Netherlands.

Hickman, M., Round, F. E., 1970. Primary production and standing crops of epipsammic and epipelic algae. British Phycological Journal 5, 247–255.

HR Wallingford, 1992. Tidal transport of mud/sand mixtures. Report SR 257, Wallingford, UK.

Jacobs, W., 2011. Sand-mud erosion from a soil mechanical perspective. Doctoral Thesis, Department of Civil Engineering, Delft University of Technology, Delft, The Netherlands.

Jackson, G. A., 1990. A model of the formation of marine algal flocs by physical coagulation processes. Deep Sea Research 37, 1197–1211.

Jacobs, W., Le Hir, P., Van Kesteren, W. and Cann, P., 2011. Erosion thresholds of sand-mud mixtures. Continental Shelf research, Vol. 31 (10), S14-S25.

Jiufa, L. et al., 2001. Fluid mud transportation at water wedge in the Chiangjiang estuary, China. Sciences in China (Series B), Vl. 44

Kamphuis, J. W. and Hall, K.R., 1983. Cohesive material erosion by unidirectional current, Journal of Hydraulic Engineering, Vol. 109, 39– 62.

Kineke,G.C. and Sternberg, R.W., 1995. Distribution of fluid muds on the Amazon continental shelf. Marine Geology 125, 193-233

MUSA

Kineke, G.C., Sternberg, R.W., Trowbridge, J.H. and Geyert, W.R. 1996. Fluid-mud processes on the amazon continental shelf. Continental Shelf Research, Vol. 16, No. 516, 667-696

Kitchener, J. A., 1972. Principles of action of polymeric flocculants. British Polymer Journal 4, 217–229.

Klimpel, R. C., Hogg, R., 1986. Effects of flocculation conditions on agglomerate structure. Journal of Colloid Interface Science 113, 121–131.

Kolmogorov, A. N., 1941a. The local structure of turbulence in incompressible viscous fluid for very large Reynolds numbers. Proceedings of the USSR Academy of Sciences, 30, 301.

Kolmogorov, A. N., 1941b. Dissipation of energy in locally iscotropic turbulence. Proceedings of the USSR Academy of Sciences, 32, p16.

Kranck, K., 1984. The role of flocculation in the filtering of particulate matter in estuaries. In: Kennedy, V. (ed.), The Estuary as a Filter. Orlando, FL: Academic Press, 159–175.

Kranck, K., Milligan, T. G., 1988. Macroflocs from diatoms: in-situ photography of particles in Bedford Basin, Nova Scotia. Marine Ecology Progress Series 4, 183–189.

Kranck, K., Milligan, T. G., 1992. Characteristics of suspended particles at an 11-hour anchor station in San Francisco Bay, California. Journal of Geophysical Research 97, 11373–11382.

doi: 10.1029/92JC00950.

Krone, R. B., 1962. Flume studies of the transport of sediment in estuarial shoaling process: Final report, Hydraulic Engineering Laboratory and Sanitary Engineering Research Laboratory. Berkeley: University of California.

Krone, R. B., 1963. A Study of Rheological Properties of Estuarial Sediments. Berkeley: Hydraulic Engineering Laboratory and Sanitary Engineering Research Laboratory, University of California, Report No. 63–68.

Laflen, J. M., and Beasley, R.P., 1960. Effect of compaction on critical tractive forces in cohesive soils, Res. Bull. 749, Agric. Exp. Stat. Univ. of Missouri, USA.

Le Hir P., Monbet Y., Orvain F., 2007. Sediment erodability in sediment transport modelling: Can we account for biota effects? Continental Shelf Research 27:1116-1142

Le Hir, P., Cann, P., Waeles, B., Jestin, H., and Bassoullet, P., 2008. Erodibility of natural sediments: experiments on sand/mud mixtures from laboratory and field erosion tests. Sediment and Ecohydraulics, Intercoh 2005, Saga, Japan. Proceedings in Marine Science, Vol. 9. Edited by Kusuda, T., Yamanishi, H., Spearman, J. and Gailani, J.Z.

Lichtman, I. D., Baas, J. H., Amoudry, L. O., Thorne, P. D., Malarkey, J., Hope, J. A., Peakall, J., Paterson, D.M., Bass, S.J., Cooke, R.D., Manning, A.J., Davies, A.G., Parsons, D.R., Ye, L. (2018). Bedform migration in a mixed sand and cohesive clay intertidal environment and implications for bed material transport predictions. Geomorphology, 315, 17– 32.

Lick, W., 1994. Modelling the transport of sediment and hydrophobic contaminants in surface waters. In: U. S. / Israel Workshop on Monitoring and Modelling Water Quality, May 8–13, 1994, Haifa, Israel.

Lick, W., Huang, H., Jepsen, R., 1993. Flocculation of fine-grained sediments due to differential settling. Journal of Geophysical Research 98 (C6), 10279–10288.

Lick, W., Jin, L. and Gailani, J., 2004. Initiation of movement of quartz particles. Journal of Hydraulic Engineering, ASCE, Vol. 130, No.8, 755-761.

Lim, S.S., 2006. Experimental investigation of erosion in variably saturated clay soils. Doctoral Thesis, School of Civil and Environmental Engineering, University of New South Wales, Australia

Lin, T.W., 1983. Sedimentation and self weight consolidation of dredge spoil. Doctoral Thesis, Iowa State University, USA

Liqin Zuo, 2018. Modelling and analysis of fine sediment transport in wave-current boundary layer. Doctoral Thesis. Department of Civil Engineering, Technical University of Delft. Delft, The Netherlands

Little, C., 2000. The Biology of Soft Shores and Estuaries. Oxford: Oxford University Press.

Long, M. and Menkiti, C.O., 2007. Geotechnical properties of Dublin boulder clay. Géotechnique Vol. 57, No. 6, 595-611. Doi: 10.1680/geot.2007.57.7.595

Lu, Y.J., Ji, R.Y. and Zuo, L.Q., 2009. Morphodynamic responses to the deep-water harbor development in the Caofeidian Sea area, China's Bohai Bay. Coastal Engineering Vol 56, No.8, 831-843

LVRS, 2018. Meetrapport Scheldemetingen nabij Antwerpen. Blokzijl. The Netherlands (in Dutch)

Malarkey, J., Baas, J.H., Hope, J.A., Aspden, R.J., Parsons, D.R., Peakall, J., Paterson, D.M., Schindler, R.J., Ye, L., Lichtman, I.D., Bass, S.J., Davies, A.G., Manning, A.J., Thorne, P.D., 2015. The pervasive role of biological cohesion in bedform development. Nat. Commun. 6, 6257. https://doi.org/10.1038/ncomms7257.

Manning, A. J., 2001. A study of the effects of turbulence on the properties of flocculated mud.

Ph.D. Thesis. Institute of Marine Studies, University of Plymouth.

Manning, A.J., 2004a. Observations of the properties of flocculated cohesive sediment in three western European estuaries. Journal of Coastal Research, SI41, 70-81.

Manning, A. J., 2004b. Observations of the properties of flocculated cohesive sediment in three western European estuaries. Journal of Coastal Research 41, 70–81.

Manning, A. J., 2008. The development of algorithms to parameterise the mass settling flux of flocculated estuarine sediments. In: Kudusa, T., Yamanishi, H., Spearman J., Gailani, J. Z. (eds.), Sediment and Ecohydraulics – Proc. in Marine Science 9, Amsterdam: Elsevier,

193–210. ISBN: 978-0-444-53184-1.

Manning, A. J., Bass, S. J., Dyer, K. R., 2006. Floc properties in the turbidity maximum of a

mesotidal estuary during neap and spring tidal conditions. Marine Geology 235, 193–211.

Manning, A.J., Baugh, J.V., Spearman, J.R. and Whitehouse, R.J.S., 2010. Flocculation settling velocities of mud: sand mixtures. Ocean Dynamics 60, 237-253. Doi: 10.1007/s10236-009-0251-0

Manning, A.J., Baugh, J.V., Spearman, J.R., Pidduck, E.L., and Whitehouse, R.J.S., 2011. The settling dynamics of flocculating mud-sand mixtures, part 1: empirical algorithm development. Ocean Dynamics 61, 311-350. Doi: 10.1007/s10236-011-0394-7

Manning, A. J., Dyer, K. R., 1999. A laboratory examination of floc characteristics with regard to turbulent shearing. Marine Geology 160, 147–170.

Manning, A. J., Dyer, K. R., 2002. The use of optics for the in-situ determination of flocculated mud characteristics. Journal of Optics A: Pure and Applied Optics, Institute of Physics Publishing 4, S71–S81.

Manning, A. J., Dyer, K. R., 2007. Mass settling flux of fine sediments in Northern European

estuaries: measurements and predictions. Marine Geology 245, 107–122. doi:10.1016/j.margeo.2007.07.005.

Manning, A.J., Martens, C., De Mulder, T., Vanlede, J., Winterwerp, J.C., Ganderton, P. and Graham, G.W., 2007a. Mud floc observations in the turbidity maximum zone of the Scheldt estuary during neap tides. Journal of coastal research, SI50, 832-836.

Manning, A.J., Friend, P.L., Prowse, N. and Amos, C.L., 2007b. Preliminary Findings from a Study of Medway Estuary (UK) Natural Mud Floc Properties Using a Laboratory Mini-flume and the LabSFLOC system. Continental Shelf Research, doi:10.1016/j.csr.2006.04.011.

Manning, A. J., Schoellhamer, D.H., 2013. Factors controlling floc settling velocity along a

longitudinal estuarine transect. Marine Geology, San Francisco Bay special issue. doi.org/10.1016/j.margeo.2013.04.006.

MUSA

Manning, A. J., Spearman, J. R., Whitehouse, R. J. S., Pidduck, E. L., Baugh, J. V., Spencer, K. L., 2013. Laboratory assessments of the flocculation dynamics of mixed mud-sand suspensions. In: Manning, A.J. (ed.), Sediment Transport Processes and Their Modelling Applications. Rijeka, Croatia: InTech, 119–164.

Manning, A.J., Whitehouse, R.J.S. and Uncles, R.J., 2017. Suspended particulate matter: the measurements of flocs. In: R.J. Uncles and S. Mitchell (Eds), ECSA practical handbooks on survey and analysis methods: Estuarine and coastal hydrography and sedimentology, Chapter 8, pp. 211-260, Pub. Cambridge University Press, DOI: 10.1017/9781139644426, ISBN 978-1-107-04098-4.

Mastbergen, D.R. and Van den Berg, J.H., 2003. Breaching in fine sand and the generation of sustained turbidity currents in submarine canyons. Sedimentology. Doi: 10.1046/j.1354-3091.2003.00554.x

McAnally, W., 1999. Aggregation and deposition of estuarial fine sediment. Ph.D. Thesis, University of Florida, FL.

McAnally, W. H., Mehta, A. J., 2001. Collisional aggregation of fine estuarine sediments. In:

McAnally, W. H., Mehta, A. J. (eds.), Coastal and Estuarine Fine Sediment Processes – Proceedings in Marine Science, 3. Amsterdam: Elsevier, 19–39.

McCave, I. N., 1975. Vertical flux of particles in the ocean. Deep Sea Research 22, 491–502.

McCave, I.N., 1984. Erosion, transport and deposition of fine-grained marine sediments. In: Stow, D. A. V., Piper, D. J. W. (eds.), Fine-Grained Sediments: Deep Water Processes and Facies. Oxford: Blackwell, 35–69.

McLaughlin, R.J., 1959. The settling properties of suspensions. Journal of Hydraulics Division, ASCE, Vol. 85 (HY12), 9-41

Mehta, A.J., 1988. Laboratory studies on cohesive sediment deposition and erosion. In: Dronkers and Van

Leusen (Editors), Physical Processes in Estuaries. Springer-Verlag, 427-445.

Mehta, A.J., 1991. Review notes on cohesive sediment erosion. In: N.C. Krauss et al. (Editors), Coastal

Sediments, Vol. I, 44-53.

Mehta, A.J.,1991. Characterization of cohesive soil bed surface erosion, with special reference to the relationship between erosion shear strength and bed density," Report UFL/COEL/MP-91/4, Coastal and Oceanographic Engineering Department, University of Florida, Gainesville, FL.

Mehta, A. J., 1992. Summary of the Ad Hoc Technical Panel at the nearshore and estuarine cohesive sediment transport workshop, Cohesive Sediments Newsletter, U.S. Army Engineer Waterways Experiment Station, Vicksburg, MS, USA

Mehta, A. J., 2002. Studies on erosion and settling of organic-rich sediment from Newnans Lake and other water bodies in Florida. U.S. Army Engineer Research and Development Center, Vicksburg, MS, USA.

Mehta, A. J., 2014. An Introduction to Hydraulics of Fine Sediment Transport. Advanced Series on Ocean Engineering, Vol. 38. Hackensack, NJ: World Scientific Publishing Co.

Mehta, A. J., Kirby, R., Stuck, J. D., Jiang, J., and Parchure, T. M., 1997. Erodibility of organic-rich sediments: A Florida perspective. Coastal and Oceanographic Engineering Department, University of Florida, Report No. UFL/COEL/MP 97/01, USA

Mehta, A. J., Lott, J. W., 1987. Sorting of fine sediment during deposition. Proceedings of the Conference on Advances in Understanding Coastal Sediment Processes 1, 348–362.

Mehta, A. J., Partheniades, E., 1975. An investigation of the depositional properties of flocculated fine sediment. Journal of Hydraulic Research 92, 361–381.

Mengual, B., Le Hir, P., Cayocca, F. and Garlan, T., 2017. Modelling fine sediment dynamics: towards a common erosion law for fine sand, mud and mixtures. Water, 9,564; doi:10.3390/w9080564

MUSA

Merckelbach, L.M., 1996. Consolidation theory and rheology of mud. Report no. 9. Department of Civil Engineering. Technical University of Delft.

Mietta, F., Chassagne, C., Manning, A.J. and Winterwerp, J.C., 2009. Influence of shear rate, organic matter content, pH and salinity on mud flocculation. Ocean Dynamics, 59, 751-763, doi: 10.1007/s10236-009-0231-4.

Migniot, C., 1968. Etude des Proprietes Physiques de Differents Sediments tres fins et de leur Comportement sous des Actions Hydrodynamiques. La Houille Blanche, Vol. 23, No. 7, 591-620.

Migniot, C. 1968. Studies of physical properties of fine sediments (in French). La Houille Blanche, Vol. 23 (No. 7).

Migniot, C., 1989. Bedding-down and Rheology of Muds, Part 1. La Houille Blanche, Vol. 44, No. 1, 11-29

Mikeš, D. and Manning, A.J., 2010. An assessment of flocculation kinetics of cohesive sediments from the Seine and Gironde Estuaries, France, through laboratory and field studies. Journal of Waterway, Port, Coastal, and Ocean Engineering (ASCE), Volume 136, Issue 6, 306-318, doi: 10.1061/(ASCE)WW.1943-5460.0000053.

Min Su, 2016. Progradation and erosion of a fine-grained tidally dominated delta. Doctoral Thesis, Department of Civil Engineering, Delft University of Technology, Delft, The Netherlands

Mitchener, H. and Torfs, H., 1996. Erosion of mud/sand mixtures. Coastal Engineering, Vol. 29, 1-25.

Mitchener, H. J., Torfs, H., Whitehouse, R. J. S., 1996. Erosion of mud/sand mixtures. Coastal Engineering 29, 1–25 [Errata, 1997, 30, 319].

Mobley, J., Melville, J. and Parker, F., 2009. Evaluation of scour potential of cohesive soils. Report 930-644. Highway Research Center, Auburn University, Alabama, USA

Mostafa, T.S., Imran, J., Chaudhry, M.H. and Kahn, I.B., 2008. Erosion resistance of cohesive soils. Journal of Hydraulic Research, Vol. 46, No. 6, 777-787

Murphy, B., Parsons, D., Rosewell, K., Ruessink, G., Schrijvershof, R., Wu, X., Ye, L., 2014. Wave ripples in mixtures of cohesive clay and cohesionless sand: preliminary results. Proceedings of the HYDRALAB IV Joint User Meeting, Lisbon, July 2014, pp. 1–9.

Noack, M., Gerbersdorf, S.U., Hillebrand, G. and Wieprecht, S. 2015. Combining field and laboratory measurements to determine the erosion risk of cohesive sediments beds. Water Vol. 7, 5061-5077 (doi:10.3390/w7095061).

Ockenden, M. C., Delo, E. A., 1988. Consolidation and erosion of estuarine mud and sand mixtures – an experimental study. HR Wallingford Report, SR 149.

Odd, N. V. M., 1988. Mathematical modelling of mud transport in estuaries. In: Dronkers, J., van

Leussen, W. (eds.), Physical Processes of Estuaries. Berlin: Springer Verlag, 503–531.

Opera 2015. Properties and behavior of the Boom Clay. Vlissingen, The Netherlands (www.covra.nl)

Otsubo, K. and Muraoka, K., 1988. Critical shear stress of cohesive bottom sediments. Journal of Hydraulic Engineering, Vol. 114, No. 10.

Panagiotopoulos, I.P., 1996. Clay influence on the threshold of movement and physical parameters of sand-mud deposits. Doctoral Thesis. Department of Oceanography, University of Southampton, UK.

Parchure, T.M. and Mehta, J.A., 1985. Erosion of soft cohesive sediment deposits. Journal of Hydraulic Engineering, ASCE, Vol. 111, No. 10.

Parchure, T. M., McAdory, R. T., Teeter, A. M., and Brown, B., 2002. Design of traps for sediment management in harbors and navigation channels, Proceedings of PACON 2002 International Conference held at Chiba, Japan.

Parchure, T.M. and Davis, J.E., 2005. Effect of organic materials on bulk density and erodibility of fine sediment beds. Report ERDC/CHL TR-05-07, US ARMY Corps of Engineers, Research and Development Center, Vicksburg, USA

MUSA

Parker, D. S., Kaufman, W. J., Jenkins, D., 1972. Floc break-up in turbulent flocculation processes. Journal of the Sanitary Engineering Division 98 (SA1), 79–97.

Parsons, D. R., Schindler, R.J., Hope, J.A., Malarkey, J., Baas, J.H., Peakall, J., Manning, A.J., Ye, L., Simmons, S., Paterson, D.M., Aspden, R.J., Bass, S.J., Davies, A.G., Lichtman, I.D. and Thorne, P.D., 2016. The role of biophysical cohesion on subaqueous bed form size, Geophys. Res. Lett., 43, 1566–1573, doi:10.1002/2016GL067667.

Partheniades, E., 1962. A study of erosion and deposition of cohesive soils in salt water. Doctoral Thesis, University of California, Berkeley, USA.

Partheniades, E., 1965. Erosion and deposition of cohesive soils. J. Hydraul. Div. Proc. ASCE, 91(HY1), 105-137.

Paterson, D. M., Hagerthey, S. E., 2001. Microphytobenthos in contrasting coastal ecosystems: Biology and dynamics. In: Reise, K. (ed.) Ecological Comparisons of Sedimentary Shores, Ecological Studies, vol. 151. Berlin: Springer, 105–125.

Peng Yao, Min Su, Wang, Z., Van Rijn, L.C., Zhang, C., Chen, Y. and Stive, M.J.F., 2015. Experiment-inspired numerical modeling of sediment concentration over sand–silt mixtures by Coastal Engineering, Vol. 105, 75-89

Peng Yao, 2016. Tidal and sediment dynamics in a fine-grained coastal region. Doctoral Thesis, Department of Civil Engineering, Delft University of Technology, Delft, The Netherlands

Peng Yao et al. 2015. Experiment inspired numerical modeling of sediment concentration over sand–silt mixtures by Coastal Engineering, Vol. 105, 75-89

Puls, W., Kuehl, H., Heymann, K., 1988. Settling velocity of mud flocs: results of field measurements in the Elbe and the Weser Estuary. In: Dronkers, J., Van Leussen, W. (eds), Physical Processes in Estuaries. Berlin: Springer-Verlag, 404–424.

Raudkivi, A. J., 1998. Loose Boundary Hydraulics. 3rd Edition. Rotterdam: Balkema.

Richardson, J.F. and Zaki, W.N., 1954. Sedimentation and fluidisation: Part I. Trans. Instn. Chem. Engrs., Vol. 32, 35-50

Richardson, J.F. and Meikle, R.A., 1961. Sedimentation and fluidisation: Part II. Trans. Instn. Chem. Engrs., Vol. 39, 348-356

Righetti, M. and Lucarelli, C., 2007. May the Shields theory be extended to cohesive and adhesive benthic sediments? Journal of Geophysical Research, Vol. 112.

Rijkswaterstaat 1996. Clay for dikes. TAW Technical Report. Department DWW, Delft, The Netherlands

Rijkswaterstaat/RIKZ 2002. Evaluation of the effects of the dispersal of Boom Clay in the Western Scheldt (in Dutch). Report 2002.052, Rijksinstituut voor Kust en Zee, The Hague, The Netherlands

Roberts, J., Jepsen, R., Gotthard, D. and Lick, W., 1998. Effects of particle size and bulk density on erosion of quartz particles. Journal of Hydraulic Engineering, ASCE, Vol. 124, No. 12.

Ross, M. A., 1988. Vertical structure of estuarine fine sediment suspensions. Ph.D. thesis, University of Florida, Gainesville.

Sanford, L.P.,Halka,J.P.,1993. Assessing the paradigm of mutually exclusive erosion and deposition of mud, with examples from upper Chesapeake Bay. Marine Geology 114,37–57

Schindler, R.J., Parsons, D.R., Ye, L., Hope, J.A., Baas, J.H., Peakall, J., Manning, A.J., Aspden, R.J., Malarkey, J,, Simmons, S., Paterson, D.M., Lichtman, I.D., Davies ,A.G., Thorne, P.D., Bass S.J., 2015. Sticky stuff: redefining bedform prediction in modern and ancient environments. Geology 43:399–402.

Shepard, F.P., 1954. Nomenclature based on sand-slit-clay ratios. Journal of Sedimentary Petrology, Vol. 24, 151-158

Sheremet, A., Sahin, C. and Manning, A.J., 2017. Flocculation: A General Aggregation-Fragmentation Framework. Proceedings of the 35th International Conference on Coastal

MUSA

Engineering - ICCE 2016, Antalya, Turkey, 2016, Editor: P. Lynett, Vol. No. 35, Sediments Article 28, ISBN: 978-0-9896611-3-3.

Shields, A. 1936. Anwendung der ähnlichkeitsmechanik und der turbulenz forschung auf die geschiebebewegung. Mitt. der Pruess. Versuchsamst. für Wasserbau und Schiffbau. Heft 26, Berlin, Germany

Shi, Z. and Zhou, H.J., 2004. Controls on effective settling velocities of mud flocs in the Changjiang Estuary, China. Hydrological Processes 18, 2877-2892. Doi: 10.1002/hyp.1500

Shynu, R. et al. 2017. Suspended matter and fluid mud off Alleppey, southwest coast of India. Estuarine, Coastal Shelf Science, vol.185(5); 31-43

Smerdon, E.T. and Beasley, R.P., 1961. Critical tractive forces in cohesive soils. Agricultural Engineering, St. Joseph, Mich., 42(1), 26–29.

Smith, J, Perkey, D. and Priestas, A., 2015. Erosion thresholds and rates for sand-mud mixtures. Technical Report, US Army Engineer Research and Development Center, Vicksburg, MS, USA

Soulsby, R. L., L. Hamm, G. Klopman, D. Myrhaug, R. R. Simons and G. P. Thomas, 1993. Wave-current interaction within and outside the bottom boundary layer. Coastal Engineering 21: 41–69.

Soulsby, R. L., 1997. Dynamics of Marine Sands. London: Thomas Telford.

Soulsby, R.L., Manning, A.J., Spearman, J. and Whitehouse, R.J.S., 2013. Settling velocity and mass settling flux of flocculated estuarine sediments. Marine Geology, doi.org/10.1016/j.margeo.2013.04.006.

Spearman, J. and Manning, A.J., 2017. On the hindered settling of sand-mud suspensions. Ocean Dynamics, DOI 10.1007/s10236-017-1034-7.

Spearman, J.R., Manning, A.J. and Whitehouse, R.J.S., 2011. The settling dynamics of flocculating mud:sand mixtures: Part 2 – Numerical modelling. Ocean Dyn., doi: 10.1007/s10236-011-0385-8.

Spearman J R, Taylor J, Crossouard N, Cooper A, Turnbull M, Manning A.J., Lee M and Murton, B., 2020. Measurement and modelling of deep sea sediment plumes and implications for deep sea mining, Nature Scientific reports 10 (1), 1-14.

Stokes, G. G., 1851. On the effect of the internal friction on the motion of pendulums, Transactions of the Cambridge Philosophical Society, 9, 8–106.

Stolzenbach, K. D., Elimelich, M., 1994. The effect of density on collisions between sinking

particles: implications for particle aggregation in the ocean. Journal of Deep Sea Research I 41, 469–483.

Sutherland, T.F., Amos, C.L. and Grant, J., 1998. The effect of buoyant biofilms on the erodibility of sublittoral sediments of a temperate microtidal estuary. Limnology Oceanography, Vol. 43, No. 2, 225-235.

Tambo, N., Hozumi, H., 1979. Physical characteristics of flocs – II. Strength of flocs. Water Research 13, 441–448.

Tambo, N., Watanabe, Y., 1979. Physical characteristics of flocs – I. The floc density function and

aluminium floc. Water Research 13, 429–439.

Te Slaa, S., 2020. Deposition and erosion of silt-rich sediment-water mixtures. Doctoral Thesis, Department of Civil Engineering. Delft University of Technology, Delft, The Netherlands

Te Slaa, S., He, Q., Van Maren, D.S. and Wintwerwerp, J.C., 2013. Sedimentation processes in silt-rich sediment systems. Ocean Dynamics, Vol. 63 (4), 399-421

Thomsen, L. and Gust, G., 2000. Sediment erosion thresholds and characteristics of resuspended aggregates on the Western European Continental margin. Deep-Sea Research I, Vol. 47, 1881-1897

Thorn, M.F.C., 1981. Physical processes of siltation in tidal channels. Proc. Hydraulic Modelling, Paper No. 6, ICE, London, UK.

Tolhurst, T. J., Gust. G., Paterson, D. M., 2002. The influence on an extra-cellular polymeric

substance (EPS) on cohesive sediment stability. In: Winterwerp, J.C., Kranenburg, C. (eds.), Fine Sediment Dynamics in the Marine Environment – Proceedings in Marine Science 5, Amsterdam: Elsevier, pp. 409–425.

Tolhurst, T.J., Riethmueller, R. and Paterson, D.M., 2000. In situ versus laboratory analysis of sediment stability from intertidal mudflats. Continental Shelf Research, 20, 1317-1334.

Torfs, H., Mitchener, H., Huysentruyt, H and Toorman, E., 1996. Settling and consolidation of mud/sand mixtures. Coastal Engineering 29, 27-45

Uncles, R. J., Bale, A. J., Brinsley, M. D., Frickers, P. E., Harris, C., Lewis, R. E., Pope, N. D.,

Staff, F. J., Stephens, J. A., Turley, C. M., Widdows, J., 2003. Intertidal mudflat properties,

currents and sediment erosion in the partially mixed Tamar Estuary, UK. Ocean Dynamics 53, 239–251. DOI: 10.1007/s10236-003-0047-6.

Uncles, R. J., Bale, A. J., Stephens, J. A., Frickers, P. E., Harris, C., 2010. Observations of floc sizes in a muddy estuary. Estuarine, Coastal and Shelf Science 87, 186–196.

Underwood, G. J. C., Kromkamp, J., 1999. Primary production by phytoplankton and microphytobenthos in estuaries. Advances in Ecological Research 29, 93–153.

Underwood, G. J. C., Paterson, D. M., 2003. The Importance of Extracellular Carbohydrate

Production by marine Epipelic Diatoms. Advances in Botanical Research (incorporating Advances in Plant Pathology), Vol. 40. Amsterdam: Elsevier, 183–240.

Van, L.A., Villaret, C., Pham Van Bang, D. and Schuettrumpf, H., 2012. Erosion and deposition of the Gironde mud. ICSE 6, Paris.

Van den Berg, J.H. and Van Gelder, A., 1993. Prediction of suspended bed material transport in flows over silt and very fine sand. Water Resources Research, Vol. 29, No. 5 p. 1393-1404

Van den Berg, J.H., Van Gelder, A. and Mastbergen, D.R., 2002. The importance of breaching as a mechanism of subaqueous slope failure in fine sand. Sedimentology Vol. 49, 81-95

Van de Koppel, J., Herman, P.M.J., Thoolen, P., Heip, C.H.R., 2001. Do alternate stable states occur in natural

ecosystems? Evidence from a tidal flat. Ecology 82 (12), 3449–3461.

Van der Lee, W.T.B., 2000. The settling of mud flocs in the Dollard estuary., The Netherlands. Doctoral Thesis Department of Physical Geography, University of Utrecht, The Netherlands

van der Lee, E. M., Bowers, D. G., Kyte, E., 2009. Remote sensing of temporal and spatial patterns of suspended particle size in the Irish Sea in relation to the Kolmogorov microscale. Continental Shelf Research 29, 1213–1225.

van de Ven, T. G., Hunter, R. J., 1977. The energy dissipation in sheared coagulated soils. Rheologica Acta 16, 534–543.

Van Kessel,T., and Van Lede, J., 2009. Impact of harbour basins on mud dynamics in the Scheldt estuary. Deltares & Flanders Hydraulics Report No. 1200253, Delft, The Netherlands**.**

van Ledden, M., 2002. A process-based sand-mud model. In: Winterwerp, J.C. Kranenburg, C. (eds.), Fine Sediment Dynamics in the Marine Environment – Proceedings in Marine Science 5, Amsterdam: Elsevier, 577–594.

MUSA

van Ledden, M., 2003. Sand-mud segregation in estuaries and tidal basins. Ph.D. Thesis, Delft University of Technology, The Netherlands, Report No. 03–2, ISSN 0169-6548, 217pp.

Van Ledden, M., Van Kesteren, W.G.M. and Winterwerp, J.C., 2004. A conceptual framework for the erosion behaviour of sand-mud mixtures. Continental Shelf Research 24, 1-11.

van Leussen, W., 1988. Aggregation of particles, settling velocity of mud flocs: A review. In:

Dronkers, J., van Leussen, W. (eds.), Physical Processes in Estuaries. Berlin: Springer-Verlag, 347–403.

Van Leussen W., 1994. Estuarine Macroflocs and their Role in Fine-grained Sediment Transport. Doctoral Thesis. University of Utrecht, Utrecht.

Van Leussen, W., 2011. Macroflocs, fine-grained sediment transports and their longitudinal variations in the Ems estuary. Ocean Dynamics 61, 387-401. Doi: 10.1007/s10236-011-0384-9

Van Maren, D.S., Vroom, J., Fettweis , M., Vanlede, J., 2020. Formation of the Zeebrugge coastal turbidity maximum: The role of uncertainty in near-bed exchange processes. Marine Geology, 425. Doi: https://doi.org/10.1016/j.margeo.2020.106186

van Olphen, H., 1977. An introduction to Clay Colloid Chemistry. For Clay Technologists, Geologists, and Soil Scientists, 2nd edition. New York: John Wiley and Sons.

Van Rijn, L.C., 1984. Sediment pickup functions. Journal of Hydraulic Engineering, ASCE. Vol. 110, No 10

Van Rijn, L.C. 2016. Deposition and dredging of a small ferry channel through sand-mud flats in Dutch Wadden Sea, LVR-Sediment Consultancy, Blokzijl, The Netherlands (www.leovanrijn-sediment.com)

Van Rijn, L.C., 2018. Consolidation of mud-sand mixtures. LVR-Sediment Consultancy, Blokzijl, The Netherlands (www.leovanrijn-sediment.com)

Van Rijn, L.C., 2019. Erodibility of mud-sand bed mixtures. Journal of Hydraulic Engineering, ASCE, USA. Doi: 10.1061/(ASCE)HY.1943.7900.0001677

Van Rijn. L.C., 2019. Settling velocity of mud. www.leovanrijn-sediment.com

Van Rijn, L.C. and Louisse, C.J., 1987. The Effect of Waves on Cohesive Bed Surfaces. Proc. Coastal and Port Eng. Cnf., Beijing, China.

Van Rijn, L.C., and Barth, R. 2019. Settling and consolidation of soft mud-sand layers. Journal of Waterway, Port, Coastal and Ocean Engineering, ASCE, Vol. 145(1). DOI: 10.1061/(ASCE)WW.1943-5460.0000483

Van Rijn, L.C., Riethmueller, R. and Rarth, R. 2018. Erodibility of mud-sand mixtures. Report of experimental results. www.leovanrijn-sediment.com

Van Rijn, L.C., Bisschop, R. and Van Rhee, C. 2019. Modified Sediment pick-up function. Journal of Hydraulic Engineering ASCE, Vol. 145(1). DOI: 10.1061/(ASCE)HY.1943-7900.0001549

Vinzon, S.B. and Mehta, A.J., 2003. Lutoclines in high concentration estuaries: some observations at the mouth of the Amazon, p. 243-253. Journal of Coastal Research, Vol. 19, No. 2

Wacholder, E., Sather, N. F., 1974. The hydrodynamic interaction of two unequal spheres moving under gravity through quiescent viscous fluid. Journal of Fluid Mechanics 5, 417–437.

Wang, Y.P. et al., 2012. Sediment transport over an accretional intertidal flat with influences of reclamation, Jiangsu coast, China. Marine Geology, 291: 147-161.

Waterproofbv, 2019. Metingen Holwerd-Ameland; meetresultaten en laboratoriumanalyse metingen januari-maart 2019. Rapport WP2018_1155-R3r2, Lelystad, The Netherlands (in Dutch)

Waterproofbv, 2020. Metingen Holwerd-Ameland; meetresultaten en laboratoriumanalyse T1 metingen september-october 2019. Rapport WP2019_1176-R1r1, Lelystad, The Netherlands (in Dutch)

Literature review on sand and mud
16 November 2020

MUSA

Whitehouse, R. J. S., Soulsby, R., Roberts, W., Mitchener, H. J., 2000. Dynamics of Estuarine Muds. London: Thomas Telford Publications.

Wiberg, Patricia L., Brent A.Law, Robert A. Wheatcroft, Timothy G. Milligan, Paul S. Hill, 2013. Seasonal variations in erodibility and sediment transport potential in a mesotidal channel-flat complex, Willapa Bay, WA. Continental Shelf Research 60S, S185–S197.

Widdows, J., Blauw, A., Heip, C. H. R., Herman, P. M. J., Lucas, C. H., Middelburg, J. J.,

Schmidt, S., Brinsley, M. D., Twisk, F., Verbeek, H., 2004. Role of physical and biological processes in sediment dynamics of a tidal flat in Westerschelde Estuary, SW Netherlands. Marine Ecology Progress Series 274, 41–56.

Widdows, J., Brinsley, M.D., Salkeld, P.N., Lucas, C.H., 2000. Influence of biota on spatial and temporal variation in sediment erodability and material flux on a tidal flat (Westerschelde estuary). Marine Ecology Progress Series 194, 23–37.

Widdows, J. P.L. Friend, A.J. Bale, M.D. Brinsley, N.D. Pope, C.E.L. Thompson, 2007. Inter-comparison between five devices for determining erodability of intertidal sediments. Continental Shelf Research 27, p. 1174–1189

Williamson, H. J., Ockenden, M. C., 1993. Laboratory and field investigations of mud and sand mixtures. In: Wang, S. S. Y (ed.), Advances in Hydro-science and Engineering, Proceedings of the First International Conference on Hydro-science and Engineering, Washington D.C. (7–11 June 1993), Volume 1. University, MS: Center for Computational Hydroscience and Engineering, the University of Mississippi, 622–629.

Winterwerp, J. C., 1998. A simple model for turbulence induced flocculation of cohesive sediment. Journal of Hydraulic Engineering 36, 309–326.

Winterwerp, J. 1999. On the dynamics of high-concentrated mud suspensions. Doctoral Thesis, Department of Civil Engineering, Technical University of Delft, The Netherlands

Winterwerp J.C., 2007. On the deposition flux of cohesive sediment. In: Maa J, Sanford L, Schoelhamer D, Proceedings of the 8th International Conference on Nearshore and Estuarine Cohesive Sediment Transport Processes, INTERCOH-2003, Gloucester Point, USA, pp. 209–226

Winterwerp, J.C., 2011. Fine sediment transport by tidal asymmetry in the high-concentrated Ems river: indications for a regime shift in response to channel deepening. Ocean Dynamics

Winterwerp, J.C., Cornelisse, J.M. and Kuijper, C., 1991. Erosion of natural sediments from The Netherlands. ReportZ161-35/37. Deltares, Delft, The Netherlands

Winterwerp, J.C. and Van Kesteren, W.G.M., 2004. Introduction to the physics of cohesive sediment in the marine environment. Elsevier, Developments in sedimentology, ISBN 0-4444-51553-4.

Winterwerp, J.C., Van Kesteren, W.G.M., Van Prooijen, B. and Jacobs, W., 2012. A conceptual framework for shear flow-induced erosion of soft cohesive sediment beds. Journal of Geophysical Research, Vol. 117, C10020, Doi: 10.1029/2012JC008072

Wolanski, E., 2007. Estuarine Ecohydrology. Amsterdam, The Netherlands: Elsevier.

Wolters, G., Nieuwenhuis, J.W., Van der Meer, J. and Klein Breteler, M., 2008. Large scale tests of boulder clay erosion at the Wieringermeer dike (IJsselmeer). ICCE 2008, Hamburg, Germany

Wu, W., and Li, W., 2017. Porosity of bimodal sediment mixture with particle filling. International Journal Sediment Research, 32(2), 253-259, Doi:10.1016/j.ijsrc.2017.03.005.

Wu, W., Perera, C., Smith, J. and Sanchez, A., 2017. Critical shear stress for erosion of sand and mud mixtures. Journal of Hydraulic Research, Doi.org/10.1080/00221686.2017.1300195

Yang, H. and Hou, Z.Q., 2004. Study on siltation in the outer channel of Huanhua Harbor. Journal of Waterway and Harbor, 25: 59-63.

Zhao, Q. and Han, H., 2007. Siltation mechanisms of Huanghua Port and 3 D characteristics of nearshore suspended sediment concentration under waves. Shuidao Gangkou (Journal of Waterway and Harbor), 28(2): 77-80.

MUSA

Zhang, Q.H. et al. 2010. Simulation of sorting sedimentation in the channel of Huanghua harbor by using 3d multi-sized sediment transport model of efdc. Coastal Engineering ICCE 32, Sjanghai 2010, China

MUSA

A Summary of experimental results of erosion of soft mud-sand bed mixtures

A.1 General

Various studies on soft mud-sand mixtures are available in the Literature. An important study of the erosion of soft mud-sand beds to be discussed in more detail is that of Mitchener and Torfs (1996) who presented many data of laboratory and field experiments. Both artificially made homogeneous and layered beds were tested. Field tests were done using in-situ instruments, and field samples were also returned to a straight flume. Detailed interpretation of their data is not easy, as they did not use the same definitions for defining the bed composition, while the type of erosion (particle, surface, mass erosion) and important parameters as the bed density and the percentage of the clay-dominated fractions were not always given for the mixtures of natural mud and sand. The most significant effect on erosion resistance was found by adding small percentages of kaolinite/montmorillonite clay (by weight) to sand. The mode of erosion changed from cohesionless to cohesive behaviour at low clay contents added to sand, with a transition occurring in the region 5% to 15% mud (by weight). The highest critical bed-shear stress in the case of homogeneously mixed beds was observed to occur for a percentage of mud of 50% to 70% (by weight). The erosional properties were found to be strongly dependent on the type/history of the bed deposits (mud content, homogeneously mixed or layered bed structure; weak or firmly consolidated). Some of their data from artificial mixtures of clay/mud and sand are used and discussed in this study.

Panagiotopoulos (1996) is one of the few, who studied the critical erosion velocity of artificial mud-silt-sand mixtures (density values of 250 to 1200 kg/m³) under waves and combined currents and waves in a laboratory flume. The critical erosion velocity of the sand fraction was found to increase from 30% to 50% when 50% mud was added.

Field experiments using in-situ instruments is a special class of work of utmost importance (Amos et al.,1992, 1996, 1997; Sutherland et al., 1998; Tolhurst et al., 2000; Andersen, 2001; Aberle et al., 2006 and Debnath et al., 2007; Andersen et al., 2010; Houwing, 2000; Noack et al., 2015). Various types of erosion instruments were used: in-situ circular and straight flumes; in situ EROMES-tube with propeller (also used in this study). Similarly, the critical bed-shear stress (mostly in the range of 0.2 to 1 Pa) was found to increase with dry density and the percentage of clay and fines (< 63 μm). The study of Noack et al. (2015) is important as it offers a complete data set for muddy river beds in Germany (data used in this study).

Various studies of the Literature show the presence of various modes of erosion (Partheniades, 1962, 1965; Metha 1988, 1991a,b; Winterwerp and Van Kesteren 2004; Kothyari and Jain 2008; Winterwerp et al. 2012):

- particle/floc erosion, which is the limited pick-up of individual particles and flocs of the (fluffy) top layer;
- surface erosion, which is the simultaneous mobilization of several layers of particles and flocs;
- mass erosion, which is the erosion of lumps of bed material (bed failure) when the applied fluid stresses are larger than the undrained (remoulded) soil strength of the bed.

Most of the studies reviewed did not include (or only implicitly) the effect of organic materials. An exception is the study of Parchure and Davis (2005) who analysed many field mud samples (USA) with organic matter content in the range of 1% to 75%. The bulk density decreased significantly for increasing values of the organic content (by weight). The

MUSA

dry density was about 1200 kg/m³ for 5% organic content reducing to about 200 kg/m³ for 30% organic content. The erosion rate was significantly affected by the amount of organic content. The erosion rate at a shear stress of 0.2 Pa reduced by a factor of 7 for organic contents from 10% to 60%. This shows that the content of organic matter can have a very strong effect, particularly for high values of the organic content (>> 10%).

Generally accepted relationships for the prediction of critical shear stress are not yet available in the Literature. Winterwerp et al. (2012) proposed a conceptual framework for shear-induced erosion of soft mud beds. They argue that mass erosion occurs when the flow-induced stress exceeds the undrained shear strength of the bed based on the Mohr-Coulomb approach. The undrained strength is a bulk soil property resulting from a triaxial test or a simple in situ vane test. Relationships between the (vane) shear strength and the critical shear stress for erosion have been proposed earlier (Dunn, 1959).

Ahmad et al. (2011) proposed a simple formulation for the determination of the critical bed shear stress for soft mixed beds based on the critical shear stresses for pure sand and pure mud. But the effect of the dry density of the mixed bed was not taken into account by Ahmad et al. (2011) limiting their method to a narrow range of low-density beds. Wu et al. (2017) proposed a general method for the critical bed shear stress including the effect of the dry density. The relationships proposed by Ahmad et al. (2011) and Wu et al. (2017) are tested in this study. Van Rijn (2007) has presented a unified view on the transport of sand and mud. The effect of mud on the critical stress for the sand fraction was represented by a fairly simple relationship which is improved in this study.

A.2 Pure mud beds (before 2016)

Many studies on the erodibility of pure mud beds in estuarine and marine conditions are summarized in Table A2.1 with information of the critical shear stresses for surface and mass erosion of various types of mud beds with sand percentages <10%. The results of the in-situ field tests are more representative than the results of the laboratory flume tests which involve the handling/preparation of a mud bed.

The critical bed-shear for surface erosion of a weakly consolidated mud bed with a dry bulk density <400 kg/m³ is of the order of 0.2 ± 0.15 N/m². The critical bed-shear for mass erosion of a weakly consolidated mud bed is a factor of 2 to 3 larger.

The critical bed-shear for erosion of a firmly consolidated mud bed with a dry bulk density >800 kg/m³ is of the order of 1 ± 0.5 N/m².

MUSA

Table A.2.1 Critical bed-shear stress for erosion; pure mud beds ($d_{50} < 32 \mu m$)

Mud beds	Test method	Dry bulk density (kg/m³)	Critical bed-shear stress for surface erosion (N/m²)	Critical bed-shear stress for mass erosion (N/m²)
Kaolinite (distilled water); Van Rijn 1993	Lab. flume	100-200	0.05-0.2	
Kaolinite (saline water); Van Rijn 1993	Lab. flume	100-200	0.05-0.4	
Dutch lake muds (fresh water); Van Rijn 1993	Lab. flume	100-300	0.1-0.4	0.6-0.7
Gironde subtidal mud; Van 2012	Lab. flume	300	0.2-0.3	0.7
River mud (submerged); Mostafa-Imran 2008	Lab. flume	>1000	0.05-0.3	0.3-1.5
China muds; Dou (2000)	Lab. flume	200-400	0.05-0.2	
UK muds; Thorn 1981	Lab. flume	<400	0.05-0.2	
Hong-Kong mud; Mitchener-Torfs 1996	Lab. flume	<400	0.1-0.15	
UK tidal flat muds; Mitchener-Torfs 1996	in-situ ISIS	400	0.05-0.25	
Hudson Bay subtidal mud; Amos 1996	in-situ SC	>1000	0.7-2	
Lunenburg subtidal mud; Sutherland 1998	in-situ SC	100-200	0.05-0.15	
Kongsmark tidal flat mud; Andersen 2001	in-situ EROMES	200-400	0.2-0.4	
Kjelst tidal flat mud; Andersen 2001	in-situ EROMES	200-400	0.2-0.4	

A.3 Mud-sand beds (before 2016)

Experiments of Deltares/Delft Hydraulics (1989)

Experiments were done to determine the critical bed-shear stress (in a flume) of the sand fraction of various natural bed core samples with diameter of about 0.07 m and lengths up to 2.5 m taken (using vibro-core equipment; May and June 1989) from the subtidal bed surface near a pipeline site in the Dutch Sector of the North Sea. The samples can be roughly classified as: fine sand (100 to 300 μm), silty sand and clayey silt, silty clay. The percentages of clay and very fine silt (<8 μm) were estimated to be in the range of 0 to 50%. The core samples were subdivided in subsamples with a length of about 0.1 m, which were placed in a cylindrical container at the bottom of a laboratory flume. The surface of the sample was exposed to the flow in the flume, which was successively raised until erosion of the bed surface was observed (movement of the sand particles). The critical bed-shear stress for a pure sand sample (200 μm) was found to be about 0.2 to 0.4 N/m², which is somewhat larger than the Shields value of 0.2 N/m² for sand with d_{50} of 200 μm. This may have been caused by the definition of the critical conditions for initiation of motion as used by the observers: "clear rolling of a considerable number of particles (order of dozens) during the entire test".

MUSA

Table A.3.1 Critical bed-shear stress of natural sand-mud mixtures of North Sea (Delft Hydraulics, 1989)

Type of sediment sample	Percentage of clay-dominated fraction	Ratio of critical bed-shear stress $\tau_{b,cr,sample}/\tau_{b,cr,pure\ sand}$
Fine sand (non-cohesive)	0%	1
Fine sand with silt (non-cohesive)	0 to 30%	1 to 2
Sand, very silty (cohesive)	30%	2 to 3
Silt, very clayey (grey) (cohesive)	50%	3 to 5
Clay, very silty (brown), (cohesive)	>50%	5 to 10

The critical bed-shear stress was estimated from measured critical velocities assuming a logarithmic velocity profile. The samples with $p_{clay}>0.3$ (p_{clay}=proportion of clay in bed sample) show a cohesive behaviour with relatively large critical bed-shear stresses ($\tau_{b,cr,sample}/\tau_{b,cr,pure\ sand}>2$). The sandy samples (about 200 μm) show a non-cohesive behaviour with relatively small critical bed-shear stresses ($\tau_{b,cr,sample}/\tau_{b,cr,pure\ sand} < 2$). The results are presented in Table A.3.1. The results for sand particles (>63 μm) can be roughly represented as: $\tau_{cr,bed}=(1+p_{clay})^3\ \tau_{cr,puresand}$.

Experiments of Mitchener and Torfs (1996)

They have summarized experimental results on the erodibility of mud-sand mixtures in laboratory and field conditions. Mud (or fines) is defined as clay and silt particles with sizes < 63 μm.

The data, which originate from both laboratory and field experiments, have been used to examine the physical processes behind the erosion behaviour of mud/sand mixtures. It was found that adding sand to mud, or vice versa, increases the erosion resistance and reduces the erosion rates when the critical shear stress for erosion is exceeded. The laboratory beds consist of homogeneously mixed beds and layered beds tested in flume experiments. Natural beds generally have a more layered structure. The field data from various UK-sites concern the in-situ testing of intertidal and subtidal beds using the ISIS-apparatus, which is an in-situ erosion bell consisting of an inverted, curved funnel. Water is drawn from the sides and up through the center of the funnel by pumping (HR Wallingford, 1992).

Table A.3.2 shows the critical bed-shear stresses for particle/surface erosion of laboratory and field tests based on the work of Mitchener and Torfs (1996). The field samples may have been affected by biogenic effects (not explicitly measured). The critical bed-shear stress of mud beds is related to the erosion of the topmost layer of 1 mm thick. If the mud percentage is larger than about 30%, a thin mud layer generally may have been present at the bed surface.

The critical shear stress for erosion increases when mud is added to sand, and also when sand is added to mud (mud < 63 μm). The addition of up to 50% sand to a mud bed can typically increase the critical erosion shear stress by a factor of 2. Conversely, the addition of 30% mud to a sand bed can increase the critical shear stress by as much as a factor of 10.

Table A.3.2 *Critical bed-shear stress of mud-sand mixtures (laboratory-field, Mixener and Torfs 1996)*

Type of bed	Percentage sand (150-250 µm)	Wet and dry bulk density (kg/m³)	Critical bed-shear stress of particle/surface erosion (N/m²)	
			Natural beds of UK sites (intertidal and subtidal)	Artificial beds (homogeneously mixed)
Pure mud	0%	1200-1300 (350-450)	0.05-0.25	0.1-0.15 (HK-mud)
Light sandy mud	20%	1300-1400 (450-650)	0.15-0.25	0.15-0.2 (HK-mud)
Sandy mud	40%	1400-1600 (650-950)	0.2-1.0	0.2-0.4 (HK-mud)
Muddy sand	60%	1600-1700	0.4-1.5	0.4-0.8 (K,M,S-muds)
Muddy sand	80%	1700-1800	0.6-1.8	1-3 (K,M,S-muds)
Light muddy sand	90%	1800-1900	?	0.5-1.5 (K,M,S-muds)
Pure sand (150-250 µm)	100%	1900-2000	0.15-0.2	0.15-0.2 (K,M,S-muds)

HK= Hong-Kong, S=Scheldt, K=Kaolinite, M=Montmorillonite

The critical shear stress at mud percentages of about 30% depends on the grain size of the sand (which anchors the critical shear stress at the 100% sand point) and the cohesive properties of the mud. The top layer may then consist of a thin muddy layer.

The addition of mud to sand significantly increases the critical erosion shear stress with a maximum value occurring at a mud content of between 30% and 50% by weight. If enough mud is added to sand (>50%), then the sediment mixture behaves as if it were a mud. It should also be realized that the bulk density depends on the compaction time scale for mixtures with mud contents > 30% (weakly and firmly consolidated bed mixtures can be present for mud contents > 30%).

Experiments of Roberts et al. (1998)

They have done experiments on initiation of motion of cohesive beds consisting of very small quartz particles (< 63 µm) with relatively high wet bulk densities (1600 to 1900 kg/m³). The sediments that were used in the tests consisted of quartz particles (99.5% pure) with mean diameters, *d* of 5.7, 14.8, 18.3, 48, 75, 125, 222, 432, 1,020, and 1,350 µm. Each sediment had a fairly narrow size distribution. These particle size distributions were measured by means of a Malvern particle sizer after thorough disaggregation of any flocculated sediments in a Waring blender.

In order to obtain different bulk densities for each sediment for the erosion tests, sediment cores were prepared as follows. Thirty to thirty-eight liters of each wet sediment were placed in a 45-liter cylindrical container and mixed with water for 15 to 30 min until the sediment-water mixture was homogeneous.

The amount of water added was enough to allow the mixture to be fluid, but care was taken to also keep the mixture thick so that stratification of the sediment due to differential settling of the particles did not occur. The sediment mixtures were then poured into coring tubes generally to a depth of 20 cm. These cores were then allowed to compact for 8 h to 124 days. Duplicate analysis cores were checked for repeatability and to ensure uniformity in particle size with depth. In order to determine the bulk density of the sediments at a particular depth and compaction time, the sediment analysis cores were frozen, sliced into

MUSA

3 to 4 cm sections, and then weighed (wet weight). They were then dried in the oven at approximately 75°C for 2 days and weighed again (dry weight).

For each sediment and compaction time, erosion rates were determined by means of flume tests at shear stresses from 0.2 to 6.4 N/m^2. This flume is essentially a straight flume that has a test section with an open bottom through which a rectangular cross section coring tube containing sediment can be inserted. This coring tube has a cross section that is 10 by 15 cm and, in the present experiments, is 20 to 40 cm long. Water is pumped through the flume at varying rates and produces a turbulent shear stress at the sediment-water interface in the test section. This shear stress is known as a function of flow rate from standard pipe flow theory. As the shear produced by the flow causes the sediments in the core to erode, the sediments are continually moved upward by the operator so that the sediment-water interface remains level with the bottom of the test and inlet sections.

As the rate of flow of water over a sediment bed is increased, there is a range of velocities (or shear stresses) at which the movement of the smallest and easiest-to-move particles is first noticeable to an observer. These eroded particles then travel a relatively short distance until they come to rest in a new location. This initial motion tends to occur only at a few isolated spots. As the flow velocity and shear stress increase further, more particles participate in this process of erosion, transport, and deposition, and the movement of the particles becomes more sustained. Because of this gradual increase in sediment erosion as the shear stress increases, it is difficult to precisely define a critical velocity or critical stress at which sediment erosion is first initiated. More quantitatively and with less ambiguity, a critical shear stress can be defined as the shear stress at which a small, but accurately measurable, rate of erosion occurs. This rate of erosion was chosen to be 10^{-4} cm/s; this represents 1 mm of erosion in approximately 15 min. Since it would be difficult to measure all critical shear stresses at an erosion rate of exactly 10^{-4} cm/s, erosion rates were generally measured above and below 10^{-4} cm/s at shear stresses that differ by a factor of two. The critical shear stress can then be obtained by interpolation between the two. This gives results with a 20% accuracy for the critical

In the experiments, sediments consisting of the larger particles consolidated relatively rapidly (seconds to minutes) and attained a relatively high wet bulk density (1850 to 1950 kg/m^3), which then did not change appreciably over several months. In contrast, sediments consisting of the finer particles consolidated slowly and did not reach a steady-state density over a period of several months; the range of bulk densities attained during this period of time (1650 to 1950 kg/m^3) was greater than for the larger particles.

Natural sediment beds consisting of sand, silt and clay (and organic material) have much lower densities, particularly when organic materials are involved (1100 to 1300 kg/m^3; Li et al., 2004). Based on the results of Roberts et al., it can be concluded that the critical bed-shear stress is minimum for about 63 μm. Cohesive effects become important for particles finer than 63 μm, which is manifest from the increase of the critical bed-shear stress for decreasing particle size. Experimental results of Roberts et al. for particle (quartz) sizes of 6, 15 and 50 μm in a bed with bulk density of about 1650 and 1700 kg/m^3 show critical bed shear stresses increasing from 0.08 N/m^2 to 0.25 N/m^2 for particle sizes decreasing from 50 to 6 μm. Their experiments also show that the critical bed-shear stress is affected by the packing of the bed (bulk density) and by the presence of clay particles. The presence of 2% Bentonite in a sand bed of relatively high wet density (1900 to 2000 kg/m^3) results in an increase of the critical bed-shear stress by a factor of about 1.5. The representative particle size of fine sediment beds smaller than about 32 μm is not well defined because most of the particles will not be eroded as single particles. Roberts et al. (1998) report that the silt particles (<32 μm) are eroded as aggregates (or chunks; mass erosion) which disintegrate as they are transported downstream.

MUSA

Experiments of Barry et al. (2006)

They have found a lubrication effect of clay particles on sand grain erosion. Minor changes in the mass physical properties of submerged sand beds can have significant consequences relative to bed stability against erosion. To examine the effect of small amounts of clay-sized particles in bed pore water on the critical shear stress for the erosion of sand grains, flume experiments were carried out on the erosion of quartz sand beds impregnated with clay particles. Starting with no clay, as the clay mass fraction (between 0 and 15% of the total mass of the samples; see Figure A.3.1) was increased, the critical shear stress of the sand particles at the top of the bed was found to decrease (probably due to lubrication effects) below the value for pure sand ($\tau_{b,cr,o}$) by about 40% to 50% and then reverted to $\tau_{b,cr,o}$ at a concentration $c_{clay,pore}$ and continued to increase (probably due to binding effects) as the mass fraction of clay was increased further. Post-experimental analysis suggests that $c_{clay,pore}$ is approximately equal to the pore space-filling clay fraction above which sand erosion is significantly influenced by clay. A sand bed sample has a porosity of about 0.4 or 400 liters per m^3, which can be filled with a mixture of clay (< 4 μm) of about 240 liters of clay (about 640 kg assuming porosity of 0.4 of the clay mixture) and 160 liters of pore water (40% of 400 liters) yielding an overall porosity of 0.16 of the clay-sand mixture. The wet bulk density of the clay-sand mixture is 1600 kg sand plus 640 kg clay plus 160 kg water or about 2400 kg/m^3. The maximum clay fraction filling the pores of the sand bed only is about 24% by volume (240 liters of clay/1000 liters) or 26% by mass (640/2400). The reduction effect is supposed to be caused by slider-bearing type lubrication due to the viscosity of the clay-laden interstitial fluid. It may also be a factor in the estimation of bed stability when biological activity in the benthic boundary layer introduces fine particles in clean sand beds. The reduction effect may only occur for the sand particles on top of the mixture bed. Sand particles buried in the bed may experience an increase of the critical bed-shear stress for erosion.
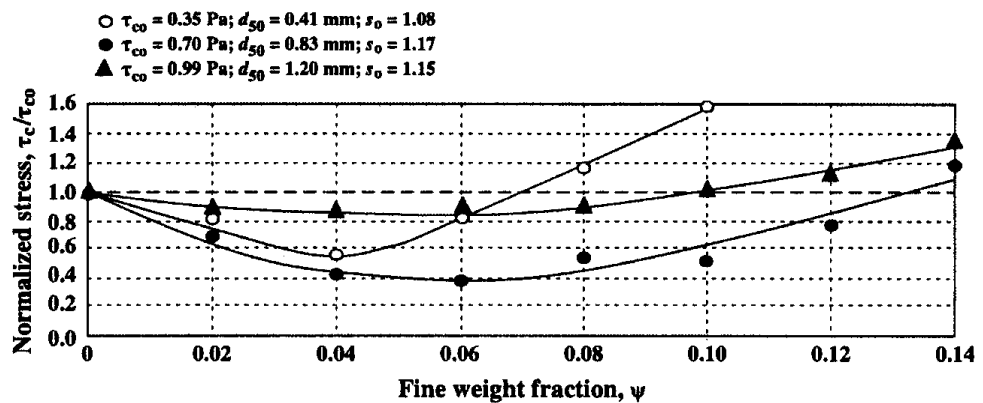

○ τ_{co} = 0.35 Pa; d_{50} = 0.41 mm; s_o = 1.08
● τ_{co} = 0.70 Pa; d_{50} = 0.83 mm; s_o = 1.17
▲ τ_{co} = 0.99 Pa; d_{50} = 1.20 mm; s_o = 1.15

Figure A.3.1 Effect of clay fraction on critical bed-shear stress of sand particles(ratio of critical stress and critical stress of pure sand on vertical axis); Barry et al. (2006)

Experiments of Jacobs (2011)

He has studied the erosion threshold stress of various mud-sand mixtures in a small-scale straight test flume (Erodimetre; length=1.2m, width=0.08 m, height=0.02 m; see Figure A.3.2; Le Hir et al., 2008.

Sediment mixtures are artificially generated using a dedicated experimental laboratory set-up at a constant temperature of 19°C. First, the individual fractions are oven-dried to disaggregate the material. Next, sand, silt and clay are manually mixed for around 10 minutes. The dry mixture is subsequently placed in a cylindrical container with a removable bottom-lid. Small holes (diameter = 3 mm) in the bottom and top-lid allow the passage of water and gas; paper filters at both ends retain the grains. The containers with dry sediments are placed in an exsiccator to remove air by lowering the pressure to 200 mbar.

Next, the exsiccator is filled with CO_2, after which the pressure is lowered again to replace enclosed air in the voids of the mixture with CO_2. Subsequently, mixtures are left for 24 hours in the exsiccator, in which a layer of water is present. The combination of the low pressure (reduced surface tension), 100% humidity and the attractive forces of the negatively charged clay particles enables water molecules to activate the clay particles in the smallest pores. The second part of the saturation process concerns the placement of a layer of 10 cm de-aired and demineralised water on top of the soil samples using the difference between the atmospheric and reduced pressure within the exsiccator. Subsequently, water percolated through the mixture, thereby completing the saturation procedure. The pressure induced by the water column corresponds with the target strength of the soil samples. Therefore, no consolidation is anticipated. The volume of water (about 0.5 liter) is sufficiently large to fill all pores and to dissolve all enclosed gas.

The saturation degree of the soil samples treated this way is about 100%. Using this method, relatively dense samples are obtained with wet bulk density values > 1800 kg/m^3. The relatively dense packing prevents segregation of the fractions during the saturation process. This experimental procedure generates reproducible and isotropic soil samples. This implies the absence of pore water pressure gradients, which would initiate swelling or consolidation. Particle size distributions were determined by using the Sedigraph and Malvern laser-diffraction methods.

The flume has a sediment container at the bottom where sediment cores can be placed and pushed upwards. Sub samples with a thickness of 2 to 3 cm were used. The surface of the soil sample was horizontally and vertically levelled with the bottom of the flume using four screws. The whole exposed surface area was presumed to contribute to erosion. The bottom of the flume was covered with sandpaper (with a roughness comparable to the applied sand fraction) to decrease differences in roughness with the sample. In practice, nearly no scour was observed at the upstream side of the samples.

A unidirectional flow generated by a re-circulating pump was accelerated step by step (average duration of a step approximately 150 - 200 seconds), until the sample was eroded by a few mm. The flow rate was controlled through a velocity meter in the pump. The volume of eroded sand was monitored at a sand trap downstream of the sediment sample, at the end of each velocity step. After the test, the total dry-mass of this material was determined. The grain size distributions of both the original soil samples and the sand trap material were determined using a laser-granulometer.

Cracks occurred for all soil samples with a dominant clay-water matrix and was characterised by cracks in the surface layer of the soil samples, and by uneven erosion patterns. Figure A.3.3 shows that both radial cracks (mostly) and cracks parallel to the flow direction exist (longitudinal cracks). Before and during the formation of the cracks, individual flocs and sand grains (particle erosion) were simultaneously eroded. Also, some aggregates of sediment randomly eroded from the cracks, which generated somewhat less accurate sand trap and concentration readings. Most soil samples did not exhibit either of the features during the surface erosion of individual sand and mud particles. Sand arrives in the sand trap within seconds after erosion. Identical behaviour was found for soil samples with kaolinite and bentonite.

Some test results are given in Table A.3.3, showing an increase of the erosion threshold stress with increasing percentage of mud.

MUSA

Table A.3.3 Critical bed-shear stress of particle/surface erosion of highly-consolidated mud-sand mixtures in laboratory flume (Jacobs 2011)

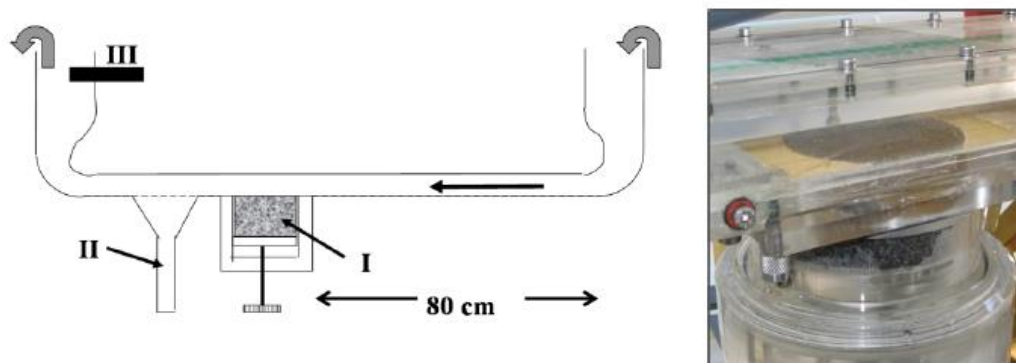| Tests	Percentage sand (%)	Percentage silt (%)	Percentage clay(%)	Percentage mud < 63 μm (%)	Mean sediment size (μm)	Wet bulk density (kg/m^3)	Critical bed-shear stress of particle/surface erosion (N/m^2)
1	90-100	< 8	<2	10	100-150	>1800	0.18$\pm$20%
13, 14	75	18	7	25	80-100	>1800	0.5$\pm$30%
18, 19	45	43	12	55	60-80	>1800	0.7$\pm$40%
5	20	65	15	80	30-60	>1800	1$\pm$40%

Figure A.3.2 Small-scale test flume with sediment lift (I=lift; II=trap)

Figure A.3.3 Examples of eroded surfaces with cracks (Jacobs 2011)

Experiments of Le Hir et al. (2008)

He has studied the erosion threshold stress in a small-scale flume of natural mud. He used firmly consolidated sample cores from the intertidal zone of the Mont St-Michel Bay (France).

The top layer of the container was eroded over a few millimeters in 1 to 2 hours. The results clearly indicate the presence of two erosion types: particle/floc erosion and surface erosion. The dominant size of the sand is about 140 μm. The dominant clay minerals are kaolinite and illite; carbonates are also present. Organic content is low (<2%). Results are given in Table A.3.4.

MUSA

Table A.3.4 Critical bed-shear stress of erosion of consolidated mud-sand mixtures (Le Hir et al. 2008)

Percentage mud < 63 μm (%)	Critical bed-shear stress of particle/surface erosion (N/m²)
20	0.25±20%
30	0.4±20%
40	0.6±20%
60	1.1±25%
70	1.5±25%
90	2.0±30%

Experiments of Houwing (2000)

He has used an in-situ erosion flume to determine the critical bed-shear stress for erosion of sand-mud mixtures at tidal mud-sand flats in the southern Wadden Sea (The Netherlands). His results are presented in Table A.3.5. The critical bed-shear stress for an almost pure sand bed (d_{50}= 80 μm, d_{10}=65 μm, d_{90}=110 μm; p_{clay}=4%) is about 0.18 N/m², which agrees rather well with the Shields-value for fine sand of 110 μm. The critical bed-shear stresses for 7 stations with p_{cfs} of about 20% are in the range of 0.1 to 0.18 N/m². The critical bed-shear stress for 1 station with p_{clay}=35% is larger than 0.5 N/m² (outside maximum range of in-situ erosion flume). For p_{clay}<25% the critical bed-shear stress for erosion is hardly affected by the presence of clay, which is an indication of the non-cohesive behaviour of most samples. One sample with p_{clay}=35% shows a typical cohesive behaviour. Hence, the critical clay-silt content for this site (tidal mud-sand flat) is about $p_{clay,cr}$= 30%. The erodibility of the bed surface decreases with increasing clay-silt content (Table A.3.5).

Table A.3.5 Critical bed-shear stress of natural sediment mixtures for intertidal flats (Houwing, 2000)

Type of sediment sample		Percentage of clay + fine silt materials	Critical bed-shear stress of particle erosion (N/m²)	Erodibility of bed (kg/m²/s)
1 station (18)	(non-cohesive)	4%	0.18	0.003
1 station (12)	(non-cohesive)	8%	0.15	0.002
7 stations	(non-cohesive)	13 to 23%	0.10-0.18	0.00008 to 0.002
1 station (10)	(cohesive)	35%	>0.5	0.00006

Experiments of Amos et al. (1997)

They have studied the stability and erodibility of fine-grained sediments on the foreshore and upper foreslope of the tidal Fraser River delta (Canada) using the *insitu* sea carousel flume, see Figure A.3.4. The erosion threshold varied between 0·1 and 0·5 N/m² and was proportional to the sediment wet bulk density.

Three erosion types were observed:

- Type IA-erosion was a surface phenomenon caused by the presence of a thin organic (fluffy) layer and occurred at current speeds less than 0·3 m/s;
- Type 1B-erosion (asymptotically decaying with time) characterized the mid portions of each erosion-time series, and occurred at current speeds of 0·3–0·9 m/s; video observations showed that Type I- erosion is largely the result of entrainment of small aggregates and flocs;
- Type I/II-erosion (transitional) was largely found on the foreslope, and occurred at current speeds in excess of 0·8 m/s; Type II erosion was the result of enlargement of surface irregularities, and subsequent undercutting and release of large aggregates (mass erosion).

MUSA

Table A.3.6 Critical bed-shear stress of surface erosion at intertidal mud flats of tidal Fraser River, Canada (Amos et al., 1997)

Stations	Percentage sand (%)	Percentage silt (%)	Percentage clay (%)	Percentage organics (%)	Mean sediment size (μm)	Wet and dry bulk density (kg/m³)	Critical bed-shear stress of particle/surface erosion (N/m²)
2	5	70	25	3	8	850	0.15
1 and 14	10	70	20	2	22	1040-1270 (50-450)	0.2-0.4
13	20	50	25	3	13	1170 (450)	0.2-0.5
3 and 7	35	45	20	5	20	950-1040 (<50)	0.1-0.25

Sediment stability was measured at 12 stations across Sturgeon Bank. Stations were occupied on the inner littoral mud flat, the littoral sand flat and the sub-littoral foreshore muds. Stations 1, 2, 3, 7, 8, 13 and 14 were situated at mud-dominated locations; the other stations were at sand-dominated locations. Stations 7 and 8 were situated on the steeply dipping upper foreslope of the Fraser River delta at a depth of 15 m below lowest low water. The foreshore mud flat is bioturbated and pelletized by a diverse invertebrate infauna. The tides in the region are mixed semi-diurnal reaching 4·8 m in range. Surface currents over the foreslope flow northward at a rate of 0·3–0·5 m/s. The region is relatively sheltered from waves.

Sea Carousel was deployed from a floating pontoon during the marine inundation of the tidal flat, thereby encapsulating the natural, saturated substrata and the overlying epibenthic water mass.

Sea-bed samples of the foreshore stations were collected during tidal exposure of the flats. Bulk samples were collected by using a gravity corer and by skimming the surface veneer of sediment with a spatula. Bottles of known volume were used to collect samples for water content and wet bulk density. At some stations the wet bulk density was smaller than 1000 kg/m³, which is an indication for the presence of bioturbations, organic materials and flocculated aggregates.

The results are shown in Table A.3.6. The sedimentation rate is a dominant factor influencing sediment stability in the region. At locations where the sedimentation rates are relatively high, the bulk density and the threshold stresses are relatively low (0.15 to 0.25 N/m2).
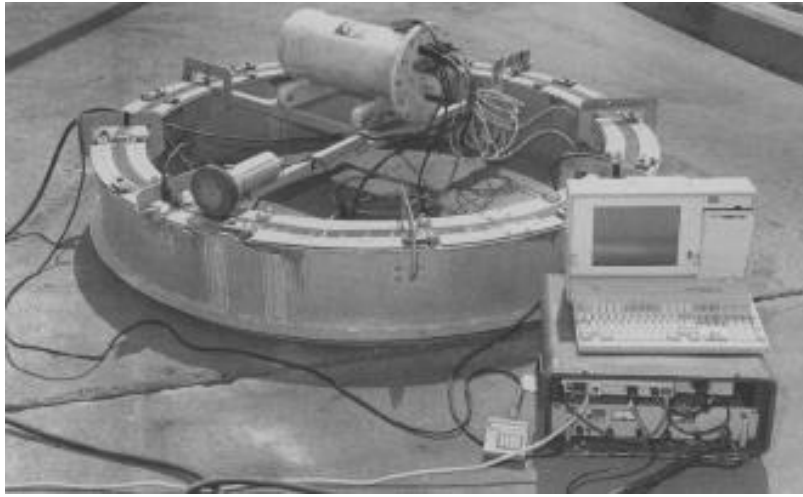
MUSA

Figure A.3.4 In-situ sea carousel flume (diameter=2 m; width=0.15 m, height=0.3 m)

Experiments of Tolhurst et al. (2000)

They have studied the critical shear stress for erosion at various intertidal mudflats using various methods. Measurement results of intertidal mudflat erosion thresholds from in-situ and laboratory erosion instruments were compared for cases with minimum (negligible) chlorophyll content. In an initial experiment, box cores were collected from the Humber estuary mudflats (April 1995) and transported back to the laboratory for measurement in a linear flume. These cores suffered visible disturbance during transport to the laboratory and their erosion thresholds were considerably higher than in-situ data obtained by the sea carousel erosion apparatus. Samples from the Sylt-Romo Bight (June 1998) were collected and transported in a manner that minimised disturbance. The stability of these cores was measured with the EROMES laboratory erosion device based on a rotating propeller in 10 cm diameter perspex cylinder and compared to in-situ measurements taken with the CSM-erosion device based on vertical water jet to erode the sediment surface. ISIS is an in-situ erosion bell consisting of an inverted, curved funnel. Water is drawn from the sides and up through the center of the funnel by pumping.

When disturbance of cores was minimised, in-situ and laboratory erosion thresholds were comparable. Basic data sets from the Sylt-Romo Bight are given in Table A.3.7. Critical shear stresses are relatively high for Chlorophyll contents > 20 mg/m^2. Biofilms (microphytobenthos) have almost no effect on the critical bed-shear stress for chlorophyll contents < 20 mg/m^2.

Table A.3.7 Critical bed-shear stresses based on EROMES erosion instrument, Sylt-Romo Bight, Germany (Tolhurst et al. 2000)

Location	Fraction < 63 μm (%)	Wet and dry bulk density (kg/m^3)		Chlorophyll a content (mg/m$^2 \cong$ μg/g)	Critical bed-shear stress of particle erosion at erosion rates < 0.01 g/m^2/s (N/m^2)
B	15-25	1600-1700	(>1000)	10-25	0.25-0.40
M	50	1350-1450	(550-750)	20-30	0.45-0.50
Ko1	40	1560	(900)	15	0.2
Ko2	80	1270	(450)	30-40	0.4-1.5

Figure A.3.5 shows the critical bed-shear stress for particle erosion as function of bulk density for samples with a low (negligible) Chlorophyll content (< 20 mg/m^2). Pure mud samples have a relatively low dry bulk density (< 400 kg/m^3). The dry bulk density increases

with increasing fine sand content. The results of various different instruments are in reasonable agreement.

Tolhurst et al. (2000) concluded that precautions should be taken to minimise disturbance during transport. Transportation times should be kept to a minimum, and measurements should be made within a few hours of collection.
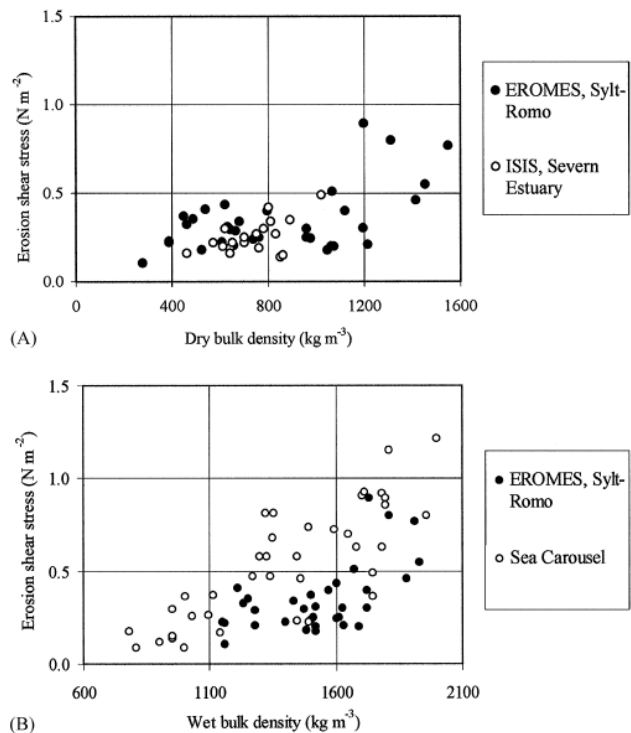
Figure A.3.5 Critical bed-shear stress for particle erosion as function of bulk density

Experiments in Germany

German authorities (Bauamt, 1987) have performed a research project in the period 1982 to 1987 to study the tidal flow velocities and mud concentrations in the subtidal channel near the ferry landing Nessmersiel.

The Nessmersiel channel has a length of 1200 m outside the landing pier. A long guiding dam with crest level varying between 0.5 and 0.9 m NN is present on the west side of the channel. The channel length between the ferry pier and the gate station (of the inland flushing lake) under the main road is about 500 m. The channel width is about 30 to 40 m. The channel bed consists of muddy/sandy sediments. Various small-scale creeks running through the extensive mud flat area drain into the channel. The surroundings of the channel undergo a longterm process of slow continuous sedimentation by fine sediments.

Various bed samples (core samples: diameter 40 mm; length= 100 mm) have been taken during conditions without any mud layer deposits on the fine sandy channel bed. The bed samples were analysed using sieve analysis and settling tests to determine the sediment composition of the bed. The settling tests consisted of the determination of the settling velocities of the sample sediments which were converted to an equivalent grain diameter using the settling velocity formula of Stokes. The percentage of organic materials was found to be relatively small (<2%). Halfway the channel length, the bed consists of fine sand with d_{50} of about 100 to 150 µm in the middle of the cross-section. The percentage of fines < 63 µm varies between 5% and 25%, mostly in the corners (east, west) of the cross-sections. The channel bed is slightly less fine near the entrance of the channel.

Measurements of tidal water levels (pressure), flow velocities (electromagnetic) and sediment concentrations (mechanical and optical) have been taken at three stations (at

MUSA

600 m, 1000 m and 1500 m from the gate station). The mud concentration measurements are largely based on the analysis of water-sediment samples taken by a pump at 0.4 m above the local bed.

The critical flow velocity for particle/surface erosion of sandy channel bed is estimated to be about 0.4 to 0.5 m/s or a critical stress of about 0.25 to 0.30 N/m^2 for the sand fraction.
The critical flow velocity for particle/surface erosion of fresh mud from the channel bed is about 0.2 to 0.3 m/s resulting a critical bed-shear stress of 0.15 to 0.2 N/m^2 (no biological effects).

Field data reported by Deltares (2016)

Deltares (2016) report field data of mud concentrations and bed samples in the Dutch Holwerd subtidal channel, which is the sailing route of the ferry between the mainland and the island of Ameland in the Dutch Wadden Sea. The tidal channel has a depth of 4 m below mean sea level and is dredged regularly to maintain the navigation depth. The channel bed is muddy-sandy (45% mud < 63 μm) in the middle of the cross-section and very muddy (75% mud < 63 μm) at the corners of the channel cross-section. The measured suspended sediment samples mainly consist of silty and clayey materials; the sand content is less than 10%.

The critical flow velocity for erosion of sand from the channel bed is estimated to be about 0.5 to 0.6 m/s or a critical stress of about 0.3 to 0.35 N/m^2 for sand.
The critical flow velocity for erosion of mud from the channel bed is about 0.3 to 0.4 m/s resulting a critical bed-shear stress of 0.2 to 0.25 N/m^2 (no biological effects).

Experiment of Van Rijn (2019)

He has presented laboratory/field data and practical relationships/graphs for the critical bed shear stresses and erosion rates of soft natural and artificial mud-sand mixtures. The percentage of sand is systematically varied in the range of 30% to 95%. These types of soft mud-sand beds have not been studied extensively in the past. Predictive equations for the critical bed shear stress of particle erosion in the case of low to medium density beds are presented. The critical shear stress of both the mud and sand fraction are addressed separately. Finally, an overall synthesis/discussion with generalized plots/graphs is presented, based on the new data and existing data from the Literature.

Three modes of erosion have been observed in this study (see also Literature review):
- particle/floc erosion; erosion of particles/flocs of the (fluffy) top layer; pick-up rates of 0.1 to 1 g/m^2/s;
- surface erosion; simultaneous mobilization of several layers of particles/flocs (failure of local networks, drained process); generation of pits, craters and grooves; pickup rates of 1 to 10 g/m^2/s;
- mass erosion; erosion of lumps of bed material, when the applied fluid stresses are larger than the undrained (remoulded) soil strength of the bed; pickup rates of 10 to 100 g/m^2/s.

All test results with soft and firm mud-sand beds (from Noordpolderzijl en Delfzijl field sites) are summarized in Table A.3.4. The bed roughness (k$_s$) of the mud bed was assumed to be in the range of 0.1-0.5 mm; 0.1 mm for a fully flat bed; 0.5 mm for a bed with small-scale erosion spots; k$_s$=3 mm for tests with significant mass erosion (test   F-N1350-ps80%-IS). Results of natural (na) and artificial (a) samples are given. The Flume data are indicated by F and the EROMES-data by E in Table A.3.8. The bed-shear stress represents the grain-related bed-shear stress. The inaccuracy of the bed-shear stress of the in-situ beds (IS) is about $\pm$20% due to presence of larger and varying roughness elements (shells, gravels, pebbles), whereas the bed-shear stress of the artificial laboratory beds is about 10% to 15% (smoother beds). The most influential parameters are the percentage of clay-dominated fraction (< 8 μm), the percentage of fines (<63 μm), and the dry bulk density of

the mud-sand mixture. It is noted that $p_{fines}+p_{sand}=1$. Column 5 gives the critical bed shear stresses for particle erosion of the fine and sand fractions. The critical stress of the fine fraction is found to be smaller (10% to 50%) than that of the sand fraction, depending on the percentage of fines and the bed density. Mud was always suspended first before sand was observed to roll into the bed load slot in the flume.

During all tests, the mud surface in the EROMES-tube with diameter of 0.1 m was much more stable (yielding higher critical shear stress values; about 10% to 15%) than the mud surface of 0.4x0.6 m^2 in the flume. Most likely, these differences are caused by differences of the bed state and the type of forcing in the tube and in the flume. In some EROMES-tests with samples containing a high percentage of fines > 70%, the bed surface was very smooth without any irregularity resulting in very high critical bed shear stresses (> 1 Pa). Once a small artificial irregularity was created (small pit) at the bed in the EROMES-tube, the erosion process started immediately. In the flume, bed irregularities were always present, particularly when small shells were present. Large-scale turbulence and near-bed pressure fluctuations were also present due to minor water surface oscillations.

Table A.3.8 *Critical bed shear stresses of present data set (Hanze Technical School HTS 2016-2018)*

Test code: F-N325-ps35%: F=Flume; N=Noorpolderzijl-mud; dry density=325 kg/m³;
na= natural sample; a= artificial sample; ps=percentage sand >63 μm=35%;
E=Eromes-tube; D=Delfzijl-mud; IS=in situ sample tested in flume or EROMES;
wet bulk density for saline water 1020 kg/m³; water depth= 0.2 m

Test	Dry/wet bulk density of layer (kg/m³)	Dry bulk density of top layer (kg/m³)	Percentage (%) > 63 μm	Critical bed-shear stress for particle erosion of fine and sand fraction > 63 μm (Pa)	Critical bed-shear stress for surface erosion of fine fraction < 63 μm (Pa)	Bed shear stress at bed failure (mass erosion) (Pa)
F-S1590-ps95% (na)	1590 (2000)	1590	95	0.15; 0.2	0.15-0.2	0.15-0.2
F-N325-ps35% (na) E-N325-ps35% (na)	≅325 (1220)	≅ 200-300	35	0.2; 0.25	0.25-0.35 local craters, grooves	0.5-0.7 top layer 10-30 mm
E-N350-ps35% (na)	≅350 (1235)	≅ 300	35	0.2; 0.3	0.25-0.35 local crates, grooves	did not occur
E-N400-ps30% (IS)	≅ 600 (1390)	≅ 400	30	0.2; 0.3	0.25-0.35 (bed hardly visible)	did not occur
E-N400-ps35% (na)	≅400 (1265)	≅ 350	35	0.2; 0.3	0.25-0.35 local craters, grooves	did not occur
F-N435-ps30% (na) E-N435-ps30% (na)	≅435 (1285)	≅ 350-400	30	0.25; 0.35	0.4-0.6 local craters, grooves	0.8-1.0 top layer 10-30 mm
F-N530-ps30% (na) E-N530-ps30% (na)	≅530 (1345)	≅ 450-500	30	0.35; 0.5	0.6-0.8 local craters/grooves	1-1.2 top layer 10-30 mm
F-N685-ps35% (na)	≅685 (1440)	≅ 600	35	0.5; 0.8	1-1.5; slight erosion at local disturbances	2-2.5; estimated not measured

Literature review on sand and mud
16 November 2020

E-N685-ps35% (na)						
E-D500-ps20% (na)	≅500 (1325)	≅500	15	0.3; 0.4	0.6-0.9; flakes are disrupted from surface	1.0-1.5
E-D300-ps20% (na)	≅300 (1205)	≅300	15	0.15; 0.2	0.2-0.3; flakes are disrupted from surface	>0.6
E-N400-ps30% (IS)	≅600 (1390)	≅400	30	0.2; 0.3	0.25-0.35 general surface erosion	did not occur
F-N530-ps45% (a) E-N530-ps45% (a)	530 (1345)	500	45	0.3; 0.4	0.6-0.7 local craters/grooves	1-1.2 top layer 10-30 mm
F-N700-ps55% (a) E-N700-ps55% (a)	700 (1450)	700	55	0.3; 0.4	0.5-0.7 local craters/grooves	1-1.2 local grooves 10 mm
F-N1100-ps70% (a) E-N1100-ps70% (a)	1100 (1695)	1100	70	0.3; 0.4	0.6-0.7 generation/ erosion of local craters/grooves	1.2-1.4 mass erosion of local grooves 1-3 mm
F-N1450-ps75% (a) E-N1450-ps75% (a)	1450 (1910)	1450	75	0.25; 0.35	0.6-0.8 local craters/grooves	1.4-1.6 local grooves 1-2 mm
F-N1450-ps85% (a)	1450 (1910)	1450	85	0.2; 0.3	0.25-0.35	did not occur
F-N1450-ps90% (a)	1450 (1910)	1450	90	0.2; 0.25	0.25-0.35	did not occur
F-N1450-ps95% (a)	1450 (1910)	1450	95	0.15; 0.2	0.2-0.25	did not occur
F-N800-ps55% (IS)	800 (1510)	800	55	0.3; 0.4	0.5-0.8	>2
F-N1200-ps70% (IS)	1200 (1760)	1200	70	0.3; 0.4	0.5-0.8	>2
F-N1350-ps80% (IS) (many shells)	1350 (1850)	1350	80	0.2; 0.3	0.4-0.7	1-1.4
F-N1425-ps90% (IS)	1425 (1895)	1425	90	0.2; 0.3	0.3-0.7	>2

Particle erosion of sand and mud fraction

The critical stress for particle erosion of the sand fraction ($\cong 100$ μm) can be determined by analyzing the results of the bed load trap (small slot) at about 1 m downstream of the sediment section in the flume. Only sand and minor silt was trapped; mud was not trapped in the small slot, not even during mass erosion conditions. Mud lumps were immediately broken and suspended. The measured bed load transport rates are used to determine the proper bed shear stress (flow stage) for critical erosion of the sand particles and to get an indication of the effect of the fine fraction on the bed load transport process. It was not possible to simultaneously measure the suspended sand transport.

The critical bed shear stresses for particle erosion of the fine fraction (Figure A.3.6), are given for four bed density ranges: (1) low dry density < 400 kg/m³ (LD); (2) low to medium dry density 400 to 800 kg/m³ (LMD); (3) medium to high dry density 800-1200 kg/m³ (MHD) and (4) high dry density 1200 to 1600 kg/m³ (HD). The critical bed shear stress is shown

MUSA

on the outside of the vertical axis, whereas the critical depth-averaged flow velocity is shown on the inside of the vertical axis. Bed shear stresses involved are the grain-related bed shear stress values.

The critical velocity is derived from the Chézy-equation: $\tau_{cr}=\rho g\ u_{cr}^2/C_{gr}^2$ or $u_{cr} = C_{gr}\ (\tau_{cr}/(\rho g))^{0.5}$, with $u_{cr}=$ depth-averaged velocity at critical conditions, $C_{gr}=$ grain-related Chézy-coefficient (about 80 to 100 $m^{0.5}/s$ for muddy field sites with depths of 1 to 5 m; the flume range is C=70 to 80 $m^{0.5}/s$). High Chézy values in the range of 80 to 100 $m^{0.5}/s$ are very typical for muddy field sites. The precise mode (p.e. or s.e) of erosion is unknown for most of the Literature data. The symbols of the HTS-data in Figure A.3.6 represent the critical stress of the fine fraction. Critical stresses of the sand fraction are only slightly higher (therefore not shown). The individual particles/flocs of the fine fraction are more easily set into motion than the sand particles, which may also be the result of the presence of a very thin mud film layer (< 1 mm) of very low density on top of the bed surface in the flume. The particles/flocs of this low-density layer are always first dislodged and immediately suspended. Most of the critical stress values are in the range of 0.15 to 0.4 Pa for LD and LMD-beds (Figure A.3.6 upper). The particle erosion of fines for soft, almost pure mud beds (p_{fines} > 80%) occurs at relatively low bed shear stresses in the range of 0.15 to 0.25 Pa (open circles, triangles). Righetti and Lucarelli (2007) have found the same critical shear stress range of 0.15-0.35 Pa (based on flume tests) for benthic muds (< 10 μm) in water depths of 10 to 50 m in several lakes in Italy. Field data for low density beds in the River Elbe and River Saale in Germany (Noack et al. 2015) show similar values:
-River Elbe: p_{fines}>85%; ρ_{wet}=1100-1150 kg/m^3 (ρ_{dry}= 125-200 kg/m^3); $\tau_{cr,fine}$= 0.15-0.35 Pa;
-River Saale: p_{fines}>90%; ρ_{wet}=1150-1200 kg/m^3 (ρ_{dry}= 200-300 kg/m^3); $\tau_{cr,fine}$=0.3-0.35 Pa.

Noack et al. (2015) observed that the silt and clay particles/flocs lying on the top bed surface as a thin fluffy layer are eroded at very low velocities and bed shear stresses in the case of a low-density top layer. In practice, this thin fluffy top layer of a low-density bed is not of much importance as it will lead to very low mud concentrations in the water column (in the range of 1 to 10 mg/l). In the case of medium to high density beds, the critical stresses are larger and clearly increase for increasing percentages of fines. (Figure A.3.6, lower). The maximum critical bed shear stress is of the order of 2 Pa for a HD-bed of pure mud with p_{fines} > 80%. Smith et al. (2015) and Wu et al. (2017) have tested HD-mixtures of Mississippi-mud (M-mud) and sand. The samples were tested in an erosion flume after 30 days of consolidation, when the dry density values were 750 to 1200 kg/m^3 (initial dry density of 700 to 950 kg/m^3). The critical shear stresses, defined as the shear stress in conditions with an erosion rate of 10^{-4}cm/s (surface erosion), are shown in Figure A.3.6 (lower). The data are in good agreement with the other data. Data of Payra mud ($p_{fines}\cong$80%; Van Rijn et al. 2018) from the offshore Bangladesh coast is also shown in Figure A.3.6 (lower). This is a very pure mud with almost no calcareous and organic materials, which consolidates within one or two days to a dry density of 1200 to 1300 kg/m^3. The texture is that of a soft buttery mud, but the critical bed shear stress for surface erosion (sudden generation of small grooves) is found to be rather high ($\cong$ 2 Pa). The critical bed shear stresses (surface/pit erosion) based on the flume tests of Kothyari and Jain (2008) for high density beds are in the range of 1 to 2.5 Pa, whereas the present HTS-data are in the range of 0.5 to 1 Pa (surface erosion) and 1 to 1.5 Pa (mass erosion) for high density beds. Most likely, this discrepancy is caused by the relatively high percentage of clay used by Kothyari and Jain (2008). The results of Debnath et al. (2007) also point to the importance of the clay content. Discrepancies between various data sets are most likely related to the sediment composition of the mixtures (percentage of clay; percentage organic materials) and the various definitions of particle/surface/mass erosion.

The results for artificial mud-sand beds and in situ mud-sand beds (IS) show no major differences. The critical bed shear stress for particle/surface erosion is in the range of 0.2 to 0.8 Pa for both type of beds.

Predictive relationships for particle erosion are given by Equations of Van Rijn, by Ahmad et al. (2011) and Wu et al. (2017). These latter two relationships refer to the critical stress for the mixture (no distinction between the fine fraction and the sand fraction). The results of Equations of Van Rijn are shown in Figure A.3.6 for a low density case ($\rho_{dry,mud}$= 300 kg/m³; LD) and a high density case ($\rho_{dry,mud}$= 1400 kg/m³; HD) using $\tau_{cr,fine,o}$= 0.1 Pa, $\tau_{cr,sand,o}$= 0.2 Pa, p_{clay}/p_{fines}=0.3, α_1=2, α_2= 1.5 for sand and α_2= 2 for fines. It is noted that the coefficients (α_1 and α_2) are derived/calibrated from the HTS-data. Reasonable agreement with the measured data can be observed for LD-beds. The critical bed shear stress for particle erosion of the fine fraction ($\tau_{cr,pef}$) is somewhat smaller than that ($\tau_{cr,pes}$) of the sand fraction in the case of LD-beds, but the critical stresses of both fractions approach each other for HD-beds with p_{fines} > 0.7. The measured critical shear stresses of HD-beds have values in the range of 1 to 2 Pa for p_{fines}> 0.7 and are somewhat underestimated by Equations of Van Rijn. The HD-data of Laflen-Beasley (1960), Kamphuis-Hall (1983), Roberts et al. (1998) and Kothyari-Jain (2008), not shown in Figure A.3.6, also point to very high critical bed shear stresses (> 1 Pa). Equations (2a,b,c) yield values which are somewhat too small for HD-beds (underprediction by about 50%). Additional research is required for the HD-range.

The relationship of Ahmad et al. (2011) is only valid for low density beds (LD) and is given by:

$\tau_{cr,mix}$= p_{fines} $\tau_{cr,fines}$ + $\tau_{cr,sand}$ exp$\{\beta(1-1/p_{sand})\}$ with $\tau_{cr,fines}$= critical shear stress for a bed bed of fines only (pure mud), $\tau_{cr,sand}$= critical shear stress for a bed bed of pure sand, β= empirical coefficient ($\cong$0.1) The predicted values are between 0.1 and 0.22 Pa for a low density bed ($\rho_{dry,mud}$=300 kg/m³) , see Figure A.3.6 (upper)

The relationship of Wu et al. (2017) is generally valid for low and high-density beds and is given by:

$\tau_{cr,mix}$= λ_{fines} $\tau_{cr,fines}$ + λ_{sand} $\tau_{cr,sand}$ with λ_{fines} and λ_{sand} = empirical coefficients depending on the ratio p_{sand}/p_{fines}; (λ_{fines} + λ_{sand}=1). The method is applied for a low density bed ($\rho_{dry,mud}$=300 kg/m³). Two approaches were used to derive the value of $\tau_{cr,fines}$: (1) constant value $\tau_{cr,fines}$ = 0.15 Pa (as measured) and (2) value based on equations 21 to 26 of Wu et al. (2017) with d_{sand}=0.1 mm and d_{mud}=0.01 mm resulting in $\tau_{cr,fines}$ = 0.17 to 0.57 Pa for p_{fines}=0.9 to 0.1. Appproach 1 yields critical stresses in the range of 0.15 to 0.2 Pa (not shown). Approach 2 yields values in the range of 0.17 to 0.35 Pa and are shown in Figure A.3.6 (upper). The predicted values are in good agreement with the measured data. The method of Wu et al. was not applied for high density beds because of uncertainty of the critical stress for a pure mud bed ($\tau_{cr,fines}$). Overall, it can be concluded that Equation of Van Rijn, that of Ahmad et al. (2011) and Wu et al., (2017) are close together for soft mud-sand beds (LD and LMD) and in reasonably good agreement with measured data.
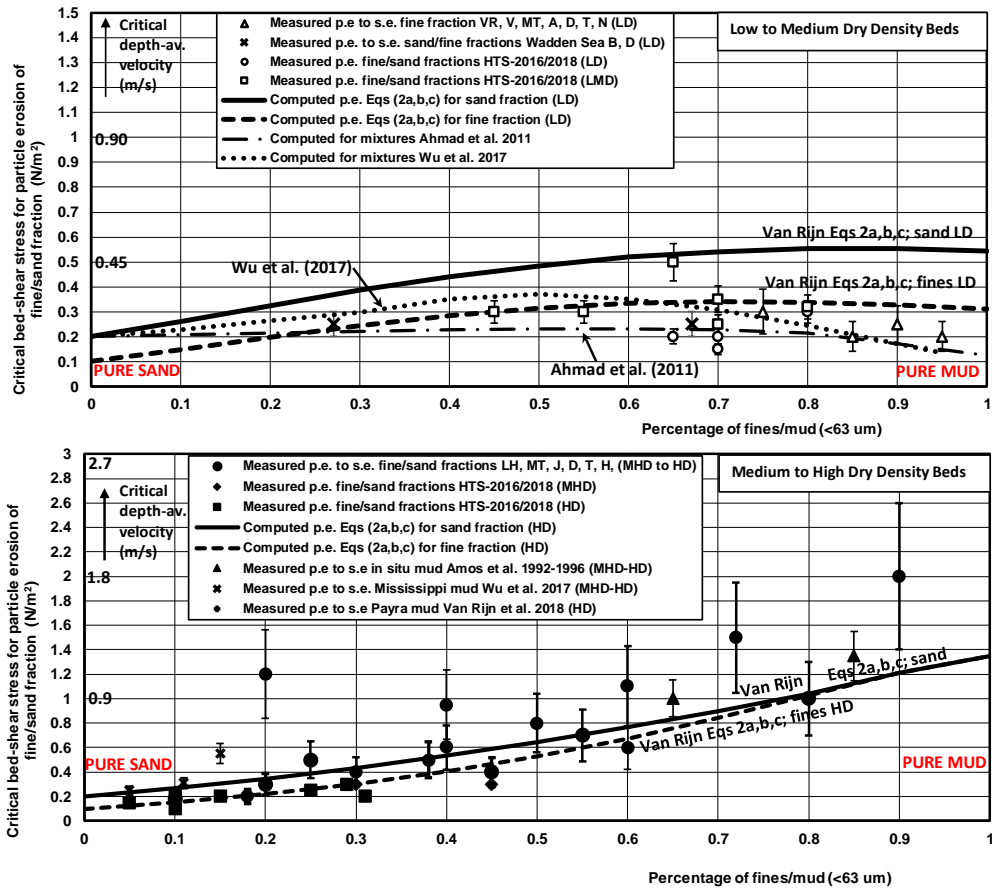
MUSA

Figure A.3.6 Critical bed shear stress for particle erosion Upper: Low to medium dry density beds Lower: Medium to high dry density beds An= Andersen 2001; B= Bauamt 1987; De= Deltares 1989, 1991, 2016; D= Dou 2000, J= Jacobs 2011; H= Houwing 2000, LH= Le Hir et al. 2008; MT= Mitchener and Torfs 1996; N= Noack et al. 2015; T= Thorn 1981; To=Tolhurst et al. 2000; V= Van et al. 2012; VR= Van Rijn 1993 p.e.= particle erosion; s.e.= surface erosion LD= low dry density beds < 400 kg/m³; LMD= low to medium dry density beds 400-800 kg/m³; MHD= medium to high dry density beds 800-1200 kg/m³; HD= high dry density beds > 1200 kg/m³

Surface and mass erosion of mixture

Surface and mass erosion are most important for the engineering practice, as these processes create relatively high mud concentrations in the water column. The transition from particle erosion to surface erosion is reasonably continuous for low to medium density beds (compare closed and open circles of HTS-data; LD and LMD), but discontinuous for higher density beds (MHD and HD), as shown in Figure A.3.7.

Both the measured data points and the trend lines are shown in Figure A.3.7. For p_{fines} between 0.1 and 0.5, the bed dry density is mostly > 800 kg/m³ (MHD to HD) and the critical stress for surface erosion gradually increases from 0.2 to 1 Pa. For p_{fines}> 0.5, the bed dry density is generally much smaller (LD to LMD) and the critical stress for surface erosion is gradually decreasing to about 0.2 Pa for p_{fines}=0.9. The critical shear stress of particle and surface erosion tend to approach a value of about 0.15 to 0.2 Pa for LD-beds with p_{fines} > 0.9 (close to gelling point of sediment; dry density of 100 to 150 kg/m³). The critical stress for surface erosion of LD to LMD-beds can be crudely related to the critical stress for particle erosion: $\tau_{cr,se}$ = 1.1 to 1.5 $\tau_{cr,pef}$;   see Eqs. (4a,b). Some of the data of Mitchener and Torfs (1996) are discussed hereafter. Their data for homogeneous mixtures refer to surface/particle erosion, as the bed surface was eroded in steps and the critical bed-shear

Literature review on sand and mud
16 November 2020

MUSA

stress was determined at the point of zero-erosion depth. Their data for relatively high percentages of fines (> 70%) are in the same range as the present HTS-data (critical stress values of 0.2 to 0.5 Pa). A marked difference occurs for mixtures with relatively low percentages of fines (< 63 μm) in the range of 10% to 20% (muddy sands). Mixtures of clay (kaolinite/Montmorillonite) and 150/230 μm-sand with percentage of clay of about 10% and dry density values > 800 kg/m³ of the MT-data had relatively high critical stresses in the range of 0.7 to 3 Pa. These values are much higher than those of the present HTS-data. The main difference is the percentage of the clay fraction within the fine fraction. The pure clay fraction is relatively high for the MT-data and relatively small for the HTS-data. Hence, relatively high percentages of clay within the fine fraction may lead to relatively high critical stresses (see also Section on Network structure: 5% to 10% clay can give complete coating of 200 μm-sand particles). This makes it important to specify the percentage of clay as a basic parameter based on the particle size distribution of the bed samples involved. The important role of the clay fraction was recently confirmed based on erosion tests with mud from Guayaquil (Ecuador) having about 20% fines < 63 μm and 10% clay and critical stress values for surface erosion in the range of 0.5 to 1.5 Pa (Van Rijn 2019).

Mass erosion of LD, LMD, MHD and HD-beds of the HTS-data occur at critical stresses of in the range of 0.7 to 2 Pa. It is noted that the measured bed-shear stress values related to mass erosion are less accurate than those for particle and surface erosion, because the mud-sand bed was eroded over maximum 10 mm resulting in a larger water depth and varying bed roughness. This was taken into account (to some extent) by using a larger water depth and a larger bed roughness (k_s). The inaccuracy of the bed-shear stress for mass erosion may be as large $\pm$30%.

The pickup rate of a cohesionless silt bed (50 μm; bed density of 1500 kg/m³) is also shown in Figure A.3.7. This value was obtained from the work of Bisschop (2018), who studied the pickup of fine silt in a recirculating pipeline system. Mass erosion was observed for a depth-averaged velocity of about 1.7 m/s in a depth of about 0.2 m ($\cong$ 2 to 2.5 m/s for a depth of 1 m). The critical stress for mass erosion of LD to LMD-beds can be crudely related to the critical stress for particle erosion: $\tau_{cr,me}$ = 2 to 3 $\tau_{cr,pef}$.
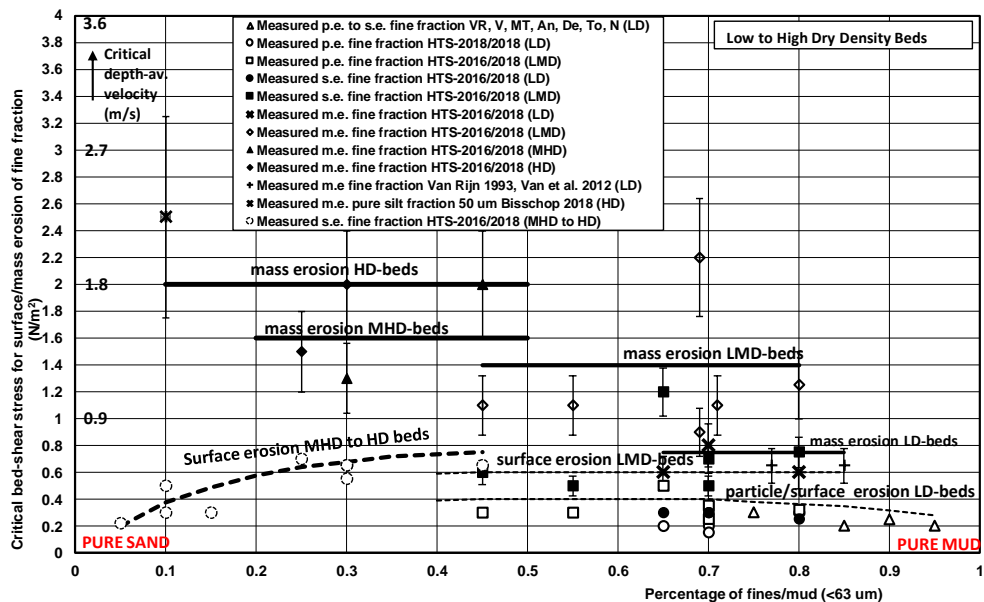

Figure A.3.7 Critical bed shear stress for surface and mass erosion; low to high dry density beds

Erosion rates

At the bed, two simultaneous processes do occur: erosion and deposition. A rough indication of the erosion rates of mud-sand mixtures observed in the present tests is given in Figure A.3.8.

The erosion rates were determined from the estimates of the eroded sediment mass and the time elapsed (flume test results; accuracy $\pm$ factor 2). For clearness the measured values (only crude estimates) are omitted. Instead the trend lines are given resulting in a type of conceptual plot identifying the influence of the most basic parameters. The erosion rate increases for increasing bed shear stress ($E \sim \tau_b^2$) and decreases strongly for increasing dry density (400, 600, 700, 800 and > 1000 kg/m³). The erosion rate of fine cohesionless sand of 63 μm measured in a high-velocity pipeline circuit is also shown (Van Rijn et al. 2019). Strong damping of turbulence at high bed shear stress was observed for cohesionless fine sand resulting in a less steep increase of the erosion rate of fine sand. The erosion rate of mixtures of clay-silt-sand is smaller than that of fine cohesionless sand due to the cohesive effects of the very fine clay fraction reducing the erosion rate of cohesive mixtures.

The deposition flux is defined as: $D = c_b w_s$ with c_b= near-bed concentration of fines (range of 10 to 100 kg/m³) and w_s= settling velocity near the bed (range of 0.1 to 1 mm/s). Using these values, an estimate of the deposition flux is 1 to 100 g/m²/s, which is of the same order of magnitude as the erosion rate. Hence, fairly stable channel beds are possible in very muddy conditions (soft mud beds, fluid mud beds).
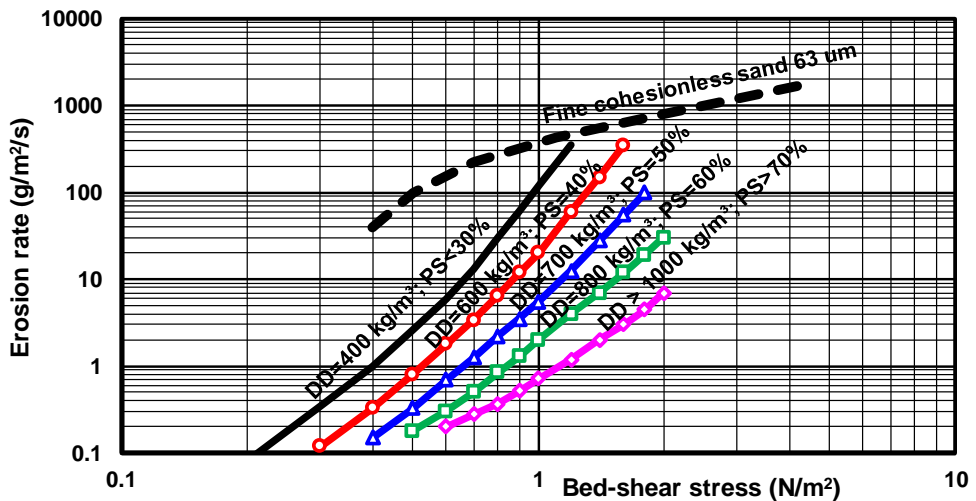

Figure A.3.8 Erosion rates of mud-sand mixtures derived from measured data
(DD=dry density; PS= percentage of sand)

Tentative equations for the critical bed-shear stress for particle erosion are:

$$\tau_{crp,finefraction} = \phi_{cohesive}\, \tau_{cr,fine,o} = (1+p_{fines})^{\beta}\, \tau_{crp,silt,o} \quad \text{for particles} < 63\ \mu m\ \text{(fine range)}$$
$$\tau_{crp,sandfraction} = \phi_{cohesive}\, \tau_{cr,sand,o} = (1+p_{fines})^{\beta}\, \tau_{crp,sand,o} \quad \text{for particles} \geq 63\ \mu m\ \text{(sand range)}$$

with:

$\tau_{crp,silt,o;}\ \tau_{crp,sand,o;}$ = critical bed-shear stress for particle erosion without cohesive effects based on Equation (1.5) resulting in $\tau_{crp,silt,o} \cong 0.1$ N/m² for silt and $\tau_{crp,sand,o} \cong 0.2$ N/m² for fine sand; $\beta = (1 + \rho_{dry,mixture}/\rho_{dry,max})^{\alpha}$ with $\rho_{dry,mixture} = (1-p_{fines})\, \rho_{dry,sand} + p_{fines}\, \rho_{dry,fines}$; $\rho_{dry,max}$ = maximum dry bulk density of mud-sand mixture ($\cong 1600$ kg/m³), p_{fines}= percentage of fines < 63 μm of the bed layer, $\rho_{dry,sand}$ = dry bulk density of sand ($\cong 1600$ kg/m³), $\rho_{dry,fines}$= dry bulk density of mud ($\cong 200$ kg/m³ for soft mud up to 1200 kg/m³ for firm mud bed); α= empirical coefficient ($\cong 2$).

MUSA

The wet density ($\rho_{dry,wet}$) can be determined most easily by the measured wet mass and volume of the sample.

The dry density follows from: $\rho_{dry,mix}=[\rho_{dry,wet}-\rho_w][\rho_s/(\rho_s-\rho_w)]$ with $\rho_s=$ sediment density ($\cong2650$ kg/m³) and $\rho_w=$sea water density ($\cong1020$ kg/m³).

If $\rho_{dry,mix}$ and p_{fines} (wet sieving using mesh of 63 μm) are known, the $\rho_{dry,mud}$ can be computed as: $\rho_{dry,mud}=[\rho_{dry,mix}-(1-p_{fines})\rho_{dry,sand}]/p_{fines}$.

The propose equations are shown in Figure A.3.9 for a dry mud density of 300 kg/m³ in the case of weakly consolidated mud and 1000 kg/m³ in the case of firmly consolidated mud. The trends of the data are reasonably well represented for $\alpha\cong2$.

Synthesis of literature results (before 2016)

Table A.3.9 summarizes the available data of critical bed-shear stress values for particle and surface erosion of mud-sand mixtures without biogenic effects before 2016.

The most influential parameters are the percentage of fines (<63 μm) and the dry bulk density of the mud-sand mixture. The precise type of erosion (particle or surface erosion) is not the same for all data. Most data are based on visual observations of particle erosion. Some data are based on definitions of erosion related to sudden changes of measured concentrations or pickup rates (plots of concentration/pickup rate against bed-shear stress).

The critical bed-shear for particle/surface erosion of a weakly consolidated pure mud bed with a dry density < 400 kg/m³ is of the order of 0.2±0.1 N/m².

The critical bed-shear for particle/surface erosion of a firmly consolidated mud bed with a dry bulk density >800 kg/m³ is of the order of 1±0.5 N/m². The critical bed-shear stress decreases to about 0.4 N/m² for $p_{fines}\cong0.3$. For $p_{fines}<0.3$, the dry density of the mud-sand mixture is relatively high > 800 kg/m³ and the critical bed-shear stress of the sand fraction is dominant with critical bed-shear stress values in the range of 0.2 to 0.4 N/m².

It is most logical to assume that the sand particles are more difficult to erode due to the binding effects of the mud particles surrounding the sand particles. Mud particles will be washed out, once sand particles are eroded. Hence, the critical stresses of both the sand and mud fraction are almost the same. Most likely, the critical stress of the mud fraction will be slightly smaller, as the skin layer of mud around the sand particles needs to be broken first.

In the case of a high mud percentage ($p_{fines}>0.7$), the bulk density of the mud-sand mixture is generally relatively low (dry density<400 kg/m³) in dynamic subtidal conditions with significant reworking of the bed surface (tidal channels). High bulk densities (> 800 kg/m³) do occur mostly in quiescent tidal environments where subtidal deposition is dominant (tidal channels with very low velocities <0.3 m/s). Intermediate bulk densities (dry density of 400-800 kg/m³) generally occur at intertidal mud-sand flats. The critical bed-shear stress of the mud fraction is dominant for $p_{fines}>0.7$. In that case, the sand particles are scattered throughout the mud fraction and surrounded by many layers of mud particles and are thus much more difficult to erode than the mud particles. Hence, the critical bed-shear stress of the sand fraction is most likely much larger than that of the mud fraction.

MUSA

Table A.3.9 Critical bed-shear stress for erosion of mud-sand mixtures without biogenic effects; literature data

Type of mud-sand mixture	Percen tage mud (< 63 μm)	Mean sediment size d_{50} (μm)	Dry bulk density top layer (kg/m³)	Critical bed-shear stress for particle (p.e.) and surface erosion (s.e.) of sand and mud fraction (N/m²)
Laboratory flume (Jacobs 2011)	10%	100-150	>1800	0.18±0.04 (p.e./s.e.)
Laboratory flume (Jacobs 2011)	25%	80-100	>1800	0.5±0.15 (p.e./s.e.)
Laboratory flume (Jacobs 2011)	55%	60-80	>1800	0.7±0.3 (p.e./s.e.)
Laboratory flume (Jacobs 2011)	80%	30-60	>1800	1±0.4 (p.e./s.e.)
Lab and field (Le Hir et al. 2008)	20%	<140	> 1500	0.25±0.05 (p.e./s.e.)
Lab and field (Le Hir et al. 2008)	30%	<140	> 1500	0.4±0.1 (p.e./s.e.)
Lab and field (Le Hir et al. 2008)	40%	<140	> 1500	0.6±0.15 (p.e./s.e.)
Lab and field (Le Hir et al. 2008)	60%	<140	> 1500	1.1±0.3 (p.e./s.e.)
Lab and field (Le Hir et al. 2008)	70%	<140	> 1500	1.5±0.4 (p.e./s.e.)
Lab and field (Le Hir et al. 2008)	90%	<140	> 1500	2.0±0.5 (p.e./s.e.)
Lab and field (Mitchener-Torfs 1996)	>70%	<63	400	0.2±0.1 (p.e./s.e.)
Lab and field (Mitchener-Torfs 1996)	40%	<100	800	0.6±0.3 (p.e./s.e.)
Lab and field (Mitchener-Torfs 1996)	30%	<100	1000	1.0±0.4 (p.e./s.e.)
Dutch Wadden Sea intertidal flats (Houwing	<10%	100-150	>1000	0.1-0.2 (p.e.)
Dutch Wadden Sea intertidal flats (Houwing 2000)	15%-20%	100-150	>1000	0.1-0.2 (p.e.)
Dutch Wadden Sea intertidal flats (Houwing 2000)	35%	50-100	>1000	>0.5 (p.e.)
Dutch Wadden Sea subtidal channel Holwerd (Deltares 2016)	70%	20-50	300-500	0.2-0.25 mud fraction 0.3-0.35 sand fraction (surface erosion)
Dutch North Sea bed (subtidal) (Deltares/Delft Hydraulics 1989)	0-30%	100-150	>800	0.2-0.4 (p.e.)
Dutch North Sea bed (subtidal) (Deltares/Delft Hydraulics 1989)	50%	50-100	>800	0.6-1.0 (p.e.)
German Wadden Sea intertidal flats	15%-30%	100-150	> 1000	0.2-0.5 (p.e.)

MUSA

(Tolhurst et al. 2000)				
German Wadden Sea intertidal flats (Tolhurst et al. 200)	40%-50%	50-100	>800	0.2-0.5 (p.e.)
German Wadden Sea subtidal channel Nessmersiel (Bauamt 1987)	5%-30%	60-100	300-500	0.15-0.2 mud frac. (s.e) 0.25-0.3 sand frac. (s.e)
Lunenburg basin (subtidal), Nova Scotia, Canada (Sutherland et al. 1998)	20%-30%	30-40	<400	0.05-0.15 (p.e.)
Minas basin (subtidal), Bay of Fundy, Canada (Amos et al. 1992)	65%	20-30	>1000	0.5-1.5 (p.e.)
Tidal fraser river (intertidal), Canada (Amos et al. 1997)	65%-90%	10-20	<400	0.15-0.5 (p.e.)
Hudson Bay (subtidal), Canada (Amos et al. 1996)	40%-50%	40-60	>1000	> 3.5 (p.e)

p.e.= particle erosion; s.e.= surface erosion

Experiments of Waterproofbv and LVRS Holwerd (2019)

Flume experiments have been done in the small flume (Figure A.3.9) of Waterproof in Lelystad to determine the critical shear stress and erosion rates of various samples taken from the ferry channel between Holwerd and the island of Ameland in January-February and September-October 2019, The Netherlands.

Figure A.3.4 Small flume of Waterproof (width=0.15 m)

The muddy and sandy bed samples were taken at different locations from the landing pier (0, 1, 2 and 6 km).

The current velocity in the flume was raised in small steps until particle, surface (small pits, craters and grooves) and mass erosion was observed visually. Maas erosion is the sudden failure of the bed of part of the bed. The bed-shear stress is computed as: $\tau_b = \rho g (u_m/C)^2$ with: ρ= fluid density water, g=9.81 m/s^2, u_m= depth-mean current velocity, C= Chézy-coefficient= 5.75 $g^{0.5}$ log(12h/$k_{effective}$), h= water depth (m), k_{eff}= effective bed roughness height ($\cong$0.0001-0.0005 m); C $\cong$ 63-75 m$^{0.5}$/s. The test results are given in Table A.3.10**.**

Figure A.3.10 shows the critical bed-shear stress fore surface-erosion as function of the dry density of the sample and the percentage of fines (pf) < 63 μm. The vertical axis also shows the depth-mean current velocity for h=3 m; k_{eff}=0.001 m and C=80 m$^{0.5}$/s. The most important features are:

MUSA

- critical stress increases for increasing dry density.
- critical stress is about 0.2 to 0.4 Pa for a dry density of 250 to 350 kg/m³ (soft mud);
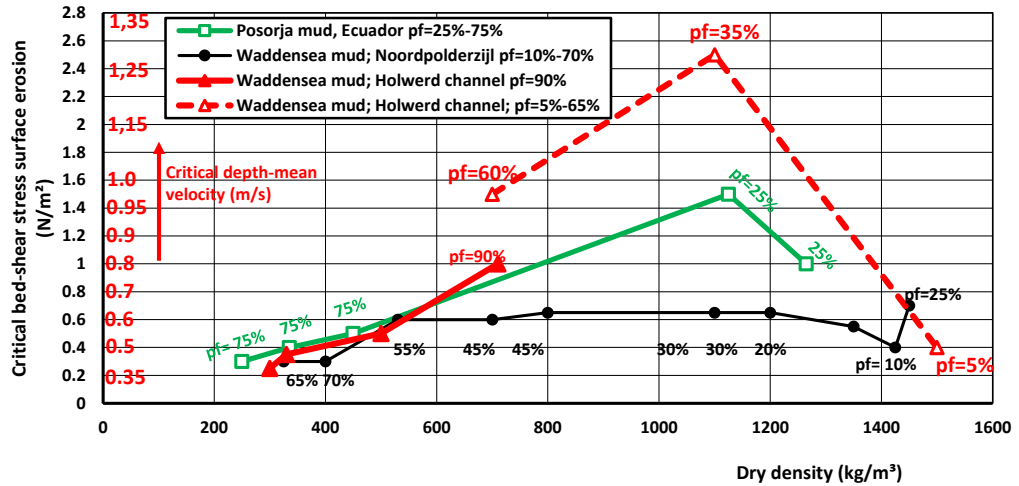- critical stress increases to about 1 Pa for a dry density of about 700 kg/m³.

Figure A.3.5 Critical bed shear stress of surface erosion as function of dry density; mud-sand Holwerd channel; pf= percentage fine sediment < 63 µm; January-February 2019

Measured erosion rate (g/m²/s) based on the eroded sediment volume at the end of the test are given as function of the excess shear stress in Table A.3.10 and in Figure A.3.11. The layer of sediment (δ_e) erode over time dt can be estimates using $\delta_e = E \, \Delta t / \rho_d$
with: E= erosion (kg/m²/s), Δt = time (s) and ρ_d = dry density (kg/m³). For example: E = 0.005 kg/m²/s, Δt = 3600 s, ρ_d = 400 kg/m³ (soft mud), the layer thickness is δ_e = 0.01x3600/400=0.045 m.

Table   A.3.10 Erosion of Holwerd mud

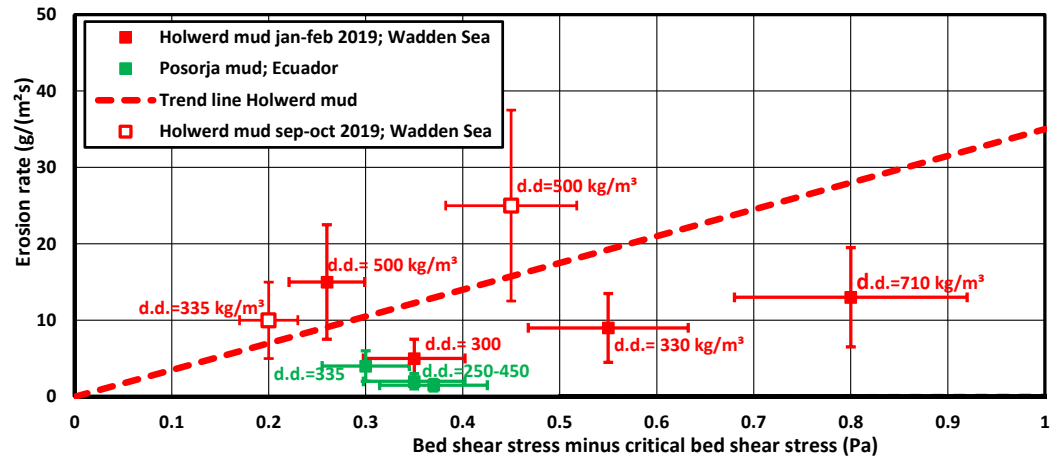| Parameters	Erosion Holwerd-mud January-February 2019 p_{fines}=85%; p_{clay}= 10%; p_{sand}= 15%.				Erosion Holwerd-mud September-October 2019 p_{fines}=57%-80%	
	Dry density 710 ± 50 kg/m³	Dry density 500 ± 30 kg/m³	Dry density 330 ± 30 kg/m³	Dry density 300 ± 30 kg/m³	Dry density 500 ± 30 kg/m³	Dry density 335 ± 15 kg/m³
Critical bed-shear stress for surface erosion (N/m²)	1	0.45	0.35	0.25	0.85	0.4
Bed shear stress (N/m²)	1.8	0.72	0.9	0.6	1.3	0.6
Erosion rate (g/m²/s)	13	15	8	5	25	10

MUSA

Figure A.3.11 Erosion rates of Holwerd mud (d.d=dry density)

B Summary of experimental results of erosion of firm mud-sand beds

B.1 General

Many past studies were focused on the critical bed-shear stress of artificially compacted mud beds of pure clay, mixtures of clay, silt and fine sand or pure silt in laboratory current flumes (Smerdon and Beasley,1959, 1961; Laflen and Beasley, 1960; Kamphuis and Hall, 1983; Panagiotopoulos,1996; Roberts et al.,1998; Kothyari and Jain, 2008; Le Hir et al., 2008; Jacobs (2011) and Jacobs et al., 2011; Smith et al., 2015 and Wu et al., 2017).

In some tests, the mud bed was quite large, while in other tests only small mud cores were pushed upwards through the flume floor at a rate equal to the pickup rate of the recirculating flow (Le Hir et al., 2008; Jacobs, 2011; Jacobs et al., 2011; Smith et al., 2015; Wu et al., 2017). Various methods were used to compact the mud bed mixtures (moulding, drying, rolling, pressing, etc). Dry density values were in the range of 900 to 1900 kg/m³ for varying percentages of clay, silt and fine sand. The measured critical bed-shear stress of the tested mud beds was often quite high with values up to 20 Pa (Kamphuis and Hall, 1983). Most critical bed-shear stress values were found to be in the range of 1 to 3 Pa for firmly compacted mixtures with clay percentages of 10% to 50%. Generally, the critical stress was found to increase for increasing bulk density (packing of the bed) and percentage of clay. Often, the pure high-density clay beds had the largest critical stress. Compacted beds of pure silts also have relatively high critical stresses up to 1 Pa (Roberts et al.,1998).

B.2 Firm consolidated mud-sand beds

Very early work on firmly consolidated mud beds of clay (mean diameter about 2 μm; 61% clay) and clay-silt (about 20 μm; 14% to 22% clay) was done by **Smerdon and Beasley (1959)** and **Laflen** and **Beasley (1960)** in a flume.

Experiments of Smerdon and Beasley (1959)
They tested natural clay-silt samples in a flume. Eleven soils from the State of Missouri (USA) were selected for testing. These soils were chosen to give considerable range in physical properties, particularly concerning cohesion of the soil and the ease with which the aggregates were dispersed in water. The soil was placed in the flume in a layer of 2.5 inches thick. The remaining portions of the flume bottom were covered with a concrete fill (2.5 inches thick). Approximately 1200 pounds of soil were used for each flume test. The soil was placed in the flume and thoroughly mixed. Lumps of soil were broken up by hand and all foreign particles were removed. The soil was then carefully leveled using a specially constructed template which used the sides of the hy-draulic flume as guides. This assured that the depth of the soil sample was the same as the depth of the concrete fill upstream and downstream from the test section. No attempt was made to compact the soil any more than that which naturally occurred in the process of leveling the bed. The soil was then wetted by slowly admitting water into the flume until the bed was completely soaked. A small amount of coarse gravel was placed on the bed nearest the upper con-crete fill co increase the stability at this critical point. After the bed was wetted, the flume was permitted to drain and the soil sample permitted co dry and consolidate for approximately 20 hours. The rate of flow was then increased to give a depth of flow over the bed of about 0.05 feet. The process of increasing the flow by increments and recording data was continued until general movement of the bed material was observed. Bed failure was defined at the point at which the bed material was in general movement. The particles were carried down the

MUSA

flume past the transparent flume sides as bed-load. The bed was not considered to have failed until the tractive force was sufficient to cause general movement of the bed material. The highest and lowest value of each soil type are given in Table A.2.1.

Experiments of Laflen and Beasley (1960)

They tested natural clay-silt samples from the State of Missouri (USA) in a flume. The soil samples were moulded and saturated with water. The beds were artificially compacted to obtain the desired voids ratios in the range of 1 to 2 (dry density in the range of 900 to 1300 kg/m^3). The flow rate was increased by small increments to remove loose aggregates. The flow rate was raised to a value with ongoing erosion of aggregates during some time and used to determine the critical stress for erosion. The critical bed-shear stress (range of 0.6 to 2.5 N/m^2) increased for increasing bulk density. The pure clay bed had the largest critical stress (1.5 to 2.5 N/m^2). The values are given in Table A.2.1.

Experiments of Kamphuis and Hall (1983)

They studied the critical bed-shear stress of highly consolidated cohesive mixtures (dry density > 1500 kg/m^3) in a flume with velocities up to 3.5 m/s. Consolidated clay was taken from the bottom of the Mackenzie River in Canada and at some nearby land-based locations. The in-situ water content was in the range of 30% to 50% (dry density in the range of 950 to 1350 kg/m³. The cohesive samples were artificially compacted in a specially designed press. The dry density of the samples after compaction is herein assumed to the in the range of 1200 to 1600 kg/m³. Two markedly different highly consolidated soil samples were tested: Series A and B consisting of natural clay-silt samples with p_{clay}=50%-60%, p_{silt}=35%-45% and p_{sand}< 5% and Series D with p_{clay}=15%-35%, p_{silt}=35% and p_{sand}=30%-50%. Test series C, D and E were made from the samples of Series A by mixing with fine sand (d_{50}=0.105 mm). The clay from sample A was dried, pulverized and mixed with sand and water was added and compacted in a press.

The measured velocity at 3 mm above the bed surface was taken as the critical velocity when erosion was defined to occur as the onset of pit and streak marks (surface erosion) became apparent and used to determine the critical stress.

The onset of surface erosion was observed to occur as:
- generation of pits, parallel streaks;
- removal of flakes;
- general erosion over entire surface.

When erosion was noticed, the velocity was kept constant for 24 to 36 hours. The critical bed-shear stress for erosion was found to be in the range of 10 to 20 N/m^2 for Series A and 1 to 10 N/m^2 for series D with larger sand content. This shows that the critical stress decreases for decreasing percentage of clay.

Some characteristic data of Kamphuis and Hall (1983) are given in Table A.2.1.

Experiments of Lim (2006)

He studied the critical shear stress of various stiff clay samples from sites in Australia and USA in a rotating cylinder. In this test, the soil sample is placed between steel plates in a cylinder filled with water, and the shear stress is applied to the soil surface through rotating the cylinder relative to the soil. The torque required to keep the soil sample stationary against the spinning water and cylinder is measured and converted to the shear stress. The data of critical stress are given in Table A.2.1.

Experiments of Mostafa et al. (2008)

They studied the erosive behaviour of various clay-type soils. Erodibility tests were performed on field samples of natural cohesive soils obtained from several different locations in South Carolina (USA). The cohesive soils were collected from different bridge sites in the form of large undisturbed chunks. The soil chunks were scooped from the

MUSA

bottom and removed as a single piece, wrapped in plastic sheets and placed in a covered container for transportation to the laboratory. In the laboratory, the chunks were cut slowly and carefully with a thin sharp-edged knife to form an even-sized sample that would fit into a sediment indentation in the flume. Surface erodibility tests were performed in a laboratory flume that is 14.5 m long, 1.2 m deep and 0.75 m wide, has constant bottom slope of 0.0033 and an average Manning roughness coefficient of 0.018. The soil sample was placed in a small sediment lift. The sediment surface was flush with the flume bottom. The thickness of the sample was usually between 4 cm and 8 cm. The flow rate was increased in steps and each flow rate was maintained for two hours. If erosion was not observed, the flow was increased and maintained for two hours again. Erosion was observed by means of 1 cm siphon tubes close the flume bottom downstream of the sample. The eroded particles collected in an observation bucket located outside of the flume. Shear stress was calculated from the near-bed Reynolds stresses obtained from the instantaneous velocity measurements using a acoustic doppler velocity probe (ADV).
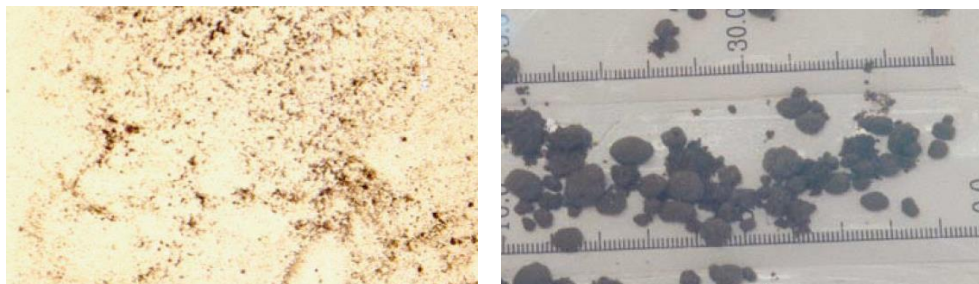

Figure B.2.1 Soil fragments related to particle/surface (left) and mass erosion (right)

Particle erosion and mass erosion were observed, see Figure B.2.2. Particle erosion started to occur when fine dispersed clay particles were collected by a siphon in the observation bucket. The erosion mode changes to mass erosion if the bottom shear stress increases sufficiently. Mass erosion was considered to occur in the experiment when small masses (2 to 5 millimeters) of clay were eroded from the soil surface and were collected by the siphon in the observation bucket. Results are given in Table A.2.1.

Experiments of Jacobs (2011)

He studied the erosion threshold stress of various mud-sand mixtures in a small-scale straight test flume (Erodimetre; length=1.2m, width=0.08 m, height=0.02 m). Sediment mixtures were artificially prepared using a dedicated experimental laboratory set-up at a constant temperature of 19°C.

Relatively dense samples were obtained with wet bulk density values > 1800 kg/m^3 (dry density > 1250 kg/m³). The relatively dense packing prevents segregation of the fractions during the saturation process.

The flume has a sediment container at the bottom where sediment cores can be placed and pushed upwards. Sub samples with a thickness of 2 to 3 cm were used. The surface of the soil sample was horizontally and vertically levelled with the bottom of the flume using four screws. The whole exposed surface area was presumed to contribute to erosion. The bottom of the flume was covered with sandpaper (with a roughness comparable to the applied sand fraction) to decrease differences in roughness with the sample. In practice, nearly no scour was observed at the upstream side of the samples.

A unidirectional flow generated by a re-circulating pump was accelerated step by step (average duration of a step approximately 150 - 200 seconds), until the sample was eroded by a few mm. The flow rate was controlled through a velocity meter in the pump.

Cracks occurred for all soil samples with a dominant clay-water matrix and was characterized by cracks in the surface layer of the soil samples, and by uneven erosion patterns. Before and during

MUSA

the formation of the cracks, individual flocs and sand grains (particle erosion) were simultaneously eroded.

Some test results are given in Table A2.1, showing an increase of the erosion threshold stress with increasing percentage of mud.

Le Hir et al. (2008) has studied the erosion threshold stress in a small-scale flume of natural mud. He used firmly consolidated sample cores from the intertidal zone of the Mont St-Michel Bay (France).

The top layer of the container was eroded over a few millimeters in 1 to 2 hours. The results clearly indicate the presence of two erosion types: particle/floc erosion and surface erosion. The dominant size of the sand is about 140 μm. The dominant clay minerals are kaolinite and illite; carbonates are also present. Organic content is low (<2%). Results are given in Table A.2.1.

Experiments of Wolter et al. (2008)

They studied the behavior of boulder clay for the outer protection of dykes. A large-scale model test (scale 1 to 1) of the erosion resistance of boulder clay in dikes under wave attack was carried out in the Delta Flume of Deltares (Figure B.2.3). Boulder clay is a clay-like material which has been used in dikes since 1920.

Boulder clay can be found at the edges of glaciers. Boulder clay consists of varying fractions of clay, silt and sand with pieces of shingle. The high gradation ensures a high density of approximately 2000 kg/m^3 and a low water permeability. During the construction phase of the Wieringermeer dike for example the unprotected boulder clay dike was able to withstand flow velocities of 3-3.5 m/s without failure (shear stress of about 20$\pm$5 N/m^2 for C=70 to 80 m$^{0.5}$/s). The boulder clay blocks of 10 ton were taken from an old dike and tested in the wave flume. The significant wave height was in the range of 1.1 to 1.6 m with peak periods of 5 to 6 s.

The first 10 minutes of testing caused strong erosion. Individual waves were observed to quarry large chunks of boulder clay out of the slope (resulting in a horizontal erosion length of 1.1 m with an erosion depth of 0.3m). Most of the erosion was found just beneath the waterline. After the first 10 minutes the erosion visibly slowed. The starting erosion revealed stones of 5-15 cm diameter which were embedded in the boulder clay and a large quantity of roots was also revealed. These can have a destabilizing effect on the boulder clay and can reduce the erosion strength. The maximum cumulative (horizontal) erosion length found after testing was about 5,4 m and the maximum cumulative erosion depth (measured vertically) was about 1,9 m after 5 hours of testing.

Using a peak velocity of V=2 m/s and C-values of 70 to 80 m$^{0.5}$/s, the peak shear stresses are about: $\tau_{max}=\rho g (V/C)^2 \cong 7 \pm 2$ N/m^2. Based on this the critical shear stress of boulder clay is at least 5 N/m^2.

The study showed that the behavior of boulder clay is significantly different from clay. Clay erosion is usually faster at the erosion begin but with time diminishes below that of boulder clay.

Experiments of Long and Menkiti (2007)

They have determined the geotechnical properties of Dublin boulder clay (DBC), as follows:
Wet bulk density=200-2300 kg/m^3; Moisture Content= 10-15%; Plasticity Index= 15-20%
Permeability=10^{-9} -10^{-11} m/s; p_{clay}=10-15%; p_{silt}=15-30%; $p_{sand-gravel}$=50-70%. The percentage of gravel is relatively large with 30% to 45%.

MUSA

Figure B.2.3 Dutch boulder clay (upper: excavation at local dike; lower: tests in Delta flume)

Experiments of Mobley et al. (2009)

They studied the erodibility of stiff clay-type material in a pipeline circuit in which a sediment lift was installed (Figure B.2.4). Analysis of sediment composition showed only 15% < 75 μm (sandy clay), see Table B.2.1. A 1 mm thick portion of soil is pushed into a stream of water and the time required for erosion noted to establish an erosion rate (mm/hour). Core tube samples were provided from borings for a culvert replacement project in Talladega County, USA. Borings were mostly to a depth of around 4.5 meters. The boring logs described the soil encountered as stiff or very stiff clay with occasional chert pebbles. A common erosion pattern was observed for every tested sample. Silty, clayey emission occurred around the sample edges, and erosion began to occur on the upstream surface. Occasionally large erosion holes/spalls (10 mm) would suddenly occur on the sample surface. Some samples were tested in different way. The testing difference was that the soil was trimmed flush with the bottom of the flume rather than projecting 1 mm into the flow. The critical shear stress was found to be in the range of 0.6 to 1 N/m², see Table

MUSA

B.2.1. The erosion rate was about 0.3 mm/hour for τ=1.2 N/m^2 and 1.5 mm/hour for τ=3.2 N/m^2.
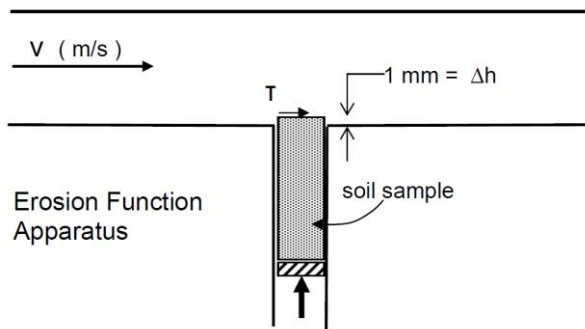

Figure B.2.4 Pipeline circuit with sediment lift

Table B.2.1 Critical stresses of firm clay-type soils

Authors	Sample	Mean size (µm)	p_clay (%)	p_silt (%)	p_sand (%)	Plasticy index (%)	Water content (%)	Dry density (kg/m³)	Critical velocity (m/s)	Critical shear stress (N/m²)
Smerdon and Beasley (1959)		20	15			10		1140		1.0
		20	17			12		1080		1.6
		22	17			7		1010		0.76
		13	24			14		1190		1.05
		10	30			14		1100		2.2
		<10	58			44		955		4.3
		15	23			14		1070		1.6
		15	17			8		1105		1.1
		11	31			18		1140		1.2
		11	25			15		935		1.8
		4	44			30		1010		2.6
Laflen and Beasley (1960)	MS	12	22			4		1140		2.5
	MS	12	22			4		970		1.45
	KS	20	14			4		1120		0.7
	KS	20	14			4		1205		0.5
	KSS	18	24			13		1230		1.1
	KSS	18	24			13		1015		0.5
	MSS	2	61			17		1050		2.3
	MSS	2	61			17		1000		1.6
	MES	20	18			5		1320		2.45
	MES	20	18			5		1030		1.8
Kamphuis and Hall (1983)	A-5		60	35	5	18	37	>1200	1.95	9
	A-9		60	35	5	34	31.5	>1200	2.6	15.7
	A-11		60	35	5	33	33.3	>1200	2.8	18

MUSA

	B-4		60	35	5	33	31.8	>1200	2.1	11
	C-2		48	35	17	20	30.9	>1200	1.6	6.5
	D-2		36	35	29	11	22.9	>1200	0.95	2.6
	D-3		36	35	29	13	22.6	>1200	1.35	5.0
	E-1		15	35	50	-	20.5	>1200	0.75	1.7
Lim (2006)	Soil A		22	36	42	16	17	1750		2±1
	Soil B		22	9	69	9	12	1945		4±2
	Soil C		35	24	41	18	19	1720		7±2
	Soil D		27	50	23	16	18	1750		>10
	Soil F		16	21	63	8	13	1875		5±2
	Soil G		22	59	21	22	20	1690		5±2
	Soil H		77	9	14	60	41	1250		10±5
	Soil S		27	37	36	19	22	1615		10±5
Mostafa et al. 2008	Soil 1	8.5	40	48	12	22	35	1250		0.55-2.7
	Soil 2	18	26	56	18	15	19	1205		0.3-1.7
	Soil 3	12.2	39	55	6	16	22	1365		0.4-1.6
	Soil 7	6.5	46	46	8	24	33	1460		0.45-2.2
Mobley et al. 2009	Talladega soil		<15%		85	6±1	18±7	1750±150		0.8±0.2
Jacobs 2011		120	2	<8				1200-1600		0.2
		90	7	18				1200-1600		0.5
		70	12	43				1200-1600		0.7
		45	15	65				1200-1600		1
Le Hir et al. 2008			7	13				1200-1600		0.25
			10	20				1200-1600		0.4
			13	27				1200-1600		0.6
			20	40				1200-1600		1.1
			23	47				1200-1600		1.5
			30	60				1200-1600		2.0

Kamphuis and Hall (1983) measured the flow velocity at 3 mm above the bed

Mostafa et al. (2008) have measured critical shear stress for particle and mass erosion; both values are given

MUSA

C   Summary of experimental results of settling velocity

C.1   All experiments

Experimens of Van Leussen (1994, 2011) and Van der Lee (2000)

Deltares has developed an insitu video camera system (VIS) for determination of floc sizes and settling velocities in tidal environments. The VIS-system was used by Van Leussen (1994) and Van der Lee (2000).

The VIS consists of an underwater housing that contains a settling tube and video camera. When the VIS is immersed in the water, flocs can settle from above into the settling tube. In the settling tube the flocs are illuminated by a light sheet, filmed by a CCD camera and recorded by a super VHS video camera. The VIS can be deployed from a research vessel floating with the current, in a quasi-Lagrangian approach. The VIS floats some 30 meters away from the research vessel at about 3 m below the water surface and is connected to the research vessel by power and video cables. Floating with the current is done to reduce the effect of turbulence around the VIS.

Video images of VIS cover an area of 6.5 mm (vertical) x 10 mm (horizontal). The images are digitised and processed to obtain size and settling velocity of the observed mud flocs. The floc size is defined as the equivalent diameter of a circle with the same surface area as the surface area of the floc measured with the VIS. Floc sizes smaller than 80 μm cannot be detected. Settling velocities were determined for flocs that appeared in consecutive images. The time interval (about 0.1 s) between consecutive images depended on the settling speed of he flocs, their size and the water movement in the VIS. Often the settling velocity of the same floc was determined several times in consecutive images. Each of these floc settling velocity determinations are used for the calculation of average floc settling velocities. So flocs that appear longer in the consecutive images contributed more often to the average. Data processing to obtain floc settling velocities is laborious and more time consuming than measuring floc sizes.

Van Leussen (1994, 2011) used the VIS-system in the Ems estuary and along the Dutch coast near Hook of Holland (close to Rotterdam, The Netherlands).

The macroflocs in the Ems estuary (Ranselgat, Oost Friesche Gaatje and Emder Vaarwater) had sizes in the range of 200 to 700 µm, sometimes more than 1000 µm, and survived high current velocities. The settling velocities were in the range of 0.5 to 8 mm/s. Settling velocities are lowest during conditions with low concentrations around slack tide.

Ranselgat (2—50 mg/l): during high flow velocities, the settling velocities increased to about 4 mm/s, both during flood and ebb. The corresponding floc sizes were 400–600 µm.

Oost Friesche Gaatje (concentrations of 50 to 200 mg/l): the results are quite similar, although the suspended sediment concentrations are considerably higher than in the Ranselgat (20–50 mg/l) during high flow velocities. In the turbidity maximum area, the suspended sediment concentration was much higher (> 1000 mg/l). However, the settling velocities at periods of high flow currents were somewhat smaller (3 mm/s). Also, in the River Ems location, the suspended sediment concentration was fairly high (500–1500 mg/l) and the settling velocities of the macroflocs showed comparable results: an increase of the settling velocities up to several millimeters per second shortly after maximum flow velocity. During the field cruise, measurements with the RWS field settling tube have also been carried out. The settling velocities are in the range of 0.01 to 1.5 mm/s for concentrations between 10 and 1000 mg/l. Settling velocities higher than 1.5 mm/s were not observed due to the absence of macroflocs (fragile structure) which are thought to be destroyed during sampling.

Van Leussen (1994) used the VIS-system to measure floc sizes and settling velocities in the North Sea near Hook of Holland (The Netherlands). The results of 14 November 1990 shows few macroflocs in the range of 200 to 350 μm with settling velocities of 0.5 to 2 mm/s during peak flow conditions (0.7 m/s) and mud concentrations of about 50 mg/l. Microflocs < 80 μm with low settling velocities were dominant. These microflocs cannot accurately be detected by the VIS-system.

Van der Lee (2000) used the VIS-system in the tidal channel Groote Gat in the Dollard estuary (The Netherlands). Typical results for three days are, as follows:
- 11 October 1996 springtide: settling velocities in the range of 1.5 to 3.5 mm/s for flocs in the range of 80 to 650 μm; floc sizes are highest when the mud concentrations are relatively high (300 to 400 mg/l);
- 29 May 1996: large flocs up to 1000 um were observed in conditions with a rapid decline of the plankton bloom;
- 8 August 1996: a record of 20 minutes with about 500 data points shows floc sizes, settling velocities and concentrations as given in Table C.1.1.

The overall mean floc sizes of all data in 1995 and 1996 was about 150 μm, except end of May when the average floc size increased to about 300 μm (maximum flocs of 1000 μm) due to rapid decrease of plankton bloom. The percentage of organic material in suspended samples varied in the range of 15% to 30%.

Van der Lee (200) also used the Owen-settling tube to determine the settling velocities. The measured settling velocities were in the range of 0.1 to 1 mms/s. Larger settling velocities (due to macroflocs) were not observed.

Table C.1.1 Mud concentrations, floc sizes and settling velocities in Dollard estuary, The Netherlands

Concentration (mg/l)	Floc size (μm)	Settling velocity (mm/s)	Floc density (kg/m³)
100-200	100-150	1.5-2	1300-1350
200-300	150-200	2-3	1250-1300
300-400	200-250	2.5-3.5	1150-1250
400-500	250-300	3.5-5.5	1050-1150

Experiments of Shi and Zhou (2004)
The Changjiang Estuary is a meso-tidal estuary with a mean tidal range of 2 to 9 m. It consists of the North Branch, the South Branch, the North Channel, the South Channel, the North Passage and the South Passage. The North Passage has been chosen for the deep-water navigational channel and it is being regulated and dredged. The estuary is characterized by extensive areas of tidal mud Hats and salt marshes. The mean annual river discharge is 3 104 m³/s; Salinity ranges from 1 to 24 psu. Maximum and minimum annual suspended sediment loads are in the range of 3.5 to 7 10^8 t. More than 90%; consists of fine sediments (<32 μm). Clay minerals of the fine sediments are mainly classified as illite (73%,), montmorilonite (6-7%), kaolinite (10%) and chlorite (10%).
The effective settling velocity was derived from the fitting of measured mud concentration profiles over the tidal cycle, resulting in the following distribution:
- 5% with w_s=0.1-0.095 mm/s;
- 42% with w_s=1-2 mm/s;
- 39% with w_s=2.1-3 mm/s;
- 5% with w_s=3.1-4 mm/s;
- 9% with w_s=4.1-5 mm/s.

Based on this, the characteristic settling velocity are: $w_{s,10}$=0.8 mm/s, $w_{s,50}$=1.6 mm/s and $w_{s,90}$=4.3 mm/s.

MUSA

The settling velocities increase for increasing current-related bed-shear stresses. Higher shear stresses erode larger aggregates leading to higher concentrations and thus larger settling velocities due to the flocculating effect, see Table C.1.2.

Table C.1.2 Settling velocity as function of bed-shear stress and concentration (Shi and Zhou, 2004)

Bed-shear stress (N/m^2)	Concentrations (mg/l)			
	300	600	900	1200
0.25-0.5	w_s=0.1-1 mm/s	0.15-1	1-2	2-2.5
0.5-0.75	w_s=0.7-1.5 mm/s	0.7-1.2	1.5-2.5	1.8-2.5
0.75-1.0	w_s=1-1.5 mm/s	1-3	1.5-4	2.5-4
1.0-1.25	w_s=1-1.8 mm/s	1-3	1.5-3	3-4

Experiments of Dankers (2006)
The experiments of Dankers (2006) present data of the hindered settling of mud suspensions and the settling of sand particles in mud suspensions.

Hindered settling of mud suspensions
The experiments were carried out with natural (pure) mud, dredged by the Harbour Authority of Rotterdam from the Calland-Beer Channel in the Port of Rotterdam. The mud was stored in a dark place before it was shipped to Oxford University, where the experiments took place. The mud was kept at 4 °C during the period in which the experiments occurred.
Four settling columns were used in the experiments. The columns were made of acrylic and had a height of about 1.9 m and an inner diameter of 100 mm. The hindered settling velocity was determined from the sinking of the mud-fluid interface in a settling column. The initial mud concentration was in the range of 11 to 76 kg/m^3, but all suspensions were prepared in the same manner. Mud was diluted with salt water (5 ppt) to the desired density. This mixture was stirred overnight in order to regain room temperature. The value of the effective settling velocity of the mud suspension was, as follows:
- 1 to 3 mm/s for concentrations of 10 to 20 kg/m^3;
- 0.7 to 1 mm/s concentrations of 20 to 30 kg/m^3;
- 0.4 to 0.7 mm/s for concentrations of 30 to 60 kg/m^3.

Settling of sand in mud suspension
Two types of quartz sand were used in the experiments. A light colored sand with d_{50} = 110 µm and a silversand with d_{50} = 360 µm. A sand dispersal system was mounted on top of the columns, increasing the columns' height by 214 mm. The sand dispersal system consisted of a perspex base with a diameter of 440 mm in which a stainless steel dispersal system was placed, on which the sand was placed. The dispersal system had remotely controlled Venetian blinds which could be opened rapidly. After opening, the blinds shook for a few seconds in order to release all sand placed in the dispersal system.
The settling velocity of the sand grains (concentrations < 10 kg/m^3) at approximately 1 m below the input level was determined by using an optical method. The effective settling velocities was about 1.5 to 3.5 mm/s for mud concentrations of 10 to 20 kg/m^3 and in the range of 1 to 2.5 mm/s for concentrations of 30 to 40 kg/m^3. The settling velocity is much smaller than the Stokes' settling velocity for a single grain in clear water (10.9 mm/s for sediment with d_{50}= 110 µm).
The test results show:
1. settling sand particles penetrate into the mud suspensions and sink through the small drainage channels;

MUSA

2. small sand pockets are formed in the mud suspension; larger grains penetrate to the bottom of the settling column;
3. effective settling velocity of sand particles is effectively reduced by factor 3 to 10 depending on the mud concentration.

Experiments of Manning et al. (2007, 2010)

Manning et al. (2007, 2010) used the INSSEV-video camera system to measure floc sizes and settling velocities in an annular flume and in field conditions (Deurganckdok in Port of Antwerp).

The flume channel was filled with 45 l of saline water (salinity=20±0.2), to a level that reached the top of the annular ring (0.13 m depth). Pre-mixed mud/sand slurries of pre-determined ratios (75% mud and 25% sand; 50% mud and 50% sand; and 25% mud and 75% sand) were introduced into the mini-annular flume water column. Three total suspended particulate matter (SPM) concentrations were used at each ratio: 200 mg/l (±3%), 1000 mg/l (±4.3%) and 5000 mg/l (±4.7%).

For each run, four increments of rotational motor speed were used to shear the sediment slurries at shear stresses ranging from 0.06 to 0.9 Pa (at the floc sampling point). Sediment mixtures were sheared for 30 min at each stress increment. Each run was initiated at the fastest rotational velocity and decreased towards the slowest speeds as the run progressed.

Floc population sampling comprised careful extraction of a suspension sample from the same height in the water column. The floc sample was then quickly transferred to a perspex settling column, whereby each individual floc was observed using a high-resolution (10 µm lower limit) miniature underwater video camera as they were settling. Floc size D and settling velocity w_s were recorded during settling and the values obtained by video image post-processing. The video camera floc images are silhouettes enabling the floc/particle structure to be more visible.

Table C.1.3 Measured settling velocities of micro and macroflocs in annular flume with saline water using INSSEV-video camera system; mud from Tamar estuary (Manning et al., 2010)

Shear stress in flume (N/m²)	Concentration (mg/l)	Average settling velocity (mm/s) for various mud-sand fractions				Average settling velocities (mm/s)
		100% mud	**75% mud 25% sand**	**50% mud 50% sand**	**25% mud 75% sand**	
0.35	200	micro: 0.4 mm/s macro: 1.0 mm/s	0.7 (50-160 µm) 0.7 (160-200 um)	1.5 0.7	2.0 1.0	0.7-2.0 0.7-1.0
	1000	micro: 0.8 mm/s macro: 1.5 mm/s	0.7 1.0	1.0 1.3	3.0 1.0	0.7-3.0 1.0-1.3
	5000	micro: 0.6 mm/s macro: 3.5 mm/s	1.3 (50-160 µm) 3.0 (160-700 µm)	1.3 2.0	2.0 1.5	1.2-2.0 3.0-1.5
0.6	200	micro: 0.4 mm/s macro: 2.5 mm/s	1.0 1.5	2.5 1.5	2.0 1.0	1.0-2.5 1.5-1.0
	1000	micro: 0.8 mm/s macro: 3.0 mm/s	1.0 2.5	1.5 2.0	3.5 (40-160 µm) 1.5 (160-250 µm)	1.0-3.5 2.5-1.5
	5000	micro: 0.6 mm/s macro: 4.5 mm/s	2.5 7.0	3.5 5.5	4.0 3.5	2.5-4.0 7.0-3.5
0.9	200	micro: 0.4 mm/s macro: 1.0 mm/s	1.0 0.8	2.5 0.7	1.0 3.0	1.0-2.5 0.8-3.0

MUSA

	1000	micro: 0.8 mm/s	2.0	2.0	1.0	2.0-1.0
		macro: 1.5 mm/s	1.0	1.5	3.0	1.5-3.0
	5000	micro: 0.6 mm/s	2.5	2.5 (30-160 μm)	2.0	2.5-2.0
		macro: 3.0 mm/s	3.5	3.0 (160-250 μm)	3.5	3.0-3.5

microflocs: flocs< 160 μm with floc densities 200-1600 kg/m³; macroflocs: flocs > 160 μm with floc densities 20-200 kg/m³;

sand: d_{10}=70 μm; d_{50}=110 μm d_{90}= 170 μm; $w_{s,10,sand} \cong$ 3 mm/s; $w_{s,50,sand} \cong$7 mm/s;

water depth= 0.15 mm; samples taken at 0.022 m above bottom

(floc sizes are given between brackets)

Table C.1.4 Measured settling velocities of micro and macroflocs in annular flume with saline water using INSSEV-video camera system; mud from Portsmouth harbour (Manning et al., 2010)

Shear stress in flume (N/m²)	Concen tration (mg/l)	Average settling velocity (mm/s) for various mud-sand fractions	
		70% mud **30% sand**	**38% mud** **62% sand**
0.35	2000	micro: 2-8 mm/s (60-160 μm)	0.4-20 mm/s (30-160 μm)
		macro: 4-12 mm/s (160-700 μm)	1-10 mm/s (160-320 μm)

microflocs: flocs< 160 μm; macroflocs: flocs > 160 μm;

water depth= 0.15 mm; sampes taken at 0.022 m above bottom

(floc sizes are given between brackets)

The sand was the Redhill 110 type, which is a well-rounded and closely graded silica sand and has a d_{50} (d is sand grain size) of about 110 μm, with a d_{10} and d_{90} of 70 μm and 170 μm, respectively. The experimental mud sample was obtained from the surface down to a depth of about 50 mm from the Calstock region of the upper Tamar Estuary (UK). The measured results for mud of the Tamar estuary are given in Table C.1.3 and in Figure C.1.1. The measured results for mud of Portsmouth harbour are given in Table C.1.4.

The results of the settling tests of Manning et al. (2010) are shown as function of the bed-shear stress in the flume in Figure C.1.1. The vertical lines represent the settling velocities for various conditions. For the case of 100% mud (no sand), the lower end of the line is the settling velocity of the macroflocs and the upper end of the line is the settling velocity of the macroflocs. The length of the lines for mud fractions of 25%, 50% and 75% represent the variation range for concentrations of 200 to 5000 mg/l. The results for microflocs and macroflocs are represented by different line (dotted lines for microflocs and solid lines for macroflocs.

The most important characteristics are:
- settling velocities of microflocs in 100% mud suspensions are in the range of 0.4 to 0.8 mm/s;
- settling velocities of macroflocs in 100% mud suspensions are in the range of 1 to 4.5 mm/s;
- settling velocities of micro flocs in suspensions with mud and sand are in the range of 0.7 to 4 mm/s, which is partly caused by the enclosure of fine sand particles;
- settling velocities of microflocs and macroflocs are not very different for suspensions with mud and sand; most values in the range of 1 to 3 mm/s; an exception is the case with a shear stress of 0.6 N/m^2 with relatively large settling velocities of macroflocs up 7 mm/s;

MUSA

- settling velocities are smaller for larger bed-shear stresses due to breakup of flocs by larger velocity gradient (shear stresses);
- results may be biased towards the settling of larger flocs, as it is more difficult to detect the very fine mud floc/particles (lower limit of camera is 10 micron)
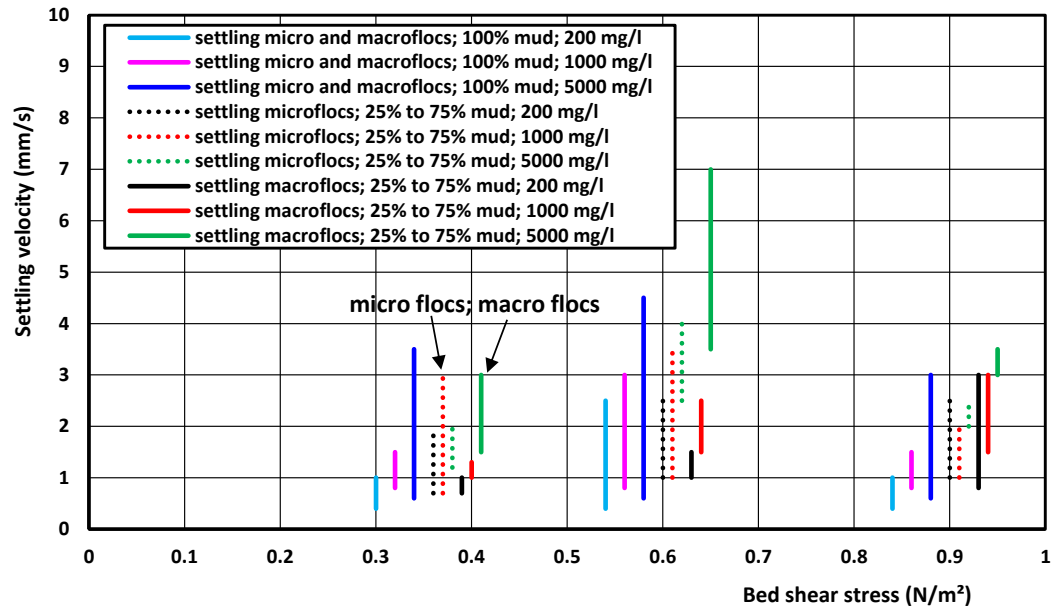

Figure C.1.1 Settling velocity of micro and macroflocs as function of bed-shear stress for different concentrations (Manning et al. 2010)

The measured data of the experiments in the entrance of Deurganckdok in the Port of Antwerp are shown in Table C.1.5. The INSSEV-camera was operated at 0.65 m above the bed surface in a depth of about 17.3 m at HW during a neap tidal cycle with tidal range of 4.8 m. The peak velocity was about 0.6 to 0.7m/s. The local mud concentrations were in the range of 50 to 250 mg/l over the tidal cycle. Floc sizes and settling velocities were measured every 30 minutes. The results for three characteristic times are given in Table C.1.5.

The data of Table C.1.5 can be interpreted, as follows:
- settling velocities of macroflocs up to 3 mm are highest during conditions with low velocities around the slack tidal periods;
- settling velocities of micro and macroflocs are in the range of 0.1 to 1.5 mm/s during peak tidal flow due to floc breakup by turbulent eddies (relatively high shear stresses);
- macroflocs have relatively low densities (< 50 kg/m³) and are delicate aggregates which are easily broken down resulting in their original microfloc sub-structures;

Table C.1.5 Measured floc sizes and settling velocities of micro and macro flocs in Deurganckdok, Port of Antwerp (Manning et al., 2010)

Tidal stage	Current velocity (m/s)	Mud concentration (mg/l)	Micro flocs			Macro flocs		
			Size (µm)	Settling velocity (mm/s)	density (kg/m³)	Size (µm)	Settling velocity (mm/s)	density (kg/m³)

HW+ 1 hrs	0.15	150	30-160	0.15-6	≅200	160-3000	0.4-1.5	<50
HW+ 2 hrs	0.65	70	60-160	0.15-1.5	≅200	160-280	0.1-1.5	<50
LW slack	0	60	70-160	0.15-2	≅200	160-700	0.5-4	<50

Critical comments: The results of the video-camera system were not compared to results from settling test. This latter method could also have been used during the annular flume tests. Samples extracted from the flume could have been used to do a settling test for comparison. The results of the INSSEV-camera may be biased towards the macroflocs which are easier to detect. The sample extraction method is not explicitly described.

Experiments of Deltares (2016) and Van Rijn (2019)

Mud samples were taken from various locations in the Dutch Wadden Sea (Holwerd ferry channel and tidal channel near Noordpolderzijl). Samples were also taken from the Scheldt tidal river in Belgium and from Payra channel in Bangladesh. Most samples were transferred to the laboratory for a settling tube test in (native) saline water. Deltares (2016) used a settling tube with underwaterbalance. Van Rijn used a settling tube from which subsamples were extracted by a small tap outlet.

One experiment of Van Rijn is discussed in more detail. The horizontal WASED-tube was used from the quay wall at the ferry landing near Holwerd (June 2017), The Netherlands. Four samples were taken at about 0.5 to 1 m above the local bed at about 2 hours after HW. The local water depth was about 3.5 m at the start of the tests and about 3 m at the end of the tests.

Particle size analysis of a bed sample and a suspended sample shows the following results:
- bed sample: percentage mud=53%; percentage sand=47%, d_{50}=55 μm;
- suspended sample: percentage mud=75%; percentage sand=25%, d_{50}=25 μm.

The test procedure was, as follows:
- samples 1 and 2: horizontal WASED-tube is lowered to the sampling point at about 0.5 m to 1 m above the bed; valves are closed after about 1 minute and the tube is raised; the water-sediment sample is poured into a large closable bucket, which is returned to the laboratory for analysis;
- sample 3: horizontal WASED-tube is lowered to the sampling point at about 0.5 m to 1 m above the bed; valves are closed after about 1 minute and the tube is raised; the water-sediment sample is poured into a large bucket; and then (using a funnel) into a vertical settling column at the quay wall (in the back of a small fan); the sample is stirred to make a uniform suspension and the settling test is started;
- sample 4: horizontal WASED-tube is lowered to the sampling point at about 0.5 m to 1 m above the bed; valves are closed after about 1 minute and the tube is raised; the Wased-tube is shaken and put into a vertical position and the settling process is started;
- sample 5; a bed mud sample was taken using the Van Veen grab and a settling test was performed in the laboratory using a settling tube.

The settling curves are shown in Figure C.1.2. The initial concentrations of samples 2 and 4 are extremely high as the samples are taken relatively close to the bed near the big steel poles of the quay wall creating additional turbulence resulting in high near-bed concentrations.

The median settling velocity ($w_{s,50}$) of samples 1, 2, 4 and 5 are in the range of 1.5 to 3.5 mm/s expressing the presence of fine sand. The results are fairly close together despite different analysis methods were used.

The median settling velocity ($w_{s,50}$) of sample 3 is about 0.4 mm/s expressing the presence of fines in the water column.

MUSA

The results of all tests are summarized in Table C.1.6 and Figure C.1.4.

Figure R3 shows the settling velocity as function of the mud concentration for all test results. Results from other sites (Van Rijn 1993; Deltares 2016) are also shown.

The maximum settling velocity of N-mud due to the flocculation effect is about 2 mm/s at a concentration of about 6 kg/m^3. The settling velocity decreases due to hindered settling effects to about 0.05 mm/s at a very high concentration of about 100 kg/m^3.

Non-flocculated mud is mostly present at low concentrations < 100 mg/l around slack tide, whereas flocculated mud generally is present at high concentrations (> 500 mg/l) in the near-bed zone (within 1 m of the bed) around maximum flow.

The settling velocities of N-mud and P-mud are smaller than those of the H-mud, which may be caused by the larger clay fraction (about 30% for N-mud/P-mud and about 10% for H-mud).

Literature review on sand and mud
16 November 2020

MUSA

Figure C.1.2 Settling columns (left: standard settling tube; right: WASED-tube in vertical position)
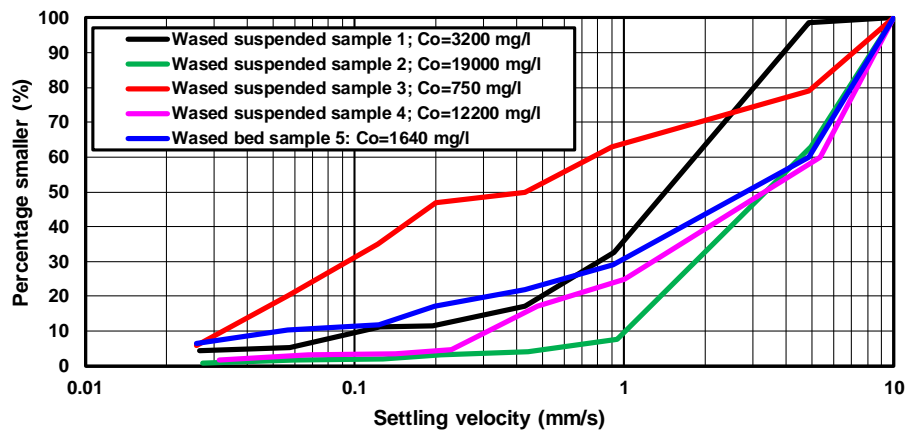

Figure C.1.3 Settling velocity curves of mud samples from quay wall near Holwerd, The Netherlands
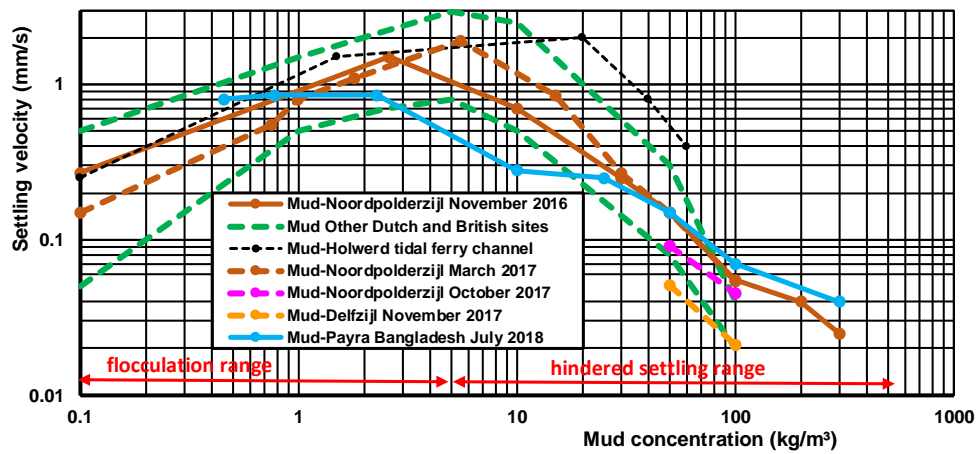

Figure C.1.4 Median settling velocity as function of mud concentration of various mud samples

Table C.1.6 Summary of settling velocities; mud from field sites in Bangladesh, Belgium and The Netherlands

Type of mud	Settling velocity of bed samples		Flocculated settling velocity of in-situ suspended samples (mm/s)
	flocculated settling velocity (mm/s)	hindered settling velocity (mm/s)	
N-mud Noordpolderzijl (NL) p_{clay}= 20% p_{silt}= 45% p_{sand}=35%	$w_{s,50}$=0.55 mm/s (c_o=750 mg/l) $w_{s,50}$=0.8 mm/s (c_o= 990 mg/l) $w_{s,50}$=1.1 mm/s (c_o=1755 mg/l) $w_{s,50}$=1.1 mm/s (c_o=2130 mg/l) $w_{s,50}$=1.5 mm/s (c_o=2635 mg/l) $w_{s,50}$=1.9 mm/s (c_o=6025 mg/l)	w_s=0.85 mm/s (c_o=15 gr/l) w_s=0.25 mm/s (c_o=30 gr/l) w_s=0.15 mm/s (c_o=50 gr/l) w_s=0.055 mm/s (c_o=100 gr/l)	$w_{s,50}$=0.4 mm/s (c_o=105 mg/l) $w_{s,50}$=0.75 mm/s (c_o=530 mg/l) $w_{s,50}$=1.4 mm/s (c_o=900 mg/l)
D-mud Delfzijl (NL) p_{clay}=40% p_{silt}=40% p_{sand}= 20%		w_s=0.051 mm/s (c_o=50 gr/l) w_s=0.021 mm/s (c_o=100 gr/l)	
H-mud; Holwerd (NL) p_{clay}=25% p_{silt}=50% p_{sand}=25%	$w_{s,50}$=0.2 to 1 mm/s (c_o< 1000 mg/l) $w_{s,50}$=1-2.5 mm/s (c_o=1000 to 5000 mg/l)	w_s=2.3 mm/s (c_o=20 gr/l) w_s=0.5 mm/s (c_o=40 gr/l) w_s=0.25 mm/s (c_o=60 gr/l)	
P-mud Payra Bangladesh p_{clay}=30% p_{silt}=50% p_{sand}=20%	$w_{s,50}$=0.85 mm/s (c_o=2275 mg/l) $w_{s,50}$=0.85 mm/s (c_o=775 mg/l) $w_{s,50}$=0.8 mm/s (c_o=455 mg/l)	w_s=0.28 mm/s (c_o=10 gr/l) w_s=0.25 mm/s (c_o=25 gr/l) w_s=0.15 mm/s (c_o=50 gr/l) w_s=0.07 mm/s (c_o=100 gr/l) w_s=0.04 mm/s (c_o=300 gr/l)	
S-mud; Scheldt river near Antwerp p_{clay}=40% p_{silt}=45% p_{sand}=15%	$w_{s,50}$=0.85 mm/s (c_o=2275 mg/l)		

p_{sand}= percentage of sand >63 μm ; p_{clay}=percentage of fines < 8 μm; p_{silt}=percentage of fines 8-63 μm

Experiments of Waterproof (2019, 2020) and LVRS (2018)

Holwerd mud

Various suspended samples were taken by a sampler bottle (2 liter) in the ferry channel near Holwerd landing pier, The Netherlands. The suspended samples were stirred again and analyzed in the laboratory using settling tests in native saline water. The results are summarized in Tables C.1.7, C.1.8 and in Figures C.1.5 to C.1.7.

In February 2019, the median settling velocity is relatively flow (0.1 mm/s) for low concentration of about 200 mg/land increasing to about 1 to 2 mm/s for high concentrations of 10,000 mg/l. The suspended material mainly consists of fine silt of 30 to 40 μm.

In September 2019, the median settling velocities are much lower in the range of 0.1 to 0.25 mm/s, because the mud concentrations are significantly smaller (500 to 1000 mg/l after summer period) than in February (5000 to 10000 mg/l in winter period with more wave activity).
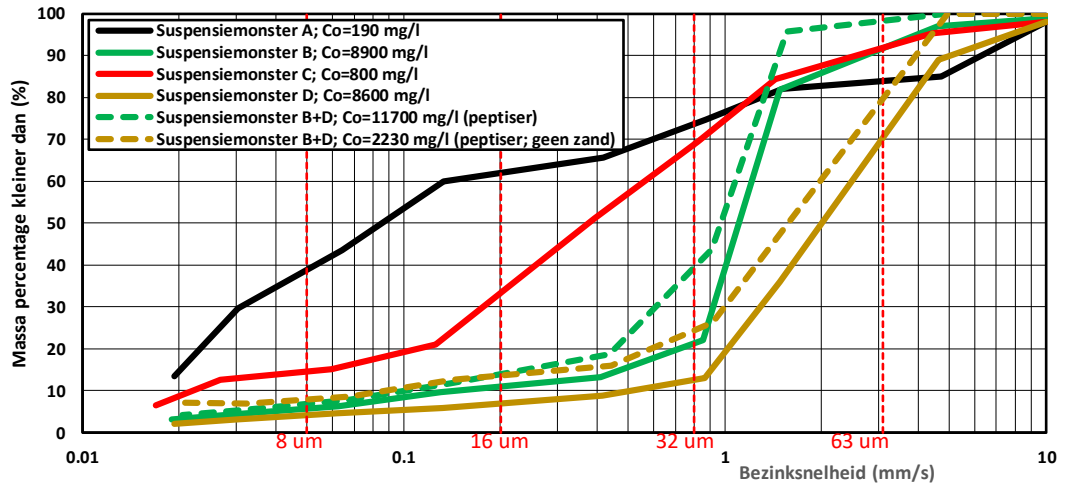
MUSA

Figure C.1.5 Settling velocities of samples; Location near Holwerd ferry landing pier; 27 February 2019
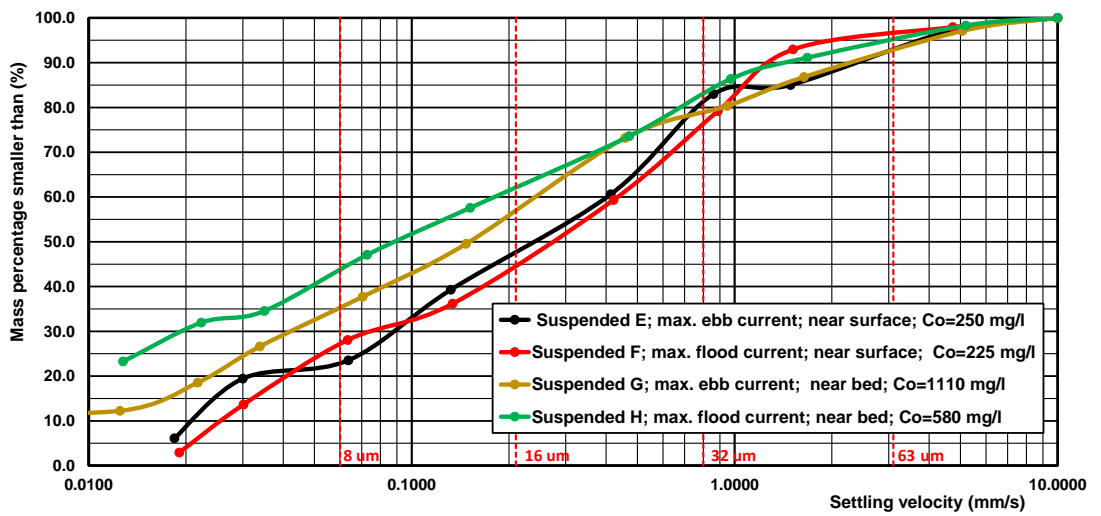

Figure C.1.6 Settling velocities of samples; Location near Holwerd ferry landing pier; 25 September 2019
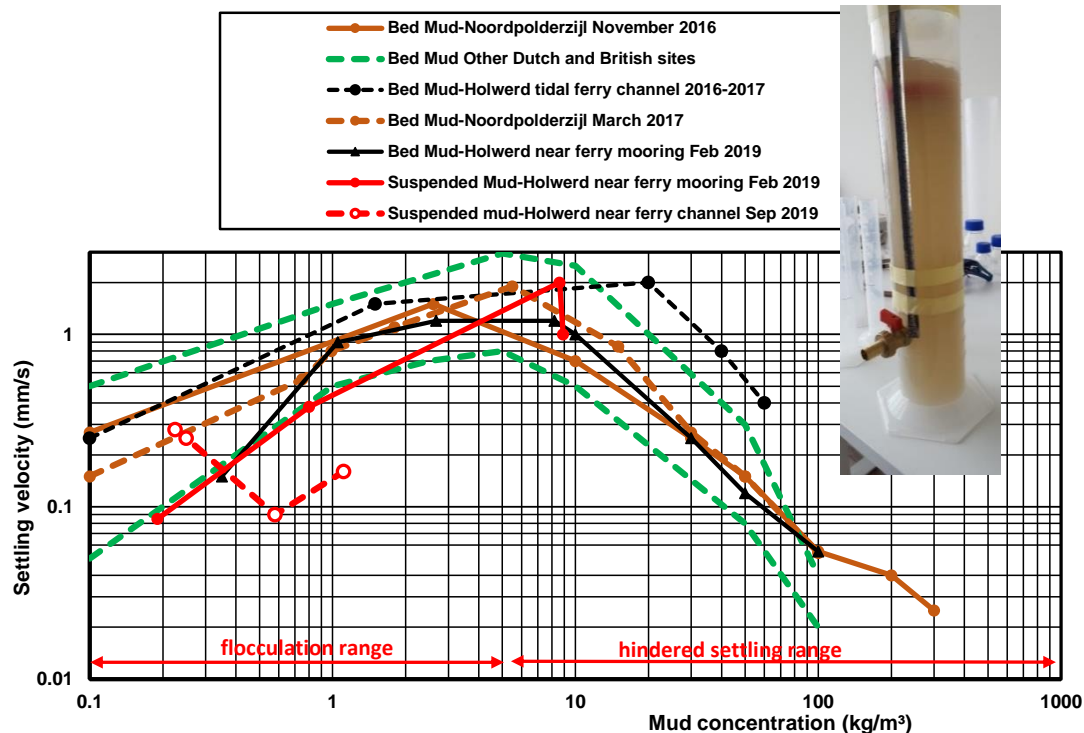
Literature review on sand and mud
16 November 2020

Figure C.1.7 Settling velocity as function of concentration

Table C.1.7 Settling velocities in native saline water; Holwerd mud; 8 February 2019

Location of samples	Settling velocity in native saline water			
	Initial concentration (mg/l)	$w_{s,10}$ (mm/s)	$w_{s,50}$ (mm/s)	$w_{s,90}$ (mm/s)
Suspended sample A; water surface -0,5 m; 1 hour before max ebb current	190	0.018	0.085	6.5
Suspended sample B; bed +0.2 m; max flood current	8900	0.15	1.1	2.8
Suspended sample C; water surface -0,5 m; max. flood current	800	0.022	0.38	2.7
Suspended sample D; bed +0,2 m; 1 hour before max ebb current	8600	0.05	2	5.0
Suspended sample B+D; with peptiser anti-flocculation agent	11700	0.1	1	1.6
Suspended sample B+D; with peptiser anti-flocculation agent; sand fraction removed by sieving 63 μm	2230	0.1	1.7	4
Bed sample	350	0.015	0.15	4
	1050	0.03	0.9	7
	2670	0.06	1.2	8
	8200	0.5	1.2	2
	10.000 (consolidation test)		1.0	
	30.000 (consolidation test)		0.25	

Literature review on sand and mud
16 November 2020

MUSA

| | 50.000 (consolidation test | | 0.12 | |
| | 100.000 (consolidation test) | | 0.055 | |

Table C.1.8 Settling velocities in native saline water; Holwerd mud; 25 September 2019

Location of samples	Settling velocity in native saline water			
	Initial concentration (mg/l)	$w_{s,10}$ (mm/s)	$w_{s,50}$ (mm/s)	$w_{s,90}$ (mm/s)
Suspended sample E; water surface -0,5 m; max. ebb current	250	0.02	0.25	2.5
Suspended sample F; water surface -0,5 m; max. flood current	225	0.025	0.28	1.3
Suspended sample G; bed +0,15-0,65 m; max. ebb current	1110	0.01	0.16	2.2
Suspended sample H; bed +0,15-0.65 m; max. flood current	580	0.01	0.09	1.5

Schelde mud

Various samples have been analyzed in the laboratory of Waterproof (Lelystad) by use of settling tests. Samples C and D are split in 2 subsamples to do tests with and without peptiser (anti-flocculation agent). The results are shown in Table C.1.9 and Figure C.1.8. Results of tests with Holwerd mud are shown for comparison.

The most important features are:
- the settling velocity of suspended Schelde mud is rather low with values ($w_{s,50}$) between 0.07 and 0.1 mm/s (0.085 ± 0.015 mm/s), which points to a low degree of flocculation; settling velocities of suspended Holwerd mud are much higher (factor 5 to 10) with values of about $w_{s,50} \cong 0.8$ mm/s;
- the equivalent particle size is about 10 ± 2 μm.

Most of the suspended samples of water and mud were taken by using a small pulsation pump, which may have destructed the size and structure of the mud flocs. Some samples were taken by using the VanDorn bottle sampler (2 liters; equipped with string valves on both sides). These samples are fairly undisturbed. All samples were taken at the same height above the bed. The mud concentrations are very similar (about 155 mg/l). The median settling velocity of both samples (pump and bottle) is between 0.04 and 0.07 mm/s (0.055 ± 0.015 mm/s).
The largest settling velocity ($w_{s,90}$) of macroflocs is in the range of 1.5 to 3.5 mm/s.
The median settling velocity of samples treated with peptiser is a factor of 2 smaller than those of samples with peptiser-treatment. The equivalent particle size is about 5 μm.
Suspended sand was obtained by washing the samples over a sieve of 63 μm. All available suspended sand was aggregated into one collective sample to do a settling test in a long tube. The median settling velocity of suspended sand is $w_{s,50} = 14$ mm/s, corresponding to a particle size of $d_{50,sus} = 130$ μm.

Table C.1.9 Settling velocities and equivalent particle sizes of mud and sand in suspension; 28 September 2018

Sample	Height above bed	Initial concentration (mg/l)	Settling velocity			Equivalent particle size (temp. 15 ºC)		
			$w_{s,10}$	$w_{s,50}$	$w_{s,90}$	d_{10}	d_{50}	d_{90}

MUSA

	(m)		(mm/s)	(mm/s)	(mm/s)	(µm)	(µm)	(µm)
A-pump	1; ebb	510	0.02	0.088	1.3	5	11	40
B-pump	3; ebb	295	<0.02	0.098	3.5	<5	11	67
C-pump	6; ebb	335	<0.02	0.067	1.3	<5	9	40
C-pump with peptizer (deflocculation)	6: ebb	345	<0.01	0.03	1.3	<3	6	40
D-vandorn bottle	5; ebb	160	<0.02	0.038	1.3	<5	7	40
D-pump	5; ebb	150	<0.02	0.068	1.3	<5	9	40
D-pump with peptizer (deflocculation)	5; ebb	190	<0.01	0.03	0.2	<3	6	16
E	1; flood	390	<0.02	0.12	1.5	<5	12	44
Aggregated sample fine sand	0.15 -10	-	3	14	50	63	130	300
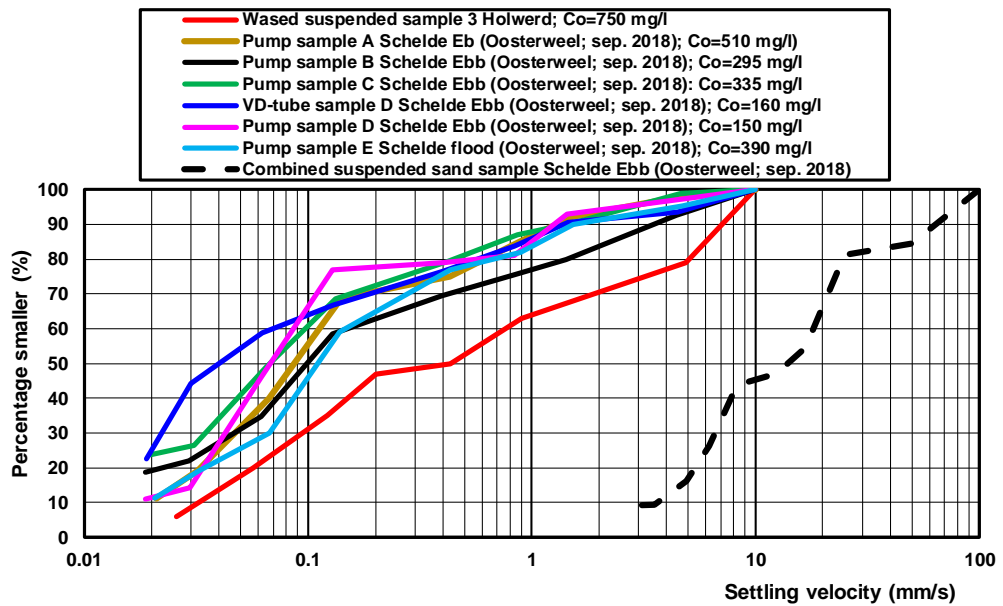
Figure C.1.8 Settling velocity of mud/sand in suspension; Schelde 28 September 2018 and Holwerd June 2018
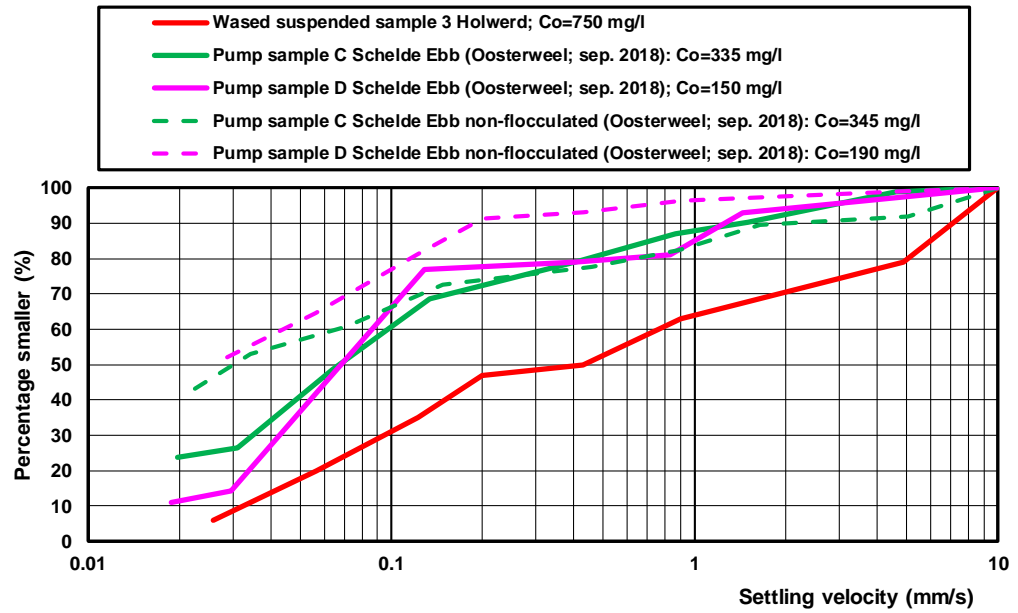
Figure C.1.9 Settling velocity of non-flocculated mud in suspension; Schelde 28 September 2018 and Holwerd Juni 2018

D Summary of experimental results of bulk density of mud-sand beds

D.1 All experiments

Experiments of van Rijn and Barth (2020)

Several consolidation tests have been carried out in transparent perspex columns with lengths of 0.5 m (inner diameter of 60 mm); 1 m (60 mm); 2 m (80 mm) and 3 m (90 mm). The consolidation tests consisted of:

- preparation of the mud suspension in a bucket (saline seawater);
- transfer of the mud suspension into the column;
- mixing of the mud suspension to make a uniform suspension (using a mechanical mixing rod with perforated plate at the bottom);
- start of test at the time that the mixing rod is removed from the column;
- reading of mud surface at various times;
- placement of a sand layer (d_{10}=95 μm, d_{50}=145 μm and d_{90}=210 μm) at a certain time (in some tests) to speed up the consolidation process.

Various types of mud have been used in the consolidation columns:

- mud from the harbour basin of Noordpolderzijl (N-mud); wet bulk density of 1470 $\pm$ 10 kg/m^3 (dry bulk density of 755 kg/m^3); 17% calcareous materials; 7% organic materials;
- mud from the harbour basin of Delfzijl (D-mud); wet bulk density of 1315 $\pm$ 10 kg/m^3 (dry bulk density of 505 kg/m^3); 18% calcareous materials; 10% organic materials;
- artificial mud-sand mixtures by adding fine sand to the base N-mud to obtain mixtures with relatively high percentages of sand (57%) and (73%).

The test program of the consolidation tests using native saline water is given in Table D.1.1. In some tests, a layer of sand was placed on top of the mud layer at a certain time to study whether this helps to speed up the consolidation process. Various repetition tests have been done to study the reproducibility with fairly good results. Details are given by Van Rijn 2018.

Laboratory tests

Various basic mud tests have been done to determine the mud particle sizes**.** As the determination of the fine mud particle sizes is not a straightforward process, three methods have been used: (i) SediGraph-method (SG); (ii) Hydrometer-method (HM) and (iii) Filtration-Wased method (FW-method). All methods basically measure the settling velocities of the particles, which are converted to particle diameters using the Stokes settling velocity formula. The tests have been done in fresh water using a peptiser-solution for deflocculation. The sand fraction was separated using wet sieving. The calcareous and organic materials were removed chemically to obtain samples with minerals only.

The SediGraph III-instrument (Micromeritics) measures the decrease of the mud concentrations in a small-scale settling cell. The mud concentrations are determined by direct (precalibrated) x-ray absorption.

The hydrometer test is based on the measurement of the decreasing sediment mixture density (initial concentration of 30 gr/l) by using a floating body in a column with settling mud particles over a period of 2 days. The sinking of the floating body is minimum at initial time with maximum mud concentration and maximum in clear water at the end of the test.

MUSA

Table D.1.1 Test program of columns 1 m, 2 m and 3 m; Noordpolderzijl-mud and Delfzijl-mud

Column		Type of mud	Initial concentration	Initial height of mud suspension	Duration	Additional sand load (d_{50}=145 μm) on top of mud layer		Settling height at end of test	Density at end of test
No	**Length (m)**		**(kg/m³)**	**(mm)**	**(days)**	**Thickness (mm)**	**At time (days)**	**(mm)**	**(kg/m³)**
1A	1	N	50 (ps=40%)	900	19	none	-	76	590 (19 d)
1B	1	N	100 (ps=40%)	900	19	none	-	147	610 (19 d)
1C	1	N	200 (ps=40%)	900	19	none	-	302	595 (19 d)
1D	1	N	300 (ps=40%)	900	19	none	-	392	690 (19 d)
2A	2	N	50 (ps=40%)	1850	39	none	-	129	715 (39 d)
2B	2	N	100 (ps=40%)	1850	30	none	-	293	630 (30 d)
2C	2	N	200 (ps=40%)	1850	37	185 (10% of i.h)	11	602	615 (37d)
2D	2	N	300 (ps=40%)	1850	116	370 (20% of i.h.) 555 (30% of i.h.)	11 60	778	715 (116 d)
3A	3	N	300 (ps=40%)	2800	102	560 (20% of i.h.)	22	1213	692 (102 d)
3C	3	N	300 (ps=57%)	2800	69	none	-	1212	693 (69 d)
3D	3	N	300 (ps=73%)	2800	69	none	-	956	878 (69 d)
1E	1	D	50 (ps=20%)	900	83	none	-	114	395 (83 d)
1F	1	D	100 (ps=20%)	900	83	none	-	225	400 (83 d)
1G	1	D	200 (ps=20%)	900	83	none	-	422	426 (83 d)
1H	1	D	300 (ps=20%)	900	83	none	-	596	453 (83 d)
2E	2	D	300 (ps=20%)	1850	76	none	-	1202	462 (76d)
2F	2	D	300 (ps=20%)	1850	76	185 (10%)	13	1156	480 (76 d)
2G	2	D	300 (ps=20%)	1850	76	370 (20%)	13	1156	480 (76 d)

N= mud from Noordpolderzijl; D= mud from Delfzijl-harbour
ps= percentage sand; d= days; i.h.= initial height of mud

MUSA

The filtration-Wased method is based on the settling of suspended sediments in a special settling column (Wased-column) with a height of 0.5 m. Small subsamples are taken at various preset times from the suspension at 70 mm above the bottom of the column. The mud concentration is determined by filtration of mud from the sample using glass-fibre filters with 0.45 µm pore size.
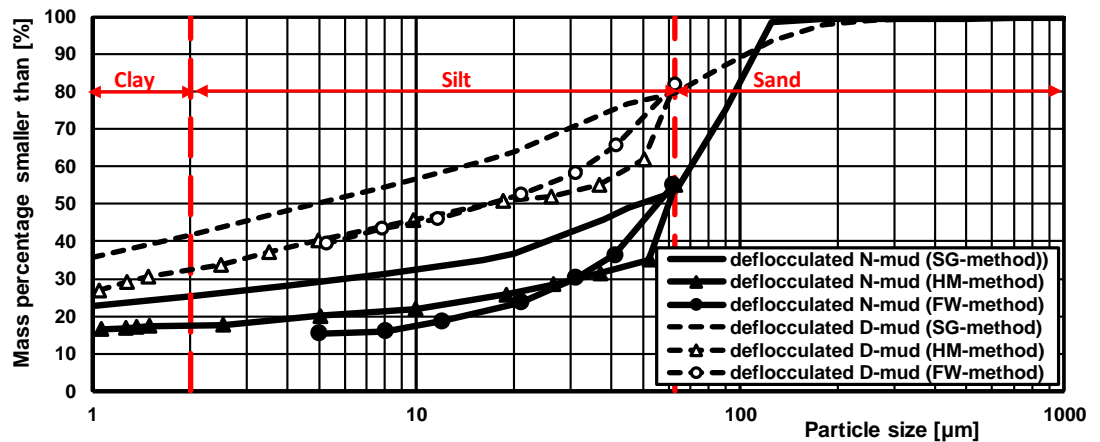

Figure D.1.1 Particle size distribution of deflocculated N-mud and D-mud

SG=SediGraph method; HM=Hydrometer method; FW=Filtration-Wased method; S= Sieving method for sand fraction

Table D.1.2 Mud data of Noordpolderzijl and Delfzijl

Parameter	Mud Noordpolderzijl (N-mud) (October 2017)		Mud Delfzijl (D-mud) (November 2017)	
	Minerals + calcareous + organic materials	Minerals only	Minerals + calcareous + organic materials	Minerals only
Particle diameter of mud-sand d_{50}; d_{90} (µm)	30; 110	30; 110	4; 100	5; 100
Particle size (µm) of sand fraction > 63 µm	85	85	120	120
Fluid density seawater (kg/m³)	1010	1010	1007	1007
Sediment density (kg/m³)	2570	2570	2560	2560
Wet bulk density (kg/m³)	1470±10	1470±10	1310±10	1310±10
Dry bulk density (kg/m³)	755±10	755±10	505±10	505±10
Percentage organic material	7%	0%	10%	0%
Percentage calcareous materials	17%	0%	18%	0%
Percentage sediment > 63 µm	40%	45%	20%	20%
Percentage silt 2 to 63 µm	35%-40%	30%-35%	40%-50%	40-50%
Percentage clay < 2 µm	20%-25%	20%-25%	30%-40%	30%-40%
Plasticity index (difference in water content to go from semi-solid state to liquid state)	33%	n.m.	35%	n.m.

n.m.= not measured; SG= SediGraph-method yields largest percentage clay < 2 µm

The test results are given in Table D.1.2 and in Figure D.1.1, which shows the particle size distribution of the N-mud and the D-mud based on the three methods. As regards the N-

mud, the percentage of fine sand is about 45% based on wet sieving. The SG-method yields a size distribution with smaller values ($d_{50} \cong 45$ μm) than those of the HM and FW-methods ($d_{50} \cong 60$ μm). The percentage of clay < 2 μm is about 25% based on the SG-method and about 15% based on the HM and FW-methods.

The D-mud is much finer than the N-mud. The percentage of fine sand of the D-mud is about 20%. The SG-method yields a size distribution with much smaller values ($d_{50} \cong 5$ μm) than those of the HM and FW-methods ($d_{50} \cong 18$ μm). The percentage of clay < 2 μm is about 40% based on the SG-method and about 30% based on the HM and FW-methods.

Field tests

The bed of the tidal channel of Noordpolderzijl (Groningen, The Netherlands) is situated between the landward harbour basin and the seaward Wadden Sea and consists of a soft layer of sandy mud with a thickness of 0.5 to 0.7 m on top of a more compacted sandy subsoil. A male person will sink into the mud near the harbour basin over about 0.5 m. The vertical distribution of the wet end dry bulk density of the soft top layer was studied by analyzing field samples. In June 2017, various mud samples were taken at different locations along the tidal channel of Noordpolderzijl (length of about 3 km; width of about 15 m). The channel bed is exposed (almost dry) at low water. Bed samples were taken over the upper 0.5 m in the middle and at the eastern side of the channel bed at low water with exposed bed. The dry bulk density and the percentage of sand (> 63 μm) have been determined in the laboratory. The d_{50} of the sand fraction varies between 95 μm at the landward end to about 120 μm at the seaward end. The ratio of the fraction of clay (< 2 μm) and silt (2-63 μm) is about 1 to 2; ($p_{silt} \cong 2 p_{clay}$).

Synthesis

The consolidation process of mud mixtures strongly depends on three parameters: percentage of clay/lutum< 2 to 4 μm, percentage of sand particles > 63 μm and the layer thickness. Other parameters like the type of mud (mineral composition) and the percentage of organic materials are less important. Natural muds may have a percentage of sand in the range of 10% to 50%.

Mud suspensions with initial concentrations of 50 to 100 kg/m^3, as present in near-bed layers of a natural muddy tidal channels, can consolidate to a dry density of about 150 to 200 kg/m^3 during a period of 3 hours, which is a typical value for the tidal slack period when deposition takes place. The hindered settling process is not so much affected by the sand content. The transition from the hindered settling phase to the primary consolidation phase is characterized by the formation of a network structure. The gelling concentrations with some degree of matrix (skeleton) structure are in the range of 100 to 150 kg/m^3.

Natural muds with initial concentrations of 150 to 300 kg/m^3 and a low sand content (< 20%) can reach a dry density of about 350 kg/m^3 after 1 day. Natural muds with high sand content (40%-50%) can reach a dry density of about 450 kg/m^3 after 1 day. Dry density values in this range are the onset of the primary consolidation phase with the gradual buildup of grain stresses in a matrix-type network structure.

The primary (short-term) consolidation process proceeds fairly quickly (10 to 50 days) if the percentage of sand (> 62 μm) is larger than about 30%, as shown in Figure D.1.2, which is based on the data from the present study and the Literature. Natural muds with low sand content ($\cong$ 20%) and thickness of 1 to 2 m can consolidate to 400 to 450 kg/m^3 after 20 to 50 days. Natural muds with a high sand content of 40% to 50% and thickness of 1 to 3 m can consolidate to dry density values of 600 to 700 kg/m^3 after 10 to 30 days. The time scale is relatively small (up to 60 days) for a small thickness of 1 m and relatively large (up to 180 days) for a large mud thickness of about 3 m and low sand content. The available data suggests an almost linear relationship between the time scale of the primary consolidation period and the mud layer thickness.

Literature review on sand and mud
16 November 2020

The vertical distribution of the dry density shows relatively high values (15% to 20% larger than depth-mean) in the near-bottom zone and relatively low values (15% to 20% smaller) in the near-surface zone. The end density values of the N-mud and D-mud in the laboratory columns were about 10% smaller than the in-situ density values at the field site where the base mud was taken.
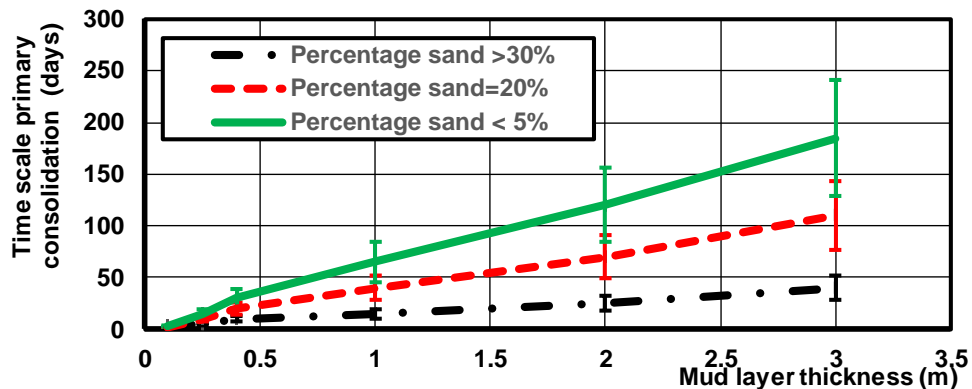

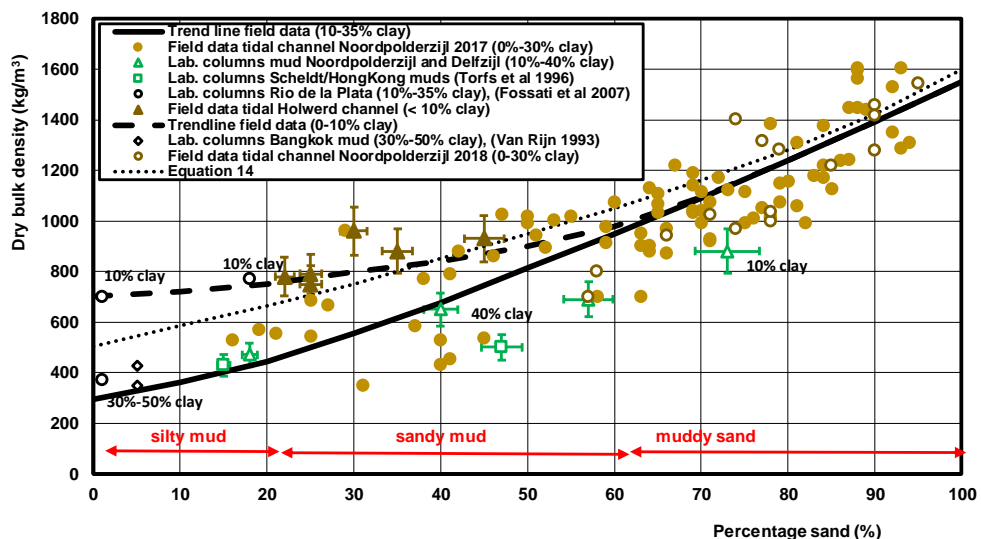Figure D.1.2 Time scale of primary consolidation process

Figure D.1.3 End dry density of primary consolidation period as function of percentage of sand and clay

The end dry bulk density of the primary (short-term) consolidation phase of mud mixtures with a layer thickness of 1 to 3 m strongly depends on the percentage of sand (ps), as shown in Figure D.1.3 with data from the present study and from the Literature (Table D.1.3). The end density increases from about 450 kg/m³ for ps=20% to about 880 kg/m³ for ps=73%. The end density is higher if the percentage of clay is lower. The dry density values derived from laboratory columns with vertical drainage processes only are somewhat smaller than the values based on field tests. In field conditions, the consolidation processes are also influenced by lateral drainage resulting in larger dry density values (15%).

The end density can be increased by 5% to 10% by placing a sand layer load on top of the mud surface after about 10 days, once the upper mud layer has developed a network structure. The placement of a top sand load is not very effective as the draining structure of the mud layer itself is not affected except for the upper mud layer in contact with the

MUSA

sand load layer. If sand is available, it is much more effective to mix the available sand through the mud beforehand than to use the sand as a top load. By mixing of mud and sand, the (end) density at the end of the primary consolidation process can be increased by about 50%.

An empirical equation (Van Rijn and Barth, 2019) is also shown in **Figure RB3** for realistic values of p_{org}, p_{clay} and p_{silt}.

Table D.1.3 Laboratory and field data of end dry density values at end of short-term consolidation period

Type of mud	Layer thickness (m)	Percentage clay < 2/4 μm (%)	Percentage sand > 63 μm (%)	Percentage organic materials (%)	Time scale of primary consolidation period (days)	End dry density of primary consolidation (kg/m³)
Lab. colums: Bangkok mud (Van Rijn 1993)	1	30-50	5	-	90	420
	2	30-50	5	-	180	350
Lab. columns: Scheldt mud (Torfs et al. 1996)		n.m	15	n.m.	60	430
Lab. columns; Hong Kong mud (Torfs et al. 1996)	0.1	40	47	n.m.	<5	500
Lab. columns: Rio de la Plata muds (Fossati et al. 2015)	1	35	1	n.m.	60	370
	1	10	1	n.m.	<1	700
	1	10	18	n.m.	<1	770
Lab. columns: Delfzijl mud (present study)	2	40	18	10	50	470
Lab. columns: Noordpolderzijl mud (present study)	2-3	30-40	40	7	40	650
	2-3	20	57	7	40	690
	2-3	10	73	7	40	880
Field: Holwerd channel (Deltares 2016; Van Rijn 2016)	1-2	<10	22	7	<30	780
	1-2	<10	25	7	<30	750
	1-2	<10	25	7	<30	790
	1-2	<10	30	7	<30	960
	1-2	<10	35	7	<30	880
	1-2	<10	45	7	<30	930
	<1	n.m.	20-50	n.m.	<90	400-800

Literature review on sand and mud
16 November 2020

MUSA

Field:	<1	n.m.	50-60	n.m.	<90	800-1000
Noordpolderz	<1	n.m.	60-70	n.m.	<60	800-1200
ijl	<1	n.m.	70-80	n.m.	<30	1000-1400
(Van Rijn 2017)	<1	n.m.	80-90	n.m.	<30	1000-1600

n.m.= not measured

Figures D.1.2 and D.1.3 can be used to get an estimate of the in-situ density of muddy layers to be dredged from navigation channels and harbour basins. It is most efficient to start dredging when the bulk density of the deposited material is as high as possible. The maximum time scale of the primary consolidation phase is of the order of 6 months for a muddy layer of 3 m, see Figure D.1.2. Hence, the dredging interval should not be smaller than about 6 months in a situation with a thick muddy layer with low sand content. Predictions of siltation rates generally yield quantities of sand, silt and clay in tons/year, which can be converted to an in-situ dry bulk density and layer thickness using Figure D.1.3.

MUSA

E   Summary of experimental results of bedforms in mud-sand beds

E.1   Abiotic experiments

Laboratory experiments of Baas et al. (2013)

Limited studies on bedform development in mud-sand mixture are available, despite the wide recognition of the importance of sedimentary bedforms.

Baas et al. (2013) developed the first systematically acquired set of laboratory flume data on the development of current ripples in mixed, cohesive sand–mud beds under steady, uniform flow conditions. The results were compared with the results of previous experiments in which cohesive forces in high concentration clay flows dominated bedform development (by Baas et al, 2011). The experiments were conducted in a 10-m-long and 0.3-m-wide recirculating flume, with a 50-mm-thick layer of mixed sediment consisting of fine-grained and moderately sorted sand (D_{50} =143 µm, σ=0.93) and kaolin with a D_{50} of 7.3 µm, with the particle size distribution spanning the clay and silt classes (referred to as mud, note: no field mud). The main findings of this study are:

- The *development curves* of the bedforms in mixed sand–mud and pure sand have the same basic asymptotic shape (i.e. initial bedform growth rates are similar), although several mixed sand–mud experiments showed a delay in the appearance of the first ripples on the flat bed, with the longest delays emerging from the runs with the highest clay values.

- Linear regression F-tests suggest a strong inversely proportional relationship between *bedform height* and initial bed mud fraction and a weak inversely proportional relationship between *bedform wavelength* and initial bed mud fraction: the ripple height decreases, and current ripple wavelength is more or less constant as bed mud fraction is increased from 0% to 13%. The ripples are significantly smaller above 13%, and height and wavelengths appear to remain constant up to bed mud fractions of 18%.

- The bed *sediment fluxes by current ripple migration* on the mixed sand–mud beds were consistently lower than on the mud-free sand bed, with a decreasing trend for an increasing initial mud fraction.

- *Winnowing* of clay from the mixed sediment bed is highly efficient (promoted by scouring and bedform migration), up to the point where the bedforms to resemble clean-sand current ripples, particularly at low initial bed mud fractions. However, strong bed cohesion and bed armouring may significantly delay or fully prevent the mixed-sediment bedforms from reaching the size of their clean-sand equivalents.

- Clay-rich, cohesive flows tend to act as a local sink of fine cohesive sediment, while clay-poor flows that move across mixed sand–mud beds tend to act as a local source of fine cohesive sediment (because of the winnowing).

A qualitative comparison is presented between bedform development in cohesive beds with bedform development under cohesive, turbulence-modulated flows. The main outcomes are presented in Table E.1.1.

MUSA

Table E.1.1 Bed form development in mud-sand beds

Cohesive forces in bed dominate bedform dynamics	Cohesive forces in flow dominate bedform dynamics
Erosional bedforms prevail	Depositional bedforms prevail
Deep erosional scours, and erosional base of bedforms	Scouring is most common below high-concentration clay flows
Bedforms evolve through stage with sandy crest and mixed sand-mud core; angle-of-repose cross-lamination prevails	Bedforms go through same stage, but low angle cross lamination is more common
Highly efficient winnowing of clay; sandy bedforms	Clay winnowing is less common; bedforms consist of muddy sand
Texture of bedforms contrasts with texture of mixed sand-mud bed underneath	Less contrast in textures
Winnowed sand tends to 'heal' irregular scoured topography; thus, re-establishing classic quasi-triangular bedform shapes	Healing processes are confined to LTPF (Lower Transitional Plug Flows); bedforms have variable shapes
Bedform height tends to decrease with increasing initial clay content in the bed; wavelength is constant below f0=13%	Bedform height and wavelength tend to increase with increasing clay concentration in the flow
No backflow ripples present in bedform trough	Backflow ripples present in bedform trough
No dewatering structures observed	Dewatering structures in mixed sand-mud

These findings are supported by a later experimental study of Schindler et al. (2015), whose results not only revealed a dramatic influence of initial bed clay content on mean bedform dimensions, but also on the steepness. Hence, the bedforms in clay-rich sand have lower amplitudes, lower wavelengths, and flatter geometries (see Figure E.1.1) than in clay-poor sand.
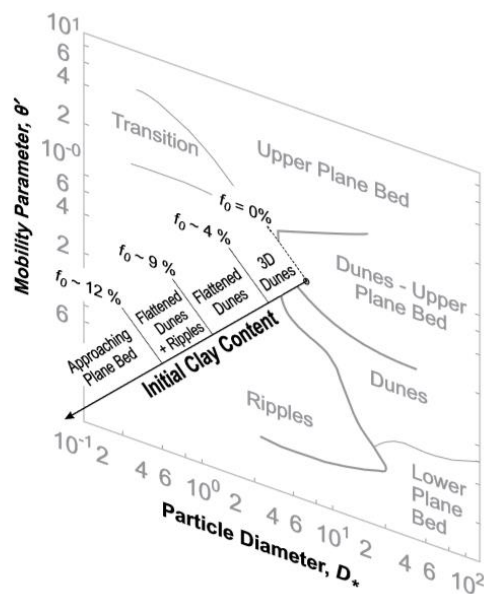

Figure E.1.1 Conceptual modification of phase-space diagram that includes third axis to incorporate cohesion. The z-axis shows approximate boundaries of initial clay content (f0) that distinguish between bedform types for the experimental conditions (by Schindler et al., 2015, modified after van den Berg and van Gelder, 1993).

Literature review on sand and mud
16 November 2020

MUSA

Experiments of Baas et al. (2014)

Baas et al. (2014) performed flume experiments with a wave generator, to study wave ripples in mixed sand-clay environments (using medium-grained sand, D_{50}=496 µm and kaolin clay). Wave ripples also developed in the mixed sand-clay, but at a slower rate than in the clean sand, even though the wave conditions were similar in all experiments. Yet, the equilibrium dimensions of the wave ripples were not affected by the bed clay fraction; the wave ripples have similar dimensions for different clay fractions (here, H_{eq} ~ 20 mm and L_{eq} ~ 120 mm, for clay fractions 0-5.5 %)), provided that the ripples are given enough time to attain their equilibrium size. This was explained by the fact that the waves were highly efficient in suspending clay particles from the pores in between the sand grains. Recorded sediment cores that penetrated ripple crests revealed 100% clean sand between the sediment surface and the base of the bedforms. Moreover, SPM concentrations were an order of magnitude higher than at the experiment without clay. Clay winnowing from the ripple troughs was less efficient (86.3%), probably because the troughs are more protected from near-bed oscillatory flow than the crests.

However, clay winnowing may not have been the only process by which the waves formed the clean sand ripples. Underneath the ripples, the final bed sand fraction was lower and the final bed clay fraction was higher than the initial bed fractions, suggesting that this part of the bed gained clay particles. The authors hypothesize that the waves acted as a pump that not only winnowed clay, but also pushed clay particles deeper into the bed. The high permeability of the medium-grained sand used in the experiments may have promoted this process.

Compared to the results of Baas et al. (2013) (current ripples), the winnowing efficiency was higher, even though these experiments were conducted at depth-averaged flow velocities that were higher than the maximum near-bed orbital velocity in the wave study (0.36 ms-1 and 0.34 ms-1, respectively). This agrees with the common notion that waves are more effective at entraining sediment than currents (van Rijn, 1993).

E.2   Experiments including biotic effects

Experiments of Malarkey et al. (2015)

In addition to these results, Malarkey et al. (2015) studied the effect of biologically cohesive extracellular polymeric substances (EPS) generated by microorganisms on bedform formation. They showed that the pervasive distribution of low levels of EPS throughout the sediment, rather than the high surficial levels of EPS in biofilms, is the key control on bedform dynamics. The first main effect of the EPS was to dramatically increase the time at which the bedforms first appeared (t_i=0.1–7.9 h), even for the comparatively small amounts of EPS used (0–0.125 %), see Figure E.2.1. This is a much stronger effect than for physical cohesion, where t_i does not increase significantly below a mud content of 16% (Baas et al., 2013). Besides, the total development time was also increased by two orders of magnitude as EPS content increased from 0 to 0.063% (T_H=1.1–115.2 h and T_L=1.3–92.2 h). This is again a far stronger effect than for physical cohesion, where T_H and T_L show no significant change up to mud contents of 12%. An EPS of 0.125% was determined as the upper limit for bedform formation.
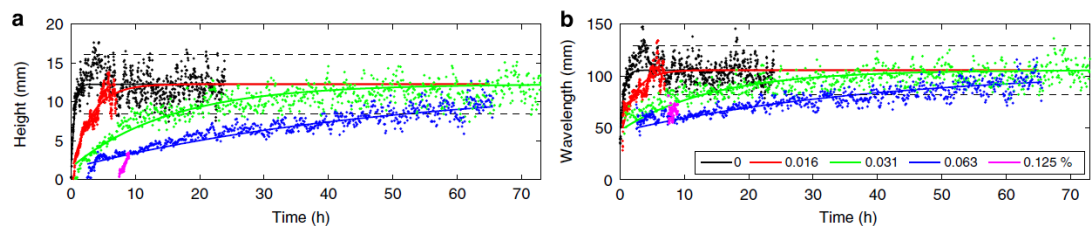

Figure E.2.1 Ripple height (a) and wavelength (b) plotted against time for various initial EPS contents

MUSA

Experiments of Parsons et al. (2016)

These findings are supported by the research of Parsons et al. (2016), who conducted controlled laboratory experiments to identify the influence of physical and biological cohesion on equilibrium dune morphology and examined the nature of the cohesive bonding mechanisms in three-way mixtures of mud, sand, and EPS (simulating both low and high primary production rates). Their results (see Figure E.2.2) reveal a substantial influence of initial bed mud and EPS content on bed form height (H), length (L), steepness (H/L), and bed roughness ($k_s = 25H^2/L$), and that EPS are by far the most effective of the two components in reducing bed form dimensions and steepness, due to their stronger interparticle bonding. The combined effect of biological and physical cohesion has been shown to alter bed form dimensions by up to an order of magnitude and bed roughness by up to 2 orders of magnitude. These large changes result from the suppression of dunes in favour of ripples as the dominant bed form.
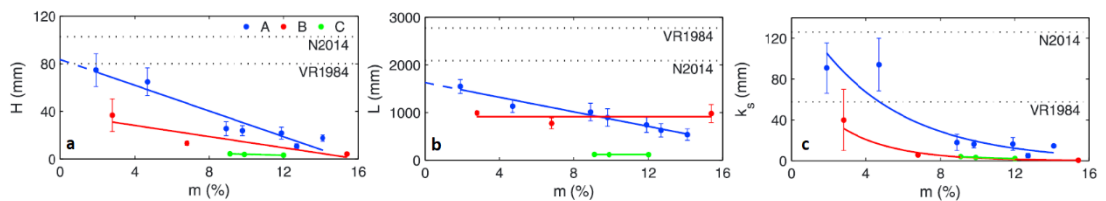
Figure E.2.2 (a) Relationship between bed form height, H, and initial mud content, m, for series A (blue, no EPS), B (red, low EPS), and C (green, high EPS). (b) Relationship between bed form wavelength, L, and initial mud content for series A–C. (c) Relationship between bed roughness, ks= 25H2/L, and initial mud content for series A–C. Error bars represent the variability from the mean across three longitudinal transects. All graphs also show predictions, based on non-cohesive sand experiments, as dotted lines (VR1984 and N2014), after van Rijn [1984] and Naqshband et al. [2014], respectively. The linear fits to H and L in series A can be used to infer clean sand values of H = 83mm and L = 1627 mm.

Field experiments of Lichtman et al. (2018)

Lichtman et al. (2018) collected data on three intertidal flats in the Dee Estuary (near West Kirby, NW England) over a spring-neap cycle to determine the bed material transport rates of bedforms in biologically-active mixed sand-mud. They performed a field-laboratory comparison of their data (under the influence of currents and waves) and the laboratory-based migration data of Baas et al. (2000). From the data, the effects of physical and biological cohesion could not be distinguished from each another, as the variation in EPS content is linearly related to the variation in cohesive clay content. Therefore, the term *cohesive clay* represents both physical and biological cohesion. An inverse relationship between the duration of tidal inundation and clay content was found: as the tide progressed from spring towards neap, and wave forcing decreased, the sediment bed at the field sites changed rapidly from weakly cohesive (<2 vol% cohesive clay) to strongly cohesive (up to 5.4 vol% cohesive clay).

The results demonstrate that the bedform migration rate and the bed material transport rate of mixed sediments in the field were significantly different from that of sand-only bedforms, even when clay and EPS fractions in the bed were below 2.8 vol% and 0.05 wt%, respectively. Below these limits the bed material transport rate reduced as the bed cohesive clay and EPS content increased. Above these limits, which correspond approximately to the points where clay and EPS began to significantly affect the migration rate in the mixed clay-sand laboratory experiments of Baas et al. (2013) and the mixed sand-EPS laboratory experiments of Malarkey et al. (2015), bedform migration and bed material transport were below measure able limits in the study area.

MUSA

F   Summary of experimental results on effects of biogenetic factors

F.1   Effects of biota on the erodibility of mudflats

Field experiments by Amos et al., 1992

Amos et al. (1992) have studied the erodibility of fine-grained sediments in Minas basin within the Bay of Fundy (Canada) using the benthic annular flume, Sea Carousel.

Minas basin: bed of 30% to 40% sand, 40% to 60% silt and 10% to 20% clay and wet bulk density of 1800 kg/m^3. Surface sediments are biologically active (diatoms) and the pelletization process is high. Each winter, ice removes the upper 0.10 m of the mud bed surface at Minas basin. The surface layer is regenerated through tidal sedimentation each spring. Deposition occurs at concentrations below 50 mg/l. The repetitive measurements of sediment erodibility were made during July and August 1989 and July, 1990 at three stations along a transect of a littoral mudflat in the Southern Bight of Minas. This basin is strongly macro- tidal (semi-diurnal mean tides of 11.5 m tidal range) and is subject to intermediate wave activity and ice cover.

Surface erosion (Type I-erosion) occurred at imposed bed stresses between 0.5 and 1.5 N/m2 at Minas basin and between 1 and 2.5 N/m2 after a bloom of diatom production, see Table F.1.1. Surface erosion occurred only in the uppermost 0.5 mm of the bed. At deeper layers Type II-erosion was dominant. Type II-erosion (mass erosion) was constant with time was independent of changes in bulk bed shear strength with depth.

Table F.1.1 Critical bed-shear for erosion at sand-mudflat, Minas basin, Bay of Fundy, Canada

Bed type	Percen tage mud (<63 μm)	Mean size d$_{50}$ (μm)	Dry bulk density (kg/m³)	Chlorophyll content	Critical shear stress for surface eosion (N/m²)
Minas basin; Bay of Fundy, Canada	65%	30-40	> 1000	not measured	0.5-1.5

Field experiments of Herman et al (2001)

Herman et al (2001) review and summarize the results of the ECOFLAT project with respect to the interaction between biota and sediment. Measurements were performed at the Molenplaat, a small intertidal flat in the turbid, nutrient-rich and heterotrophic Western Scheldt estuary. Five sites were selected for intensive measurements, based on sedimentology and composition of the fauna from a preliminary survey in 1995. Four intensive campaigns were organized, in May–June 1996, September 1996, June 1997 and September 1997. Each campaign lasted 14 days and included a spring and neap tide. Permanent measurements of current velocity at four heights above the bed were performed, as well as determinations of suspended sediment, chlorophyll, water temperature and salinity.

Measurements of erodibility as a function of tidal current showed a biological control on this variable. Benthic microalgae stabilize the sediment surface. Benthic macrofauna were shown to have two distinct effects on benthic–pelagic exchange (see also Widdows et al., 2000). Their filtration of suspended matter resulted in biodeposition of fines, thus increasing the flux of material from the water column to the sediment. The bioturbation caused by their movement through the upper sediment layers, and probably also their direct grazing pressure on the microalgae on the sediment surface, resulted in a significant increase of

MUSA

the mass eroded once the critical erosion current velocity had been reached (destabilizing effect). It is unclear, in the long term, which of the two opposing effects is the most important for sediment dynamics.

Mathematical model of van de Koppel et al., 2001

Van de Koppel et al. based a dynamic mathematical model on two assumptions, validated by field and laboratory measurements during ECOFLAT (see Herman et al., 2001) and by literature reports. The assumptions were: microalgal biomass accumulate faster on muddy than on sandy sediments and microalgal biomass reduces the erodibility of the sediment. Given these properties, which were translated mathematically into generalized conditions of the type "erosion rate of mud decreases with increasing microalgal biomass" without the need to specify the dynamic equations, they showed that a microalgae–mud system has two stable equilibrium states: one with low mud and low microalgal biomass and one with high mud and high microalgal biomass. At high bottom shear stress, only the latter equilibrium is expected to occur; at low shear stress only the former. However, there is an intermediate range of bottom shear stress where both states are possible, and the system may flip from one state to another. Figure F.1.1 illustrates the theory of these stable states as a function of bottom shear stress. Field data from the Molenplaat confirmed the existence of this intermediate range where the distribution of sediment mud content is bimodal.
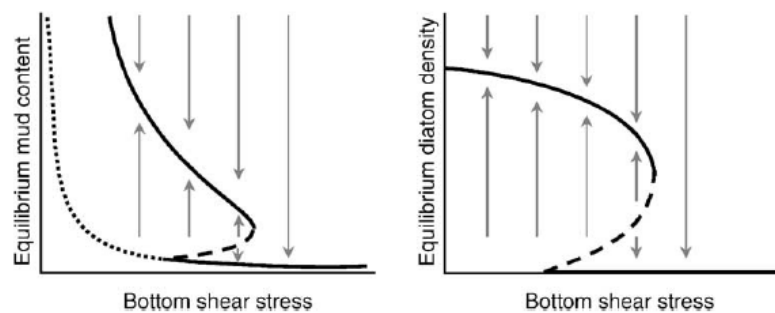

Figure F.1.1 Dynamics of the mud–microalgae interactions in the model by Van de Koppel et al. (2001). Equilibrium states for mud content and diatom density are shown in bold. Dashed lines indicate unstable equilibrium states, whereas the dotted line for mud content shows the mud content in the absence of microalgae. At intermediate values of bottom shear stress, two alternative stable states occur. Above and below this range of bottom shear stress, only one stable state is possible.

Field work of Andersen et al. (2001)

Andersen (2001) have studied the erodibility of two microtidal mudflats in the Danish Wadden Sea over a year at monthly intervals using the in-situ EROMES erosion instrument. One site was dominated by macrofauna, whereas the other was only sparsely inhabited by macrofauna with the temporary formation of diatom biofilms. The sites are situated in the microtidal Lister Dyb tidal area (Kongsmark) and the microtidal Ho Bugt, Gradyb tidal area (Kjelst), both in the Danish part of the European Wadden Sea area.

The tidal range in the Lister Dyb tidal area is 1.8 m compared to a tidal range of 1.6 m in Ho Bugt. The tidal flats in both tidal areas are generally sandy but the study sites are situated in sinks for fine-grained material and the mean grain-size is approximately 10 μm at both sites. About 80% of the dispersed material show equivalent settling diameters finer than 2 μm and the organic content of the bed material varies generally between 8 and 15%. These mudflats are generally very flat with no distinct bedforms or channels and the relief is typically 1 to 2 cm and the slope about 1‰. Small ripples (height 2 mm and length 50 mm) are often found despite the very fine-grained texture of the primary grains and this shows that the bed-material is highly aggregated. A hummocky surface is occasionally formed when the mudflats are undergoing erosion, especially in areas of patchy biofilms.

MUSA

The Kongsmark site has a relatively large macro-faunal population. Fecal pellets make up a large portion of the bed material at Kongsmark during most seasons and typical lengths and densities of these pellets are 0.1 to 0.3 mm and 1030 to 1140 kg/m^3. The macro faunal population at the Kjelst site is smaller due to the much more variable salinities.

The erosion device used for the determination of erosion threshold and erosion rate was a portable version of the German EROMES apparatus, originally developed by the GKSS research centre.

It was found that a critical value of 0.1 g/m^2/s was suitable to discriminate between the erosion of the fluffy top-layer and the erosion of the bed itself. This value corresponds to 360 g/m^2/hr or 0.5 to 1 mm/h for the dry bulk densities found for the bed sediments at the sites.

For each erosion experiment two sediment samples were collected. One sample consisted of the surface scrape of the topmost 1 to 2 mm of the bed and was analysed for grain size, fecal pellet content, chlorophyll a and phaeopigment. The second sample consisted of five subsamples of the topmost 5 mm of the bed taken with a 20-ml syringe, in total 10 ml. This sample was used for the determination of wet and dry bulk density and water content. Grain size analyses were undertaken on selected samples and carried out by use of both a Sedigraph 5100 (giving the equivalent settling diameter) and a Malvern Mastersizer/E laser-sizer (giving the volume diameter). The chlorophyll a content of the surface layer of the bed was used as an indicator of the number of living diatoms.

The fecal pellet content of the bed material and calibration samples for the OBS-sensor were determined by gentle wet-sieving of a sub-sample at 63 μm and examination of the retained material under microscope in order to estimate the fecal pellet content in this material (generally in the order of 90%). The retained material was subsequently given an ultrasonic treatment for 2 minutes and wet-sieved at 63 μm again in order to retain sand and shell-fragments.

The dry bulk density varied between 200 and 350 kg/m^3 for both sites. Particularly high dry densities with an average of 450 kg/m^3 were measured at the Kongsmark site in December 1999 after a period of weak erosion of the mudflat and deposition of fecal pellets. The organic content was variable with averages between 7 and 14% and no distinct temporal trends were found.

Fecal pellets were mostly absent at Kjelst but occasionally pellets were found at some stations. At Kongsmark, high contents of fecal pellets (generally about 50 to 60%) were found in the period May to October and low contents (generally 10 to 20%) were found in the months November to March.

For both sites the erosion threshold was significantly correlated with the Chl a content. For the Kongsmark site, average chlorophyll a contents were less than 50 μg/g dry weight for all study periods and the erosion thresholds were generally between 0.2 and 0.5 N/m^2. However, patchy diatom mats were present at the most seaward station during most of the study period and the erosion threshold varied between 0.8 and 1·9 N/m^2 at this station and with Chl a contents up to 190 μg/g dry weight. For the Kongsmark site a negative correlation was also observed between the fecal pellet content and the erosion threshold. The Chl a content at the Kjelst site was much more variable both spatially and temporally and the average content varied between 20 and 180 μg/g for the different study periods. The mean erosion threshold at Kjelst shows more variation than at the Kongsmark site and generally higher values were found with average thresholds ranging between 0.35 and 1.3

MUSA

N/m^2. Visible biofilms were found at the mudflat surface during both spring and late summer/early autumn and during these periods erosion thresholds above 2.2 N/m^2.

The erosion thresholds plotted as a function of the fecal pellet content indicates that thresholds are low and fairly constant at high fecal pellet contents whereas both high and low thresholds are found at sites with low fecal pellet contents.

Figure F.1.2 shows the temporal variation of the average erosion thresholds and chlorophyll *a* contents for both sites. The chlorophyll *a* contents are fairly low and stable at the Kongsmark site whereas a much larger variation is observed at the Kjelst site. At this site a maximum was observed both in the spring and in the late summer/early autumn. The erosion thresholds follow the variation of the chlorophyll *a* content to some extent with high thresholds at Kjelst in spring and late summer/early winter but also fairly high thresholds in January 2000. The erosion thresholds at Kongsmark slowly decreased from February 1999 to October 1999 and later higher values were found in both December 1999 and March 2000.

The erosion threshold at the Kongsmark site shows dependence on the content of fecal pellets with higher thresholds in the cold seasons when the content of fecal pellets is low and low thresholds in the warmer seasons when contents are high. However, the dependence on fecal pellet content is not very strong and it is probably the varying content of benthic diatoms that is governing the erosion threshold. The data showed no dependence of either erosion threshold or erosion rate on the dry bulk density of the top bed material.
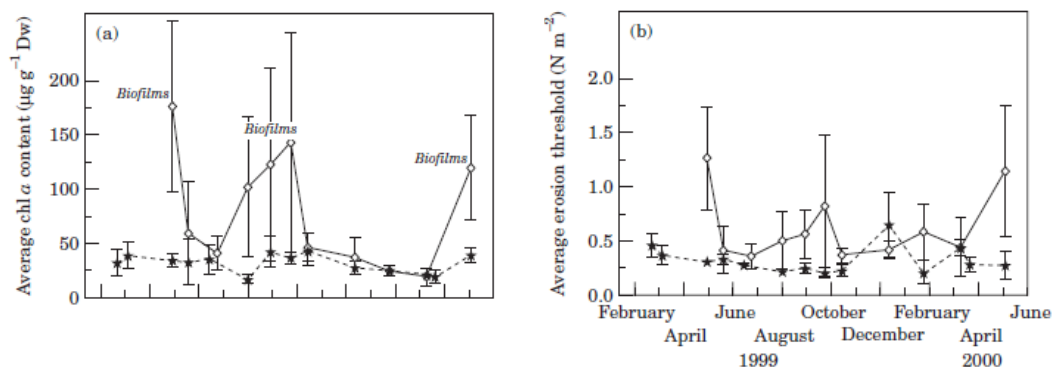

Figure F.1.2 Temporal variation of critical shear stress for erosion (solid symbols= Kongsmark; open symbols= Kjelst)

The study confirms that the erodibility of a mudflat is controlled by both the presence of macrofauna and benthic diatoms and shows that the seasonal variation of erodibility may be very different depending on the biological community structure. Biofilms did not form at sites with high densities of macrofauna and the erodibility of these sites were high due to the high contents of fecal pellets in the bed material.

It must be noted that the results are only applicable to the top few mm of the bed. Deeper layers generally possess higher resistance against erosion and the erosion rate will therefore decline rapidly with time for a given bed shear stress. Consequently, the vertical variation of erosion threshold is needed for a full numerical modelling of the erosional behavior.

The critical bed-shear stresses of almost pure mud are in the range of 0.2 to 0.4 N/m^2 at both sites, see Table F.1.2

MUSA

Table F.1.2 Critical bed-shear for erosion at sand-mudflat, tidal flats, Denmark

Bed type	Percentage mud (<63 μm)	Mean size d_{50} (μm)	Dry bulk density (kg/m³)	Chlorophyll content (μg/g)	Critical shear stress for surface eosion (N/m²)
Kongsmark tidal flat, Denmark	80-100%	10	200-400	<50	0.2-0.4
Kjelst tidal flat, Denmark	80-100%	10	200-400	50-150	0.4-0.8

Field work of Andersen et al. (2005)

This study was carried out to describe the difference in erodibility and aggregation in a tidal basin including both subtidal and intertidal study sites and to use these results to explain the shifting erosion/deposition cycles at the sites. The investigation sites are situated in the microtidal Romo Bight which is part of the Lister Dyb tidal basin. The tidal range is 1.8–2.0 m and the water column is well mixed due to low freshwater inflow and frequent mixing by wind waves. The sediment in the tidal basin is generally sandy but muddy sediments are found in the sheltered parts of the basin. Two main investigation sites were chosen in Romo Bight—a mudflat site and a small tidal channel. Both sites have been studied in detail recently and data on seasonal bed-level changes, suspended sediment transport, erodibility and 210Pb-dating have been reported. Both study sites show net accumulation of about 15 mm/year.

Erosion thresholds, erosion rates and settling velocities of the eroded material were measured at a mudflat transect and at sediment cores taken from a nearby tidal channel during surveys made in May 2000 and March 2002 (using a portable EROMES erosion equipment). Surface samples were analysed for grain-size, chl. a content, faecal pellet content, dry bulk density and organic content. Additionally, surface samples were taken at eight occasions in the period January 2002 to May 2003 from shallow tidal channels in the area. These samples were analyzed for mud content and showed that major shifts in sediment distribution occurred in the period.

The erodibility of the mudflat was generally high due to pelletization by the mudsnail Hydrobia ulvae but close to the salt marsh much lower erodibility was found, probably due to stabilisation by microphytobenthos. In contrast, the erodibility of the channel bed seemed to be very little influenced by biological activity and the relatively low erodibility found here was caused by physical characteristics of the sediment.

Both formation of biofilms and pelletization of the bed material showed a temporal variation which supports previous results from the mudflat (Andersen, 2001). In contrast, the erodibility of the tidal channel sediments did not show any significant temporal variation and the sediments seemed to be less affected by both macrozoobenthos and microphytobenthos. This is a result of the very small macrozoobenthic population at the site and limited availability of light for microphytobenthic growth due to the larger water depth and generally high turbidity of the water column. Temporal variations of the mudflat stability and hydrodynamics resulted in temporal variations of deposition and erosion and the changing stability at the mudflat is likely to be one of the main reasons for a general transport of fine-grained sediment from the mudflat to the channel in the cold seasons and vice versa during the rest of the year (see Figure F.1.3 for a conceptual diagram).

Literature review on sand and mud
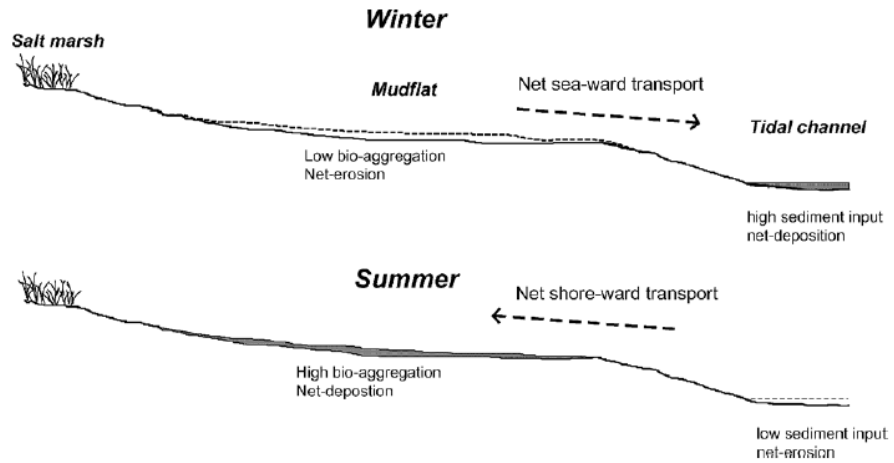16 November 2020

MUSA

Figure F.1.3 The conceptual model showing the general net-transport direction of fine-grained sediment during winter and summer. Low biological activity at the mudflat during the winter causes a net sea-ward transport, whereas the higher biological activity in the summer reverses the net transport direction.

The authors stress that, whereas a quite large data-set of erodibility/settling measurements has been collected from mudflat sites in the Danish Wadden Sea, only the two measuring campaigns reported here have been carried out in tidal channels. Consequently, it is possible (and likely) that other fine-grained channel-beds may show different characteristics as a result of different texture and/or biological community.

Field work of Andersen et al. (2010)

Andersen et al. (2010) studied a mixed mudflat situated on ''Dornumer Nacken'' in the tidal basin behind the barrier islands Baltrum and Langeoog in the East Frisian part of the German Wadden Sea. The basin is mesotidal with a tidal range of approximately 2.6 m. The basin consists largely of intertidal sand flats and mixed mudflats. The fine sediment fraction < 63 μm is in the range of 30% to 40% (mud content). The average inundation period during each tidal cycle is 7 hours during calm weather conditions and maximum tidal current velocities are about 25 cm/s.

Bed samples were taken by scraping of the topmost 1 mm of the bed and were analyzed for grain-size distribution, fecal pellet content, organic content, content of chlorophyll a, water extractable colloidal carbohydrate and extracellular polymeric substances (EPS). Analyses of carbohydrates were only carried out in June and September. Additional samples of the topmost 5 mm of the bed were taken with a suction needle (syringe with diameter 21 mm, five samples pooled into one sample) and analyzed for dry bulk density. Grain-size analyses were carried out by use of a Malvern Mastersizer/E laser-sizer after careful dispersion (deflocculation) and ultrasonic treatment prior to analysis. Fecal pellets were abundant at the site and the pellet contents of the bed material and calibration samples for the OBS-sensor were determined by gentle wet-sieving of a sub-sample at 63 μm and examination of the retained material under microscope in order to estimate the fecal pellet content in this material. The retained material was subsequently given an ultrasonic treatment and wetsieved at 63 μm again in order to separate fecal pellet material and sand and shell-fragments. Organic contents were determined. Chl a contents were determined after extraction in 90% acetone by high performance liquid chromatography and by spectrometry. The contents of colloidal (water extractable) carbohydrate and EPS were quantified using the phenol-sulphuric spectrometric assay/procedure.

The sediment from each erosion core was sieved at 1 mm and the macrozoobenthos were described and counted (range of 100 to 3000 individuals per m^2).

MUSA

The erosion experiments were carried out using a portable EROMES erosion apparatus. Additional experiments were carried out using the original laboratory version of the same instrument. Undisturbed sediment cores were brought ashore and analyzed in the laboratory EROMES.

The erosion thresholds were determined by use of plots of erosion rates versus applied bed stress. A linear fit was made through the data points in the region of the onset of erosion and the threshold was determined as the bed shear stress at the intercept of this line with a critical erosion rate; the erosion rate above which significant erosion of the sediment surface starts to take place. A critical erosion rate of 0.01 $g/m^2/s$ was used which corresponds to the erosion of the least stable material at the surface (low-density flocs and bio-aggregates). Samples for the calibration of the OBS-sensor were withdrawn from the tube during each experiment and filtered. The aggregation and settling velocity of the eroded material were analyzed as part of the erosion experiments by monitoring the change in suspended concentration as the propeller was turned off after the last step and the suspended material could settle. In order to make the data directly comparable (compensate for the changing viscosity of the water with changing temperature), the settling velocities were converted to equivalent settling diameters by use of Stokes' law. The actual diameter of the aggregates is larger, often much larger, due to the lower density and irregular shape of the aggregates.

The surface sediments at the site were a mixture of very fine-grained sand and mud and the grain-size distributions of the bed material were bi-modal and showed that the surface material consisted of well-sorted sand with an average grain-size of about 105 μm and poorly sorted silt and clay with a mode at about 15 μm.

The mud content of the surface material was about 35% and showed no significant temporal variation but a decrease with depth was observed, reaching about 15% mud at 20 cm depth.

The erosion thresholds for the sediments generally varied between 0.2 and 0.6 N/m^2 (Table F.1.3) but significantly higher thresholds (up to 1.8 N/m^2) were observed in September and April. Similarly, significantly higher contents of chlorophyll a were observed in September and April and lower contents in the rest of the study period.

Table F.1.3 Critical bed-shear for erosion at sand-mudflat, East Frisian Wadden Sea, Germany

Bed type	Percentage mud (<63 μm)	Mean size d_{50} (μm)	Dry bulk density (kg/m^3)	Chlorophyll content ($mg/m^2 \cong \mu g/g$)	Critical shear stress for surface eosion (N/m^2)
Dornumer Nacken, East Frisian German Wadden Sea	35%	15-100	700-1120	<10	0.2-0.3
				10-20	0.2-0.6
				20-40	0.4-1
				40-80	1-2

(1 mg/m^2 in layer of 1 mm thick $\cong$ 1mg/kg $\cong$ 0.001 mg/g $\cong$ 1 μg/g)

Figure F.1.4 shows a comparison of the average suspended concentration data from the experiments in September 2002 and February 2003.
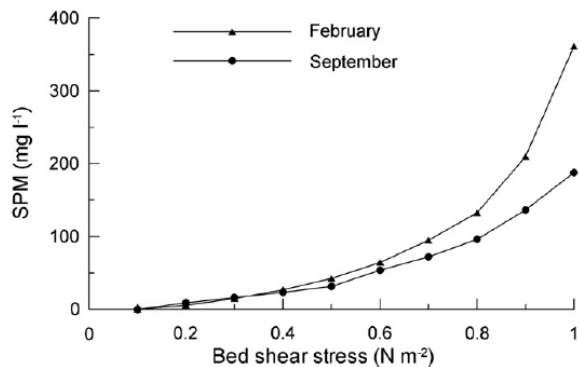
MUSA

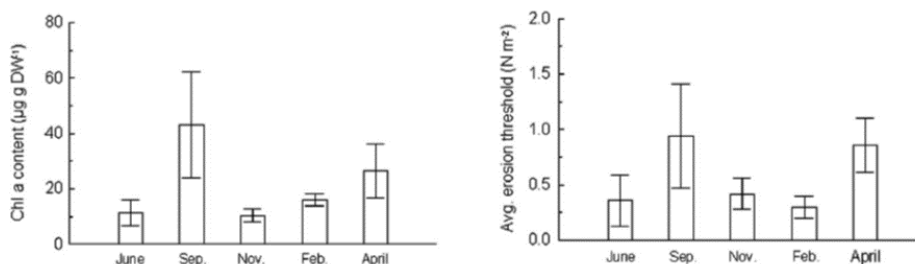*Figure F.1.4 Suspended concentrations in September 2002 and February 2003*

Figure F.1.5 Temporal variation of critical stress and Chl a-content, East Frisian Wadden Sea, Germany

Figure F.1.5 shows a plot of the temporal variation of the Chl a content and erosion threshold. Colloidal carbohydrates and EPS were only measured in June and September and much larger values were observed in September.

The dry bulk density of the sediment varied between 700 and 1150 kg/m^3 and organic content between 1.3% and 3.6%. Neither macrofauna densities, dry bulk density, fecal pellet content or organic content showed significant temporal variations.

No significant differences were observed in June but the chlorophyll a contents were higher on crests than in troughs in September. In November, erosion thresholds were higher on crests than in troughs. Bedforms were absent in February and April 2003.

The erosion thresholds were especially well correlated to the contents of chlorophyll a, colloidal carbohydrates and EPS. The site was primarily controlled by microphytobenthos, which may vary considerably temporally and spatially. Its effect is smaller in autumn and winter due to lower light-intensity and higher wave action. Drying will also contribute to differences in erodibility during warm periods with high evaporation.
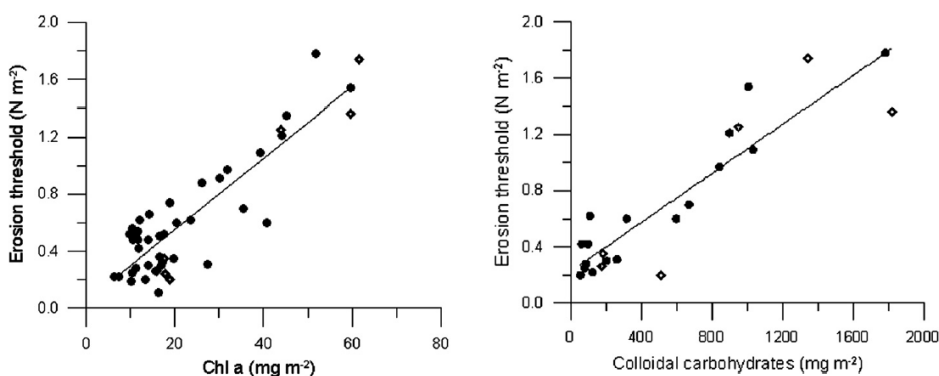

Figure F.1.6 Critical bed-shear stress as function of Chl a-content and colloidal carbohydrates-content (solid circles= in-situ EROMES; diamonds= laboratory EROMES); East Frisian Wadden Sea
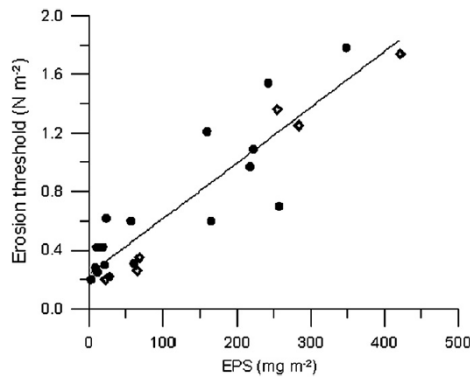
Figure F.1.7 Critical bed-shear stress as function of EPS-content; East Frisian Wadden Sea, Germany (solid circles= in-situ EROMES; diamonds= laboratory EROMES).
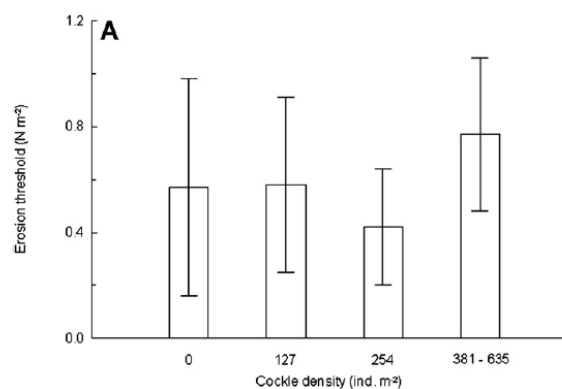

Figure F.1.8 Critical bed-shear stress as function of cockle density; East Frisian Wadden Sea, Germany

In the order of 80% of the variance in the erosion thresholds can be explained by these indirect measures of microphytobenthic stock. There was no correlation between the erodibility of individual sediment cores and the density of the cockles in the cores (Figure F.1.8). The presence of cockles may lead to increased erodibility of the sediments caused by burrowing activity (rougher surface) and the exhalent jets from the cockle's siphons.

A biostabilization index can be calculated as the ratio of the erosion thresholds with and without biological influence. If the hypothetical case of complete absence of colloidal carbohydrates and/or EPS is considered, an expected erosion threshold of about 0.2 N/m^2 can be found based on the linear fits in Figures F.1.6 and Figure F.1.7. Using this value as a best estimate of the erosion threshold at abiotic conditions a stabilization index of 4.7 is found in September and 4.3 in April. The content of sand in suspension was still lower than the bed material.

A direct influence of Cerastoderma edule on erodibility was not observed, in contrast to other recent studies. The presence of C. edule at the site results in biodeposition of fine-grained material and the presence of C. edule will therefore probably increase the content of fine-grained sediments at the surface compared to an abiotic situation. Increasing the amount of fine-grained material in mixed sediments has previously been shown to reduce the erodibility of the sediments and C. edule will therefore in this way indirectly (feedback) stabilize the bed. However, the presence of other and more vigorous bioturbators and deposit-feeding species may completely hide this effect on sediment erodibility.

Literature review on sand and mud
16 November 2020

Field experiments of Harris et al., 2016

Sediments were sampled at different times (2011–2012) from 45 points across intertidal sandflat transects in three New Zealand estuaries (Whitford, Whangamata, and Kawhia) encompassing a wide range in mud (≤63 μm) content (0–56 %) and macrofaunal community structure. The aim was to quantify the influence of biotic (benthic microbial biomass and macrofauna community structure) and abiotic (sediment mud content and grain size) variables on sediment movement. Small bioturbators dominated the macrofauna, and on average their abundance increased with mean grain size.

Three distinct measures of sediment erosion potential were calculated using an EROMES: erosion threshold (τ_c; N m−2), erosion rate (ER; g m−2 s−1), and change in erosion rate with increasing bed shear stress (m_e; g N−1 s−1). Collectively, these measures characterized surface (τ_c and ER) and sub-surface (m_e) erosion.

Results indicated that small bioturbating macrofauna (predominantly freely motile species <5 mm in size) destabilized surface sediments, explaining 23% of the variation in τ_c ($p \leq$ 0.01) and 59%of the variation in ER ($p \leq 0.01$) (see Figure F.1.9). Alternatively, mud content and mean grain size cumulatively explained 61% of the variation in m_e ($p \leq 0.01$), where increasing mud and grain size stabilized sub-surface sediments (see Figure F.1.10).
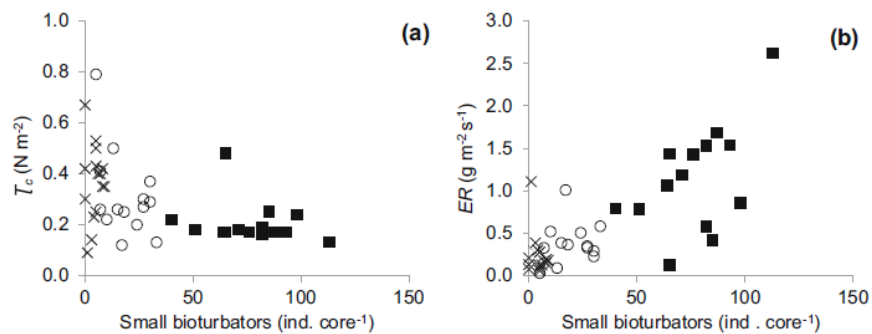

Figure F.1.9 Effect of small bioturbators on initial bed erosion (τ_c) (a) and erosion rate (ER) (b). Symbols denote estuaries Whitford (x), Whangamata (■), and Kawhia (○)
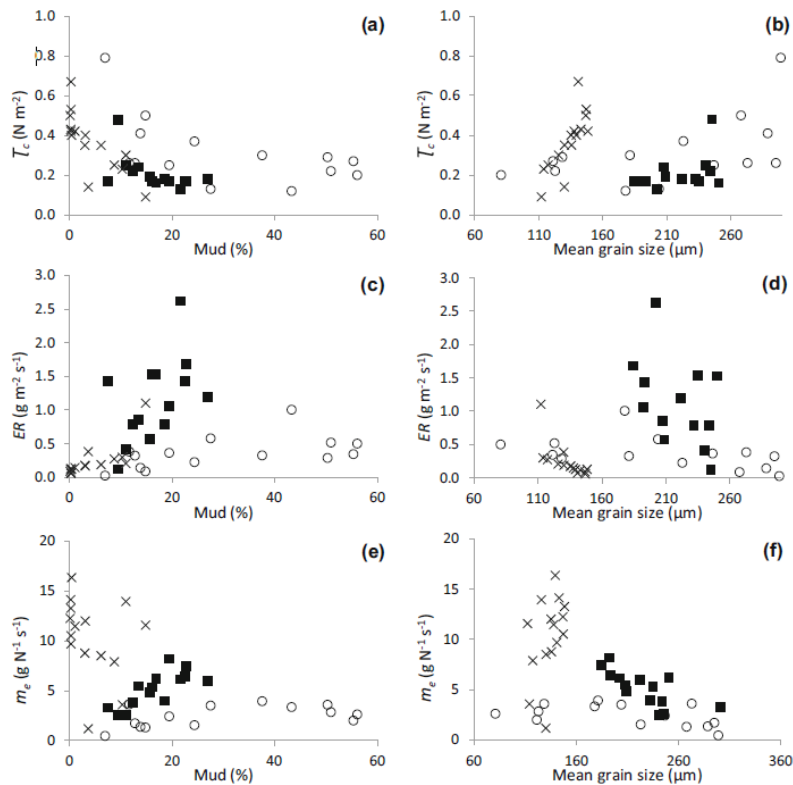
Figure F.1.10 Initial bed erosion (τc; a, b), erosion rate (ER; e, d), and erosion constant (me; e, f) as a function of sediment mud content and grain size. Symbols denote estuaries Whitford (x), Whangamata (■), and Kawhia (○)

These results reveal differences among the three measures of erosion potential, suggesting that multiple stages/depths of erosion should be considered when accounting for ecological processes. For instance, local biota was important to early/ surface erosion, yet once the surface layer was eroded/resuspended, mud/microbes appeared to stabilize sediments. In other words, the importance of biotic and abiotic predictors varies with erosion stage. Functional group classifications are a useful way to determine the impact of benthic macrofauna on sediment erodibility across communities with different species composition.

Lab experiments of Chen et al., 2017

Laboratory-controlled sediment beds were incubated with *Bacillus subtilis* for 5, 10, 16, and 22 days before performing erosion experiments to study the temporal and spatial variations in sediment stability caused by the bacterial secreted EPS. Although most previous studies focused on the surface phenomenon caused by EPS (reflected by the increase in the critical shear stress for erosion), biogenic stabilization is not necessarily confined to the presence of a surface biofilm: EPS may penetrate the surface of the sediment matrix and establish a vertical profile.

The results showed that erosion processes were significantly mediated by bed age-associated biostabilization. In the first stage of bio-maturity (5 days), the biosedimentary bed was more easily eroded than the clean sediment. With increasing growth period, bound EPS became more widely distributed over the vertical profile resulting in bed stabilization. After 22 days, the bound EPS was highly concentrated within a surface biofilm, and a relatively high content also extended to a depth of 5 mm and then decayed sharply with depth.

Literature review on sand and mud
16 November 2020

MUSA

The protection of EPS against erosion of the bed was twofold: 1) it increased the critical shear stress of the bed and 2) it enabled the bed to withstand threshold conditions for an increased period as the biofilm degraded before eroding. Moreover, after full erosion of the biofilm protection, the high EPS content in the sublayers continued to stabilize the sediment (hindered erosion) by binding individual grains. Consequently, the bed strength did not immediately revert to the abiotic condition but progressively adjusted.
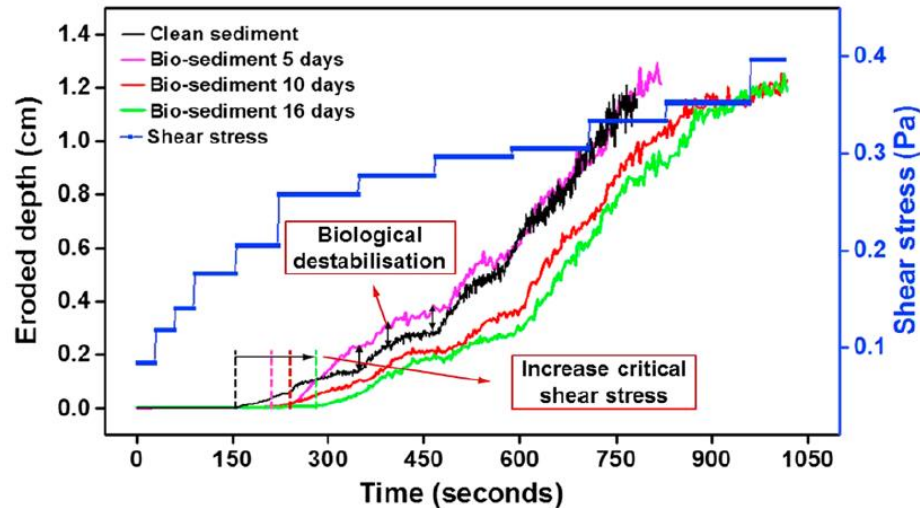

Figure F.1.11 Erosion curves of bio-sediment (5, 10, and 16 days) and controlled clean sediment represented by eroded depth value increasing with stepwise increment of shear stress (Chen et al., 2017).

Modelling study of Le Hir et al (2007)

Le Hir et al. (2007) described state-of-the-art sediment transport models accounting for biological processes and explored the effects of marine vegetation, microphytobenthos, and macrofauna on long-term morphodynamics. Marine vegetation enhances the bottom dissipation of current energy and reduces shear stress at the sediment–water interface, which can be significant when the shoot density is high. Microphytobenthos and secreted EPS stabilize the sediment, and an increase of up to a factor of 5 can be assigned to the erosion threshold on muddy beds. In addition, the development of benthic diatoms tends to be seasonal, so that stabilizing effects are likely to be minimal in winter. Macrofaunal effects are characterized by extreme variability: for muddy sediments, destabilization seems to be the general trend. This can become critical when benthic communities settle on consolidated sediments that would not be eroded if they remained bare. Biodeposition and bioresuspension fluxes are mentioned, for comparison with hydrodynamically induced erosion rates. Unlike the microphytobenthos, epifaunal benthic organisms create local roughness and are likely to change the BSS generated by the flow.

The seasonal presence of microphytobenthos generates sediment level changes of about 5 cm. However, these effects disappear in autumn and winter when the erosion threshold returns to its abiotic value, even in simulations where wave erosion is ignored. Consequently, local stabilization by the microphytobenthos does not have a significant long-term effect (see Figure F.1.12). In contrast, the simulations show a potentially strong long-term effect of vegetation by protection of sediment from wave erosion. This was concluded from simulation results where a reduction of bed shear stress in the upper flat was implemented to simulate the effect of a saltmarsh, which induced a significant seaward shift of the upper flat.
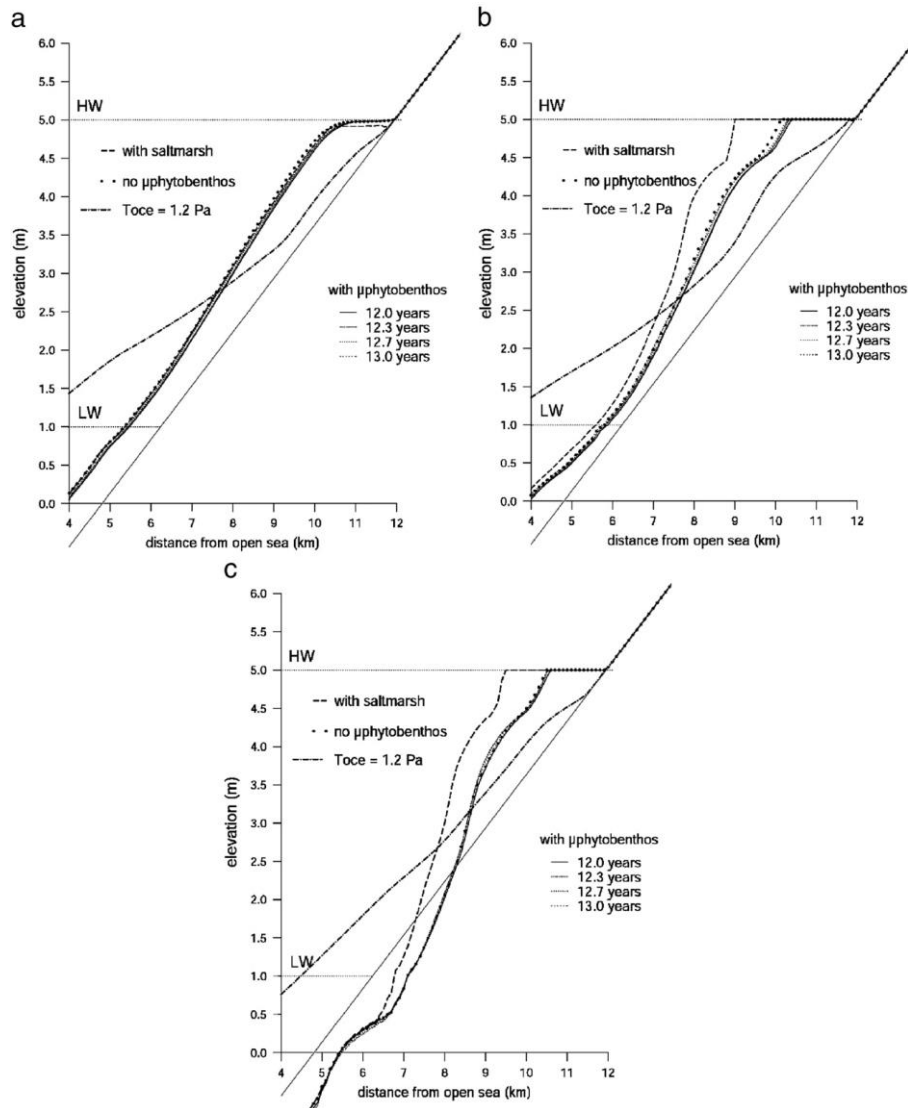
Figure F.1.12 Simulation of the bottom profile evolution after 13 years for 3 wave regimes (a–c). Results are given every 4 months for the "reference" simulation, which accounts for microphytobenthos stabilization. These profiles are compared with profiles simulated after 13 years either without microphytobenthos (bold dotted line), with microphytobenthos and saltmarsh (dashed line), or with a steadily increasing erosion threshold (mixed line). The grey line represents the initial bottom profile. Toce is the critical shear stress for erosion.

Modelling study of Borsje et al (2008)

A modelling study was performed with the aim to understand the large-scale effects of small-scale biological activity. Hereto, effects of biology were quantitatively incorporated into the process-based sediment transport module of Delft3D. The Western Wadden Sea was used as a case study.

Their results suggest that the seasonal variation in the sediment concentration is caused by the combined effect of the suspended sediment concentrations at the North Sea, wind and biological activity in the bed. Biomass bio-stabilizers (microphytobenthos) show a clear temporal variation throughout the year, inducing the temporal variation in the suspended sediment concentrations on a basin scale. The spatial variation in the fine sediment distribution on the bed must be attributed to the large modification of the transport parameters in the subtidal area where the bio-destabilizers (deposit feeders) are present.

The importance of including both the temporal and spatial variations in biological activity in bio-geomorphological models is shown in Figure F.1.13. The exceeding time of the critical bed shear stress for erosion with only spatial varying biological activity is almost similar to the simulations without biological influences. By including both spatial and temporal variations in biological activity, the amount of time that the critical shear stress is exceeded deviates strong from the default model simulations.
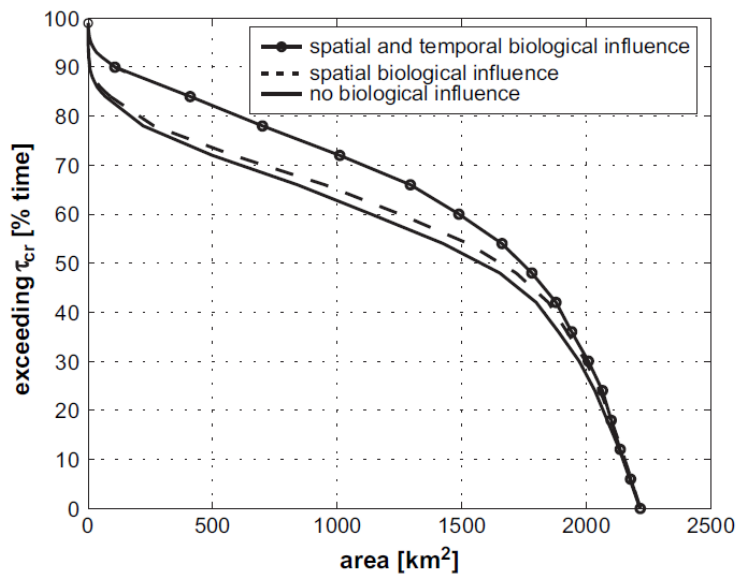

Figure F.1.13 Area of the Western Wadden Sea [km2] in which the critical shear

F.2 Effects of biota on the erodibility of subtidal estuarine environments

Field experiments by Dickhudt et al., 2009

A study was conducted on the York River estuary, a sub-estuary of the Chesapeake Bay, USA, to evaluate variation in seabed erodibility over several seasons in a cohesive estuarine environment and gain insight into the dominant physical and biological processes influencing these variations. Three sites were chosen in the York River estuary to provide variation in bed erodibility and associated physical and biologic influences. Two of these sites were located about 25 km from the York River mouth (Clay Bank), with a typical salinity of 10 to 20 ppt: one site at Clay Bank was located on the flank of the main channel at ~11 m depth (CC), while the other site was about 1 km away in a secondary channel at ~6 m depth (CS). A third site was about 10 km from the York River mouth (Gloucester Point, GP) and at a depth of 8 m and typical salinity of 13 to 23 ppt. Suspended sediment concentrations near Gloucester Point (10 s of mg l−1) are typically much less than those found at Clay Bank.

The two sites in the Clay Bank region exhibited similar, pronounced seasonal cycles in erodibility. Lowest erodibility was found in the summer and fall (July–November 2006 and July–October 2007). Erodibility was quite consistent during these periods. High levels of erodibility were found in the late winter and spring. However, erodibility at the GP site was generally low and did not exhibit the pronounced seasonal pattern found at the two Clay Bank sites.

Weak to non-existent correlations between bed erodibility, solids volume fraction, and surficial concentrations of organic matter, colloidal carbohydrate, and EPS, were not sufficient to explain the observed seasonal pattern in bed erodibility. With respect to

biological influences on erodibility, it would be expected that the magnitude of bioturbation would be in phase with seasonal variations in water temperature. So, a bioturbation maximum was expected when water temperature was high resulting in enhanced erodibility in summer and fall. Contrary to this, the highest measured erodibility occurred in the late winter and spring when the water temperature was low and before the predominantly annual benthic species successfully recruit into these habitats. EPS did not correlate well to variations in bed erodibility, probably because little light reaches the seabed during most of the year and that lacks the algal mats found on tidal mudflats. Besides, the relative constancy of EPS through time at the sites suggests that while EPS may have been an influence on sediment cohesivity in the York River estuary, it did not vary systematically, and thus did little to influence seasonal and spatial variations in bed erodibility. From this, the authors conclude that the forms of biostabilization highlighted in erodibility studies in intertidal areas may not translate to an estuarine environment where little light reaches the seabed.

Field experiments by Amos et al. (1996)

Amos et al. (1996) have studied the erodibility of natural consolidated estuarine sediments using an in-situ sea caroussel flume along a longitudinal transect of Manitounuk Sound, Hudson Bay (Canada). Water depths were in the range of 13 to 45 m and the percentage of organic materials is very small (<1%).

Sea Carousel is a benthic annular flume capable of submarine measurement of seabed stability. The annulus is 2 m in diameter, 0.3 m high and 0.15 m wide. It is equipped with three optical backscatter sensors to monitor water turbidity, an electromagnetic current meter to monitor the flow velocities, a lid rotation sensor and an underwater camera that views the eroding bed through a side window. Flow is induced by rotation of a moveable lid to which are attached eight paddles. Flow velocity is transformed to bed stress based on velocity gradients derived in a series of laboratory tests. Bed stress is increased in the flume in a series of steps of equal duration. Erosion rate (in the range of 1 to 3 g/m2/s) is evaluated as the increase in suspended mass in the flume with time. Bulk density values are based on gravity cores from each site. The sedimentary column was a highly bioturbated, mottled olive-grey silty clay, with a surface oxidized layer 0.10 m thick. Exceptions were GB13 and GB14 which showed distinct laminations and a surface layer of sandy silt.

Deployments lasted about 90 min. Each deployment comprised: (a) a slow descent of the flume to the seabed to minimize seabed disturbance on landing; (b) a still-water interval to allow settling and clearing after deployment and to derive the offsets of the flow meter and the optical backscatter sensors; (c) a period of flow during which the reference current is increased in nine steps up to 0.8 m/s and (d) a still-water period to allow settling of the material eroded in the preceding interval of flow. Water samples were collected from a port in the side of the Sea Carousel at each speed increment with the aid of a pump. The volume of the hose was flushed, and a 500-mL water sample was collected.

Table F.2.1shows the basic data and measured critical stress for erosion of the topmost layer < 1 mm. The data are grouped in three typical groups of consolidated beds with bulk densities between 1600 and 2000 kg/m3. The measured critical shear stresses for erosion are smallest for muddy-silty beds with bulk densities of 1700 to 1800 kg/m3.

MUSA

Table F.2.2 Critical bed-shear stress for erosion of consolidated beds in deeper water of Manitounuk Sound, Hudson Bay, Canada

Type of bed	Median sediment size (μm)	Percentage clay (%)	Percentage silt (%)	Percentage sand (%)	Wet and dry bulk density (kg/m³)	Critical bed-shear stress erosion of toplayer < 1 mm (N/m²)
Muddy-Silty bed (GB3-10,12,15)	3-10	20-65	30-40	5-25	1700-1800 (>1000)	0.7-2
Muddy-Silty bed (GB11,14)	30-40	30-35	15	50-60	1600-2000 (>1000)	3.5-10
Muddy-Sandy bed (GB13)	63	25	15	60	1950 (>1000)	>6

Subtidal field experiments by Sutherland et al. (1998)

Sutherland et al. (1998) used an in-situ carousel flume to study the influence of biofilms on the erodibility of a pure mud bed in a tidal channel (Upper South Cove, Nova Scotia, Canada). Upper South Cove is a shallow coastal embayment situated within Lunenburg Bay, Nova Scotia, located 63 km southwest of Halifax.

Subsamples of the material eroded within the sea carousel were collected by pumping and were analyzed for suspended particulate matter. Undistorted syringe cores of the seabed at water depths between 3 and 8 m were also collected and analyzed for major physical properties (bulk density, mineralogy, grain size) and organic character (chlorophyll, pheopigment, colloidal carbohydrate, organic content). Sediment cores (syringe cores; diameter=2.6 cm, length= 6 cm) were taken from a Van Veen Grab sample collected at each station located inside the cove. The topmost 1 and 2 mm of a second core collected from each station were analyzed for both chlorophyll and pheopigment concentrations, since the chlorophyll maximum was generally above a depth of 2 mm in the sediment. Slices of each sediment layer were cut in 1-mm depth intervals. The inner cove region where the samples were taken, is a region of net deposition of fine sediments.

Sediment in the inner cove is characterized by unconsolidated muds. The sediment is highly pelletized with an organic content of about 20% and surface porosities of up to 87%. The average current in the cove is 0.12 m/s. Resuspension of fine material occurs at peak flows of 0.3 to 0.6 m/s during flood tide. Observations made by Scuba in the cove reveal the occurrence of gel-type muds.

Seven stations were chosen along a transect extending over the inner half of Upper South Cove. The erodibility of the sediment at these stations was determined by use of the sea carousel from 16 to 19 October 1993.

The sea carousel has a diameter of 2 m, an annulus width of 0.15 m and a height of 0.30 m. The flow is driven by a movable lid with eight small paddles. A skirt is situated on the outer wall of the annulus and standardizes penetration of the flume into the seabed. Optical backscatter sensors were located inside (0.03 and 0.18 m above the skirt) and outside the annulus to measure ambient and resuspended solids. A window was situated in the inner flume wall, through which an underwater videocamera recorded erosion of the seabed. Longitudinal and vertical components of flow within the annulus were recorded with a Marsh-McBirney electromagnetic current meter.

Figure F.2.1 shows the vertical distribution of the wet bulk density over the upper 50 mm of the seabed.

Three distinct layers can be distinguished:
- biogenic gel-like layer of 1 to 5 mm thick uncosolidated mud (confirmed by diver observations) with wet bulk density of 850 to 1150 kg/m3 (including local gasbubbles of maximum 1 mm diameter causing densities < 1000 kg/m3);
- consolidating mud layer of 5 to 20 mm with wet bulk density of 1000 to 1150 kg/m3;

Literature review on sand and mud
16 November 2020

MUSA

- consoldated mud layer > 20 mm with wet bulk density of 1150 to 1300 kg/m3.

The wet bulk density is lowest in the most quiescent regions of the inner cove.
The critical bed-shear stress for erosion was found to be in the range of 0.05 to 0.15 N/m2. The critical stress increases with increasing chlorophyll content. The chlorophyll content was higher in shallower depths with higher light intensity.

Table F.2.3 Critical bed-shear for erosion at subtidal channel bed, Lunenburg Bay, Nova Scotia, Canada

Bed type	Percentage mud (<63 μm)	Mean size d_{50} (μm)	Dry bulk density (kg/m³)	Chlorophyll content (μg/ml≅μg/g)	Critical shear stress for surface eosion (N/m²)
Subtidal channel bed, Nova Scotia, Upper South Cove, Lunenburg Bay, Canada	20%-30%	30-40	< 400	< 5	0.05-0.15

Figure F.2.2 shows critical bed-shear stress as function of wet bulk density from six seabed stability studies using the sea carousel in widely varying environments. The erosion thresholds reported for pure mud of Inner Cove region (Nova Scotia) lie at the lower end of wet bulk density values. Although the sediment chlorophyll and carbohydrate contents lead to somewhat higher critical stresses, the low bulk density values may be responsible for the generally low erosion thresholds.
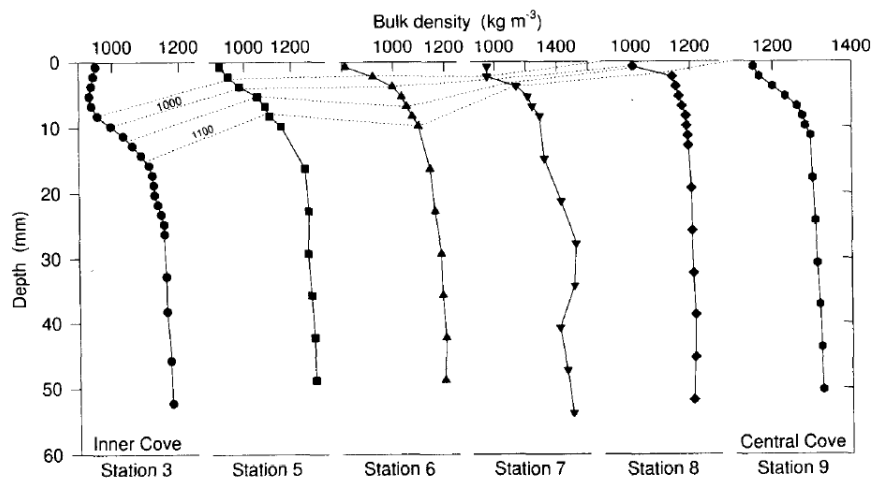

Figure F.2.1 Wet bulk density profiles at stations in water depths between 3 and 8 m, Inner cove, Canada

Literature review on sand and mud
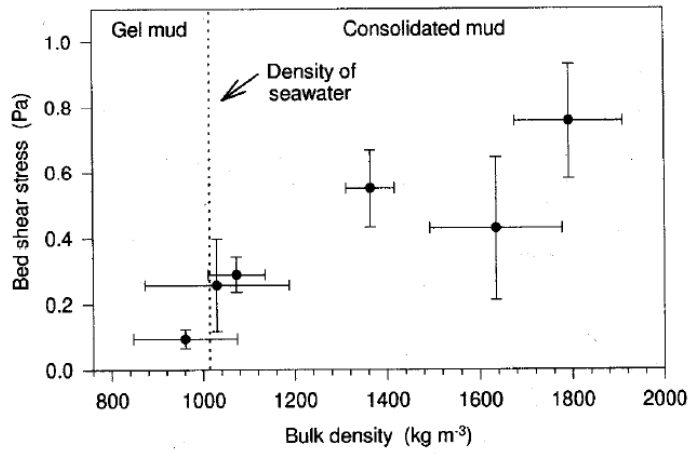16 November 2020

MUSA

Figure F.2.2 Relationship between critical bed-shear stress and bulk density; six different locations (Manitounuk Sound, Humber Estuary, Miramichi Bay, Hamilton Harbour, Fraser River, Lunenburg Bay)